SETTLEMENT ASSESSMENT OF HIGHWAY EMBANKMENT FOR SR77/1500 WEST INTERCHANGE IN SPRINGVILLE, UTAH

by

Michael Robert Platt

A thesis submitted to the faculty of
The University of Utah
in partial fulfillment of the requirements for the degree of

Master of Science

Department of Civil and Environmental Engineering

The University of Utah

May 2013

The University of Utah Graduate School

STATEMENT OF THESIS APPROVAL

The thesis of **Michael Robert Platt**

has been approved by the following supervisory committee members:

Evert Lawton	, Chair	**2/14/2013** Date Approved
Steven Bartlett	, Member	**2/14/2013** Date Approved
Chris Pantelides	, Member	**2/14/2013** Date Approved

and by **Chris Pantelides** , Chair of

the Department of **Civil and Environmental Engineering**

and by Donna M. White, Interim Dean of The Graduate School.

ABSTRACT

A research study was conducted for the Utah Department of Transportation regarding settlement caused by embankment construction for a new bridge located about ¼ mile east of the Interstate 15-State Route 77 interchange in Springville, Utah. Embankment ramps were about 425-ft long, 106-ft wide, and 30-ft tall at the highest points, with vertical side slopes supported by mechanically stabilized earth (MSE) walls. The primary objectives of this study were as follows: (1) Determine consolidation properties of the cohesive soils; (2) predict time rate of primary consolidation settlement using numerical analyses; (3) compare measured rates of primary consolidation settlement with predicted values; and (4) compare the effectiveness of Asaoka's (1978) method for predicting the time for surcharge removal with more advanced methods. These objectives were attained by performing field and laboratory investigations to determine properties of the soils at the site, installing instrumentation to measure settlement and other relevant parameters, and performing numerical analyses to predict the rate of primary consolidation settlement within each cohesive layer.

During the field investigation, undisturbed piston samples were obtained and standard penetration, cone penetration, and vane shear tests were performed. Instruments installed to monitor soil behavior included nineteen piezometers, twenty spider magnets, six settlement manometers, three push-in cells, two ShapeAccelArrays, one vertical inclinometer, one horizontal inclinometer, three pressure cells for vertical stress, and

three pressure cells for horizontal stress. The laboratory investigation included classification and constant rate of strain consolidation tests.

Primary consolidation settlement was predicted using Terzaghi's (1947) and Davis and Raymond's (1965) one-dimensional consolidation theories in conjunction with the finite difference method. Results from these two analyses were compared with measured primary consolidation settlement data obtained from field instruments. Primary consolidation settlement results using both methods proved to be reasonable, but no conclusion could be reached regarding which method yielded better predictions.

Predicted times for surcharge removal analyzed using Asaoka's method based on measured values of surface settlement were incorrect because of the erroneous assumption that the underlying soil is homogenous. Better estimates of time for surcharge removal were obtained by analyzing each of the cohesive layers separately.

TABLE OF CONTENTS

ACKNOWLEDGMENTS

I would like to first take the time to thank Dr. Evert Lawton for the opportunity to participate in the 1500 West and State Route 77 2009 Research Project located in Springville, Utah. I would also like to thank Dr. Lawton for providing guidance and instruction throughout my scholastic career at the University of Utah.

I would like to also like to thank Dan Seely at IGES Inc. for his support and instructions on performing laboratory tests that were performed during the research period.

I would like to thank my wife for her unwavering support and patience during this time of scholastic activity and for always reminding me of the important things in life.

Finally, I would like to thank my parents for teaching me integrity and hard work pays off in the end.

1 INTRODUCTION

The reconstruction of the Interstate 15/State Route 77 interchange in Springville, Utah began in the fall of 2008 and can be seen in Figure 1-1 through Figure 1-4 starting with the location of the embankment, followed by plan and profile views, and ending with preexisting conditions of the construction site.

As part of this project, a bridge was constructed over the railroad tracks and road located about ¼ mile east of the interchange, which included ramps about 425-ft long on the east and west sides of the bridge.

Figure 1-1. Aerial view of research site located east of Interstate 15 on State Route 77 in Springville, Utah (image from Google Earth).

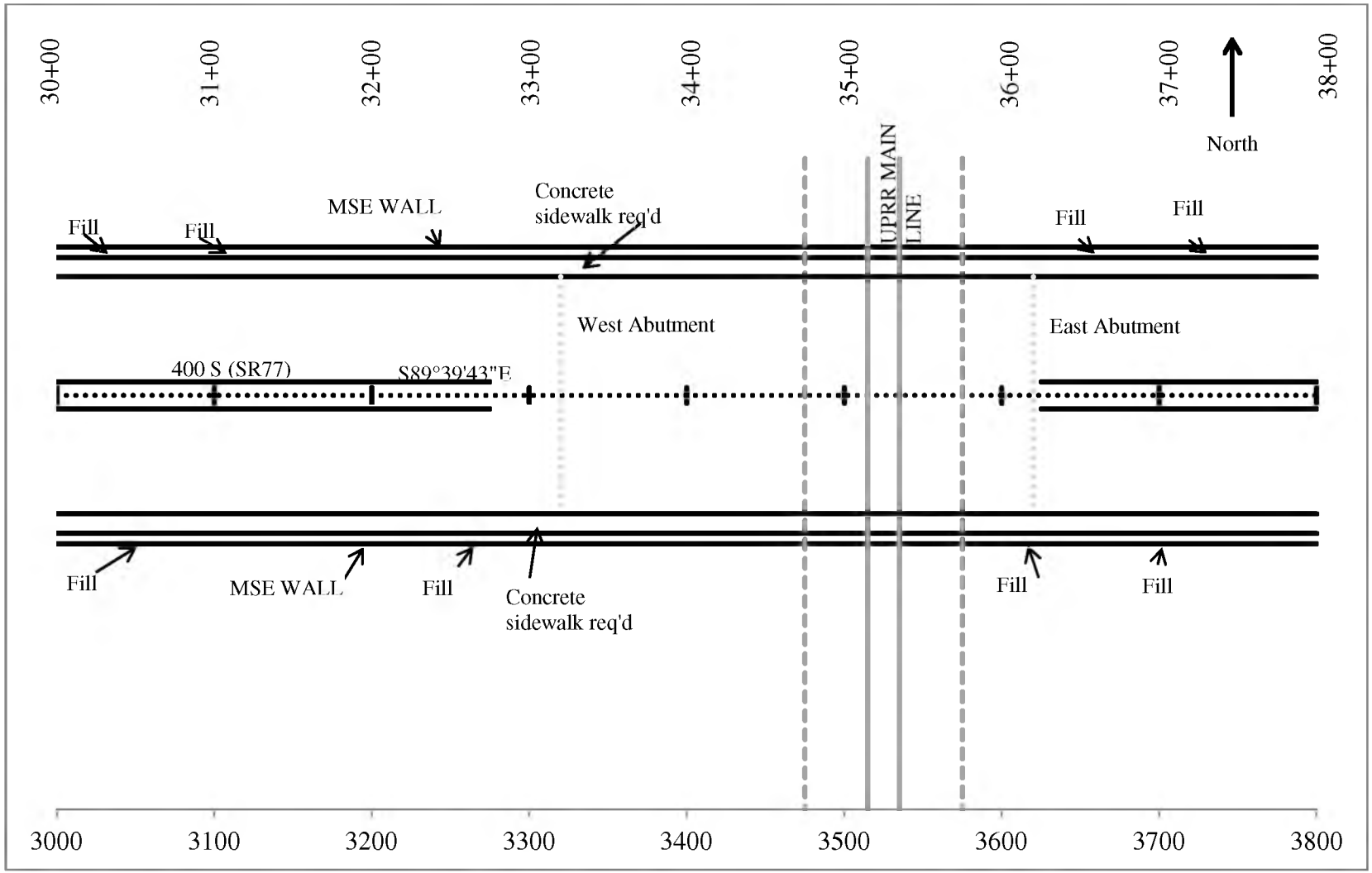

Figure 1-2 Construction drawing showing plan view of the SR-77 Bridge containing stationing and centerline.

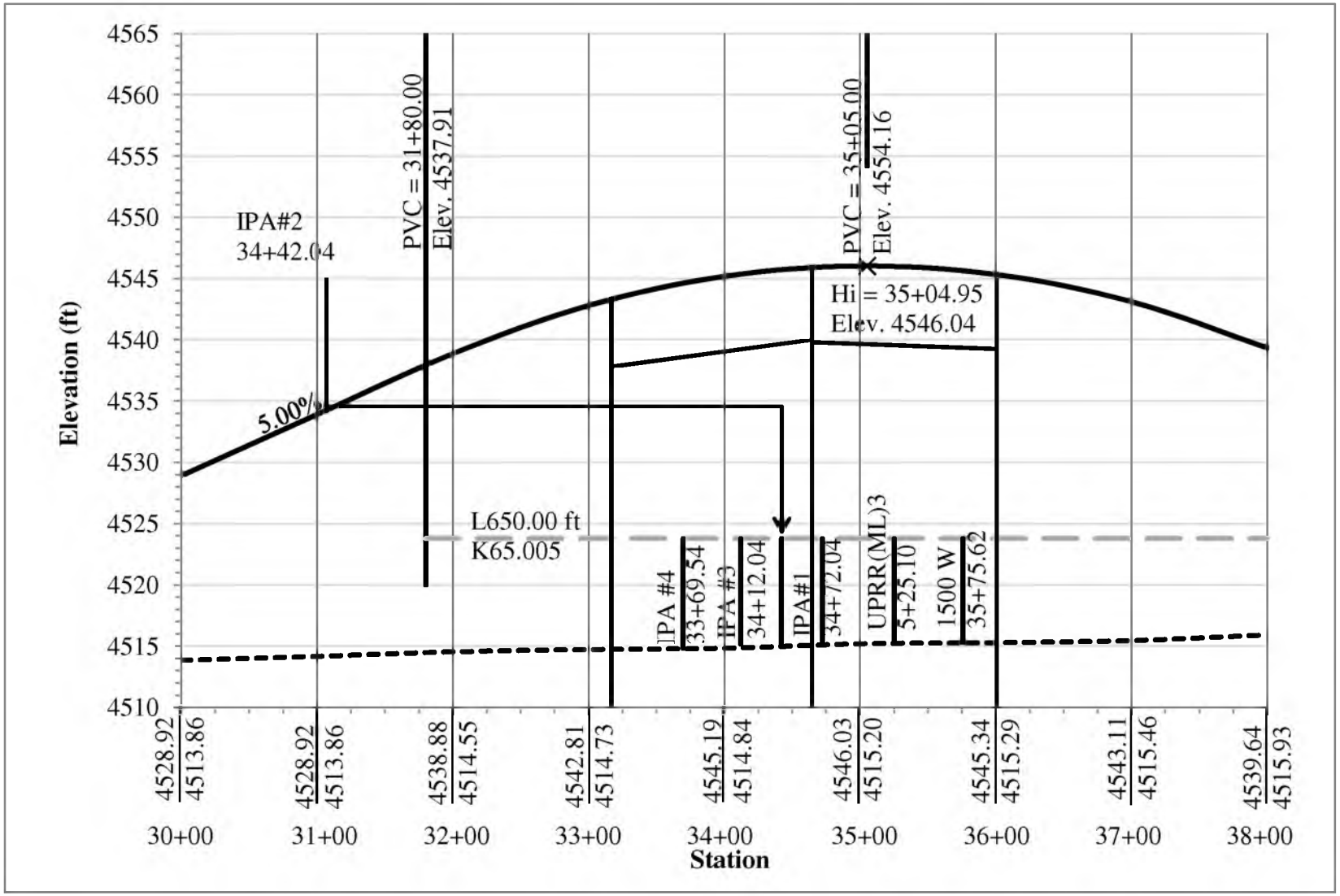

Figure 1-3 Construction drawing showing profile view of SR-77 including height of embankment with stationing going east to west.

Figure 1-4. Initial stages of construction in December 2008 looking east. Piles for the west abutment can be seen in the left foreground. The railroad crossing can be seen in the middle.

The embankment for the ramps was 106-ft wide, about 30-ft tall at the highest point, with vertical slopes on the north and south sides supported laterally by mechanically stabilized earth (MSE) walls as shown in Figure 1-4 through Figure 1-12

The Utah Department of Transportation (UDOT) selected this site for installation of a significant array of instrumentation to be monitored and the results evaluated in support of an ongoing research study titled *Improved Stability and Consolidation Assessment of Embankments* being performed by the University of Utah. The overall objectives of this study are summarized as follows:

1. Review and recommend an appropriate fully-coupled soil model to UDOT for implementation in performing fully-coupled effective stress analyses.

Figure 1-5. Steel pipe piles installed beneath MSE wall west of the bridge on the south side of SR77.

Figure 1-6. Initial fill height just after instrumentation was installed on April 20, 2009.

Figure 1-7. Compaction of fill.

Figure 1-8. Closeup of borrow material. Camera lense cap shown for scale.

Figure 1-9. Welded wire mesh used for facing of MSE wall.

Figure 1-10. Reinforcing strips.

Figure 1-11. Outside view of MSE wall west of the bridge on the south side of SR 77 during construction. Location of the research instrumentation can be seen in the middle.

Figure 1-12. Completed MSE wall on the south side of the embankment west of the bridge.

2. Develop a laboratory triaxial testing program and procedures to obtain the required soil parameters for a preselected site of interest to UDOT.
3. Develop in situ correlations with selected soil parameters so that these tests can be potentially used in the future to obtain key model parameters.
4. Validate the approach, where possible, using field/project observations from a candidate site and other embankments with high quality monitoring data.
5. Develop methods/recommendations for safe rates of embankment placement.

6. Recommend the type and amount of instrumentation that should be used to monitor future embankment construction and further validate coupled-effective stress evaluations.

The research described in this thesis constitutes a portion of the tasks required for completion of the full study. The specific objectives of the research described herein were as follows:

1. Characterize the index and engineering properties of the subsurface materials at the site.
2. Determine the magnitude and time rate of changes in the following parameters within the preexisting ground resulting from construction of the embankment and removal of the surcharge: Vertical and horizontal deformations; and total , horizontal, and pore water pressures.
3. Compare measured rates and magnitudes of primary consolidation settlement with values predicted using traditional methods of analysis.
4. Identify improved methods of analysis to predict the rate and magnitude of primary consolidation settlement.
5. Determine if a ShapeAccelArray (SAA) is a technically viable method to measure horizontal deformation versus depth within the ground.

The tasks conducted to attain these objectives were as follows:

1. Conducted detailed field and laboratory geotechnical investigations to determine pertinent index and engineering properties of the soils at the location of the instrument array.

2. Determined the location where the array of instruments were to be installed and supervised the installation of those instruments at that location.
3. Monitored all instruments and recorded the results at regular intervals during construction of the embankment and afterward.
4. Reduced and analyzed all data obtained from the instruments within the array.
5. Performed analyses to estimate dissipation of pore water pressure, time rate of settlement, and ultimate settlement using a variety of methods. Results from these analyses were compared with measured values to determine the effectiveness of the various methods in predicting dissipation of pore pressure and magnitude and rate of primary consolidation settlement.
6. Compared measurements of horizontal displacement versus depth within the original ground from a vertical inclinometer and an adjacent SAA.

The results and findings of the research conducted to achieve the objectives listed above are described in detail in this thesis. The types and number of instruments installed within the research array are discussed in Chapter 2. Research instrumentation arrays including installation, data collection, frequency of readings, and data reduction are described in Chapter 3. The geotechnical investigation consisted of a field investigation and laboratory testing and is described in Chapter 4. Chapter 5 includes the results from the instrumentation. A settlement analysis which includes the magnitude of estimated settlement and the actual magnitude of settlement, predicted and measured dissipation of excess pore pressures, and a prediction of surcharge removal using Asaoka method and the individual layer method is discussed in Chapter 6. A summary of the research and

major conclusions obtained are described in Chapter 7. Specific details regarding important calculations and methods of analysis are provided in the appendices.

2 BACKGROUND AND LITERATURE REVIEW

Settlement of an embankment constructed on ground containing soft cohesive soil is an important aspect of the construction process that requires effective communication between the contractor and the geotechnical engineer if the project is to be completed in a timely manner. Three main issues must be addressed for these conditions: (1) The large amount of total settlement that typically will occur, (2) the slow rate at which settlement from primary consolidation will occur unless measures are undertaken to accelerate this process, and (3) the rate and magnitude of settlement from secondary compression that will occur. The first two issues are addressed in the research described in this thesis.

Primary consolidation settlement within thick layers of soft cohesive soil will generally occur over a period of years or sometimes even decades unless measures are undertaken to accelerate this process. Preloading, which is also known as surcharging, is one method that can be used to accelerate primary consolidation and involves placing temporary additional fill on top of the permanent embankment. In addition, preloading has the advantage of reducing long-term settlement from secondary compression if the surcharge is left in place long enough to achieve a significant change in the properties of the soft soils. Preloading was the method used to accelerate primary consolidation for the embankment studied in this research project.

The background information related to the research performed for this thesis is described in this chapter. The various types of instrumentation used to monitor settlement, lateral deformations, and changes in pressure within the ground underlying the embankment are discussed in Section 2.1. General geotechnical field and laboratory conducted during the construction of this embankment are described in Section 2.2 and Section 2.3. Methods used to predict settlement are described in Section 2.4. Techniques used to estimate the time when surcharge should be removed are described in Section 2.5. Methods used to determine or predict relevant properties of cohesive soils are discussed in Section 2.6. A discussion of previous embankment studies and findings related to this research is given in Section 2.7

2.1 Field Instrumentation

Embankment construction on soft cohesive soil requires field instrumentation to monitor soil behavior. Soil behaviors often monitored are, (1) magnitude of total settlement including components caused by distortion, primary consolidation, and secondary consolidation, and (2) time required for completion of primary consolidation. Data obtained from field instrumentation is analyzed for the purpose of understanding soil behavior. Enhancing the understanding of soft cohesive soil behavior can lead to better predictions of magnitude and rate of primary and secondary consolidation settlements.

Data obtained through field instrumentation is often used to determine changes in geotechnical parameters caused by embankment and surcharge construction such as (1) pore pressures, (2) in situ vertical and horizontal stress, and (3) vertical and horizontal

deformations. These parameters are analyzed to determine the stability of a soft soil foundation. The various types of field instrumentation used to monitor soil behavior and geotechnical parameters during this research project will be discussed in Section 2.1

2.1.1 Settlement Manometer

Settlement manometers are used to monitor vertical settlement of the original ground caused by the load of the embankment during and after construction. Settlement manometers are comprised of the following components: (a) settlement platform, (b) readout tower, and (c) polyethylene tubing filled with a solution containing a 50/50 mixture of antifreeze and water. Settlement platforms are composed of two wooden pieces extending laterally, in the shape of an H, with another piece of wood extending vertically at the center of the platform. Readout towers are made of PVC pipe with rulers connected to the inside of the readout towers. Polyethylene tubing connects the settlement platform with the readout tower. Upon connecting the readout box with the readout tower, the solution of antifreeze and water is pumped through the tubing and allowed to come to equilibrium for initial vertical settlement measurements. A settlement manometer readout tower used in this project can be seen in Figure 2-1.

Figure 2-1. Manometer used to measure settlement of the original ground surface beneath the embankment in this project.

2.1.2 Settlement Cell

Settlement cells are used to measure settlement of the original ground during and after construction of the embankment. A settlement cell system is made of the following parts (see Figure 2-2): (a) vibrating wire readout box, (b) settlement cell, (c) liquid filled reservoir, and (d) liquid filled tubing. The governing principle of this device is the same as for a manometer, except that the level of fluid within the tubing is determined electronically using a pressure transducer. The settlement cell is set at the desired depth in the original ground and connected to the electronic readout box. The readout box consists of nodes used to record electronic data obtained from the settlement cells by way of hand-held vibrating wire readout data collector.

2.1.3 Magnet Extensometer

Magnet extensometers are used to measure the changes in heights of subsurface layers of soil during and after construction. Magnet extensometers consist of PVC pipe

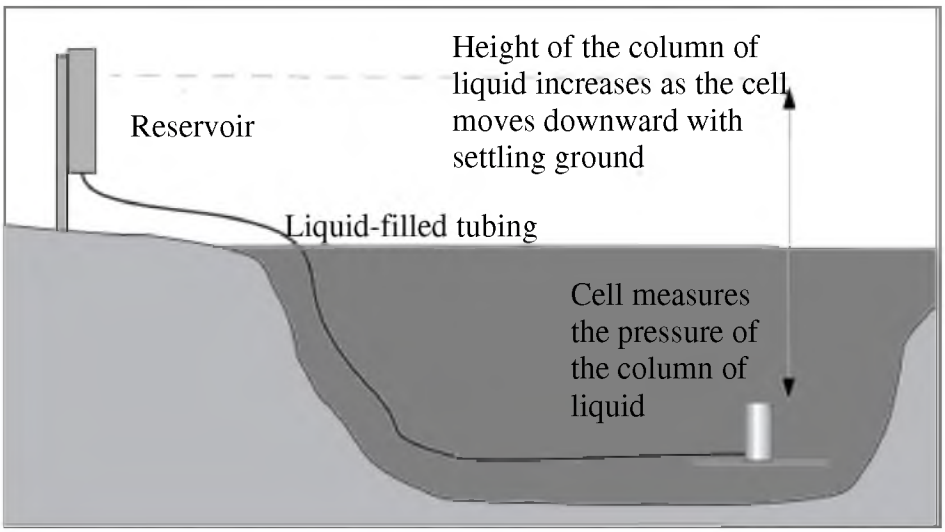

Figure 2-2. Schematic diagram illustrating how a settlement cell is used to measure settlement (Illustrations Courtesy of Geokon Inc.www.geokon.com.)

and spider magnets. Readings are taken using a probe. Spider magnets are cylindrical shaped objects with a diameter of about 1 in and a height of approximately 6 in with six legs extending from the center. Three legs extend vertically upward and three legs extend vertically downward as shown in Figure 2-3. Initially the legs are bound by a small brass chain and a steel pin. A borehole is drilled to the desired depth and the PVC pipe is placed inside the borehole with the spider magnets attached (see Figure 2-4). Once all spider magnets are in the borehole, they are released by a steel wire pulling the pin from the small brass chain binding them into the adjacent soil. The borehole is then grouted to seal the spider magnets in place relative to the soil at the same elevation.

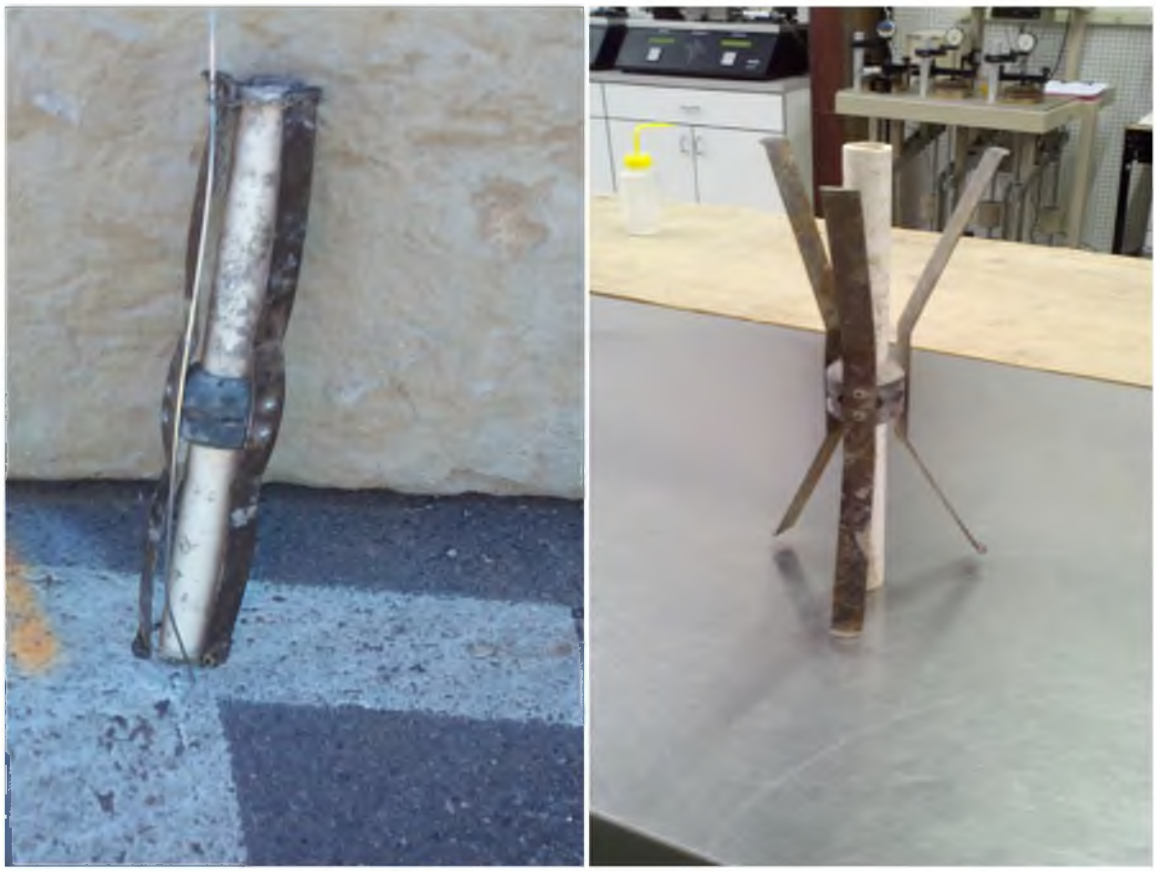

Figure 2-3. A spider magnet is shown in two positions: The legs of the spider magnet are closed (left), and the legs of the spider magnet are extended (right).

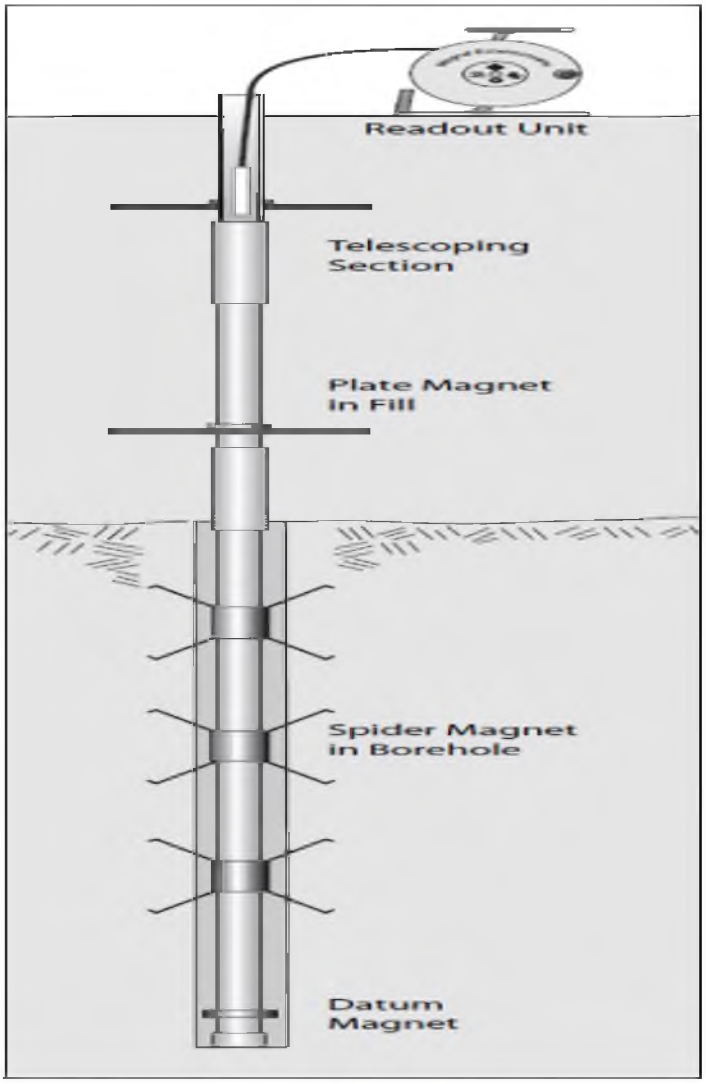

Figure 2-4. Schematic diagram illustrating installation of magnet extensometer and measurement of depths at which magnets are located (Illustrations Courtesy of Geokon Inc.www.geokon.com.).

Readings are taken by lowering a probe attached to a measuring tape down the hole in the PVC pipe. The probe beeps twice when it reaches the depth of each magnet, and the depth of the magnet below the top of the PVC pipe is determined by reading the measuring tape. The settlement of each magnet (and hence the ground at that depth) is determined in one of two ways: (1) If the datum magnet (or bottom spider magnet) is founded in ground that is not settling, the settlement of each magnet above it is

determined by changes in elevation of the magnets relative to the datum magnet; or (2) if the ground below the datum magnet is settling, the elevation of the top of the PVC pipe is determined by surveying from a bench mark located in ground that is not settling, and the elevation of each magnet is determined from its depth below the top of the PVC pipe.

2.1.4 Horizontal Inclinometer

Horizontal inclinometers, as shown in Figure 2-5, are used to measure vertical deformation (settlement or heave) across the width of the embankment. Horizontal inclinometers are comprised of the following components: (a) casing comprised of tiny grooves at the 12 and 6 o'clock positions, (b) an inclinometer probe, (c) a readout box, (d) electrical cable with markings at 2-ft intervals, and (d) a pulley system. The probe is comprised of wheels in the vertical position with the purpose of fitting into the casing. The tilt of the wheels is measured through the readout box connected to the probe. After properly securing the probe to the readout box, the probe is connected to the pulley system and pulled into the casing. Data are recorded at each 2-ft increment. Upon completion of one pass, the probe is rotated 180 degrees and sent into the casing for a second pass. Horizontal profiles comprising of settlement or heave can be determined from the data collected using the horizontal inclinometer.

2.1.5 Vertical Inclinometer

A vertical inclinometer is very similar to the horizontal inclinometer, except the vertical inclinometer is used to measure lateral deformation of the ground. The vertical

Figure 2-5. Horizontal inclinometer casing with pulley system perpendicular to the centerline alignment in this project.

inclinometer is comprised of the same components as found in the horizontal inclinometer system, except a pulley system is not used with a vertical inclinometer. The vertical inclinometer probe is connected to the readout box via electrical cable.

The vertical inclinometer is placed inside the casing and lowered to the bottom of the borehole. Readings measuring tilt of the wheels are taken from the bottom of the borehole upward using the same principles to measure deformation as used with the horizontal inclinometer. Lateral deformation profiles of a borehole can be determined from the data collected using the vertical inclinometer.

2.1.6 ShapeAccelArray

ShapeAccelArray (SAA) is a new instrument developed by Measurand Inc. to monitor or measure lateral deformation, by reporting the shape of a borehole in a manner that is similar to that of a vertical inclinometer. SAA are rigid segments connected by joints that bend in any direction as shown in Figure 2-6. Each rigid segment is comprised of three micro-electro-mechanical systems (MEMS) gravity/vibration sensors whose purpose is to measure the tilt occurring within the ground beneath or adjacent to an embankment that is under construction. The SAA slides directly into PVC casing, and can be grouted into a borehole or supported by sand if the borehole is large enough. The shape of the PVC casing is monitored by gathering continuously logged raw data from a Campbell Scientific CR1000 logger. The data logged by the Campbell Scientific CR1000, are calibrated to into x, y, and z data components using Measurand's SAA3D software. Once the data are calibrated in Measurand's SAA3D software, results for lateral deformation can be viewed using Measurand's 3D viewer software.

2.1.7 Piezometers

Piezometers are used in measuring the development and dissipation of excess pore pressures during and after embankment construction. Electronic piezometers,as shown in Figure 2-7, can be embedded in selected layers underneath and adjacent to the embankment.

A vibrating wire piezometer is comprised of the following components: (a) Pressure transducer, (b) diaphragm, and (c) vibrating wire. The fluid pressure acting on the end of the diaphragm causes the frequency in the vibrating wire to change. The

Figure 2-6. Rigid segments connected at joints allowing the SAA to move freely and monitor lateral deformation (courtesy of Measurand Inc. www.measurand.com).

Figure 2-7. Vibrating wire piezometer used to measure excess pore pressures developed during construction (Courtesy Durham Geo Slope Indicator.).

change in frequency is sensed by the vibrating wire. Piezometers installed at desired depths are connected to a readout box the in the same manner as the settlement cells. Electronic data can be obtained by way of hand-held vibrating wire readout data collector or using an automated electronic data collection system.

2.1.8 Pressure Plate

Pressure plates are used in field instrumentation with the purpose of measuring total pressure acting at the base of an embankment. Pressure plates are located at the surface or near the original ground surface so induced total vertical stress acting on the foundation can be measured. Pressure plates are thin and circular in shape and installed horizontally as shown in Figure 2-8. Two thin, flat plates are welded together along the outside edge and separated by a small gap filled with hydraulic fluid. Earth pressures acting on the plates will cause the two plates to squeeze together, thereby building up fluid pressure between the welded plates. A change in fluid pressure causes a change in frequency of the vibrating wires through a pressure transducer. Pressure plates can also be installed in a manner so that horizontal pressures can be measured by rotating the pressure plate 90 degrees so that it is oriented in the vertical position.

Figure 2-8. Pressure plate commonly used to monitor the total pressure acting on a foundation (Illustrations Courtesy of Geokon Inc.www.geokon.com).

Electronic data obtained from the pressure plates are obtained by way of hand-held vibrating wire readout data collector or using an automated electronic data collection system in the same manner as the settlement cells and piezometers.

2.1.9 Push-In Cell

Push-in cells are used to measure the total horizontal pressure within the foundation soil beneath and adjacent to the embankment. Push-in cells are thin, rectangular in shape with a pointed blade on the end, and accompanied with a piezometer to determine pore pressures, as shown in Figure 2-9. Measuring pore pressures allows for effective stresses within the foundation to be determined from data obtained through use of the push-in cell. Much like the pressure plates, the push-in cell is comprised of thin plates welded together around the exterior edge. The gap between the plates is filled with hydraulic fluid. Stresses acting on the outside of the push-in cells cause a change in fluid pressure, which is sensed by the vibrating wires. Push-in cells can be placed at depths well below the surface. Electronic data are obtained from the push-in cell in the same manner as for the settlement cells, piezometers, and pressure plates.

Figure 2-9. Push-in cell commonly used for monitoring horizontal pressure and pore pressure within the foundation soil beneath an embankment (Illustrations Courtesy of Geokon Inc.www.geokon.com)

2.1.10 Surveying Benchmarks

Benchmarks were determined before and after construction of the embankment. The purpose of the benchmarks was to provide stable elevations that would not be disturbed during or after construction. Benchmarks used during construction consisted of a piece of #3 rebar inside a steel casing. The steel casing was hammered into the ground, with the #3 bar inside and a metal cap screwed on top of the steel casing.

2.1.11 Settlement Point

Settlement points were determined to provide a manner in which post construction settlement could be monitored. Settlement points used to monitor post construction settlement consisted of Parker Kalon (PK) nails, shown in Figure 2-10, were installed within the concrete curb along the western approach to the bridge The following procedure was used to install each of the settlement points: A ¼-in diameter

Figure 2-10. Parker Kalon (PK) nails used for measuring postconstruction settlement at the bridge approach.

was drilled horizontally into the curb, epoxy was placed into the hole, and PK nails were hammered into the hole. Initial elevations were determined once the epoxy stabilizing the PK nails had cured.

2.2 Field Tests

Standard field tests performed during the geotechnical investigation of SR 77 will be discussed in this section. The objectives of the field tests were to define subsurface conditions and to obtain undisturbed soil samples for subsequent laboratory testing. The results from the field tests will be discussed in Section 4 of this thesis. The standard penetration test (SPT) is described in Section 2.2.1. Piston sampling is discussed in Section 2.2.2. The Cone Penetration Test is described in Section 2.2.3. The Vane Shear Test is discussed in Section 2.2.4.

2.2.1 Standard Penetration Test

The standard penetration test (SPT) is a common in situ test performed during a geotechnical field investigation. The details of the test are well-known within the geotechnical community, so only a brief summary will be provided here. The goal of the SPT is to drive a split-spoon sampler 18 in into the ground using a hammer weighing 140 lb dropped from a height of 30 in. Blow counts are counted and recorded for three 6-in intervals as the hammer strikes the sampler. The number of blowcounts required to drive the sampler through the last two 6-in increments is the SPT blowcount in units of blows/ft. Because significant variations in equipment and procedures are permitted in the SPT, values of blowcounts obtained in the field must be corrected for hammer energy, rod length, sampler type, and diameter of the borehole if the results are to be meaningful. Corrected blowcounts have been correlated empirically with various parameters such as compressibility and strength of granular soils. Procedures for performing the SPT in cohesive soils can be found in ASTM D1586-08a. Procedures for performing the SPT in sandy soils can be found in ASTM D6066-96 (2004).

2.2.2 Piston Sampling

Piston sampling is a common technique used to collect high quality (relatively undisturbed) samples of cohesive soil. Piston sampling requires a thin-walled Shelby tube be pushed into the ground while the piston is sealed at the lower end of the Shelby tube, free of soil intrusion. Once the desired depth for sampling is reached, a down pressure, via air or water, is applied to the Shelby tube to advance it further into the soil while the piston remains stationary. Upon completion of the Shelby tube advancement,

the tube is slowly rotated to shear the sample. The piston and Shelby tube are raised simultaneously to the surface using the friction and suction developed between the Shelby tube, piston, and sample to hold the sample intact. Detailed procedures for gathering undisturbed piston samples can be found in ASTM D6519-08.

2.2.3 Cone Penetration Test

The cone penetration test (CPT) can be used to obtain significant information during the geotechnical field investigation. During the CPT the resistance of the soil to penetration is measured much like the SPT, except a cone penetrometer (rather than a split-spoon sampler) is hydraulically pushed (rather than driven) into the soil. The CPT provides details concerning subsurface statigraphy of the geologic profile, soil behavior type, and geotechnical parameters based on empirical correlations. Properties measured from the cone penetration test are uncorrected tip resistance, sleeve friction, friction ratio, and pore pressure either behind or within the tip. Values of each of these parameters are determined for small increments of depth during the CPT. Procedures for performing a CPT can be found in ASTM D3441-05.

2.2.4 Vane Shear Test

The field vane shear test (VST) is an in situ test used to determine the peak undrained shear strength and the remolded undrained shear strength of subsurface cohesive soils. The vane shear test measures the torque caused by a four bladed vane after it is pushed into the ground and then rotated at a standard rate. The maximum

torque is theoretically related to the peak undrained shear strength by a constant, as shown in the following equation:

$$S_{u,vst} = T_{max} / K \tag{2-1}$$

where:

$S_{u,vst}$ = theoretical undrained shear strength determined from the VST

T_{max} = maximum torque developed during rotation of the vane

K = theoretical constant.

The theoretical constant depends on the size and shape of the vane being used in the test. For the vane used in this project, the equation for the theoretical constant, K, is given below in Eq. 2-2 in units of inches and pounds.

$$K = \frac{\pi}{1728} * \left(\frac{D^2 H}{2} \right) * \left[1 + \frac{D}{3H} \right] \tag{2-2}$$

where:

D and H are the diameter and height of the vane, respectively

Eq. 2-2 is based on the following two major simplifying assumptions that unfortunately do not match the real conditions very well under most conditions: (1) The strength is mobilized simultaneously at all points along the shearing surface, and (2) the strength of the soil is isotropic with respect to the direction of shear. Because of these discrepancies, a correction factor must be applied to the obtained value of $s_{u,vst}$ if the

results are to be meaningful. Three correlations are here: Lambda (λ) developed by Bjerrum (1972) shown in Figure 2-11, which was improved by Asa et al. (1986) as shown Figure 2-12, and mu (μ) found in ASTM 2573-08, which is shown in Figure 2-13.

Bjerrum (1972) introduced a correction factor for undrained shear strength based on back calculations from embankment failures. Bjerrum's correction factor is based only upon the plasticity index of the soil. Asa et al. (1986) made improvements to the correction factor by including the effects of aging and overconsolidation ratio (OCR). A third correlation found in ASTM 2573-08, is based upon the plasticity index of the soil and time of failure of the soil. Reduction of undrained shear strengths using the

$$S_{u,design} = \lambda S_{u,vst} \tag{2-3}$$

$$S_{u,design} = \mu_R S_{u,vst} \tag{2-4}$$

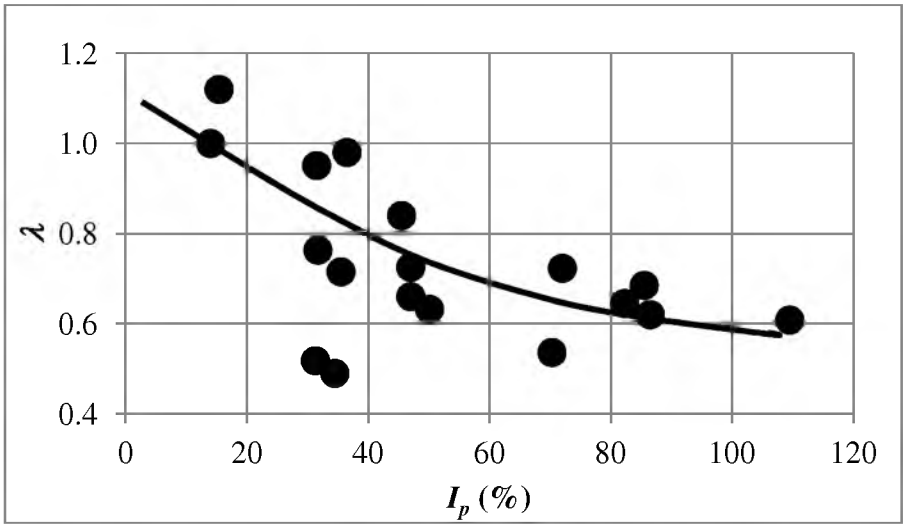

Figure 2-11. Bjerrum's (1972) correction factor for undrained shear strength (Reproduced with permission from MgGraw-Hill, from Bowles, Foundation Analysis and Design, Mc-Graw-Hill, 1996).

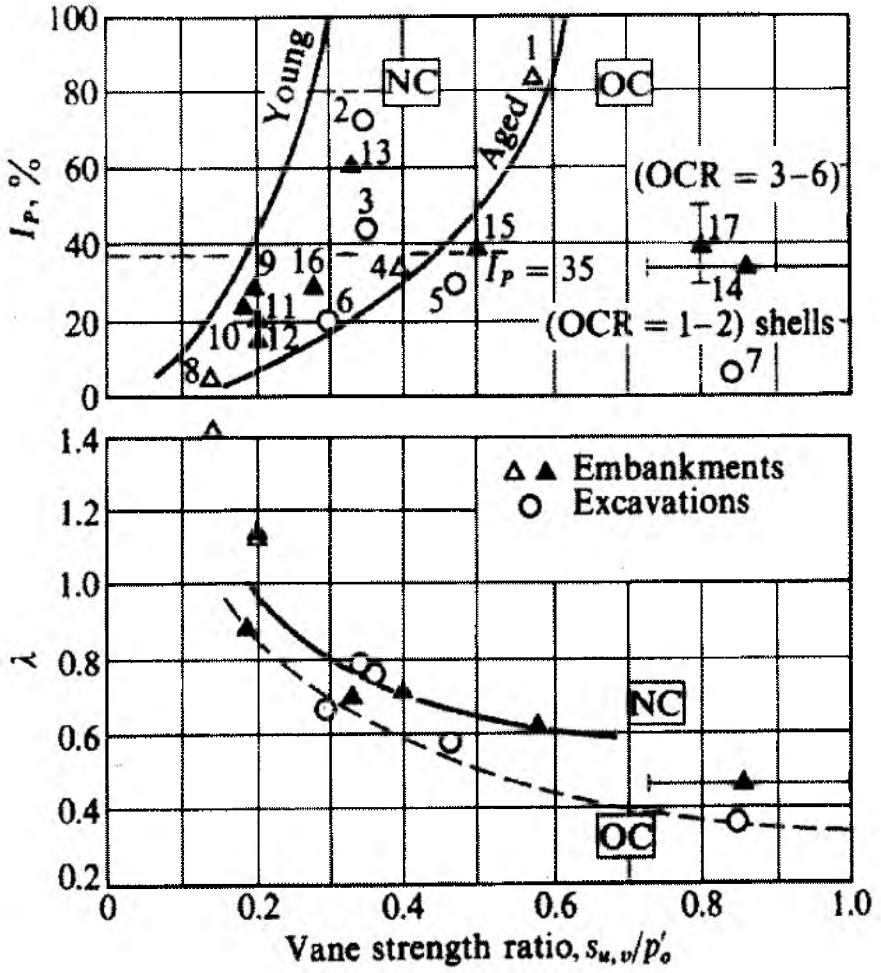

Figure 2-12. Chart developed by Aas et al. (1986) reinterpreting Bjerrum's correction factors to correlate the effects of aging and OCR with undrained shear strength (Reproduced with permission from MgGraw-Hill, from Bowles, Foundation Analysis and Design, Mc-Graw-Hill, 1996).

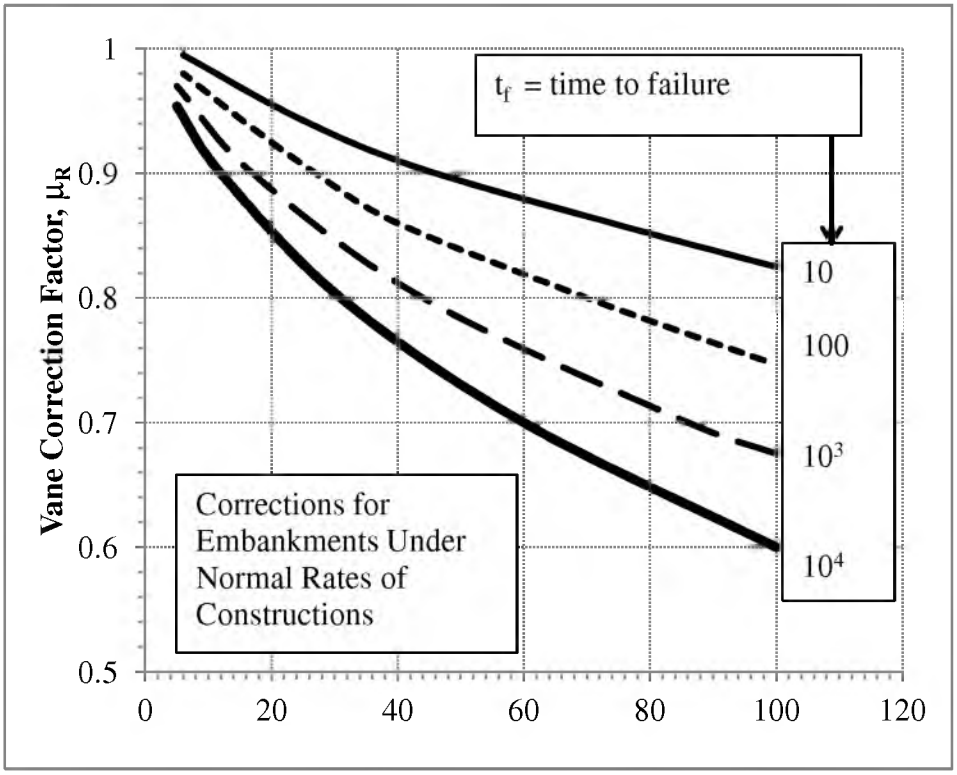

Figure 2-13. Correction factor for undrained shear strength from ASTM D2537-08 (Reprinted, with permission, from ASTM D2573-08 Standard Test Method for Field Vane Shear Test in Cohesive Soil, copyright ASTM International. 100 Bar Harbor Drive, West Conshohocken, PA 19428).

correlation factors are found Eq. 2-3 and Eq. 2-4 Detailed procedures for performing the VST can be found in ASTM D2573.

2.3 Laboratory Tests

Laboratory tests performed during the geotechnical investigation of SR 77 will be discussed in this section. Sieve analysis will be discussed in Section 2.3.1. Hydrometer analysis and Atterberg limits will be discussed in Sections 2.3.2 and Section 2.3.3, respectively. Finally, details regarding the constant rate of strain consolidation test will be discussed in Section 2.3.4.

2.3.1 Sieve Analysis

A sieve analysis, commonly known as a particle size analysis, determines the gradation of the soil retained on the No. 200 sieve and provides information that can be used to classify soil using both the United Soil Classification System (USCS) and American Association of State Highway and Transportation Officials (AASHTO) methods. Procedures for performing a sieve analysis can be found in ASTM D422-63 (2007).

2.3.2 Hydrometer Analysis

A hydrometer analysis is performed to determine the gradation of particles that pass a No. 200 sieve. A hydrometer analysis consists of placing soil in a glass jar filled with solution containing water and a dispersing agent (hexametaphosphate). The hexametaphosphate is used to disperse small clods of cohesive soil into their individual particles. Over time the soil particles begin to settle out. The rate at which the particles settle is measured using a hydrometer and Stokes Law is used to determine the gradation of the particles. Stoke's Law states that soil particles remaining in suspension are smaller than the soil particles that have already settled due to gravitational, buoyancy, and drag forces. A hydrometer analysis correlates the soil particle size concentration in the tube as a function of depth and time. Procedures for performing a hydrometer analysis can be found in ASTM D422-63 (2007).

2.3.3 Atterberg Limits

Atterberg limits are performed on fine grained soils and provide details about the plasticity of a soil through determining the liquid and plastic limits. The liquid limit is the water content at the boundary of the plastic and liquid consistency states, and the plastic limit is the water content at the boundary of the semisolid and plastic states. The difference between the liquid limit and plastic limit is known as the plasticity index. Procedures for performing Atterberg limits are found in ASTM D4318-10.

2.3.4 Constant Rate of Strain Consolidation

The constant rate of strain test (CRS) test is performed by confining a soil sample laterally while straining the sample in the axial direction at a constant rate, causing one-dimensional consolidation to occur. The objective of the CRS test is to determine the geotechnical parameters associated with the magnitude and rate of consolidation for saturated cohesive soils. During the test, axial strain, total axial stress, and pore water pressure, are constantly monitored.

The CRS test consists of a saturation phase and a consolidation phase. During the saturation phase, the specimen is subjected to a large value of back pressure (e.g., 30 psi) that forces air bubbles into the solution, thereby ensuring saturation of the specimen. In the consolidation phase, the specimen is strained at a constant rate with drainage allowed only at the top, which produces partially undrained conditions within the specimen and corresponding excess pore pressures. Full procedures of the CRS test can be found in ASTM D4186-06.

2.4 Theories to Predict Rate of Primary Consolidation

The strains accompanying consolidation settlement of a cohesive soil can occur in one-, two-, or three-dimensions, depending on the loading, geologic, and boundary conditions present at the site. The simplest case is one-dimensional consolidation in which the strains occur only in the direction of applied load. Although true one-dimensional consolidation is rare in the field, it can be closely approximated when the following conditions are present: (1) The compressible soil layer under consideration is relatively homogeneous, oriented horizontally, and of relatively uniform thickness; (2) the load is fairly uniform; and (3) the widths of the loaded area in all directions are much greater than the thickness of the compressible layer. Two-dimensional consolidation occurs when the width of the loaded area in only one direction is very large in comparison to the thickness of the compressible layer; and three-dimensional consolidation occurs when the widths of the loaded area are relatively small compared to the thickness of the compressible layer.

Certain parameters must be considered in two- and three-dimensional consolidation that are not important in one-dimensional consolidation settlement. These parameters may include isotropic versus anisotropic properties of the soil, drainage of water in the horizontal directions, and geometry of the load being placed.

Only one-dimensional consolidation will be considered in this thesis, and therefore the discussions in the following sections are limited to this topic. The first consolidation theory was developed by Terzaghi (1925) for one-dimensional conditions (see Section 2.4.1). Biot (1941) developed the first theory for three-dimensional consolidation using essentially the same assumptions as Terzaghi. Interested readers are referred to Biot's

paper for additional details. Several two-dimensional theories have been developed over the years. Selected references for this topic include Skempton and Bjerrum (1957) and Davis and Poulos (1972).

2.4.1 One-Dimensional Theories

Primary consolidation settlement of a saturated cohesive soil is a process in which excess pore pressures cause water to flow from the pore spaces of the soil to another soil or location where the total head in the water is lower. These excess pore water pressures are common by the application of the process of expulsion of water; the concomitant dissipation of excess pore pressure is time-dependent and can take anywhere from a few hours to decades or longer to occur. The primary factors determining the time of consolidation are permeability of the cohesive soil and the longest length over which water must travel to reach equilibrium.

One-dimensional consolidation settlement analysis is the most common analysis used in geotechnical engineering practice today. Terzaghi's (1925) method is the most commonly used theory used in geotechnical engineering practice to analyze the time rate at which one-dimensional consolidation settlement occurs. Unfortunately, Terzaghi made numerous simplifying assumptions to obtain his theory that are not realistically met in many practical engineering situations, even if the strain conditions are very close to one-dimensional. Therefore, many improvements have been made by various researchers over the years to overcome some of these limitations. Selected references for these improved methods include Mikasa (1963), Davis and Raymond (1965), Gibson et al. (1967), Janbu (1967), Poskitt (1969), Rokhsar (1973), Gibson et al. (1981), Choi (1982),

and Cargill (1984). Unfortunately, only the equation for Terzaghi's theory has a known closed-form solution, so numerical methods must be used to solve all the other equations. This fact has limited the use of these other equations in standard geotechnical practice. However, with modern computing tools, the solution of some of these other equations is relatively simple and these advanced methods should be used more often in geotechnical engineering practice than is the current norm. Only Terzaghi's theory and Davis and Raymond's theory are used in this research, so the discussions in the following sections are limited to those two methods.

2.4.1.1 Terzaghi is the most famous geotechnical engineer for his early work and contributions in geotechnical engineering. One of Terzaghi's most important contributions and theories still used today is his one-dimensional consolidation theory, given in Eq. 2-5 below, in which the change in excess pore pressure (u) can be determined as functions of time (t) and depth (z) within the layer undergoing settlement.

$$C_v \frac{\partial^2 u}{\partial z^2} = \frac{\partial u}{\partial t} \tag{2-5}$$

The coefficient of consolidation, c_v, is defined in Eq. 2-6.

$$C_v = \frac{k}{\gamma_w} * \frac{1 + e_0}{a_v} \tag{2-6}$$

where:

k =the coefficient of permeability

γ_w = the unit weight of water

e_0 = the initial void ratio

$a_v = -\frac{de}{d\sigma'_v}$, or the slope of the compression curve

Terzaghi made numerous simplifying assumptions in the derivation of Eq. 2-5. The most important of these assumptions are summarized as follows:

1. Water is the pore fluid.
2. The soil is homogenous, 100% saturated, and fine-grained.
3. Strain occurs only in one direction.
4. The flow of water is one-dimensional and obeys Darcy's Law.
5. No elastic distortion occurs.
6. The coefficient of consolidation (C_v) is constant.
7. No secondary compression occurs doing primary consolidation.
8. The change in void ratio is proportional to the change in effective stress.
9. The strains are small.

Assumptions 6 through 9 are known to be invalid in many situations. It is well known that C_v varies with effective stress level and that values are typically significantly higher for recompression than they are for virgin compression. Secondary compression is a fundamental property of a soil and certainly occurs during primary consolidation. For most cohesive soils the change in void ratio is generally approximately proportional to the change in the logarithm of the effective stress, which is why consolidation results are typically plotted as void ratio (or strain) versus the logarithm of effective stress. The strains in many cohesive layers are quite large and violate Terzaghi's assumption that

they are small. Most of the other theories for one-dimensional consolidation discussed above eliminate one or more of these assumptions.

2.4.1.2 Davis and Raymond (1965) developed a nonlinear theory of one-dimensional consolidation settlement that differed from Terzaghi's method in only one way - they assumed that the change in void ratio is proportional to the change in the logarithm of the effective stress. This assumption is consistent with the known behavior of most cohesive soils where the results from one-dimensional consolidation tests are typically plotted as void ratio (or vertical strain) versus logarithm of effective vertical stress so that the resulting plot is approximately linear over the regions of recompression and virgin compression (after the plot is corrected to field conditions.) The effect of this change in one assumption resulted in a much more complex equation in which the dissipation of the excess pore pressure depends on two additional parameters - the effective stress acting on the soil and the saturated unit weight of the soil, as shown in Eq. 2-7 below.

$$-C_v\left[\frac{\partial^2 u}{\partial z^2}-\left(\frac{1}{\sigma'}\right)^2 * \frac{\partial u}{\partial z} * \left(\gamma_{sat}-\frac{\partial u}{\partial z}\right)\right]=\frac{\partial u}{\partial t} \qquad (2\text{-}7)$$

There is no known closed-form solution to Eq. 2-7. Therefore, it must be solved using numerical techniques, as discussed in Section 2.4.2 below.

2.4.2 Numerical Solutions

The use of numerical methods is becoming common practice in geotechnical engineering when it is not practical or possible to use existing analytical solutions or develop new ones. The most common numerical methods used in geotechnical engineering are the finite difference and the finite element methods. Both of these methods include the separation of continuous mathematical models into discrete functions used for purposes of analysis. The finite element method is more complex than the finite difference method and generally requires a computer program to solve large matrices. On the other hand, the finite difference method, in its basic form, is relatively easy to understand and implement. Many solutions can be done in a spreadsheet program. The finite difference method is used in this research because of its straightforward approach and simplicity of modeling. Details of the finite difference method are discussed below.

The finite difference method can be used to solve ordinary and partial differential equations by replacing the derivatives in an equation with their finite difference approximations. This process is illustrated in Figure 2.14 for the case of one-dimensional consolidation, where the excess pore water pressure (u) depends on the elapsed time (t) and the depth within the cohesive layer (z).

The solid line in the figure is a graphical representation of the actual relationship for $u = f(z,t)$. A mesh is established consisting of nodal points that represent the values of the dependent variable (u) at various discrete values of the independent variables (t and z). The subscripts i and j are used to number the nodal points and keep track of their location within the system. Δz is the distance between nodal points in the z direction.

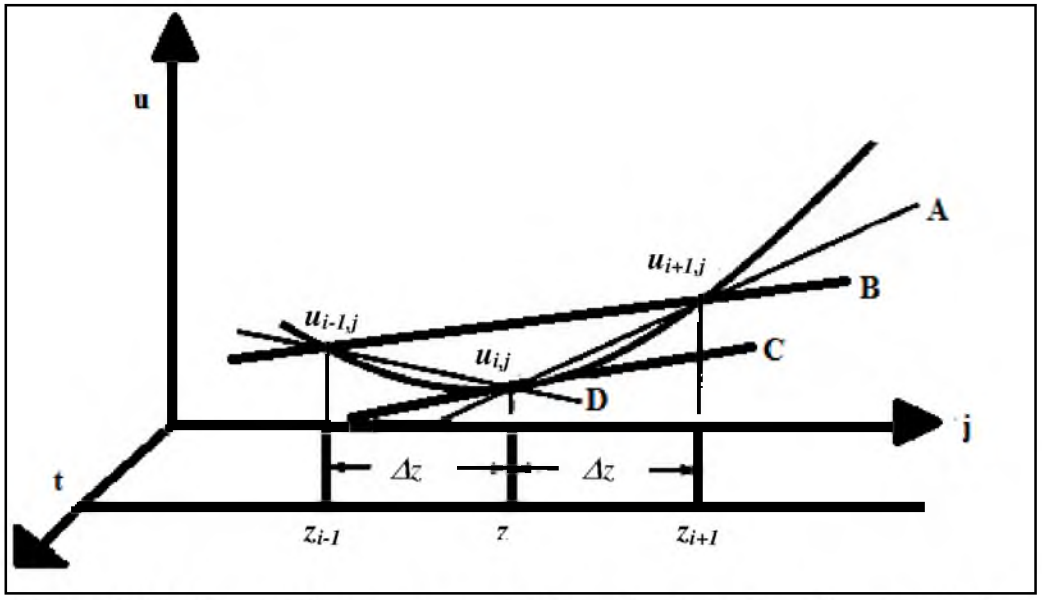

Figure 2-14. Finite difference approximation of a derivative (Courtesy Oxford University Press, Al-Khafaji and Andersland, 1992)

The approximation of the derivative $\partial u/\partial z$ at time step t_j is shown in Figure 2-14, for three different finite difference techniques: Line A represents the forward difference approximation, Line B represents the central difference approximation, and Line D represents the backward difference approximation. The equations corresponding to these three finite difference approximations are as follows:

Forward Difference:

$$\frac{\partial u}{\partial z} \approx \frac{u_{i+1,j} - u_{i,j}}{\Delta z} \tag{2-8}$$

Central Difference:

$$\frac{\partial u}{\partial z} \approx \frac{u_{i+1,j} - u_{i-1,j}}{2\Delta z} \tag{2-9}$$

Backward Difference:

$$\frac{\partial u}{\partial z} \approx \frac{u_{i,j} - u_{i-1,j}}{\Delta z} \tag{2-10}$$

Of the three methods, the central difference gives the best approximation and should be used whenever possible. However, circumstances sometimes dictate that the central difference cannot be used, requiring that either the forward or backward difference be used instead. Equations for approximations of higher order derivatives can be found in a similar manner.

The finite difference method will be used to solve both Terzaghi's and Davis and Raymond's one-dimensional consolidation equations for the time rate of dissipation of excess pore pressures. Details of these processes are described in the two subsections below. Analysis and results for dissipation of excess pore pressure using the finite difference method will be presented in Chapter 6.

2.4.2.1 Solution of Terzaghi's one-dimensional consolidation equation. The finite difference method can be used to solve Terzaghi's one-dimensional consolidation equation (Eq. 2-5) (e.g., Al-Khafaji and Andersland 1992; Holtz et al. 2011). The central difference approximation for the second order derivative for change in pore pressure with depth is defined in Eq. 2-11.

$$\frac{\partial^2 u}{\partial z^2} = \frac{u_{i-1,j} - 2u_{i-1,j} + u_{i+1,j}}{\Delta z^2} \tag{2-11}$$

The forward difference approximation for first order differential equation for change in pore pressure with change in time is defined in Eq. 2-12.

$$\frac{\partial u}{\partial t} \approx \frac{u_{i+1,j} - u_{i,j}}{\Delta t} \tag{2-12}$$

Inserting Eqs. 2-11 and 2-13 into Eq. 2-5 and solving for $u_{i,j+1,}$ the pore pressure at depth node *i* and time step *j+1* can be estimated from the pore pressures at nodes *i-1*, *i*, and *i+1* from the previous time step (*j*) using Eq. 2-12.

$$u_{i,j+1} = \alpha u_{i-1,j} + (1 - 2\alpha)u_{i,j} + \alpha u_{i+1,j} \tag{2-13}$$

where α is defined as

$$\alpha = \frac{C_v \Delta t}{(\Delta z)^2} \tag{2-14}$$

and

C_v = coefficient of consolidation

Δt = time step

Δz = depth increment

Previous research has shown that α needs to be less than 0.5 for Eq. 2-13 to be numerically stable and the most accurate results are obtained when α is equal to 1/6 (Al-Khafaji and Andersland 1992).

For Terzaghi's equation, an impervious boundary is a line of symmetry with respect to dissipation of excess pore pressure. This indicates the excess pore pressure at node *i-1* is equal to the excess pore pressure at node *i+1*, where node *i+1* is an imaginary node one step beyond the impervious boundary. In mathematical terms this relationship is represented as

$$u_{i-1,j} = u_{i+1,j} \tag{2-15}$$

When impervious boundary conditions are encountered the finite difference equation for excess pore pressure becomes:

$$u_{i+1,j} = 2\alpha u_{i-1,j} + (1 - 2\alpha) * u_{i,j} \tag{2-16}$$

One of the problems encountered in geotechnical engineering practice is that cohesive deposits are not always homogenous. The equations mentioned in this section are applicable to nodal points that could be considered in the mesh where the soil properties are constant. To handle nodal points where soil properties change along boundaries between cohesive layers, these equations need to be modified to model the appropriate behavior. The discontinuity of soil properties along these boundaries must be considered in analysis of excess pore pressure dissipation.

Along interfaces between layers within the cohesive deposits, the equation for excess pore pressure becomes (Al-Khafaji and Andersland 1992)

$$u_{i,j} = \frac{1}{1+\beta} * u_{i-1,j} + \frac{\beta}{1+\beta} * u_{i+1,j} \tag{2-17}$$

where β is defined as

$$\beta = \frac{k_2 \Delta z_1}{k_1 \Delta z_2} \tag{2-18}$$

where:

k_1 = the permeability in the cohesive layer above the interface

k_2 = the permeability in the cohesive layer below the interface

Δz_1 = the depth increment of the cohesive layer above the interface

Δz_2 = the depth increment of the cohesive layer below the interface

2.4.2.1 Solution of Davis and Raymond's one-dimensional consolidation equation. Using the finite difference method and the equations for forward, backward, and central differences, the excess pore pressures for the following time step can be determined for Davis and Raymond's one-dimensional consolidation theory. The second order differential equation for change in pore pressure with depth can be found from Eq. 2-19 using the central difference equation.

$$\frac{\partial^2 u}{\partial z^2} = \frac{u_{i-1,j} - 2u_{i-1,j} + u_{i+1,j}}{\Delta z^2} \tag{2-19}$$

The first order differential equation for change in pore pressure with depth can be found from Eq. 2-20 using the central difference equation for a first order differential equation

$$\frac{\partial u}{\partial z} = \frac{u_{i+1,j} - u_{i-1,j}}{2\Delta z} \tag{2-20}$$

The first order differential equation for change in pore pressure with time can be found from Eq. 2-21 using the forward difference method equation for first order differential equations.

$$\frac{\partial u}{\partial t} = \frac{u_{i,j+1} - u_{i,j}}{\Delta t} \tag{2-21}$$

The effective stress at a depth for a certain time is denoted by Eq. 2-22.

$$\sigma'_{i,j} = (\sigma_{ss})_{i,j} - u_{i,j} \tag{2-22}$$

where $\sigma'_{ss_{i,j}}$ is equal to the steady state effective stress.

Substituting Eqs. 2.19 – 2.22 into Eq. 2-7 and solving for the pore pressure at the next time step yields Eq. 2-23.

$$u_{i,j+1} = C_v \cdot \Delta t \left[\frac{u_{i-1,j} - 2u_{i-1,j} + u_{i+1,j}}{\Delta z^2} - \frac{1}{(\sigma'_{ss})_{i,j} - u_{i,j}} \cdot \left(\frac{u_{i+1,j} - u_{i-1,j}}{2\Delta z} \right) \cdot \left(\gamma_{sat} + \frac{u_{i+1,j} - u_{i-1,j}}{2\Delta z} \right) + u_{i,j} \right] \tag{2-23}$$

Eq. 2-17, which was derived previously for the pore pressures along the interface of two cohesive layers with different coefficients of consolidation, is also valid for Davis and Raymond's one-dimensional consolidation equation. However, an impervious boundary is not a line of symmetry with respect to dissipation of excess pore pressure in Davis and Raymond's equation. In this case the second order backward difference equation must be used for $\frac{\partial^2 u}{\partial z^2}$, which is given in Eq. 2-24.

$$\frac{\partial^2 u}{\partial z^2} = \frac{u_{i-1,j} - 2u_{i-1,j} + u_{i+1,j}}{\Delta z^2} \tag{2-24}$$

Substitution of Eq. 2-24 into Eq. 2-23 in place of Eq. 2-8 gives Eq. 2-25, which is valid for estimating the excess pore pressure along an impervious boundary when using Davis and Raymond's method.

$$u_{i,j+1} = C_v \cdot \Delta t \left[\frac{u_{i-1,j} - 2u_{i-1,j} + u_{i+1,j}}{\Delta z^2} - \frac{1}{(\sigma'_{ss})_{i,j} - u_{i,j}} \cdot \left(\frac{u_{i+1,j} - u_{i-1,j}}{2\Delta z} \right) \cdot \left(\gamma_{sat} + \frac{u_{i+1,j} - u_{i-1,j}}{2\Delta z} \right) + u_{i,j} \right] \tag{2-25}$$

2.5 Prediction of Surcharge Removal

2.5.1 Asaoka (1978) Method

The Asaoka (1978) method is an observational approach to assist in predicting the end of primary consolidation settlement and the time for removal of surcharge. In this method, a graphical procedure is used to determine the magnitude and time rate of primary consolidation settlement using measurements of surface settlement recorded at a constant time interval. Settlement observations from instrumentation readings can be obtained on a daily, weekly, biweekly, or monthly interval of time. Settlement data are plotted on a settlement versus time curve along with the height of the embankment throughout the duration of a construction project as shown in Figure 2-15. Settlement at

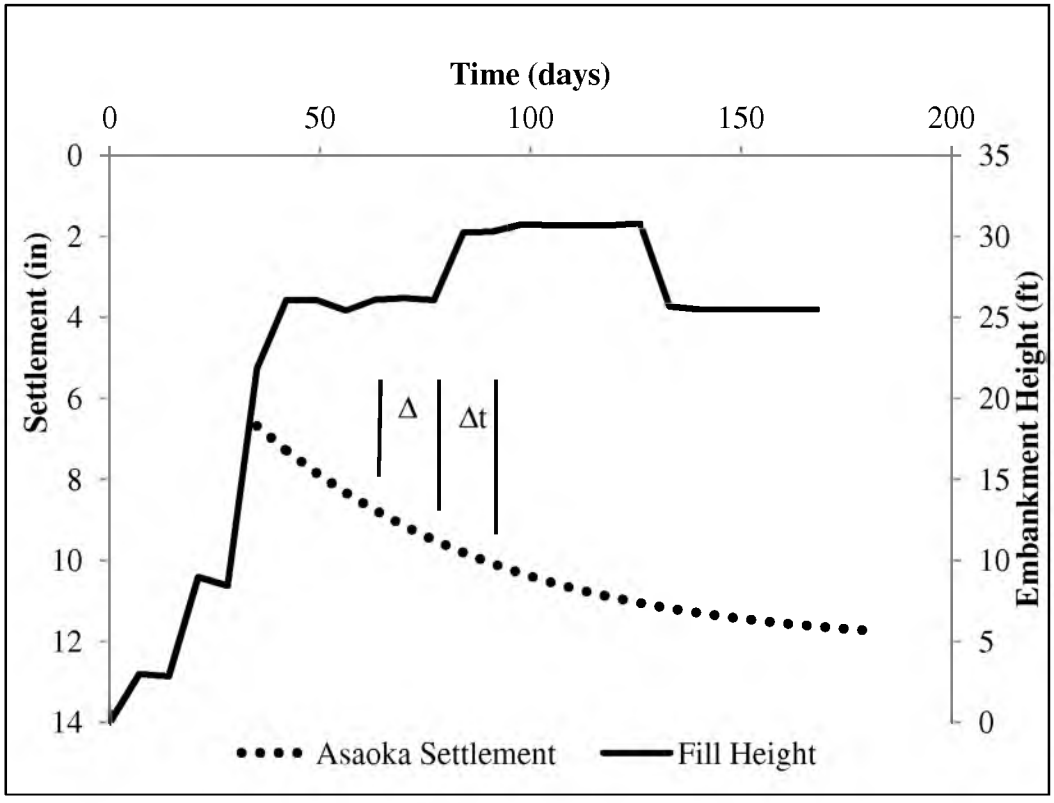

Figure 2-15. Settlement observation data plotted on settlement versus time curve.

time t (S_t) is plotted against the settlement from the preceding time ($S_{t-1} = S_t - \Delta t$), as shown in Figure 2-16.

If the data plots in a straight line, the ultimate (or final) settlement under the embankment plus surcharge load (S_f, which excludes settlement from secondary compression) can be predicted by extending the straight line through the data until it intersects a line oriented at 45 degrees.

Asaoka made three assumptions in developing this 1978 graphical procedure for ultimate primary consolidation settlement. These assumptions are summarized as follows:

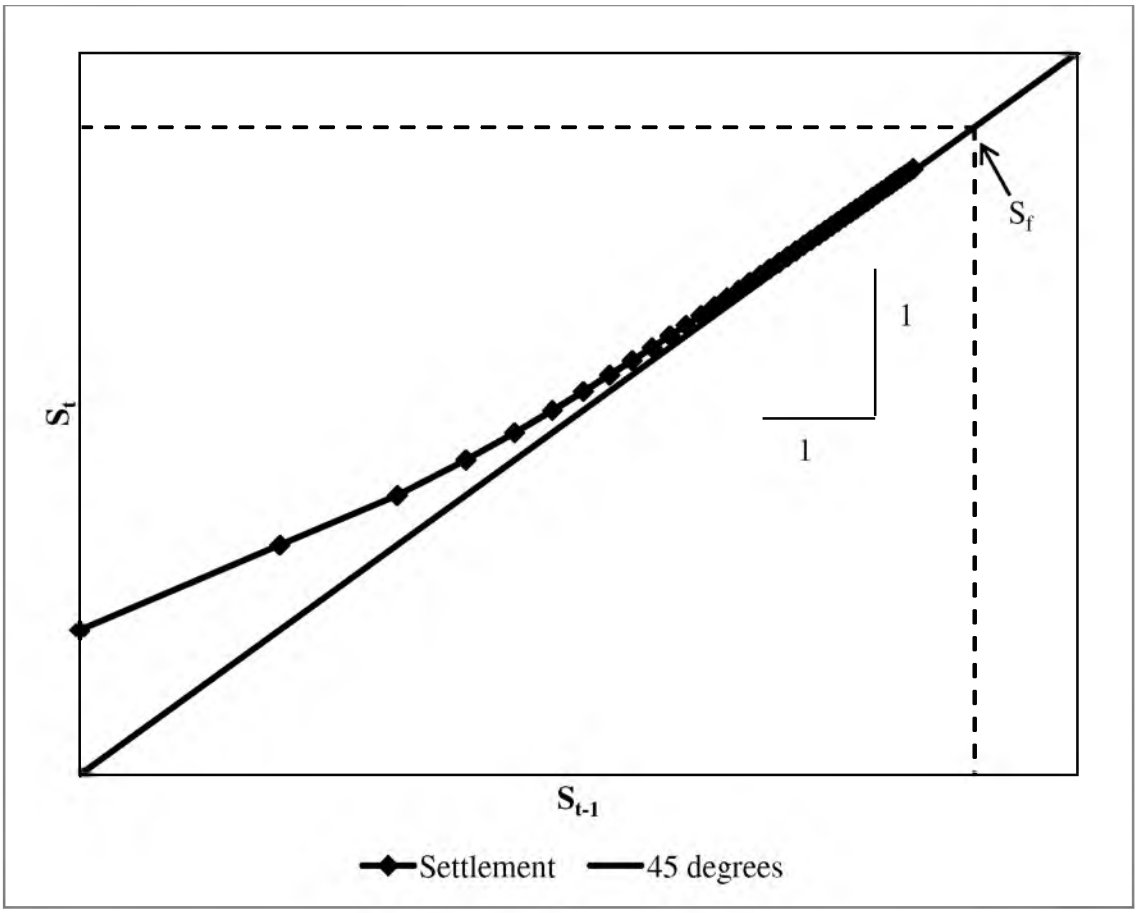

Figure 2-16. Example of plot showing settlement at time t on the ordinate, the preceding settlement at time t-1 on the abscissa.

1. One-dimensional consolidation occurs during loading.
2. Surface settlement is caused by a constant load.
3. Subsurface soil is homogenous.

It is important to note that the data will plot in a straight line only if the following conditions are met (Jamiolkowski 1985):

1. The consolidating soil is comprised of a single, relatively homogeneous layer.
2. The dissipation of pore pressures within the homogeneous soil follows the assumptions of Terzaghi's one-dimensional consolidation theory, particularly these assumptions:
    a. The flow of pore water is one-dimensional.
    b. The appropriate coefficient of consolidation (C_v for vertical flow or C_h for horizontal flow) remains constant during the primary consolidation process.
    c. No significant secondary compression occurs.

Another limitation is that the accuracy of graphical method depends on the chosen time interval Δt. The accuracy is higher for larger values of Δt.

Once the final settlement is estimated using Asaoka's Method, the time at which a certain percentage of settlement will occur can be estimated. This is accomplished by developing the settlement at time j (S_{cj}) as a function of the settlement determined by using Asaoka's method and U_{avg} developed by Eq. 2-23, Sivaram and Swamee (1977), and extrapolating the time for this percentage of final settlement determined by Asaoka's method to occur from the settlement versus time plot (shown in Figure 2-17).

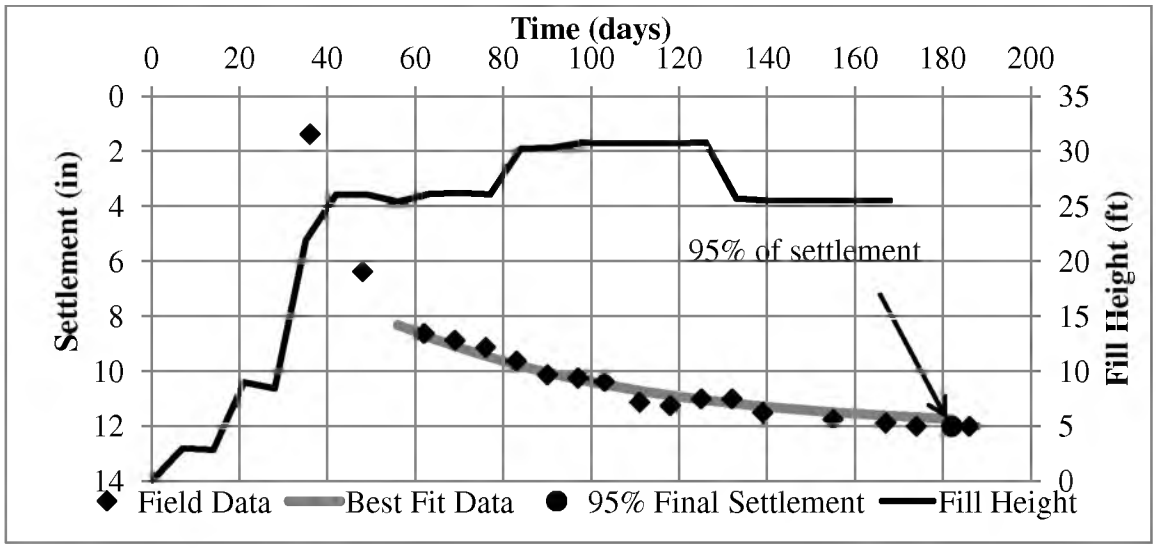

Figure 2-17. Fitting the settlement curve as a function of U_{ave} with the measured settlement obtained from field instrumentations, was determined by varying c_v/H^2_{dr},until the appropriate value best fit the actual settlement.

$$U_{avg} = \frac{\left(4T_v/\pi\right)^{0.5}}{\left[1+\left(4T_v/\pi\right)^{2.9}\right]^{0.179}} \tag{2-26}$$

$$T_v = \frac{C_v t_c}{H_{dr}^2} \tag{2-27}$$

where:

C_v = the coefficient of consolidation

t_c = the time measured from the onset of construction

H_{dr} = the height of the longest drainage path

However, it is important to understand that a percentage of final settlement is not equal to the average degree of consolidation (typically called U_{avg}). U_{avg} represents the

average degree of dissipation of excess pore pressure (and hence, the average degree of change in effective vertical stress), not the average degree of settlement, because primary consolidation settlement is not proportional to the change in the effective vertical stress, as discussed in Section 2.4.1.2.

Eq. 2-23, U_{avg} developed by Sivaram and Swamme, is applicable in solving Terzaghi's one-dimensional consolidation theory and strictly limited to one-dimensional consolidation cases.

2.5.2 Farnsworth (2009)

The reconstruction of Interstate-15 (I-15) in Salt Lake City from 1998 to 2002 provided an opportunity to gather geotechnical data pertinent to evaluating the in situ behavior of soft soil foundations (Farnsworth 2009). The purposes of this study was to (1) provide an assessment of the reliability of using Asaoka's method to determine the end of primary consolidation and the time for removal of the surcharge, (2) obtain horizontal drainage properties by back calculation of field data using Asaoka's method and radial consolidation theory, and (3) compare field settlement data with settlement results predicted using radial consolidation theory.

Stringent specifications pertaining to magnitude and time rate of primary consolidation needed to be met during the reconstruction of I-15. As previously mentioned, the time for completion of primary consolidation in soft soils, such as those found in the Salt Lake Valley, can take years or even decades to complete unless measures are undertaken to increase the rate. At the sites studied by Farnsworth, prefabricated vertical drains were installed to accelerate the consolidation process. The

specification for removal of surcharge was that 98% of the primary consolidation settlement needed to be complete before the surcharge could be removed.

One of the conclusions determined from this study was that when Asaoka's method was used, the closer the settlement got to 98% of the estimated final settlement, the farther away the predicted date for removal of surcharge was getting. Because of this situation, delays in the removal of surcharge were occurring until geotechnical engineers could determine the root of the problem. The problem was determined to be the assumption in Asaoka's method that the underlying foundation consists of a single homogenous layer. In reality, the foundations consisted of various layers with different engineering properties that were consolidating at different rates

Horizontal consolidation properties were back calculated at eleven locations using settlement data for individual cohesive layers obtained from magnet extensometers. Both Asaoka's method and radial consolidation theory were used for these analyses. It was found that the horizontal coefficient of consolidation (C_h) varied for the different cohesive layers throughout the soft soil foundations at each location. For example, at the I-15/1300 South location, C_h was determined to be 0.02 in^2/min within the lower Lake Bonneville clay layer, 0.06 in^2/min within the upper Lake Bonneville clay layer, 0.04 in^2/min within the interbed layer, and 0.02 in^2/min within the lower Pleistocene alluvium layer.

The research also was used to show the power of the finite difference method for determining settlement and back calculating horizontal drainage properties. The finite difference method was used to solve the second order differential equation for radial consolidation that simulated the horizontal drainage that was occurring because of the

presence of prefabricated vertical drains. Radial consolidation theory and the finite difference method were successfully used to estimate the magnitude and rate of primary consolidation settlement within each individual cohesive layer and to back calculate horizontal drainage properties within each individual cohesive layer, as described above. Farnsworth's research on soft soil foundations within the Salt Lake Valley provided insight into the reliability of Asaoka's method for layered soils. Farnsworth showed that Asaoka's method does not work well in layered soils due to the different rates of consolidation occurring within each individual cohesive layer. Back calculation of coefficient of horizontal consolidation from Asaoka's method, finite difference method and field data showed different rates of consolidation in each individual cohesive layer. Using Asaoka's method and treating soft soil foundations as single relatively homogenous layers can lead to erroneous estimations of magnitude of settlement and time rate of settlement. Therefore, determining the settlement behavior of each individual cohesive layer and treating underlying soils comprised of various soil properties as a multilayered system is a more correct method to analyze settlement behavior.

2.6 Estimation of Preconsolidation Stress

Methods used in this research to estimate preconsolidation stress (σ'_p) of cohesive soils will be discussed in this section. Two empirical correlations for σ'_p based on corrected tip resistance from the CPT (q_t) will be discussed in Section 2.6.1. Methods used to estimate preconsolidation stress based on the results of laboratory one-dimensional consolidation tests will be presented in Section 2.6.2.

2.6.1 Empirical Correlations based on CPT Tip Resistance

The reconstruction of Interstate 15 located in Salt Lake County yielded local correlations for various geotechnical parameters. Correlations for σ'_p, compression ratio, and compression index were developed during this research. Only the correlation for σ'_p will be discussed in this section.

Field data during construction from instrumentation, along with CPT logs of the site and results of consolidometer tests were reduced and analyzed for the purpose of correlating the preconsolidation stress with CPT parameters for Lake Bonneville clay (Ozer 2005). The field data during construction was taken from settlement plates, magnet extensometers, and surveys of fill heights versus elapsed time. A correlation developed for σ'_p is shown in Eq. 2-28.

$$\frac{\sigma'_p}{P_a} = 0.6323\left(\frac{\sigma_{v,i,j=0}}{P_a}\right)^{0.565} * \left(\frac{q_t - \sigma_{v,i,j=0}}{P_a}\right)^{0.3422} \quad (2\text{-}28)$$

where:

σ_{vo} = total overburden stress

P_a = atmospheric pressure

Empirical correlation between various geotechnical parameters can be found in almost any geotechnical engineering textbook. It is important to remember these correlations were determined from various locales and may not be applicable to all soils. A general correlation for σ'_p developed by Kulhawy and Mayne (1990) based on CPT data from many sites is provided in Eq. 2-29.

$$\sigma'_p = 0.33(q_t - \sigma_{v,i,j}) \quad (2\text{-}29)$$

2.6.2 Laboratory One-Dimensional Consolidation Tests

Casagrande's (1936) graphical technique is the most widely used method in geotechnical engineering practice to estimate σ'_p from results of laboratory one-dimensional consolidation tests. The steps for this procedure are as follows:

1) Choose by eye the point of maximum curvature from the strain versus logarithm of effective stress curve.
2) Extend a horizontal line from the point of maximum curvature.
3) Draw a line tangent to the point of maximum curvature.
4) Bisect the angle created by the horizontal line and the line tangent to the maximum point of curvature.
5) Extend a line from the virgin compression portion of the curve toward the bisector line created in step 4. The stress corresponding to the point of intersection of these two lines provides an estimate of σ'_p.

CasaGrande's method is very simple but it requires that a distinct point of maximum curvature can be determined if accurate results are to be obtained. Many samples that were tested did not have a distinct point of maximum curvature; rather, the transition from recompression to virgin compression was gradual. Thus, another method was needed to obtain estimates of σ'_p that are less subjective than Casagrande's technique.

The second method used to determine σ'_p was developed by Becker et al. (1987) and is known as the Work Method. This method was developed to estimate the yield

point (σ'_p) using work per unit volume done to the material. The work done per unit volume for a one-dimensional consolidation test (ΔW_{oed}) is expressed by Eq. 2-30.

$$\Delta W_{oed} = \left[\frac{\sigma'_{i+1} + \sigma'_i}{2}\right] * (\varepsilon_{i+1} - \varepsilon_i) \tag{2-30}$$

where:

σ'_i = Average effective stress for loading increment i

σ'_{i+1} = Average effective stress for the subsequent loading increment

ε_i = Strain at increment i

ε_{i+1} = Strain at increment i + 1

Strains that are generated within the soil are caused by a change in effective stress. Plots of cumulative work done per unit volume are plotted against the effective stress on an arithmetic scale. Fitted linear lines are drawn through the initial straight line portion of the curve and from the steepest part of the curve to the initial fitted linear line. The intersection of these two lines approximates the in situ preconsolidation stress as shown in Figure 2-18.

2.7 Determination of Field Virgin and Recompression Indices

Schertmann's method (1955) was the procedure used in determining the field virgin and recompression indices. Schmertmann developed graphical procedures for determining field and virgin recompression indices for normally consolidated and over consolidated soils. Schmertmann's procedure for over consolidated soil is shown in Figure 2-19 and is described as follows:

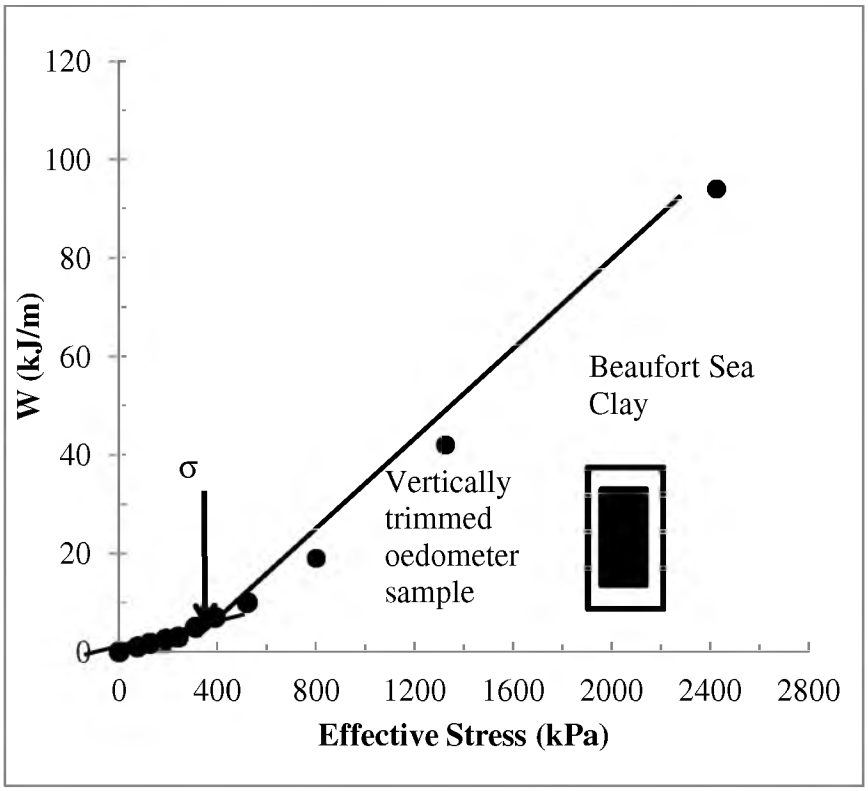

Figure 2-18. Work per unit volume plot on overconsolidated Beaufort Sea Clay (Courtesy Canadian Science Publishing/NRC Research Press Becker et al. 1987).

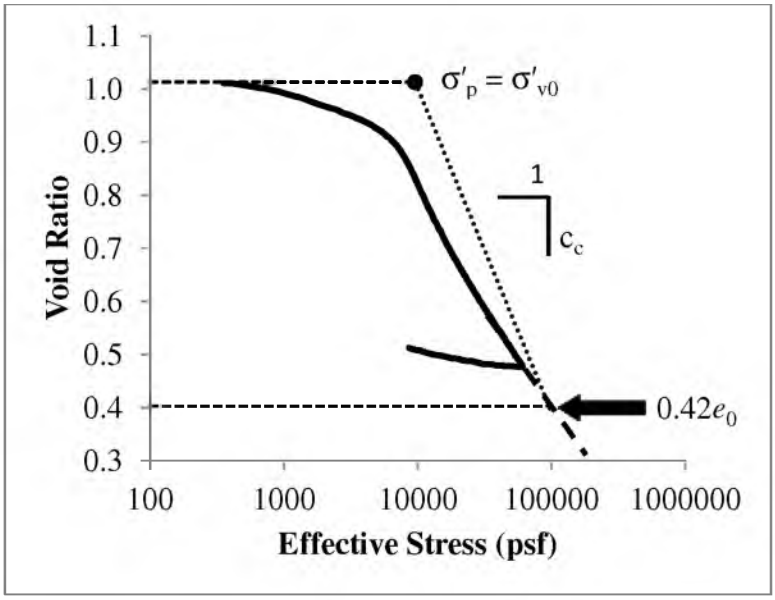

Figure 2-19. Schertmann's (1955) procedure for normally consolidated soils for virgin compression and recompression indices (adapted from Holtz and Kovac 1981).

1. Determine the initial void ratio, e_0.
2. Determine the preconsolidation stress.
3. Draw a horizontal line parallel with the abscissa from the initial void ratio to the preconsolidation stress.
4. Extend the virgin compression curve to $0.42e_0$.
5. Connect the preconsolidation stress with the intersection point of $0.42e_0$ and the extension of the virgin compression curve.
6. Determine the slope of the virgin compression curve (c_c) defined as

$$C_c = -\frac{de}{d \log \sigma'_v} \tag{2-31}$$

where:

de = the change in void ratio

$dlog\sigma'_v$ = the change in the logarithm of effective stress

The slope of the recompression curve, the rebounding section of the curve (c_r) is defined as

$$C_r = -\frac{de}{d \log \sigma'_v} \tag{2-32}$$

The modified compression index ($c_{c\varepsilon}$) or recompression ratio ($c_{r\varepsilon}$) is related c_c and c_r by the initial void ratio and is defined by Eq. 2-33 and Eq. 2-34.

$$C_{c\varepsilon} = \frac{C_c}{1 + e_0} \tag{2-33}$$

$$C_{r\varepsilon} = \frac{C_r}{1 + e_0} \tag{2-34}$$

Determining virgin compression and recompression indices for over consolidation soils is different than for normally consolidated soils. The following steps for determining field virgin and recompression indices are as follows and shown schematically in Figure 2-20.

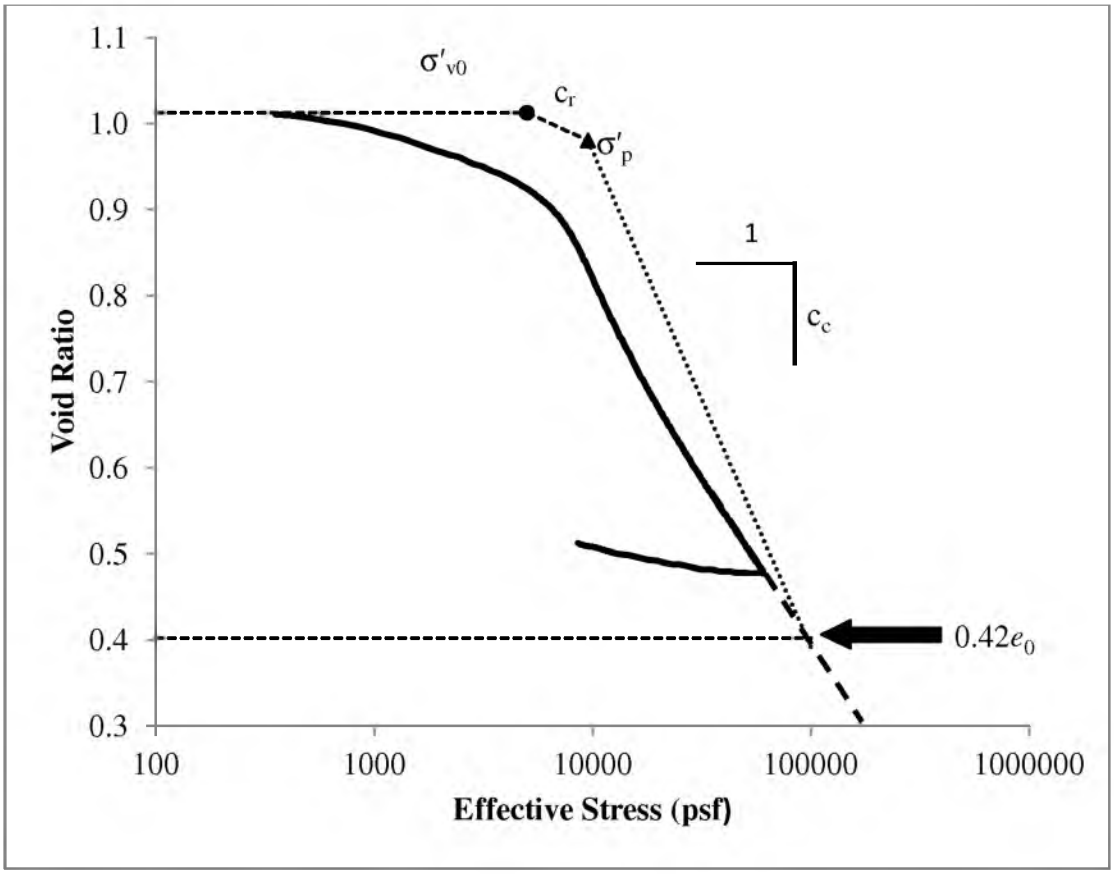

Figure 2-20. Schertmann's (1955) procedure for over consolidated soils for virgin compression and recompression indices (adapted from Holtz and Kovac 1981)

1. Determine the initial void ratio.
2. Determine the effective stress of the soil.
3. Draw a horizontal line parallel to the abscissa from the initial void ratio the effective stress.
4. Extend the virgin compression curve to $0.42e_0$.
5. Connect the preconsolidation stress with the intersection point of $0.42e_0$ and the extension of the virgin compression curve.
6. Connect σ'_{v0} to σ'_p by the recompression index, c_r.

Equations for c_c, c_r, $c_{c\varepsilon}$ and $c_{r\varepsilon}$ from normally consolidated soils are valid for over consolidated soils. Schertmann's procedure can be performed using percent strain in place of void ratio on a stress-strain plot. The same procedures for determining compression indices discussed earlier in Section 2.7 are applicable, an equivalent term for change in void ratio, Δe, is needed to use Schertmann's procedure. Modified compression index ($c_{c\varepsilon}$) and recompression ratio ($c_{r\varepsilon}$) are determined when using percent strain versus logarithm of effective stress plots. Field virgin and recompression ratios for the SR 77 research embankment site were determined by using percent strain versus logarithm of effective stress plots.

2.8 Previous Embankment Studies

Embankment construction has provided geotechnical engineers with the opportunity to use field instrumentation to monitor behavior of underlying soils. Geotechnical engineers can use results obtained through monitoring subsurface behaviors to: (1) back calculate site specific geotechnical parameters, (2) better estimate or predict

the magnitude and time rate of primary consolidation settlement, and (3) develop detailed models for future settlement analysis. Two parameters closely monitored through field instrumentation are primary and secondary consolidation settlement and the development of excess pore pressures.

2.8.1 Monitoring of Settlement through Field Instrumenation

Field instrumentation was used to monitor settlement behavior and to verify estimates of primary consolidation settlement of a test embankment located in Tacoma, WA (Chang et al. 1994). Instrumentation used included three vertical extensometers, two inclinometers, two horizontal profilers, three pneumatic piezometers, and six settlement plates. The purpose of the field instrumentation was to monitor the excess pore pressure, vertical settlement, and lateral movement. Data obtained from field instrumentation was gathered for 1 year. The height of the test embankment was 14 ft. Underlying soils at the test embankment site were comprised of soft, slightly clayey to clayey-silt and loose to medium sand in the upper 12.2 m (40 ft), followed by medium-dense to very dense, clean to silty fine coarse sand with occasional clayey silt layers to a depth of 50 ft.

Predicted primary consolidation settlement caused by the test embankment was analyzed using three methods: Winkler model, semiinfinite elastic model using Boussineq stresses being valid in a layered soil, and Terzaghi-Taylor method.

Primary consolidation settlement determined from the Winkler model was assumed to be proportional to the load acting on a settlement point. Settlement determined from the semiinfinite elastic model was found from Eq. 2-35.

$$S = \sum_{i=1}^{n} \left(\frac{\sigma_z}{E} + \nu \frac{\sigma_y}{E} + \nu \frac{\sigma_x}{E} \right)_i * H_i \quad (2\text{-}35)$$

where:

s = the stress in the x, y, or z direction

E = Young's modulus

ν = poisson's ratio of the soil

The Terzaghi-Taylor model for estimating primary consolidation settlement incorporates the stresses developed using Boussinesq. Settlements obtained from Terzaghi-Taylor model can be determined from Eq. 2-36.

$$S = \sum_{i=1}^{n} \frac{\Delta\sigma_z * h_i}{M_{DMT}} \quad (2\text{-}36)$$

where:

$\Delta\sigma_z$ = induced vertical stress component from Boussinesq theory

h_i = height of each sublayer

M_{DMT} = constrained modulus determined from a dilatometer (DMT) test

A comparison of the back calculated primary consolidation settlement determined by Chang et al. using the modified semiinfinite elastic method, Terzaghi-Taylor method, and extensometer readings at the centerline of the test embankment are shown in Figure 2-21. There were three main conclusions provided in this paper, two of which are applicable to this project. The first conclusion provides insight that a well-instrumented embankment can provide valuable data sets for better predicting future settlements. The

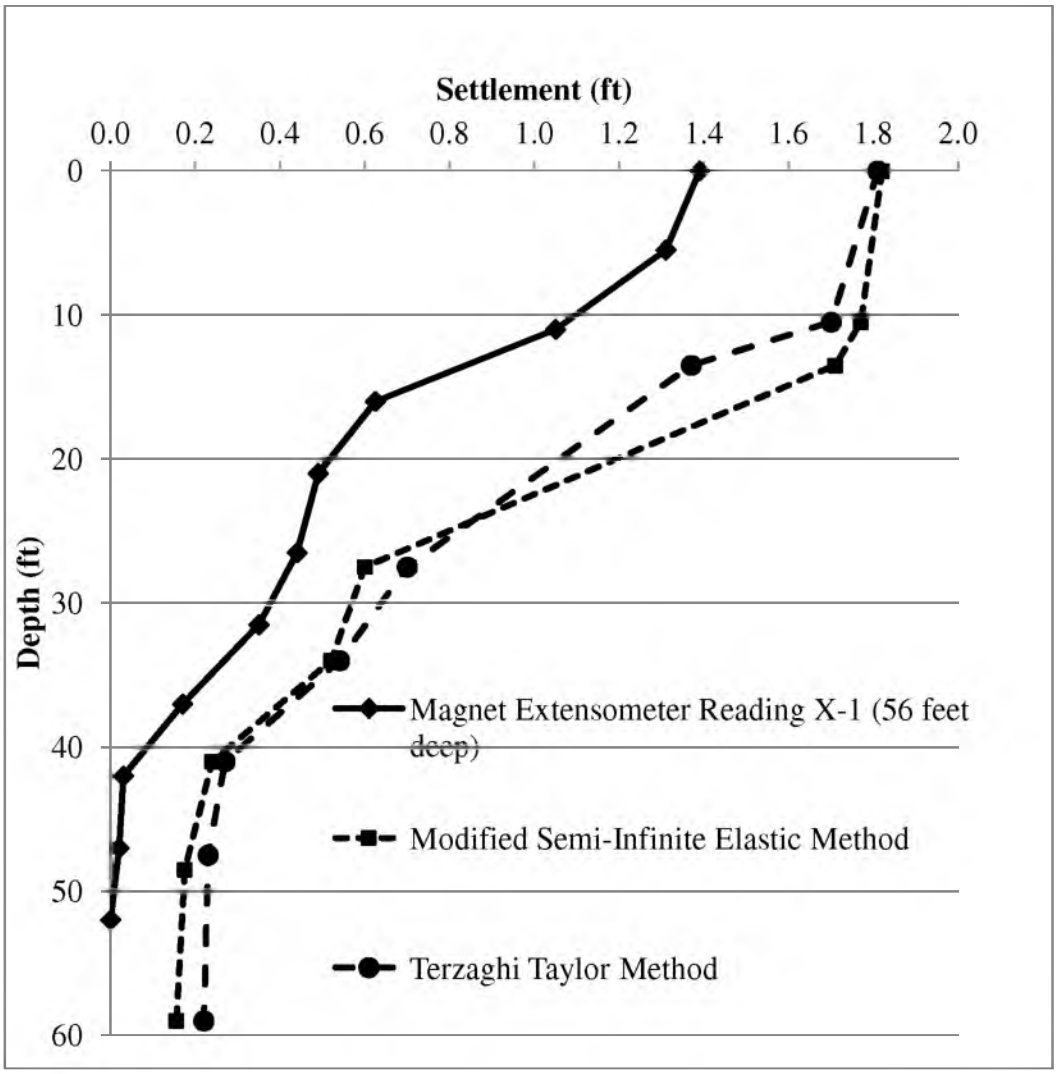

Figure 2-21. Comparison of predicted and actual settlement using an extensometer, modified semiinfinite elastic method, and Terzaghi-Taylor Method at the center of the embankment (With permission from ASCE, Chang et al. 1994).

second conclusion is that the semiinfinite elastic model yielded better predictions than the other models for this site. This conclusion allows a geotechnical engineer to assess the settlement using different models for site specific projects.

Instrumentation along Interstate 15 has been a common practice in the state of Utah. The main purposes behind placing instrumentation in embankments and soft soil foundations on various Interstate 15 projects is to discover the challenges that can be

encountered during construction and postconstruction settlement monitoring. Common challenges along Interstate 15 in the Salt Lake Valley are, compressibility and shear strength of the underlying clayey soils encountered in this region. Because of these challenges, the magnitude and time rate of primary consolidation concern local geotechnical engineers. During the 1998 redesign of Interstate 15 in the Salt Lake Valley, the Utah Department of Transportation (UDOT) had these challenges investigated

2.8.2 Monitoring Excess Pore Pressures Generated by Embankment Loading through Field Instrumentation

An important aspect in determining excess pore pressures developed from loading is Skempton's *B* parameter. The B value, as commonly referred, is the change in excess pore pressure to the change in vertical stress ($\Delta u/\Delta\sigma_v$), which will be defined as *C* in the analysis section of this thesis. $\Delta u/\Delta\sigma_v$ values range from 0 to 1, where dry soils have a ratio of 0, partially saturated soils have a B value less than 1, and completely saturated soils have a $\Delta u/\Delta\sigma_v$ value of 1. In one-dimensional loading the excess pore pressures introduced during loading is equal to the applied vertical load. Due to this assumption, the B value often used in determining excess pore pressures is 1. Assuming a $\Delta u/\Delta\sigma_v$ value of 1 can lead to settlement results that are often over estimated. The importance in determining the $\Delta u/\Delta\sigma_v$ value is to determine the magnitude of excess pore pressures induced by an applied load.

Excess pore pressures caused by an applied load are commonly measured using piezometers. Piezometers will show an increase in excess pore pressures as load is

applied, and they will also show a decrease in excess pore pressures, commonly known as dissipation, as the load stays constant. Removal of surcharge will also cause a decrease in pore pressure. The magnitude and rate of dissipation of excess pore pressures is a fundamental component in calculating primary consolidation settlement. Thus, by predicting or determining the amount of excess pore pressures, settlement calculations can be more accurately made.

Leathers and Ladd (1978) studied the possibility of predicting excess pore pressures by means of a finite element program, FEECON or elastic theory. Pore pressures were calculated using Henkel's (1960) equation for initial pore pressures, defined in Eq. 2-37.

$$u_0 = \Delta\sigma_{oct} + \alpha(\Delta\tau_{oct})^k \tag{2-37}$$

where:

$$\Delta\sigma_{oct} = \frac{1}{3}(\Delta\sigma_1 + \Delta\sigma_2 + \Delta\sigma_3) \tag{2-38}$$

$$\Delta\tau_{oct} = \frac{1}{3}\sqrt{(\Delta\sigma_1 - \Delta\sigma_2)^2 + (\Delta\sigma_1 - \Delta\sigma_3)^2 + (\Delta\sigma_2 - \Delta\sigma_3)^2} \tag{2-39}$$

$a = 0$ or 1/3

$k = 1$

The purpose of this study was to analyze the behavior of the undrained excess pore pressures associated with initial and final settlement during the construction process.

The embankment studied was built to a maximum height of 28 ft during the summer of 1971. Field instrumentation was used to monitor the behavior of the foundation soils beneath the embankment. Leathers and Ladd concluded that the excess pore pressures developed in FEECON ranged from 0.84 to 1.22 of the measured values for undrained excess pore pressures. Initial settlements predicted using a finite element program and elastic theory using undrained conditions agreed well with measured values obtained from the field instrumentation.

A later study pertaining to the construction excess pore pressures was performed by Leoroueil et al. (1978) The primary purpose of this research was to observe pore pressures and observe their behavior during construction of four test fills located in Saint-Alban.

One of the parameters studied by Leroueil et al. pertaining to this project was the ratio of induced excess pore water pressure to the change in total vertical stress ($\Delta u/\Delta\sigma_v$), referred to as r_u by Leroueil et al. This value is theoretically equal to 1 for 1-dimensional strain, soft soils, and loads that are applied instantaneously. Even if the first two conditions are met, loads in real construction projects are not applied instantaneously. Leroueil et al. discovered that the values of $\Delta u/\Delta\sigma_v$ were 0.64, 0.32, 0.47, and 0.56 for loads varying from 0 to 40 kPa at a depth of 5 m during the early stages of construction for the four test fills. They also found that $\Delta u/\Delta\sigma_v$ was less than 0.1 closer to the drainage boundaries, which indicated that a significant amount of consolidation occurred quickly at least at these locations.

During the study on the test fills at Saint-Albans a significant amount of consolidation was shown to have occurred in a thick clay deposit during a short time

frame of construction. While further loading yielded significant increases in pore pressure, the effective vertical stress remained more or less the same. This type of behavior was completely explained using the concept of limit state, as modified in the YLIGHT model proposed by Tavenas and Leroueil (1977) applied in natural clays. The YLIGHT model was used to model subsequent research embankments. Leoroueil et al. observed pore pressures developed from under 30 different embankments, and concluded that the pore pressures generated followed the same YLIGHT model developed during the original study.

The YLIGHT model led to empirical formulas for predicting pore pressures at conditions approaching failure. Leoroueil et al. concluded from all their work that continuously monitoring in situ pore pressures is the only meaningful solution for technical analysis.

Previous research from embankment construction and field instrumentation has provided insight to develop better models to predict the rate of primary consolidation settlement models. The purpose of the research described in this thesis is to provide further understanding into the complexity of estimating primary consolidation settlement for soft foundation soils beneath constructed embankments.

3 RESEARCH INSTRUMENTATION ARRAY

Vertical and horizontal positioning of field instrumentation during a construction project is vital to the success of any subsurface monitoring program. A successful instrumentation array is comprised of four parts: (1) Installation of field instrumentation, (2) data collection, (3) frequency of data collection, and (4) data reduction. Installation of field instrumentation will be described in detail in Section 3.1. The type of data collected and the frequency at which it was collected will be discussed in Sections 3.2 and 3.3. The procedures used to reduce the data will be described in Section 3.4.

3.1 Installation

The instrumentation array developed for monitoring in situ excess pore water pressure, vertical settlement, and lateral movement at the site of the SR 77 embankment construction were as follows:

- 19 piezometers
- 20 spider magnets
- 6 settlement manometers
- 3 push in cells
- 2 ShapeAccelArray
- 1 vertical inclinometer

- 1 horizontal inclinometer
- 3 pressure cells for vertical stress
- 3 pressure cells for horizontal stress

The field instrumentation was installed in March 2009 preceding the initial onset of construction. A plan view of the instrumentation referenced from the centerline of the embankment is shown in Figure 3-1.

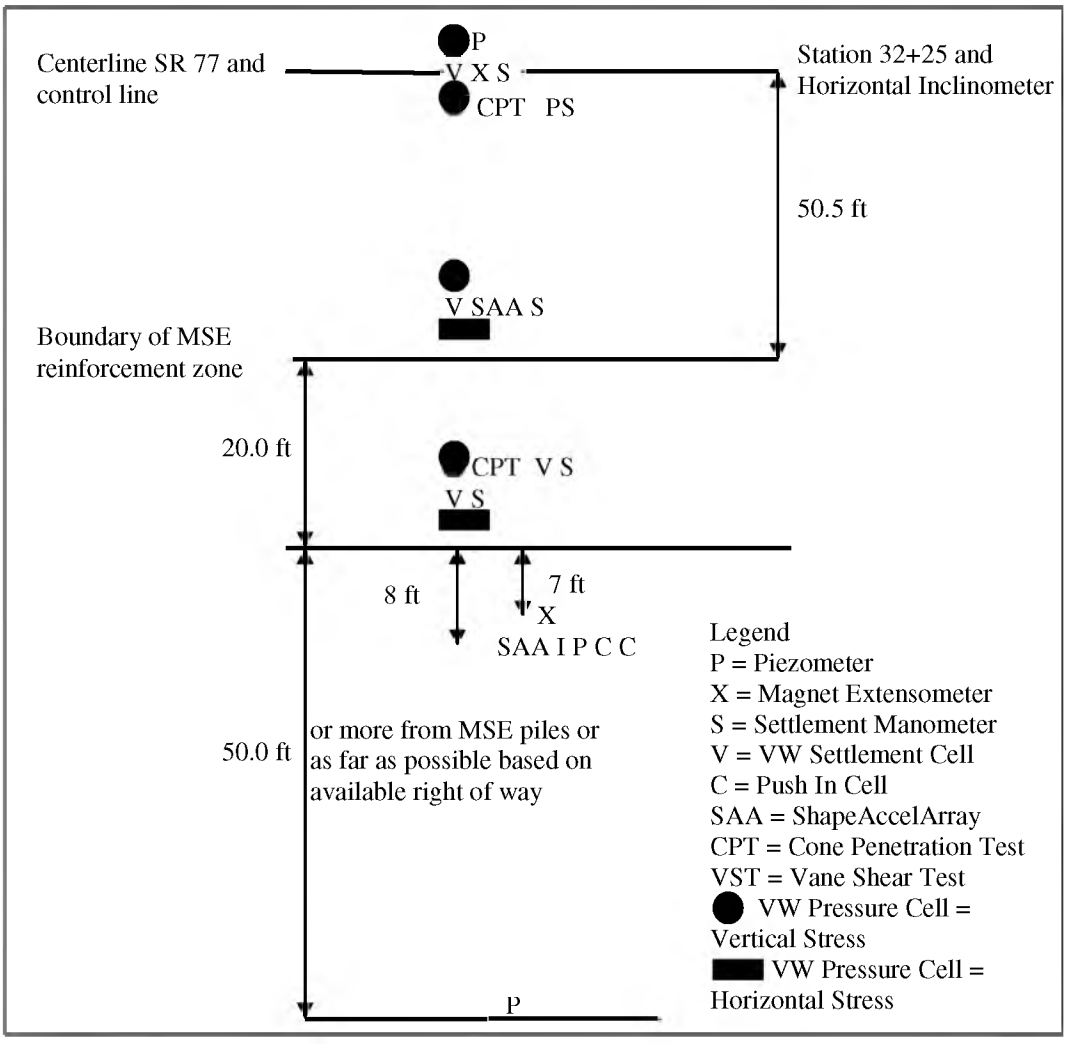

Figure 3-1. Plan view showing locations of instrumentation.

A total of 19 piezometers were installed at three different locations to monitor the excess pore pressure developed from construction of the embankment plus the surcharge. Table 3-1 shows the different locations and depths for the installed piezometers.

Twenty spider magnets were installed for the purpose of monitoring vertical settlement within layers of foundation soil. The depths and locations for these magnets are provided in Table 3-2.

The depths at which the piezometers and the spider magnets were installed for two locations (centerline and outside the MSE wall) are shown on the Cone Penetration Test (CPT) logs in Figure 3-2 and Figure 3-3 (More details on the CPT logs are provided in Chapter 4).

A total of six settlement manometers were installed, with two manometers installed at three different locations. Settlement platforms were located at the centerline of the embankment, 30 ft south of the centerline, and 8 ft inside the MSE wall.

A horizontal inclinometer was installed underneath the embankment approximately at station 32+25. The vertical inclinometer along with a ShapeAccelArray was placed approximately 8 ft outside the MSE wall.

Vibrating wire settlement cells were installed slightly below the original ground surface at three different locations – 4 ft right of centerline, 24 ft right of centerline, and 48 ft right of centerline.

Pressure cells to measure changes in both horizontal and vertical total stress were installed 4 ft right of centerline, 22 ft right of centerline, and 46 ft right of centerline.

Push-in cells were located 3 ft south of the MSE wall and were installed at depths of 11.0 ft, 15.5 ft, and 27.0 ft.

Table 3-1. Locations and depths of piezometers installed to monitor excess pore pressures.

Depth (ft) of Piezometers at Locations Shown		
Centerline	8-ft Outside South MSE wall	Free Field
5.8	16.5	16.5
16.5	50.0	50.0
33.0	68.0	68.0
37.3	79.0	79.0
41.0	115.0	115.0
58.0		
64.0		
78.0		
118.0		

Table 3-2. Depths and locations of spider magnets for monitoring vertical settlement.

Depth (ft) of Spider Magnets at Locations Shown	
7 ft Right of Centerline	3 ft Outside South MSE Wall
3.0	7.0
8.5	11.0
14.0	15.5
20.0	27.5
29.0	73.0
45.0	85.0
54.0	102.0
88.0	109.0
105.0	120.0
112.0	
124.0	

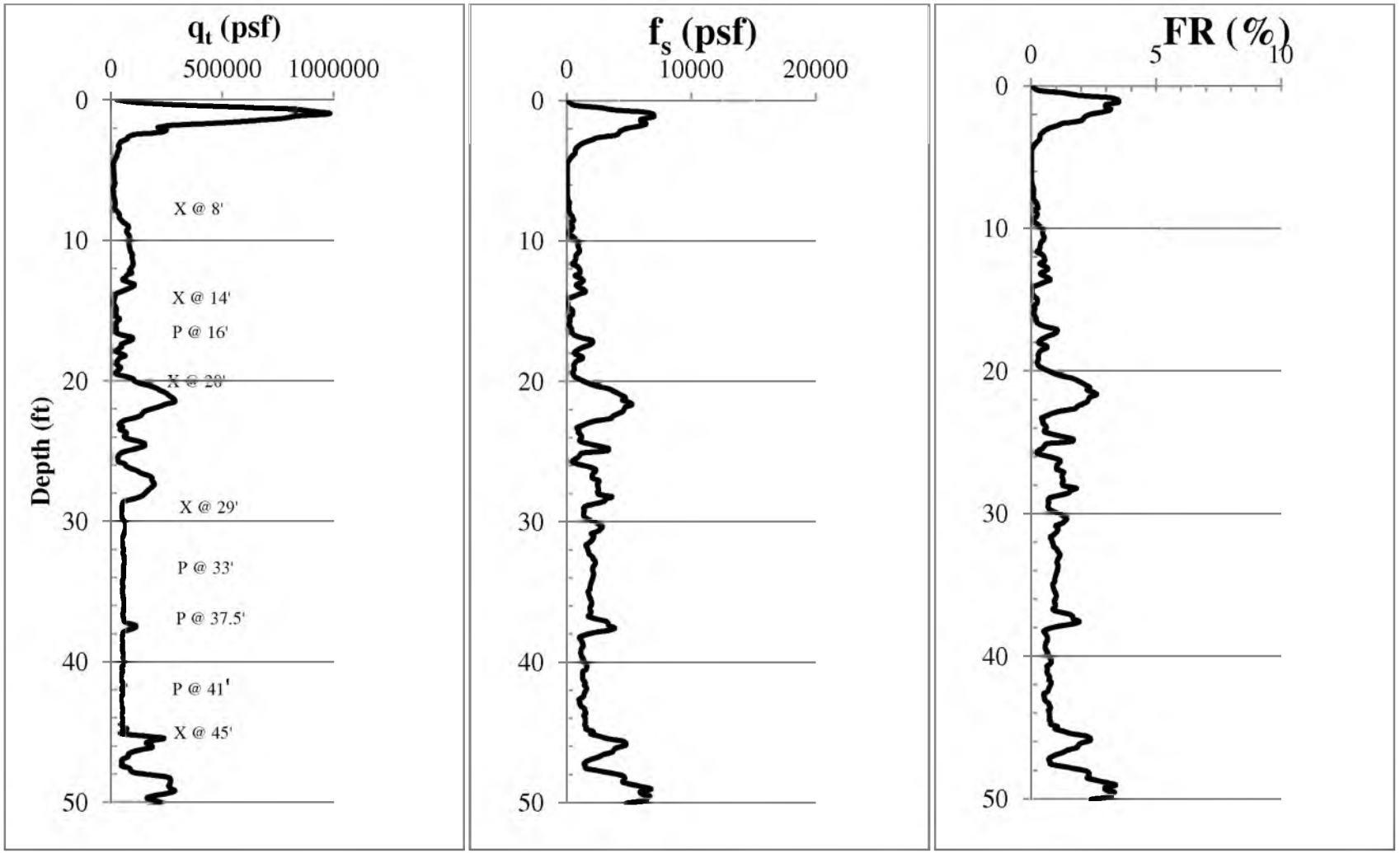

Figure 3-2. Vertical locations of vibrating wire piezometers and magnet extensometers shown on CPT logs for the location at the centerline of the embankment.

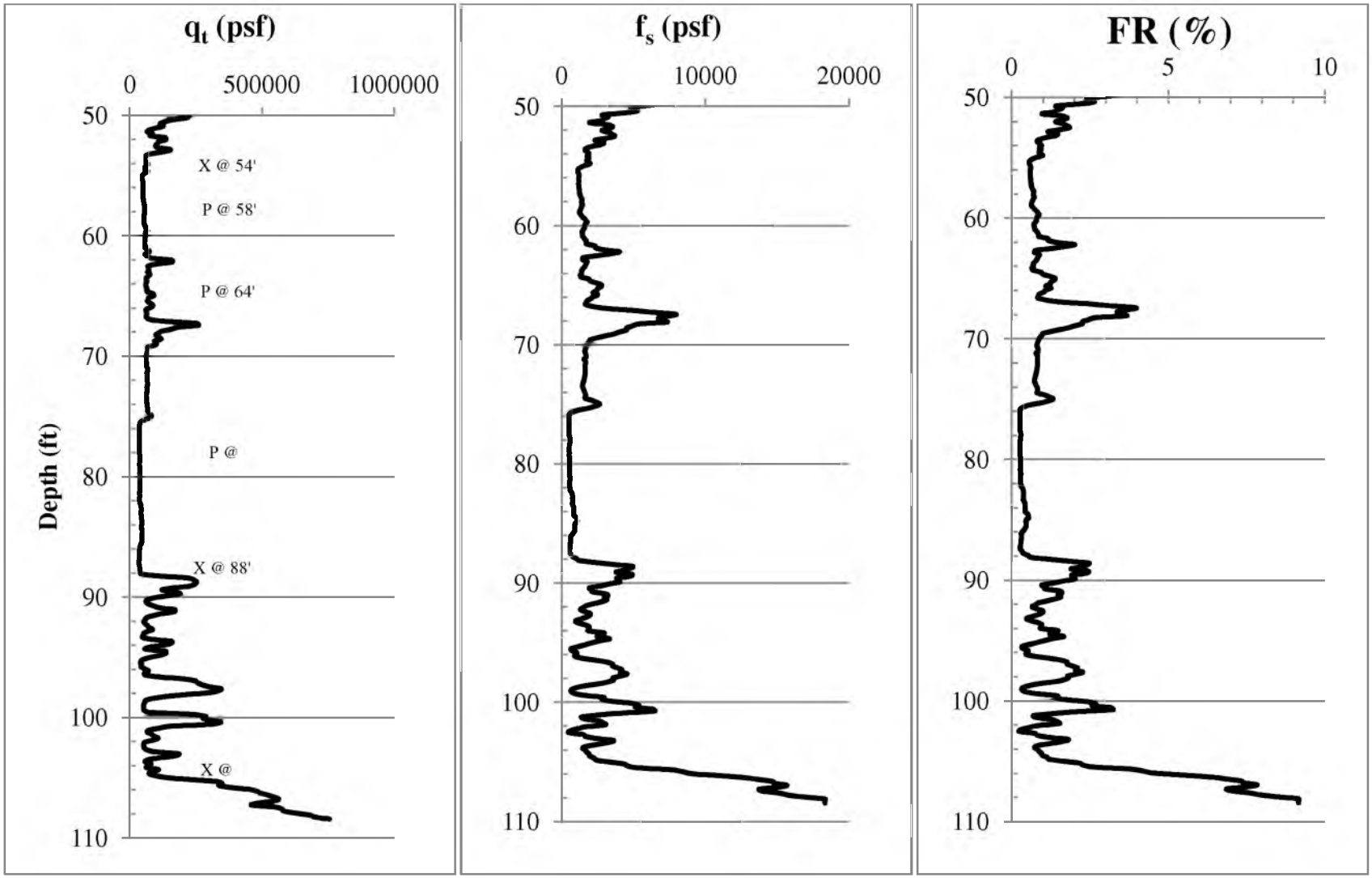

Figure 3-2 (Continued).

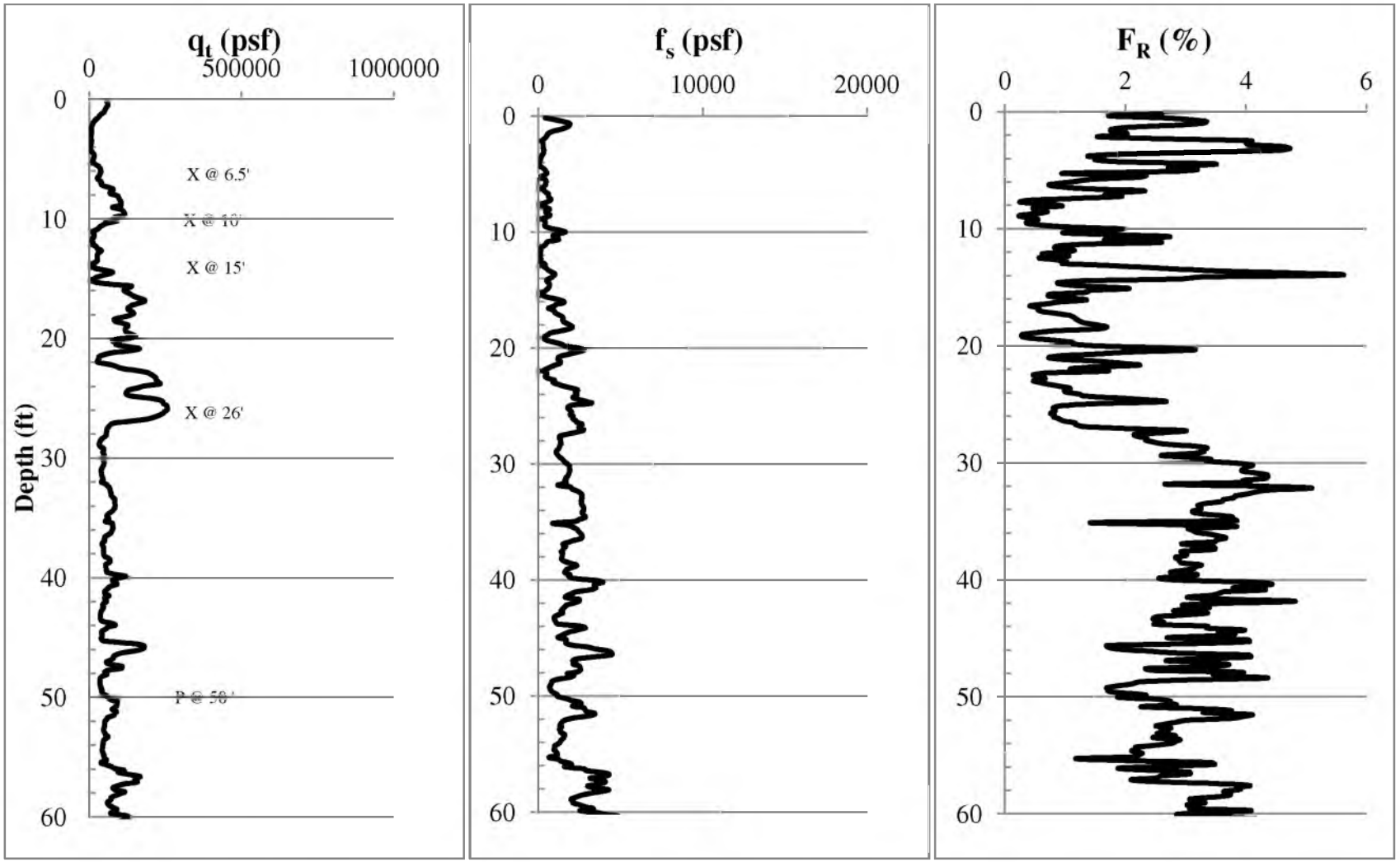

Figure 3-3. Vertical locations of vibrating wire piezometers and magnet extensometers shown on CPT logs for the location 8 ft south of the MSE wall.

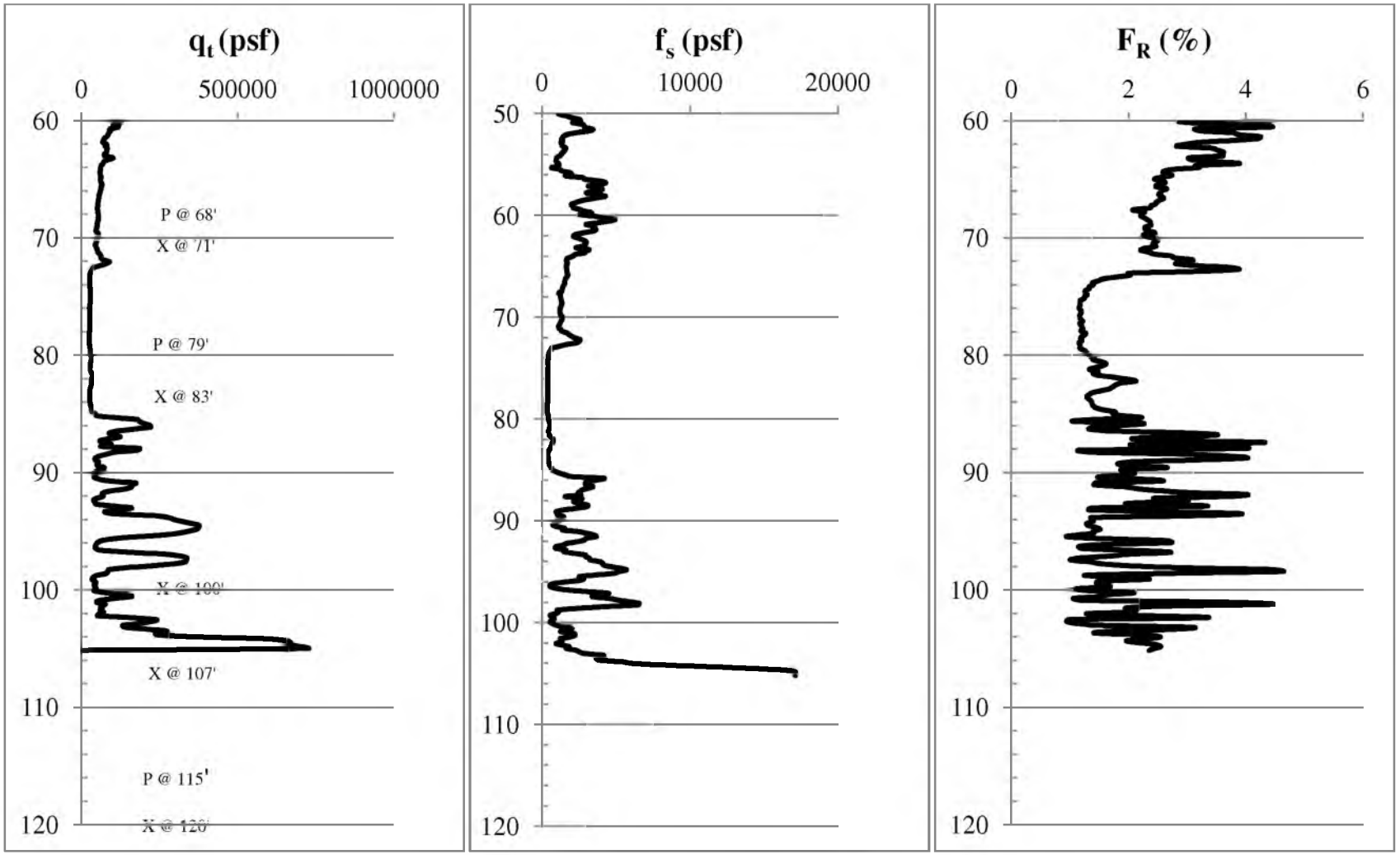

Figure 3-3 (Continued).

3.2 Data Collection

Data collection involved gathering numerical data from all the field instrumentation on site. A Campbell Scientific data collector was used to obtain hourly readings for the vibrating wire instruments. A vertical inclinometer probe and a horizontal inclinometer probe were used to obtain readings to determine vertical and horizontal deformation. Readings from the settlement manometers were collected by measuring the level of fluid inside the manometers. Elevation readings were measured with a surveying level and surveying rod. Data collection started in April 2009, shortly after the field instrumentation had been installed.

3.3 Frequency

Collecting data for the SR 77 embankment occurred on a weekly basis throughout the construction of the embankment, and a month after removal of surcharge occurred. Readings were taken on a biweekly basis as the construction of base course occurred. After placement of asphalt, data collection continued on a monthly basis. Vibrating wires were read on an hourly basis through December 1, 2009. Data from the SAA were collected hourly through December 1, 2009. The last set of vibrating wire piezometer readings was taken on September 27, 2011.

3.4 Data Reduction

Data reduction occurred on a weekly basis during the construction of the embankment and a month after removal of surcharge. Upon completion of placement of the base course material, data reduction occurred on a biweekly basis. As final asphalt was placed, data reduction occurred on a monthly basis. Data reduction was completed

with the purpose of determining the behavior of the embankment and the foundation soils. Numerical readings obtained during the data collection process were calibrated and analyzed in a spreadsheet. Various plots were developed during the data reduction process for analysis purposes. The results from the data reduction for the all field instrumentation will be discussed in detail in Chapter 5.

4 GEOTECHNICAL INVESTIGATION

The geotechnical evaluation for the research embankment site located at the intersection of SR 77 and 1500 West in Springville, Utah will be discussed in this chapter. The geotechnical field investigation included a site investigation, drilling, sampling, and multiple in situ tests. These tasks will be discussed in Section 4.1. The laboratory tests performed on the material samples obtained during the field investigation will be discussed in Section 4.2.

4.1 Site Investigation

4.1.1 Drilling and Sampling

The purpose of geotechnical investigation on the SR 77 embankment was to define the subsurface conditions of the embankment using drilling and in situ sampling to obtain undisturbed soil samples for future testing. Drilling and sampling of subsurface soil was performed by Bedke Geotechnical Services. Undisturbed piston samples were obtained by way of thin-walled Shelby tubes. Bedke Geotechnical Services began drilling and collecting samples on March 4, 2009 using a hollow stem auger. Samples were obtained every 5 ft starting at 10 ft below the original ground and finishing at 105 ft. A sample obtained using standard penetration blow counts was obtained at a depth of 35

ft. Drilling and sampling were completed upon reaching a depth of 110 ft, because a thick incompressible sand layer was encountered.

4.1.2 Cone Penetration Tests

Two cone penetrometer tests (CPTs) were conducted by ConeTec at the SR 77 research project site. The first CPT was conducted at the centerline of the embankment. The second CPT was performed 8-ft south of the south MSE wall. Results from the two CPTs are shown in Figure 4-1and Figure 4-2. The parameters shown in these figures are the total cone tip resistance, q_t, the sleeve friction resistance, f_s, the cone pore water pressure, u, the friction ratio, R_f, and the soil behavior type (SBT).

The CPT plots provided information regarding the variability in the underlying soils. Magnet extensometer spider magnets were positioned at depths in the underlying soil determined from the CPT results to delineate boundaries between layers of soil.

4.1.3 Vane Shear Tests

In addition to the drilling, sampling, and CPT tests, vane shear tests were performed within the centerline borehole of the research embankment. Five Vane Shear Tests were performed at three different depths within this borehole - 4.8 ft, 10.0 ft, and 12.4 ft. Results from the vane shear tests showing the torque of the vane plotted against the angle of rotation are shown Figure 4-3.

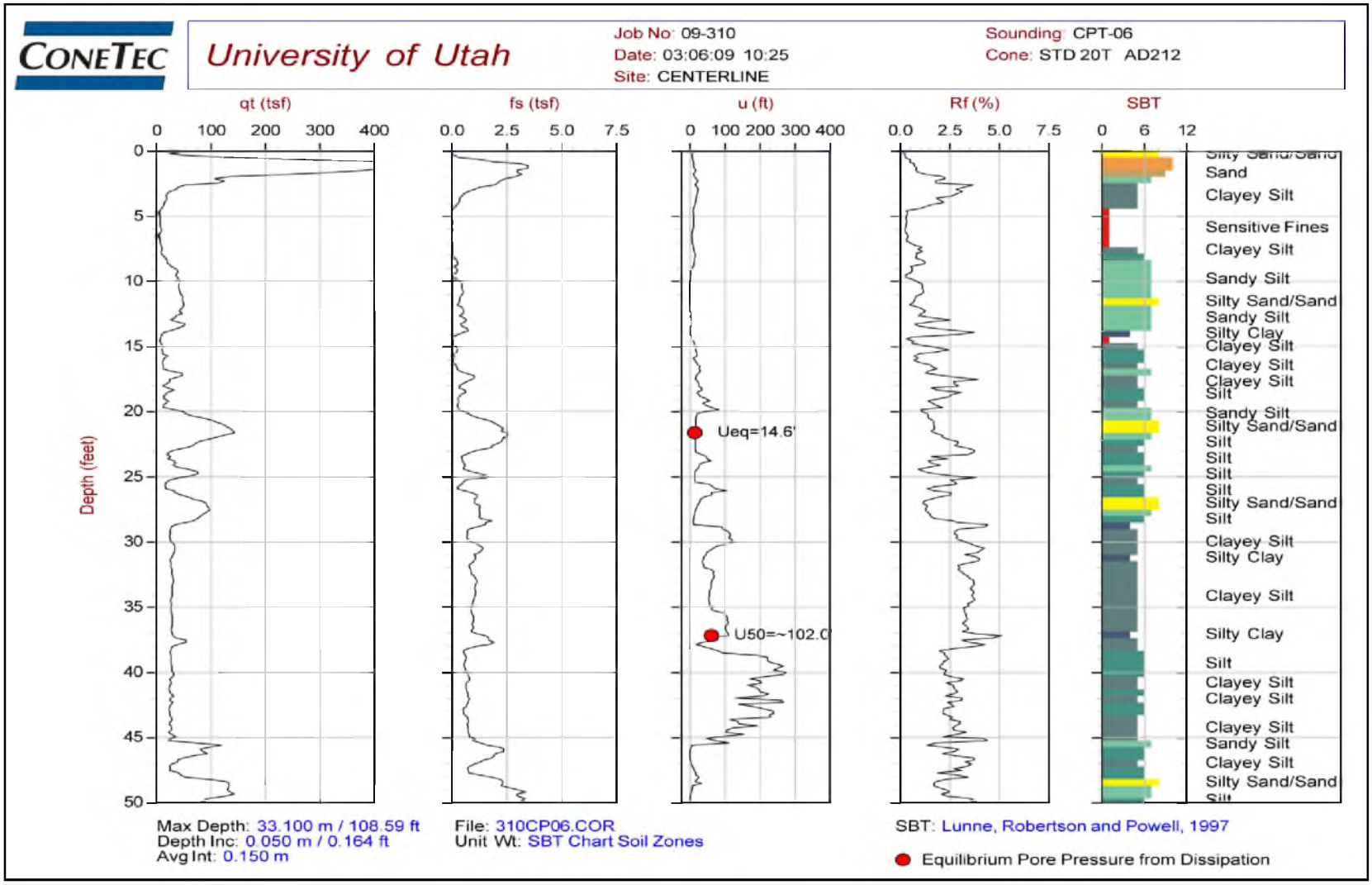

Figure 4-1. CPT log for SR 77 located at centerline

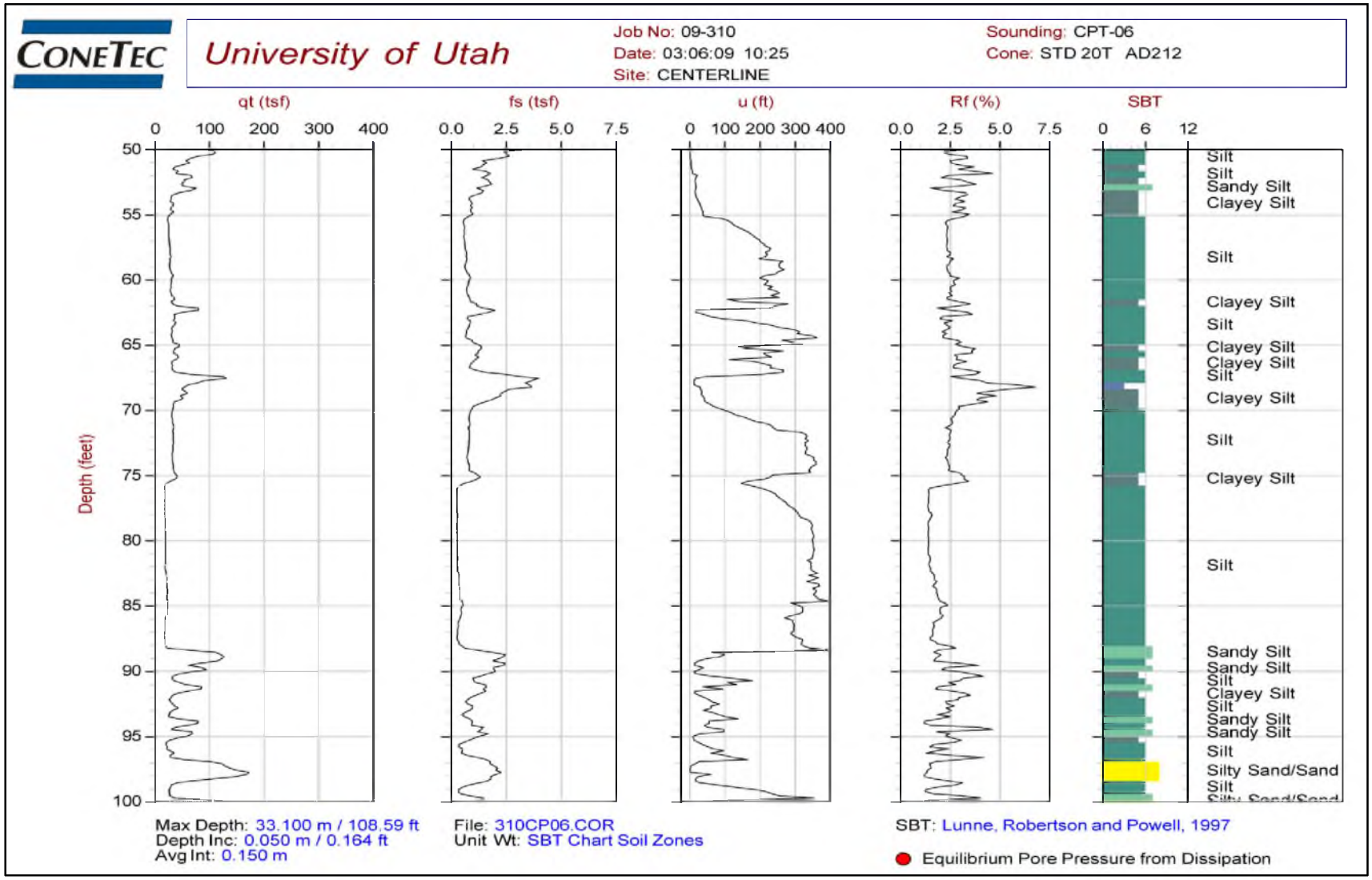

Figure 4.1 (Continued).

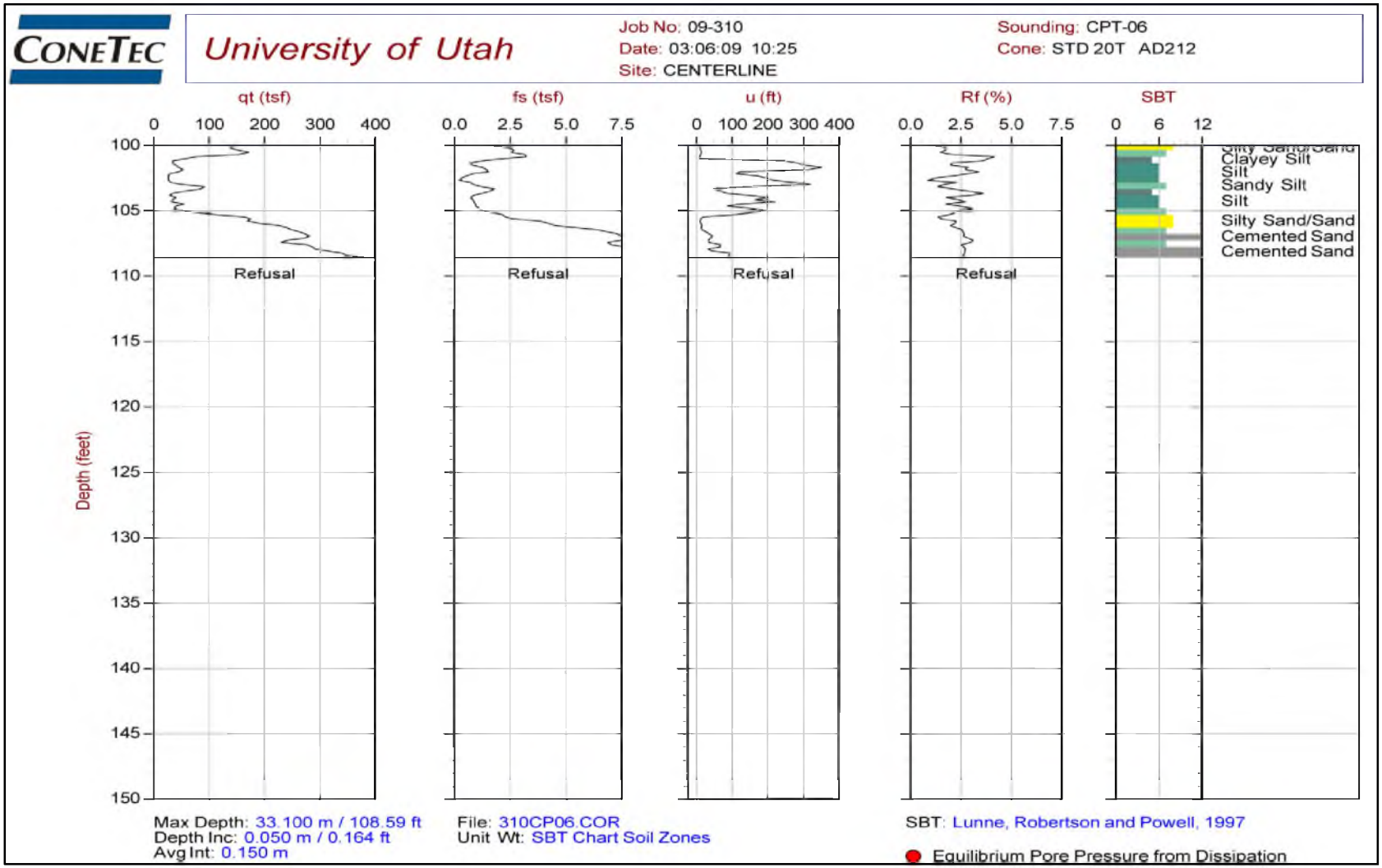

Figure 4.1 (Continued).

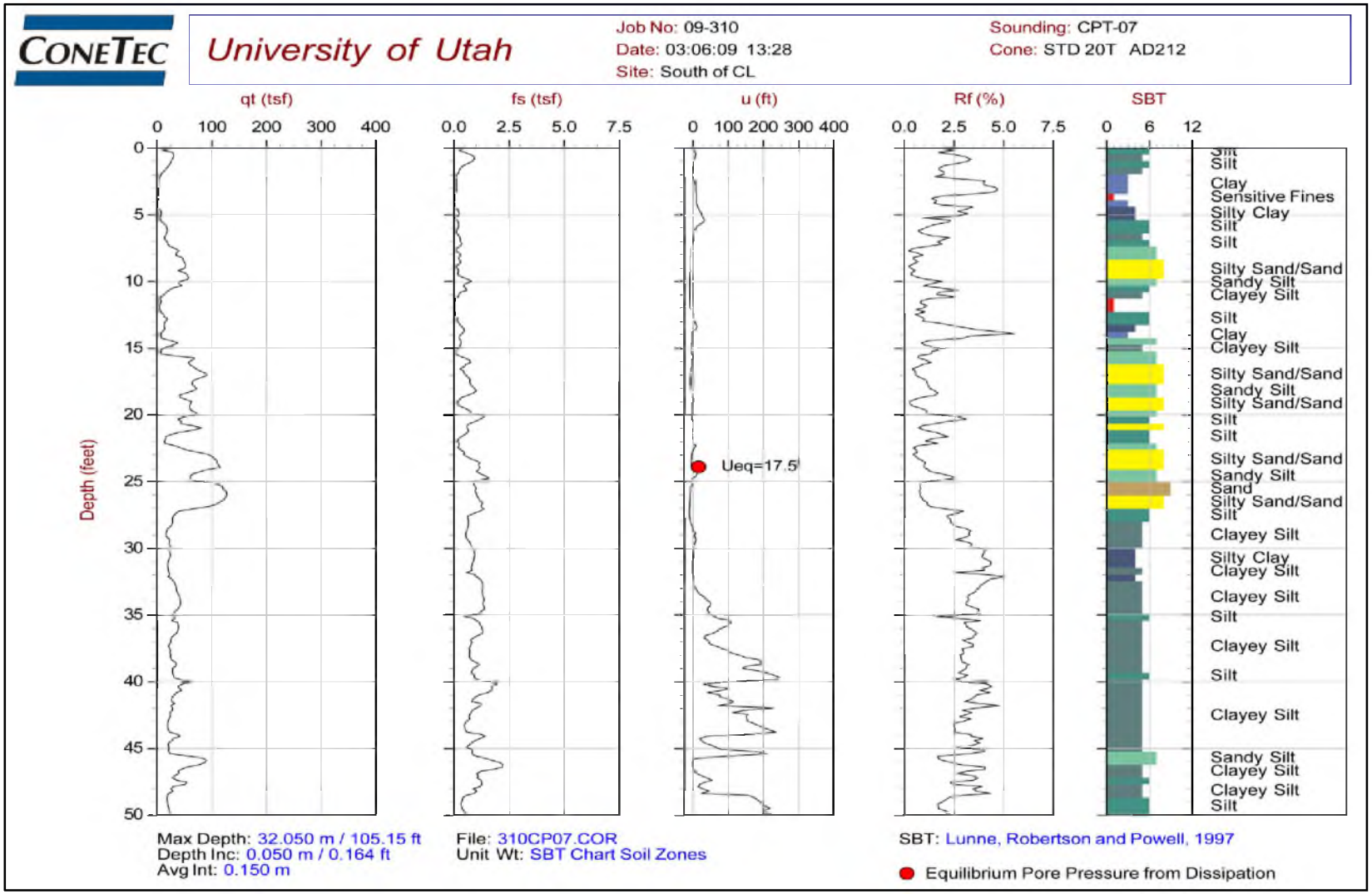

Figure 4-2. CPT log for SR 77 located 8 ft outside the south MSE wall.

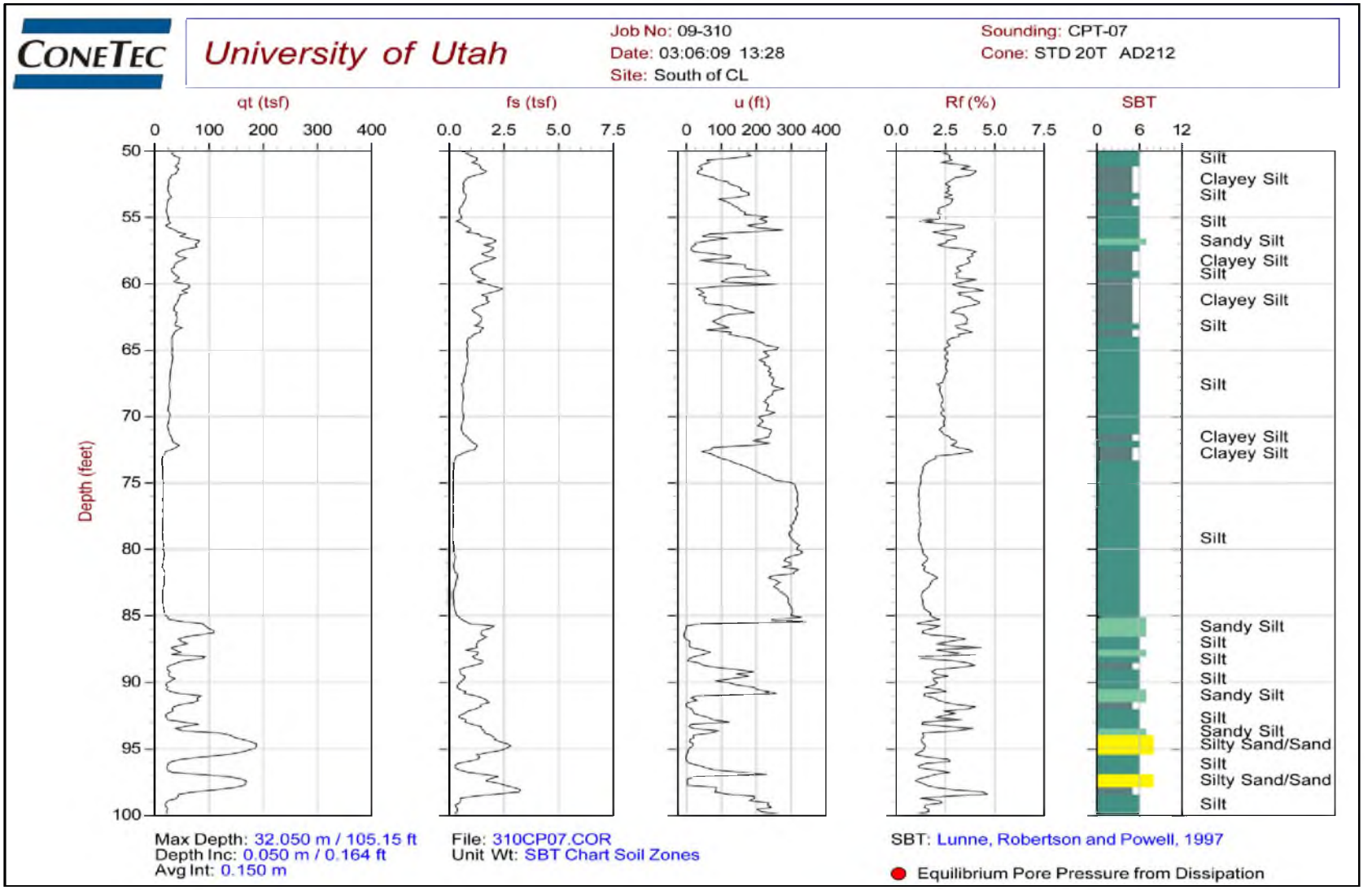

Figure 4.2 (Continued).

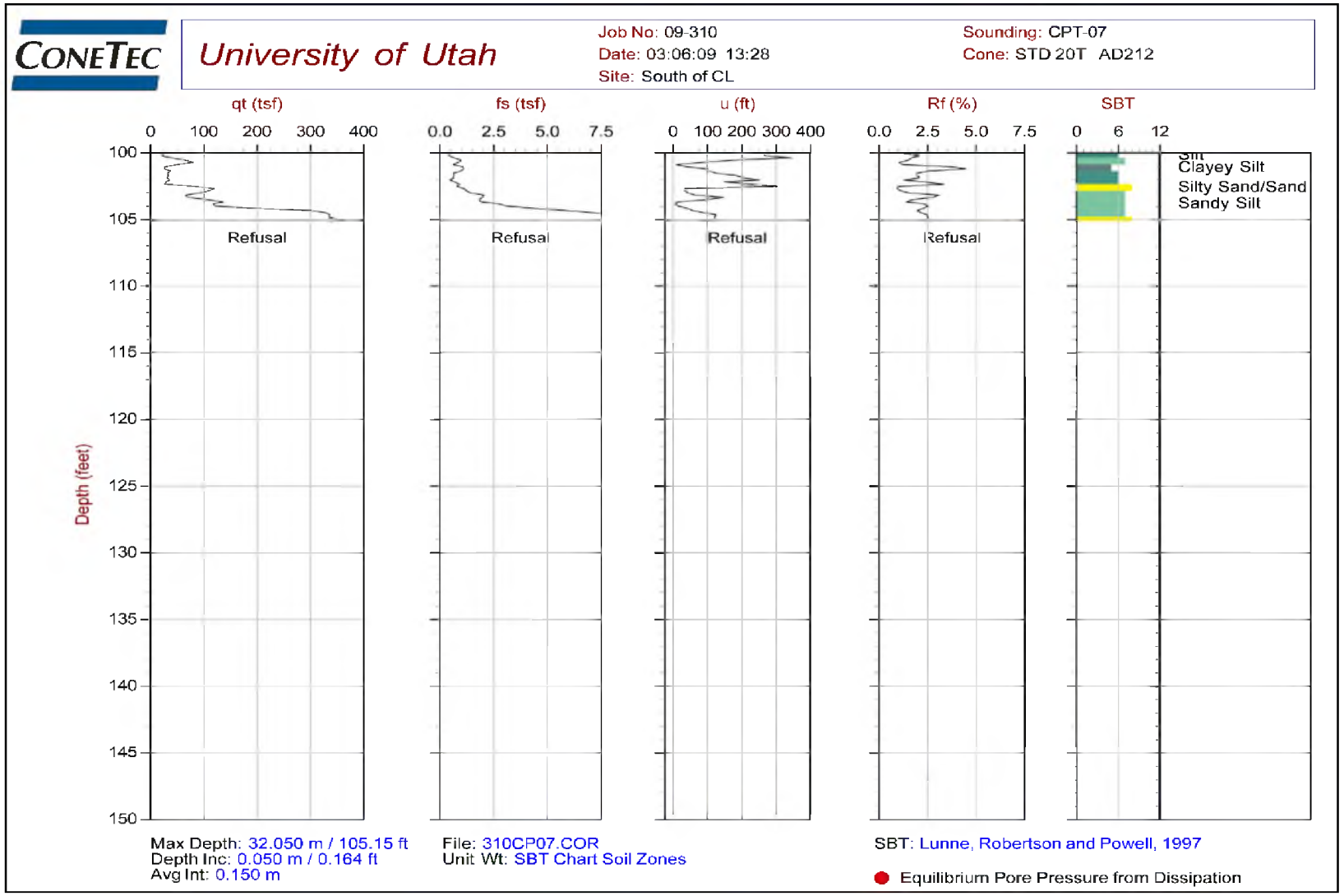

Figure 4.2 (Continued).

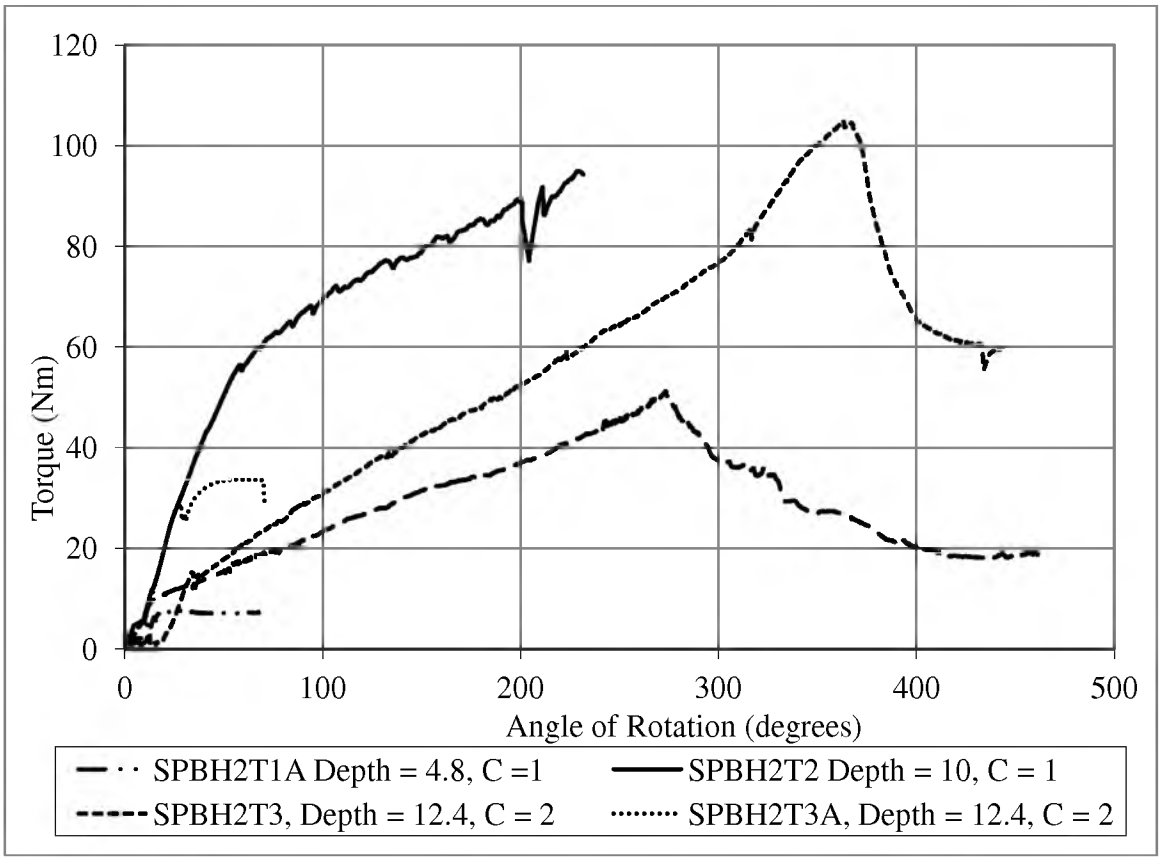

Figure 4-3. Results from field vane shear tests.

Undrained shear strengths predicted from the results of the vane shear tests using Eq. 2-1 are plotted versus depth within the borehole in Figure 4-4.

4.2 Laboratory Investigation

Undisturbed piston samples previously discussed in Section 4.1.1 were taken to the geotechnical laboratory of the Department of Civil and Environmental Engineering at the University of Utah for testing. Material indexing and soil classification tests conducted include sieve and hydrometer analysis, liquid limit, plastic limit, in situ moisture content, and total unit weight.

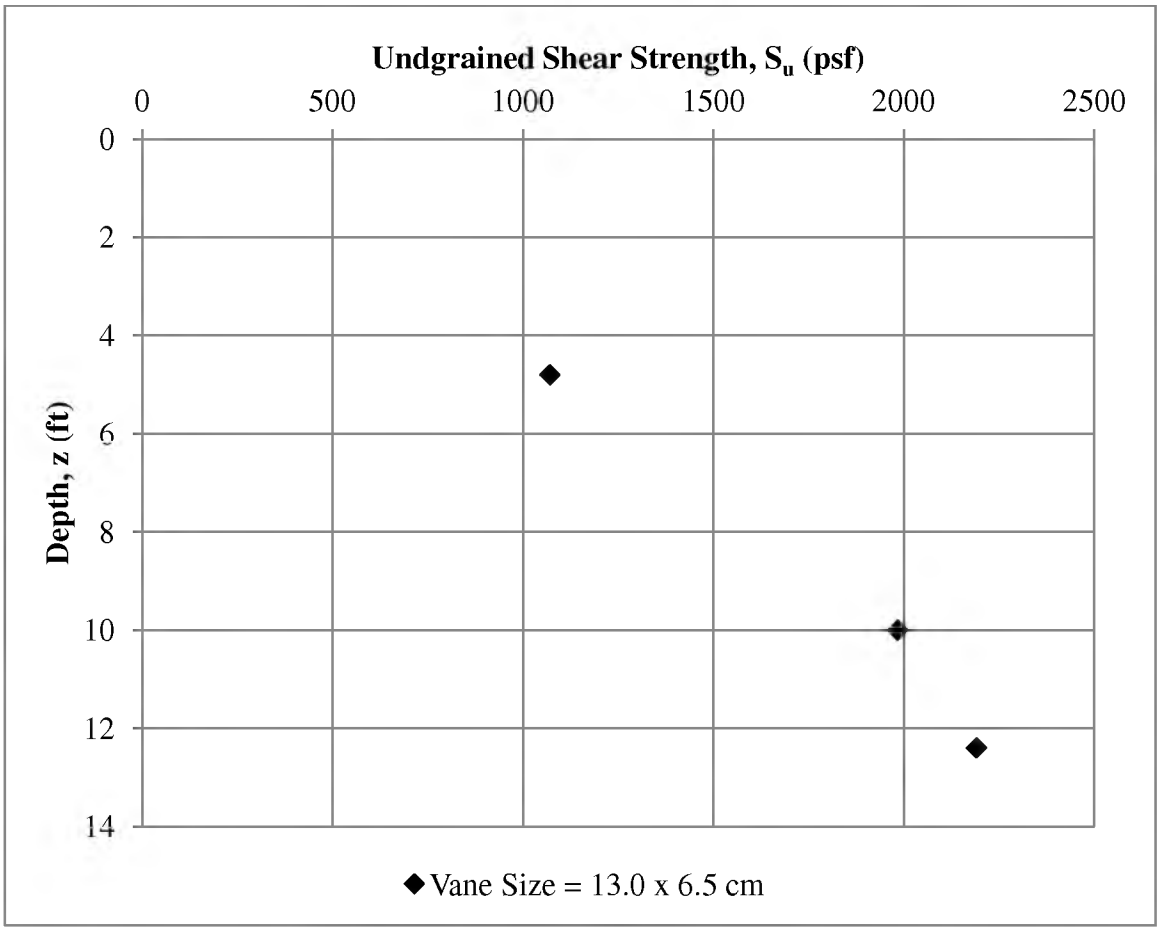

Figure 4-4. Undrained shear strength from vane shear tests plotted versus depth.

Soil classifications of the material samples are presented in Section 4.2.1. Unit weights were determined and are discussed in Section 4.2.2. Parameters determined from one-dimensional constant rate of strain (CRS) consolidation tests, including preconsolidation stress, compression indices, coefficient of consolidation, and permeability are presented in Section 4.2.3 and Section 4.2.4.

4.2.1 Soil Classification

Each undisturbed piston sample was classified following the Unified Soil Classification System (USCS) method (ASTMD 2487) and American Association of

State Highway and Transportation Officials (AASHTO) method. Grain size distribution, commonly referred to as particle size distribution tests, and hydrometer analyses were performed according to ASTM D422. The liquid limit (LL) and plastic limit (PL) tests were performed according to ASTM D4318-05. Results for PL, LL, plasticity index, USCS classification, and AASHTO classification are summarized in Table 4-1.

Table 4-1. Material Index Properties and Soil Classifications of Shelby Tube Samples

Sample No.	Sample Depth (ft)	Liquid Limit (%)	Plastic Limit (%)	Plasticity Index (%)	USCS	AASHTO
1A	5.0	23	21	2	CL-ML, silty clay	A-6(1)
1	10.3	NP	NP	---	SM, silty sand	A-2-4 (0)
2	15.3	24	20	4	CL-ML, silty clay w/sand	A-6 (1)
3	20.4	NP	NP	---	ML, sandy silt	A-4 (0)
4	25.5	NP	NP	---	ML, sandy silt	A-4 (0)
5	30.4	51	24	27	CH, fat clay	A-7-6 (31)
7	39.8	46	32	14	CL, lean clay	A-7-5 (15)
8	45.3	NP	NP	---	ML silt w/ sand	A-4 (0)
9	50.3	30	23	7	CL, lean clay with sand	A-4 (4)
10	55.4	33	23	10	CL, sandy lean clay	A-4 (11)
11	60.5	37	25	12	CL, lean clay with sand	A-4 (14)
12	65.7	27	17	10	CL, lean clay with sand	A-4 (7)
13	70.4	37	22	15	CL, lean clay	A-6 (16)
14	75.6	33	27	6	CL, lean clay	A-4 (0)
15	80.5	57	24	33	CH, fat clay	A-7-6 (38)
16	85.3	57	28	29	CH, fat clay	A-7-6 (38)
17	90.5	NP	NP	---	SM, silty sand	A-2-4 (0)
18	95.2	31	18	13	CL, lean clay	A-4 (13)
19	100.3	NP	NP	---	MH, elastic silt with sand	A-4 (0)
20	105.5	NP	NP	---	MH, elastic silt	A-4 (0)

4.2.2 Unit Weights

The total unit weight and in situ moisture content measurements were determined from the CRS test specimens that were trimmed from undisturbed piston samples. The undisturbed piston samples were trimmed to a 1.0-in thick by 2.5-in diameter CRS specimen. The unit weight (γ) and in situ moisture content (w) of trimmed CRS test specimens for each depth below the original ground surface (z) are summarized in Table 4-2.

Table 4-2. Unit weight and moisture content from the undisturbed CRS test specimens.

Depth (ft)	γ (pcf)	W (%)
5.0	112.8	22.6
10.3	126.9	25.4
16.0	112.0	28.3
20.4	127.8	25.9
25.5	121.3	26.2
30.4	127.8	24.4
40.0	111.4	26.1
45.3	124.5	19.0
50.3	127.0	21.9
55.4	122.1	23.6
60.5	119.1	25.8
65.7	112.2	27.0
70.4	121.4	19.6
75.6	127.3	24.8
80.5	112.1	36.8
85.3	111.6	19.5
90.5	120.4	30.3
95.3	119.0	29.1
100.3	124.6	25.8
105.5	121.8	25.4

4.2.3 Constant Rate of Strain Consolidation Tests

Constant Rate of Strain consolidation stress tests were performed on each undisturbed piston sample to determine the preconsolidation stress, compression indices, coefficient of consolidation, and permeability for each depth sampled. The results for preconsolidation stress (σ_p') using Ozer's (2005) local correlation, Kulhaway and Mayne's (1990) empirical formula, the strain energy method, and Casagrande's method will be presented in Section 4.2.3.1. Compression indices determined from percent strain versus logarithm of effective stress plots will be presented in Section 4.2.3.2. Results for coefficient of consolidation and permeability will be presented in Sections 4.2.3.3.

4.2.3.1. Preconsolidation stress was estimated using Ozer's (2005) local correlation for Lake Bonneville clay (Eq. 2-21), Kulhawy and Mayne's (1990) empirical formula (Eq. 2-22), the strain energy method, and Casagrande's method and is shown in Table 4-3. Judgment was needed in determining the value for preconsolidation stress for settlement calculations. Many of the logarithm of effective stress versus percent strain plots did not exhibit a classical breaking point as needed for Casagrande's method. The preconsolidation stresses estimated from Casagrande's method and strain energy method were compared at each CRS specimen depth.

The preconsolidation stress used in determining settlement behavior was determined from the strain energy for two reasons: (1) Plots developed from the work

method show a distinct point of curvature that allowed for a reasonable estimate of σ_p' to be made while the maximum point of curvature was difficult to choose for Casagrande's method due to the smoothness of the stress-strain curve and (2) plots from the strain energy method yielded more realistic results for determining the

Table 4-3. Comparison of preconsolidation stress using CasaGrande's method, strain energy method, Ozer (2005) local correlation, and Kulhawy & Mayne (1990) general correlation.

Depth (ft)	CasaGrande's Method σ'_p (ksf)	Work Method σ'_p (ksf)	Ozer (2005) σ'_p (ksf)	Kulhawy & Mayne (1990) σ'_p (ksf)
5.0	11.0	11.4	3.0	3.3
16.0	10.6	11.5	4.7	6.0
30.4	11.0	10.8	8.4	19.6
40.0	0.9	0.8	8.3	15.4
55.4	9.5	6.2	8.8	12.9
60.5	10.8	10.6	9.6	15.5
65.7	10.9	11.9	11.3	22.5
70.4	12.7	11.4	10.4	16.3
75.6	12.3	14.8	8.9	9.6
80.5	7.0	7.5	8.8	8.5
85.3	9.5	12.0	10.6	13.8

preconsolidation stress.

4.2.3.2 Virgin and recompression indices ($C_{c\varepsilon}$ and $C_{r\varepsilon}$, respectively) were calculated using strain versus logarithm of stress plots developed from the CRS test onspecimens from the cohesive layers. Results for $C_{c\varepsilon}$ and $C_{r\varepsilon}$ are presented in Table 4-4.

4.2.3.2 The coefficient of consolidation (C_v) was determined from the CRS tests for depths within the cohesive layers. The variation of the C_v with depth is shown in Table 4-5.

4.2.3.4 The coefficient of permeability (k) was determined from the CRS tests for depths within the cohesive layers. The variation of k with depth is shown in Table 4-6. The variation of k varies with depth in a manner similar to C_v.

Table 4-4. Variation of compression indices with depth.

Depth (ft)	$C_{c\varepsilon}$	$C_{r\varepsilon}$
5.0	0.167	0.0292
16.0	0.100	0.0451
30.4	0.111	0.0160
40.0	0.128	0.0110
55.4	0.095	0.0135
60.5	0.116	0.0094
65.7	0.148	0.0302
70.4	0.162	0.0114
75.6	0.178	0.0108
80.5	0.250	0.0206
85.3	0.267	0.0023

Table 4-5. Variation of coefficient of consolidation with depth.

Depth (ft)	C_v (ft^2/day)
5.0	1.00
15.2	1.85
30.4	0.16
39.8	0.08
55.4	0.45
60.5	0.73
70.4	0.03
75.6	0.62
80.5	0.07
85.3	0.05

Table 4-6. Variation of coefficient of permeability with depth.

Depth (ft)	k_{ave} (cm/sec)
5.0	1.53E-07
16.0	1.85E-07
30.4	5.18E-08
40.0	1.35E-08
55.4	4.70E-08
60.5	9.87E-08
65.7	1.24E-03
70.4	8.68E-08
75.6	4.14E-08
80.5	1.38E-08
85.3	1.35E-08

4.2.4 Profile of Index and Engineering Properties

Vertical soil profiles developed from results of the field and laboratory testing are shown in Figure 4.5. Vertical soil profiles containing geologic classification, USCS classification, soil behavior type, effective stress (------), total vertical stress (——), preconsolidation stress (●), virgin compression index (■), recompression index (◆), liquid limit (LL), plastic limit (PL), water content (W_n), and unit weights (γ) can be seen in Figure 4-5.

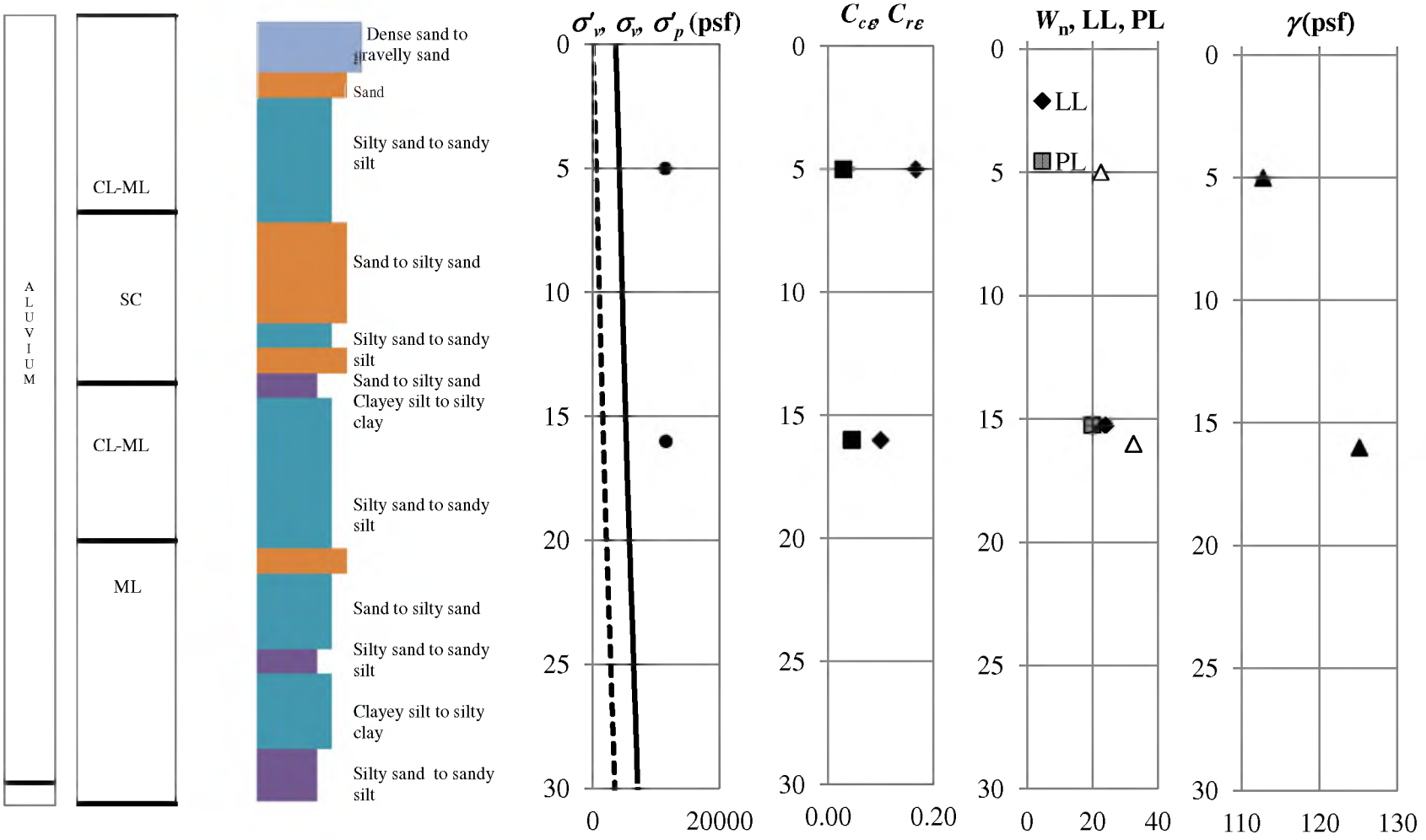

Figure 4-5. Vertical profiles showing geological classification, USCS classification, soil behavior type, vertical stress, virgin compression ratio, recompression ratio, natural water content, liquid limit, plastic limit, and unit weight.

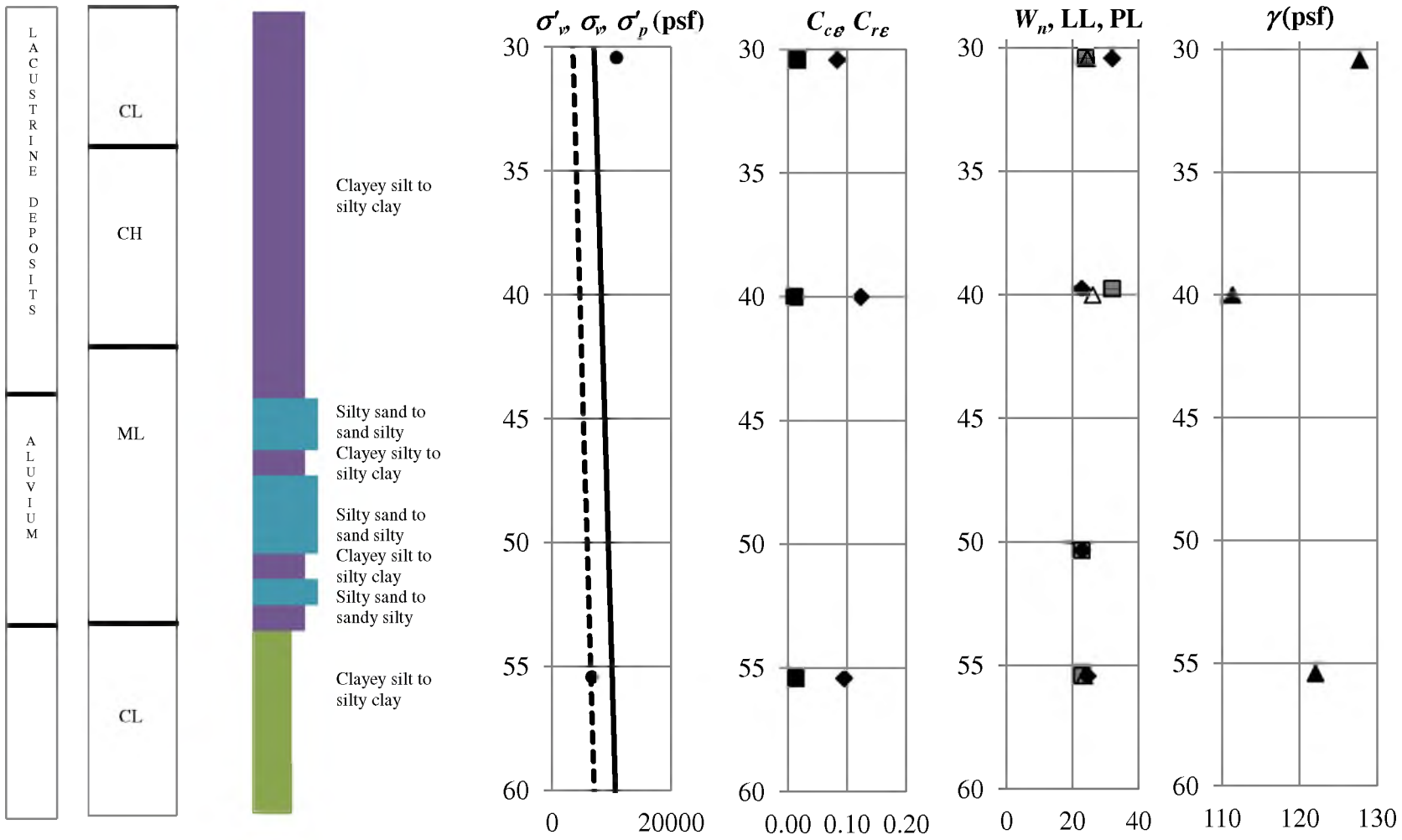

Figure 4-5. (Continued).

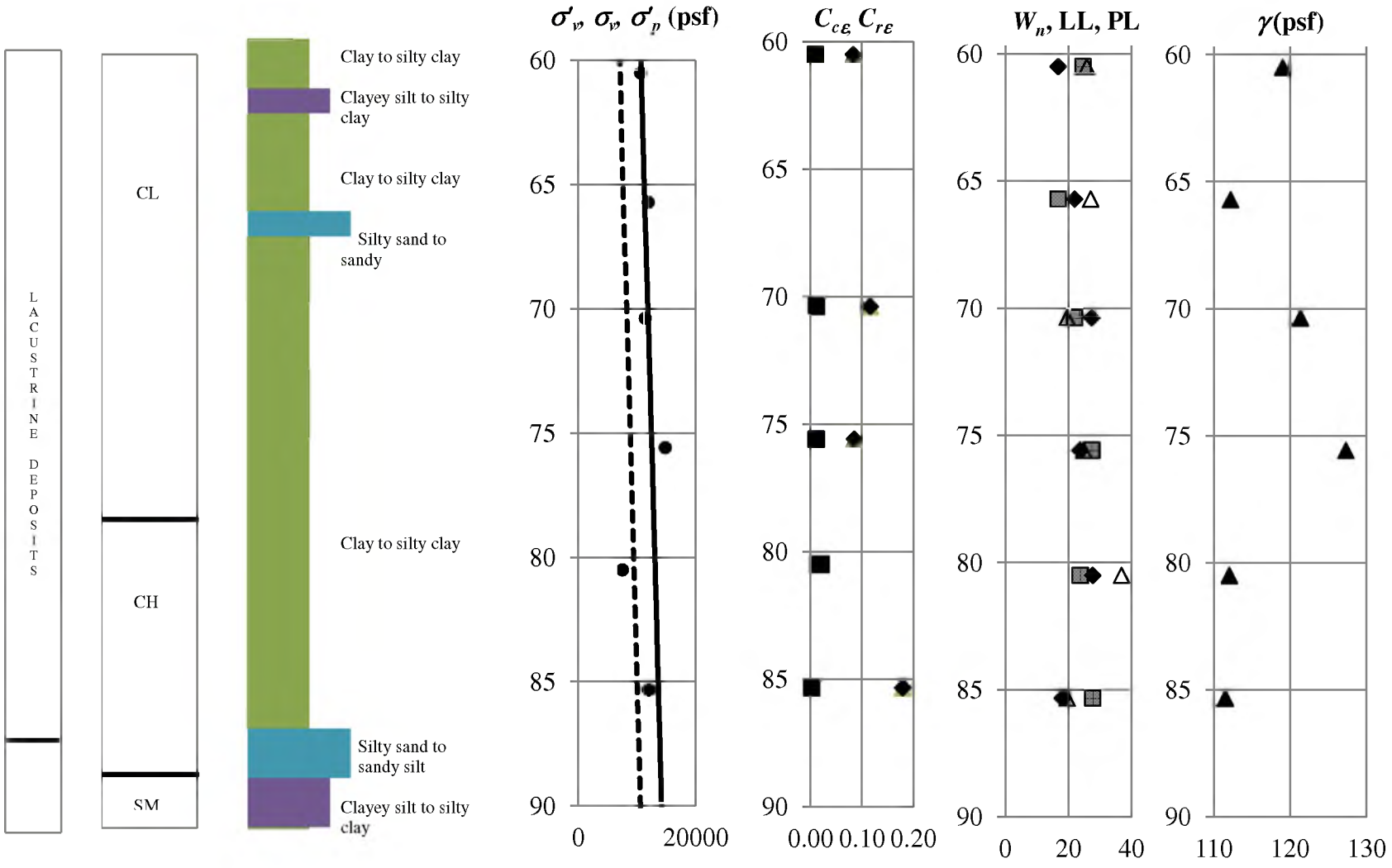

Figure 4-5. (Continued).

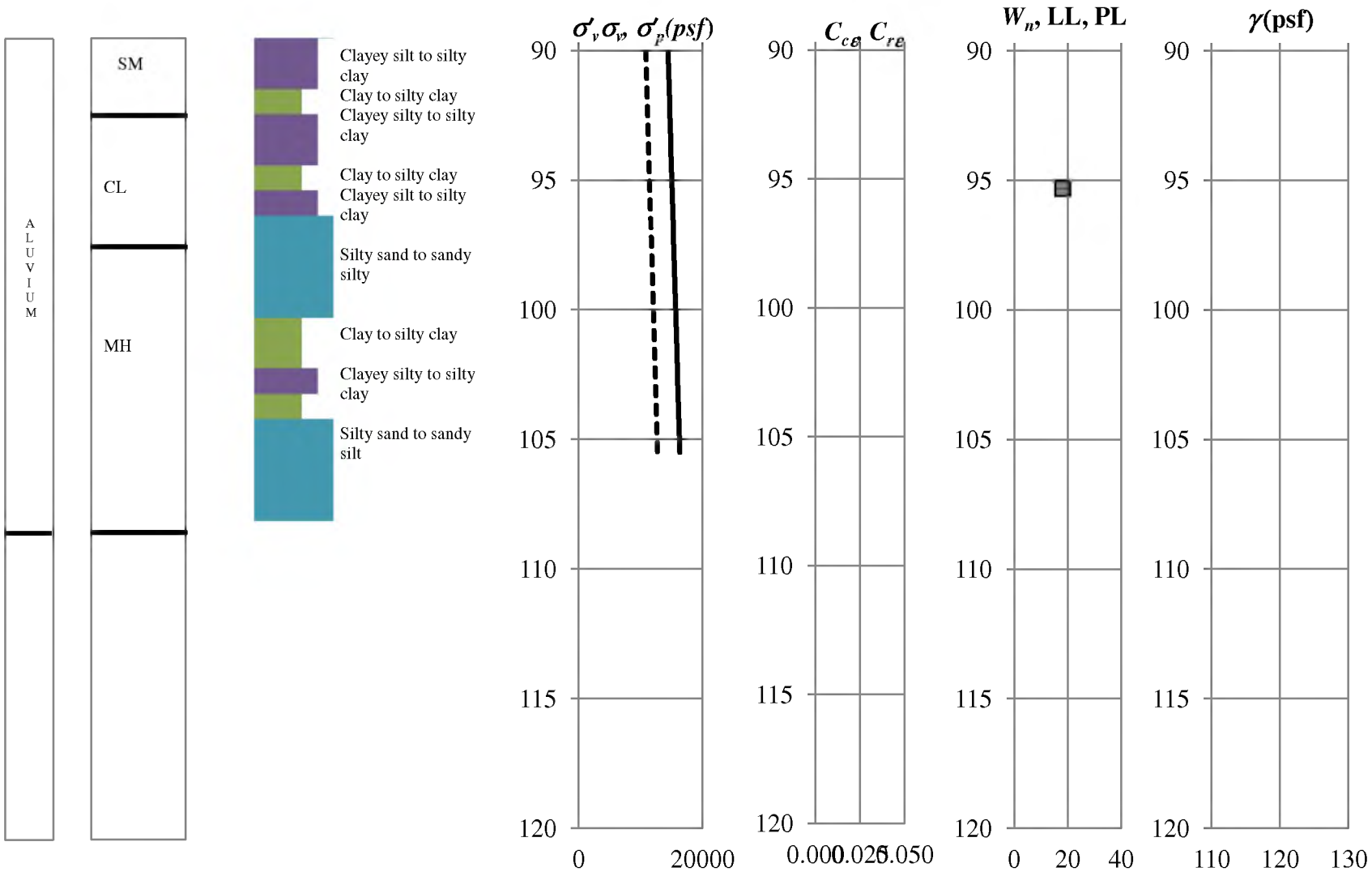

Figure 4.5. (Continued).

5 DATA AND RESULTS FROM FIELD INSTRUMENTATION

Results obtained from field instrumentation will be discussed in detail in Chapter 5. The construction schedule, including preloading, surcharging, and removal of surcharge for the embankment will be provided in Section 5.1. Results from the pressure plates used to measure the vertical stress acting on the foundation of the embankment will be discussed in Section 5.2. Results from the push-in cells for measuring the horizontal pressure acting within the foundation will be provided in Section 5.3. Pore pressure results obtained from the vibrating wire piezometers will be shown in Section 5.4 Results from the instruments monitoring settlement will be shown in Section 5.5. Results for lateral deformation as determined from the vertical inclinometer and ShapeAccelArray will be discussed in Section 5.6.

5.1 Embankment Construction

Construction of the SR 77 embankment began on April 10, 2009 and lasted 196 days. Initial elevations for monitoring placement of fill were obtained in March 2009. The maximum height of the embankment, including surcharge, was 30 ft. The final height of the embankment was 25 ft after removal of 5 ft of surcharge. Constructing the embankment was accomplished in three stages: (1) Placement of fill upon the original ground surface, (2) placement of surcharge, and (3) removal of surcharge. The first stage of construction started April 10, 2009 and lasted until July 7, 2009. During the initial

stage the embankment reached a height of 26.1 ft at the centerline. The second stage of construction included adding surcharge to the existing fill. On July 7, 2009, placement of the surcharge began being placed on the embankment's fill. A total of 5.5 ft of surcharge was added to the existing fill. Surcharge stopped being placed on July 10, 2009. The embankment, including surcharge, reached a maximum height of 30.8 ft at the centerline. The final stage of construction, the removal of surcharge, occurred on September 24, 2009. Stage construction for the SR 77 research embankment is shown in Figure 5-1 and Figure 5-2.

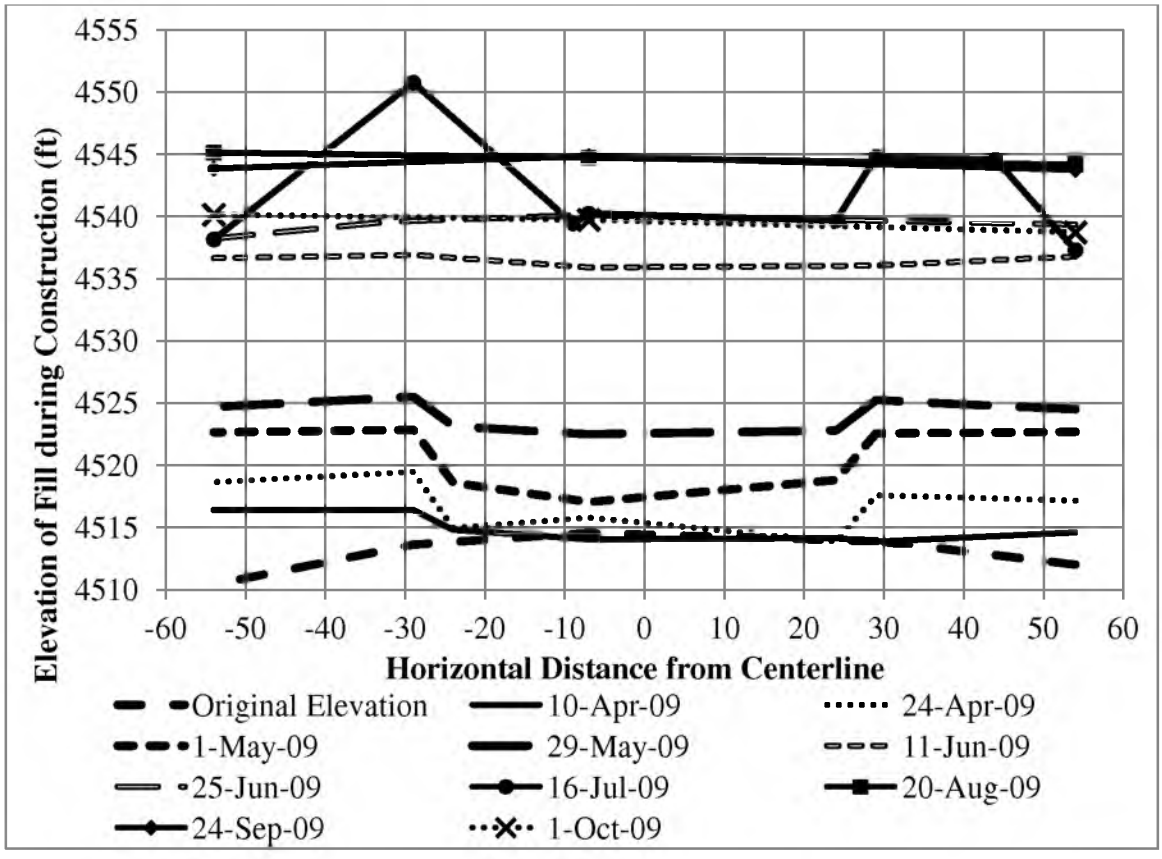

Figure 5-1. Elevation of measured fill at station 32+25 for selected dates during construction, which began on April 10, 2009 and ended on October 1, 2009.

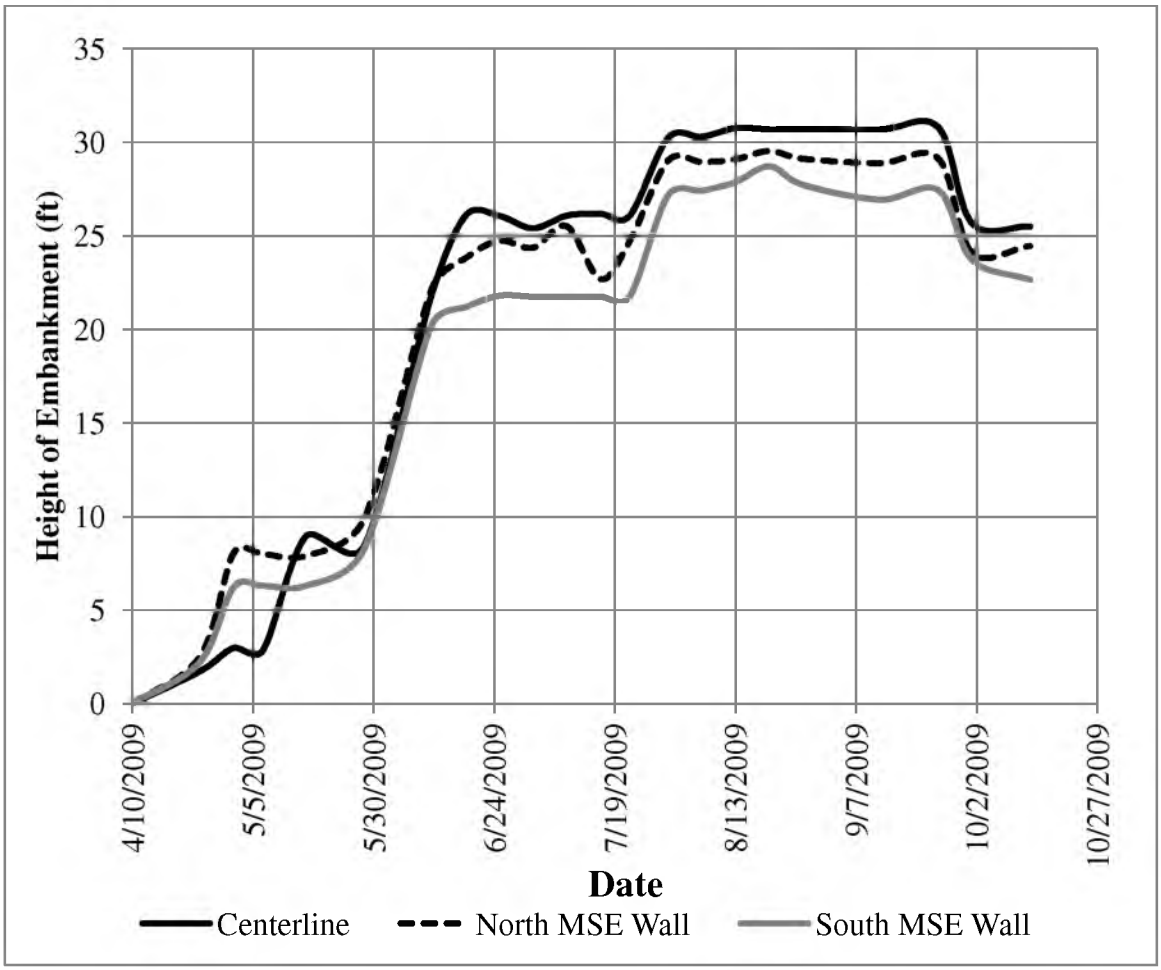

Figure 5-2. Changes in height of the embankment with time at Station 32+25 for three locations across embankment – centerline, north MSE wall, and south MSE wall.

5.2 Vertical Stress

The variations in induced vertical stresses ($\Delta\sigma_v$) at the original ground surface, as measured from four vibrating wire pressure cells oriented horizontally (see Figure 3-1), are shown in Figure 5-3 and Figure 5-4 as a function of time.

Two pressure cells were located 4 ft right of centerline, one was located 22 ft right of centerline, and one was located 46 ft right of centerline. Induced $\Delta\sigma_v$ at the centerline, 22 ft right of centerline and 46 ft right of are shown in Figure 5-3. The greatest amount

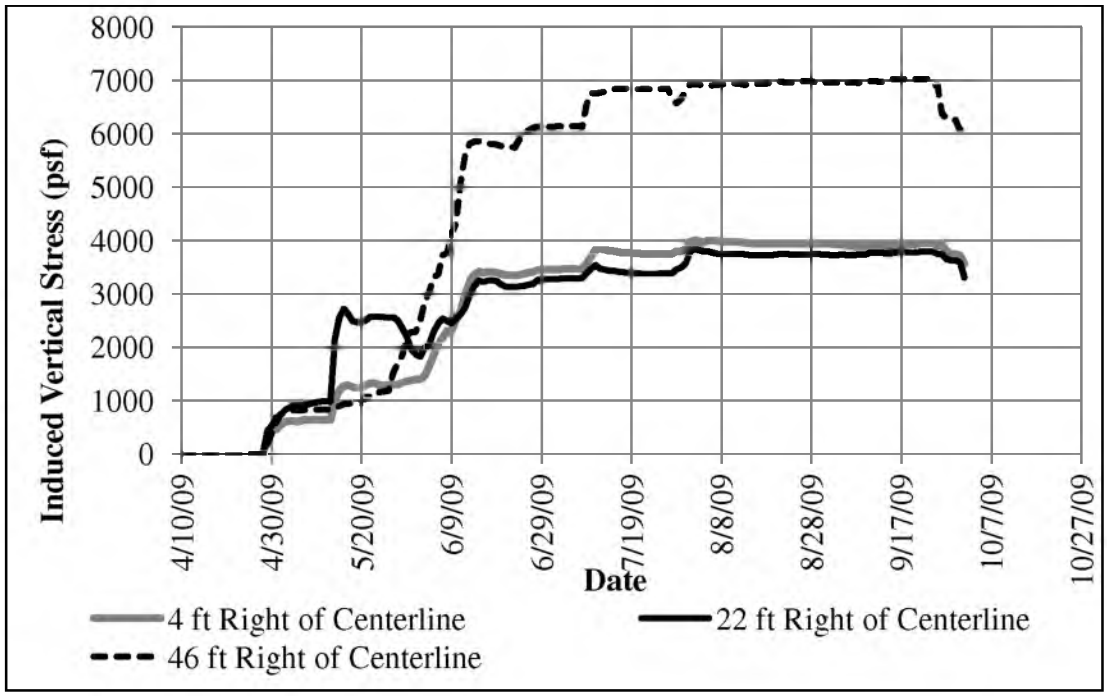

Figure 5-3. Measured vertical stress induced on the original ground surface by construction of the embankment near the centerline, 22 ft south of centerline, and 46 south of centerline.

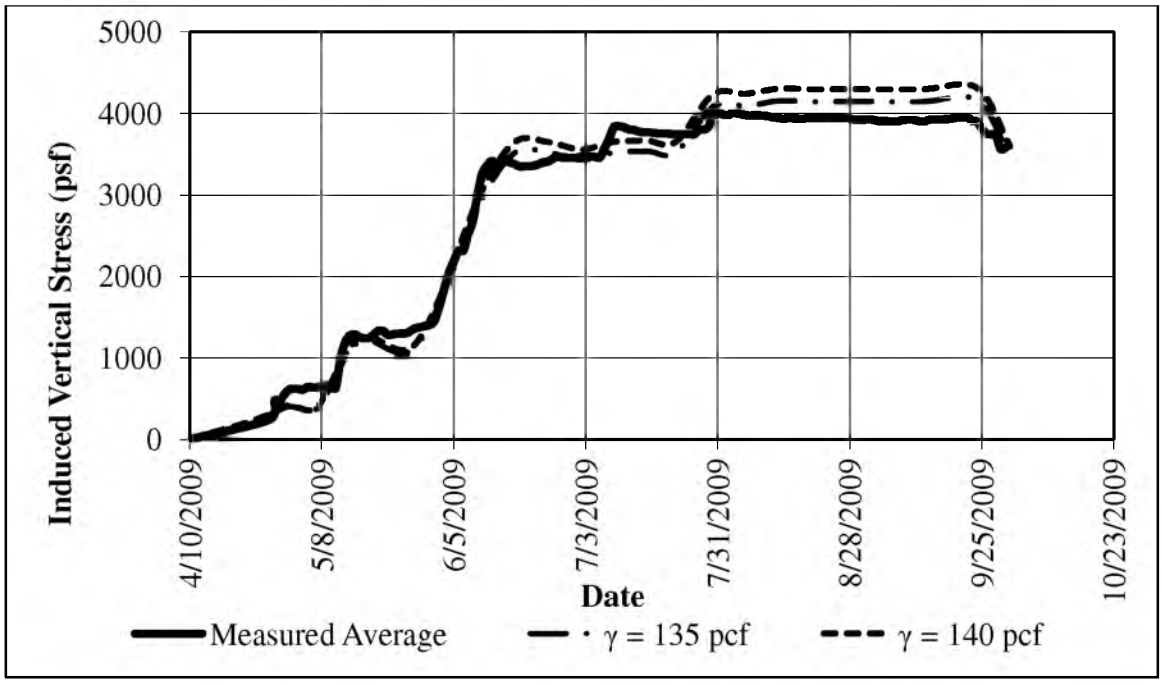

Figure 5-4. Comparison of measured and predicted vertical stress near the centerline induced on the original ground surface by construction of the embankment.

of increase in $\Delta\sigma_v$ occurred 46 ft right of centerline. The proximity of the pressure cell at this location to the MSE wall panels contributed to the greatest amount of increase of $\Delta\sigma_v$ at this location. The increase in induced $\Delta\sigma_v$ at the centerline and 22 ft right are approximately close in magnitude as seen in Figure 5-3. Because of the increase in fill height or embankment elevation (see Figure 5-1 and Figure 5-2) and the increase in $\Delta\sigma_v$ corresponding at these same dates, results for $\Delta\sigma_v$ at these locations provide a reasonable approximation of $\Delta\sigma_v$.

To determine if the measured values from the pressure cells are reasonable, the induced stresses near the centerline of the embankment were estimated by assuming a reasonable range in values of unit weight for the fill (135 to 140 pcf) and multiplying those unit weights by the height of the embankment at the same location.

Because the embankment was wide compared to the height of the fill, this method provides a reasonable approximation for the induced vertical stresses at the base of the embankment. The average measured values of $\Delta\sigma_v$ for the two pressure cells located 4 ft right of centerline are compared with the estimated values from the method described above in Figure 5-4 . It can be clearly seen from this comparison that the pressure cells were providing reasonable results for $\Delta\sigma_v$ at this location. These measured values of $\Delta\sigma_v$ are an essential component of the time-rate of settlement predictions discussed in Chapter 6.

5.3 Horizontal Stress

Induced horizontal stress was measured using push-in cells located 8 ft outside (south) of the south MSE wall at depths of 11, 15.5, and 27 ft below the original ground

surface. Results from these instruments are shown in Figure 5-5. The purpose of the horizontal push-in cells was to measure the horizontal stress at relatively shallow depths within the ground outside the footprint of the embankment to look for signs of instability. The horizontal stress at all three depths increased as embankment construction proceeded from the initiation of construction in April 2009 until May 26, 2009. An increase in horizontal stress as the vertical stress increases is normal behavior and an indicate of stability. Between May 26 and May 28, a sudden, drastic decrease in the horizontal stress occurred at these three depths. For the next several weeks the horizontal stress remained constant even though significant embankment construction occurred during part of that time. A sudden decrease in horizontal stress while the vertical stress is increasing is a sign of instability and failure. In this case, the failure mechanism was squeezing the soft soil beneath the edge of the embankment. This instability of the bearing soils beneath the edge of the embankment will be discussed in detail in Section 6.4.

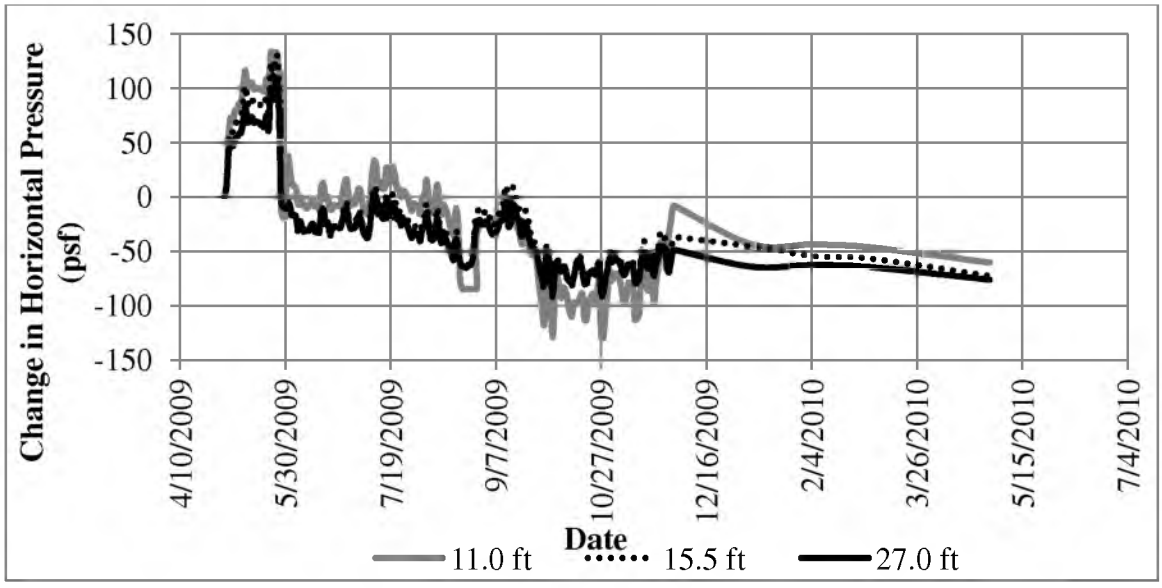

Figure 5-5. Induced horizontal stresses at depths of 11 ft, 15.5 ft, and 27 ft located south of the southern MSE wall.

5.4 Pore Pressures

Results for excess pore pressures measured during construction are shown in Figure 5-6 through Figure 5-17 beginning at a depth of 5.75 ft below the original ground surface. Excess pore pressures begin to develop during placement of the fill as shown in Figure 5-6.

Pore pressures during their steady state condition were measured by the piezometers located in the free field. Results from measured excess pore pressures at the centerline, 8 ft outside (south) of the MSE wall, and in the free field and are shown in Figure 5-6 through Figure 5-12 using 3:00 AM readings. The 3:00 AM readings were selected to eliminate variation in pore pressures caused by construction activities during the daylight hours. An increase in excess pore pressure coincided with an increase in vertical stress placed upon the foundation.

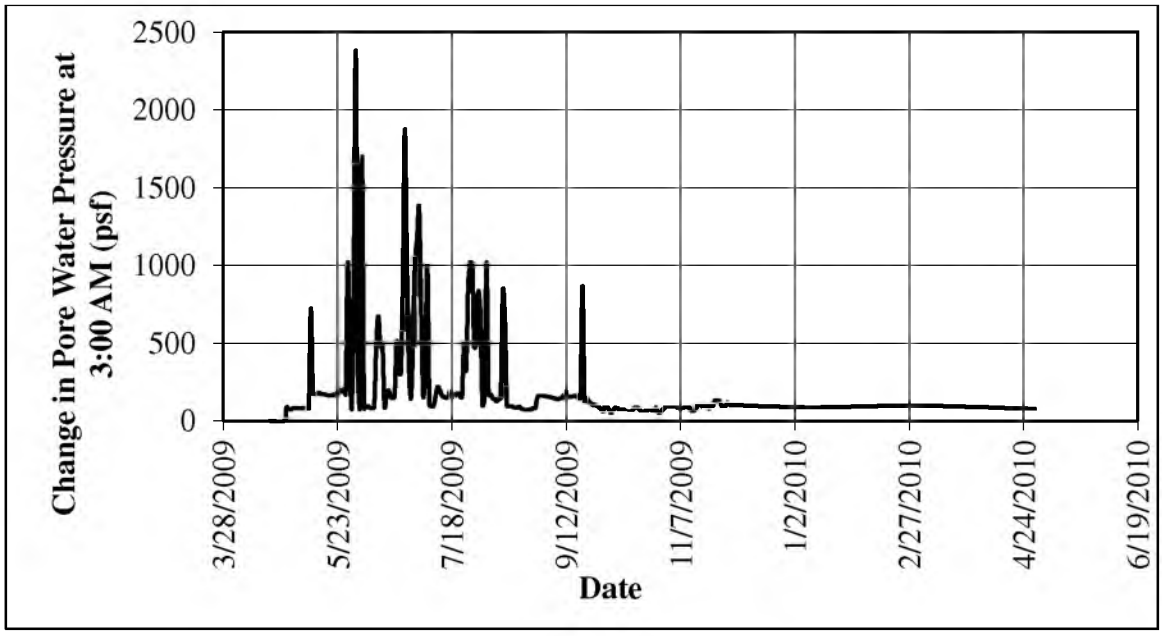

Figure 5-6 - Change in pore water pressures at 3:00 AM within cohesive layers beneath the centerline of the embankment at a depth of 5.75 ft below the original ground surface.

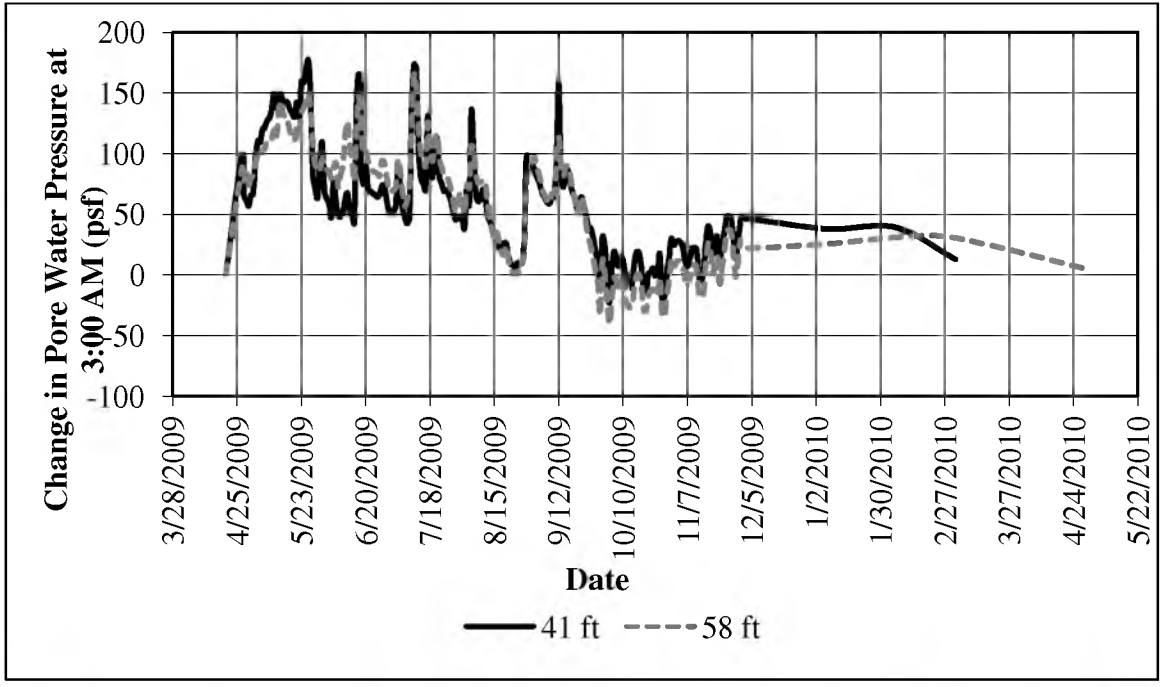

Figure 5-8. Change in pore water pressures at 3:00 AM within cohesive layers beneath the centerline of the embankment for depths of 41 and 58 ft below the original ground surface.

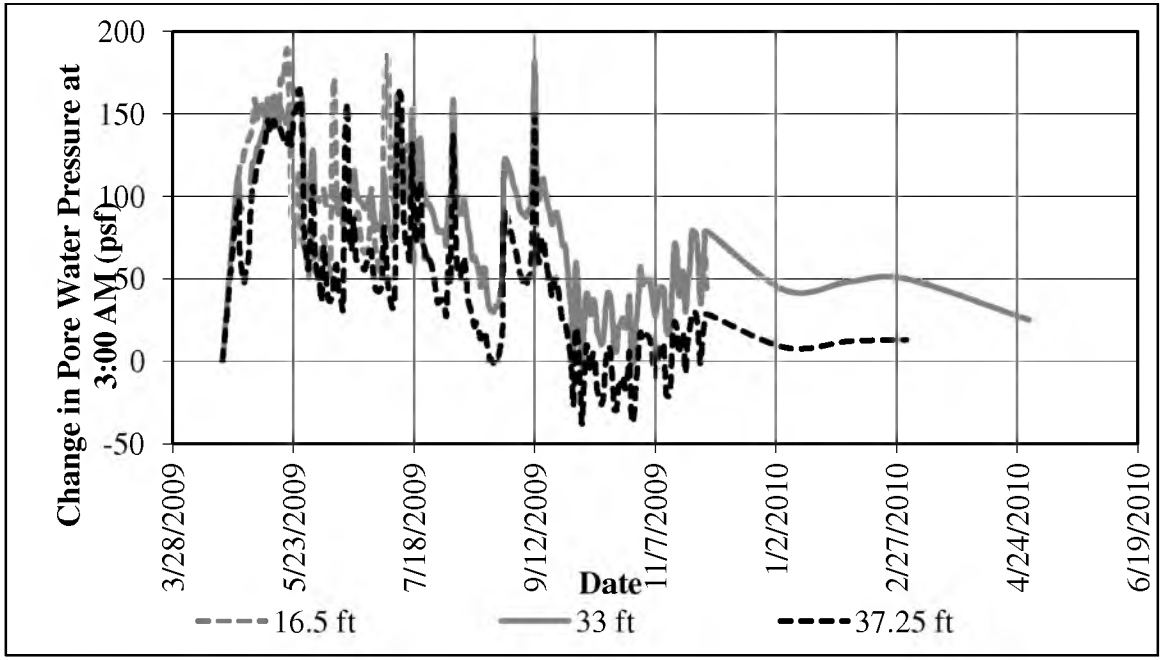

Figure 5-7. Change in pore water pressures at 3:00 AM within cohesive layers beneath the centerline of the embankment for depths of 16.5, 33, and 37.25 ft below the original ground surface.

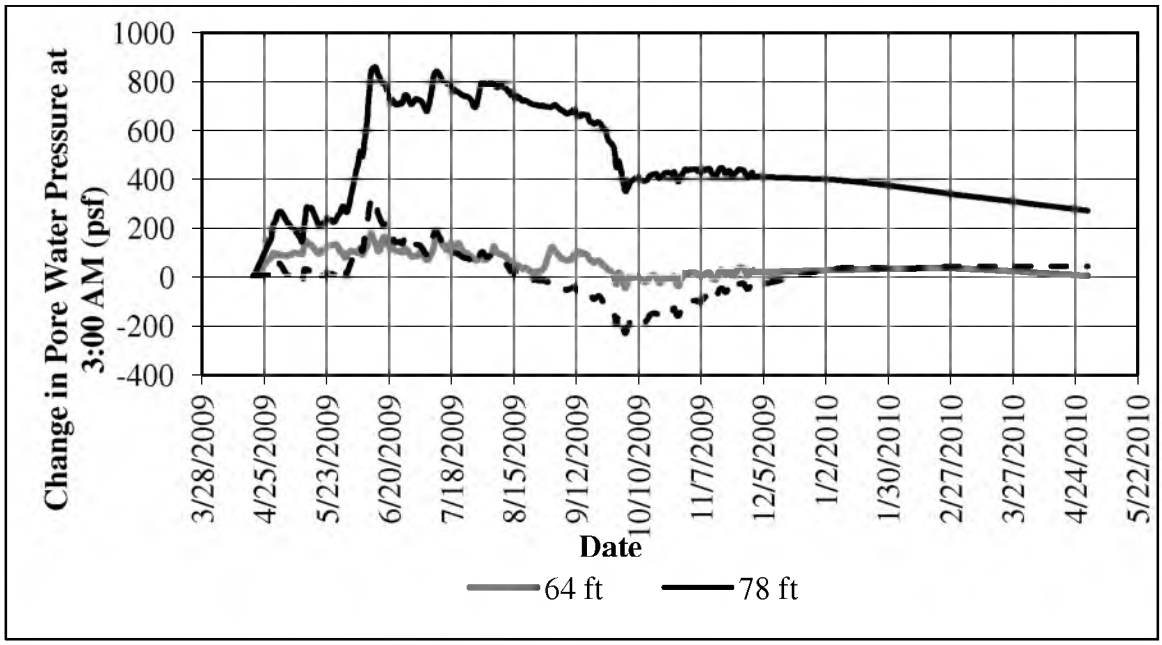

Figure 5-9. Change in pore water pressures at 3:00 AM within cohesive layers beneath the centerline of the embankment for depths of 64, 78, and 118 ft below the original ground surface.

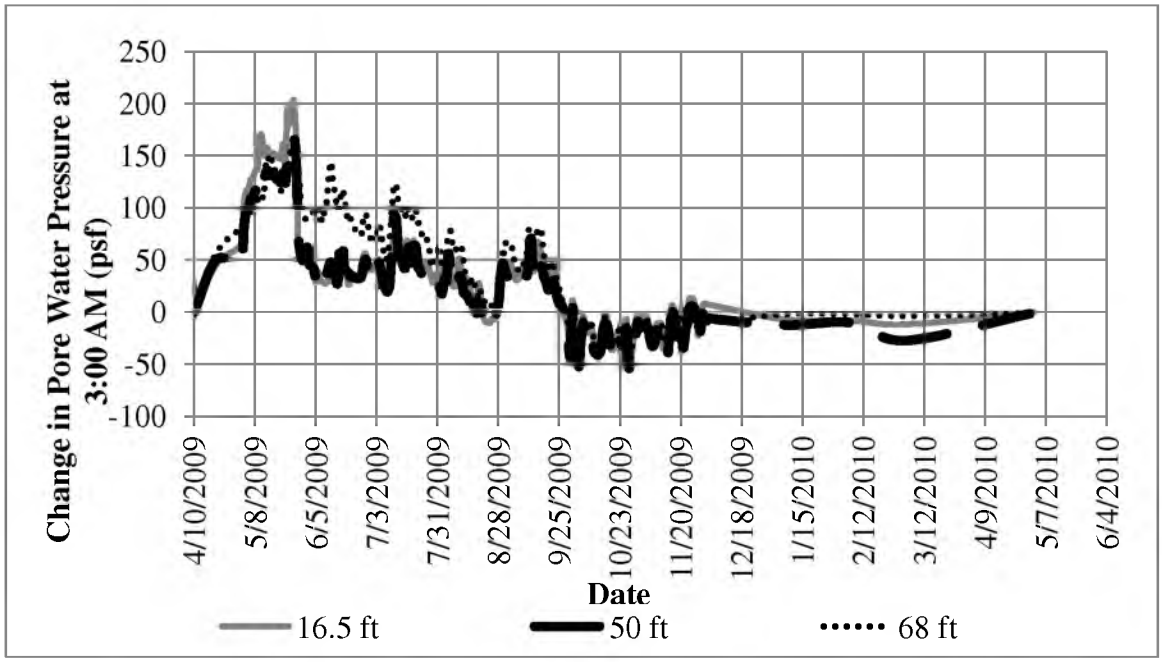

Figure 5-10. Change in pore water pressures at 3:00 AM within cohesive layers 8 ft outside the south MSE wall at depths of 16.5, 50, and 68 ft below the original ground surface.

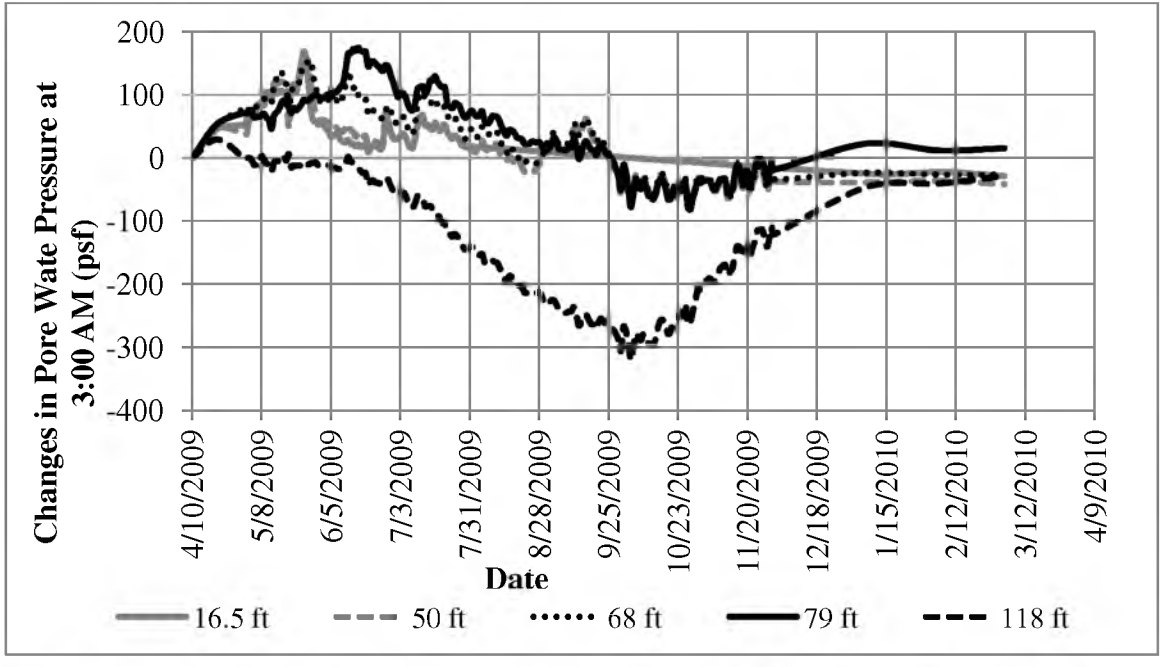

Figure 5-12. Change in pore water pressures at 3:00 AM within cohesive layers in the free field at depths of 16.5, 50, 68, 79 and 115 ft below the original ground surface.

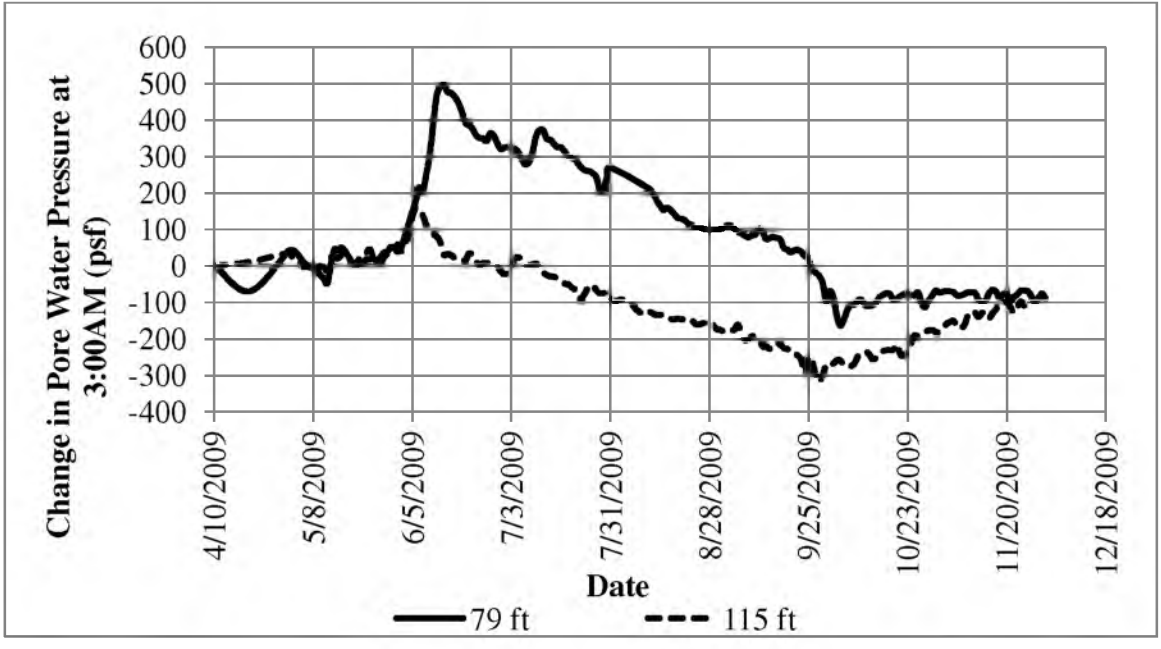

Figure 5-11. Change in pore water pressures at 3:00 AM within cohesive layers 8 ft outside the south MSE wall at depths of 79 and 115 ft below the original ground surface.

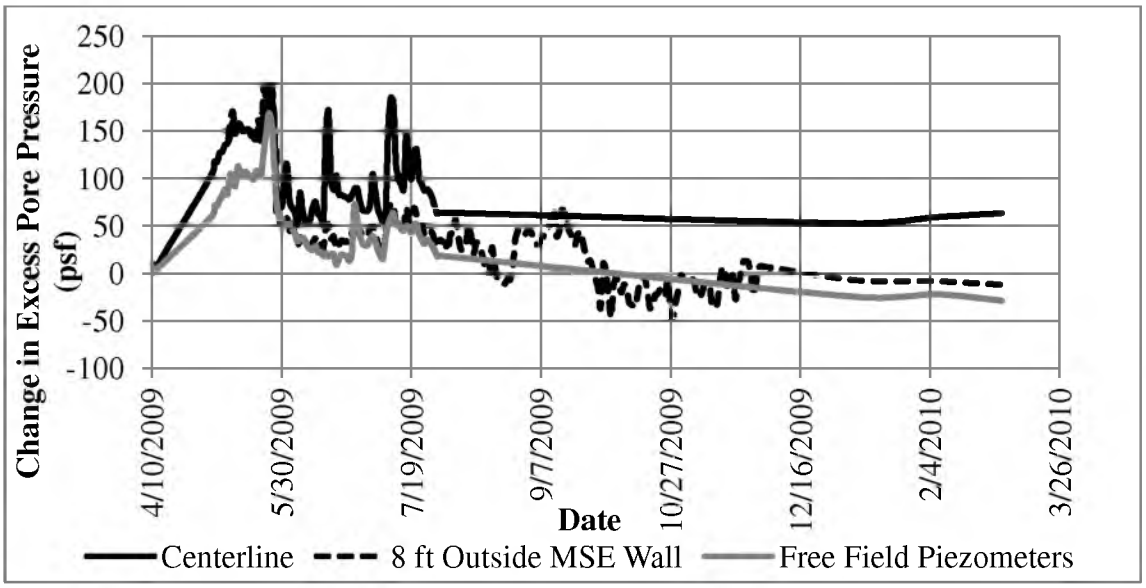

Figure 5-13. Change in excess pore pressure with time at a depth of 16.5 ft below the original ground surface.

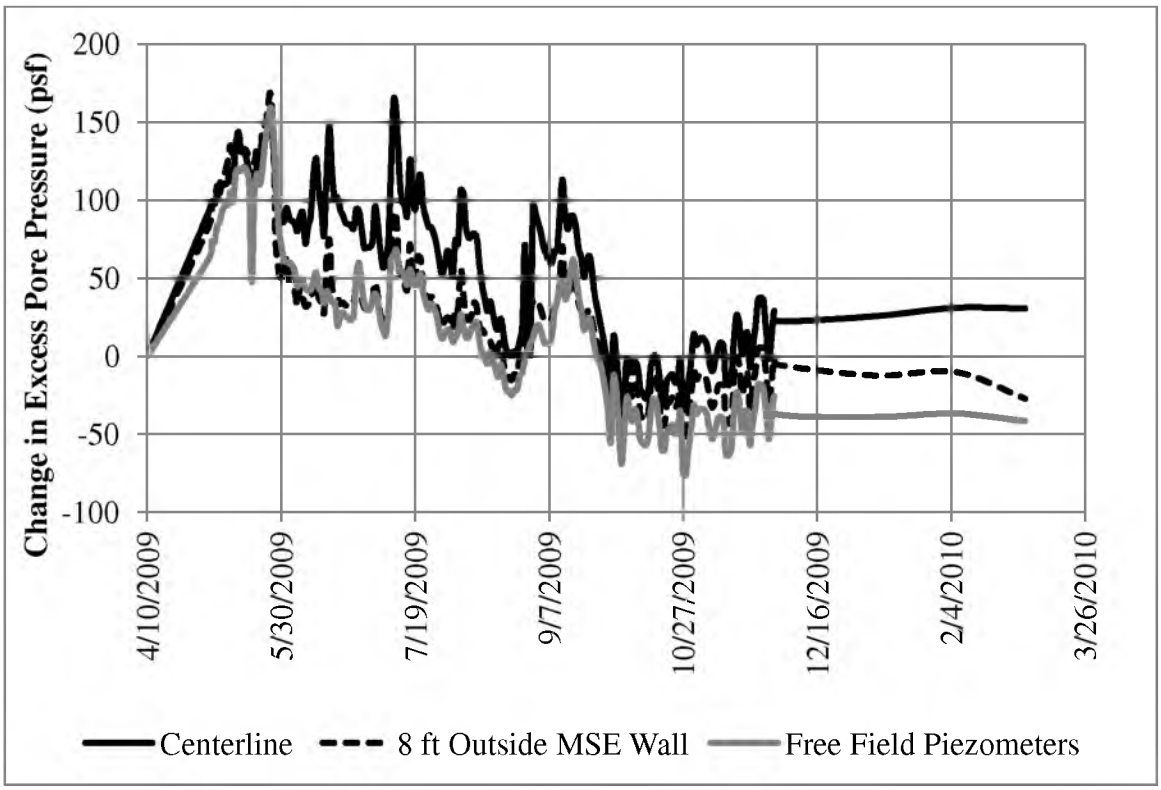

Figure 5-14. Change in excess pore pressure with time at a depth of 50 ft below the original ground surface.

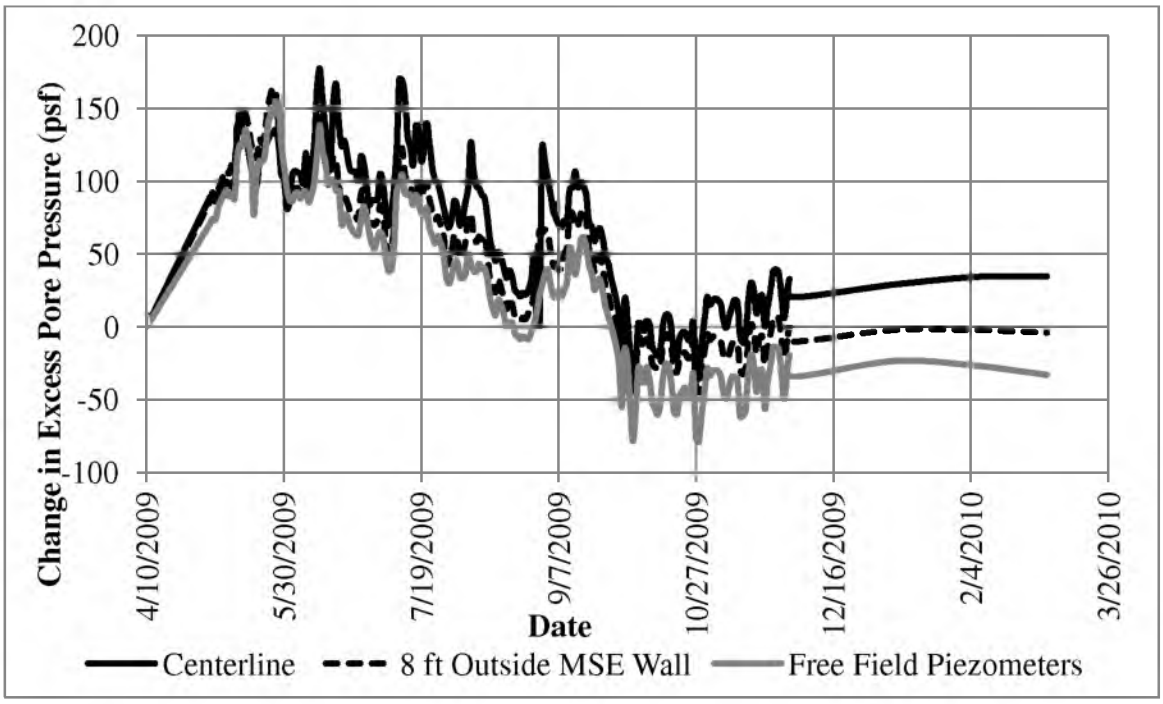

Figure 5-15. Change in excess pore pressure with time at a depth of 64 ft below the original ground surface.

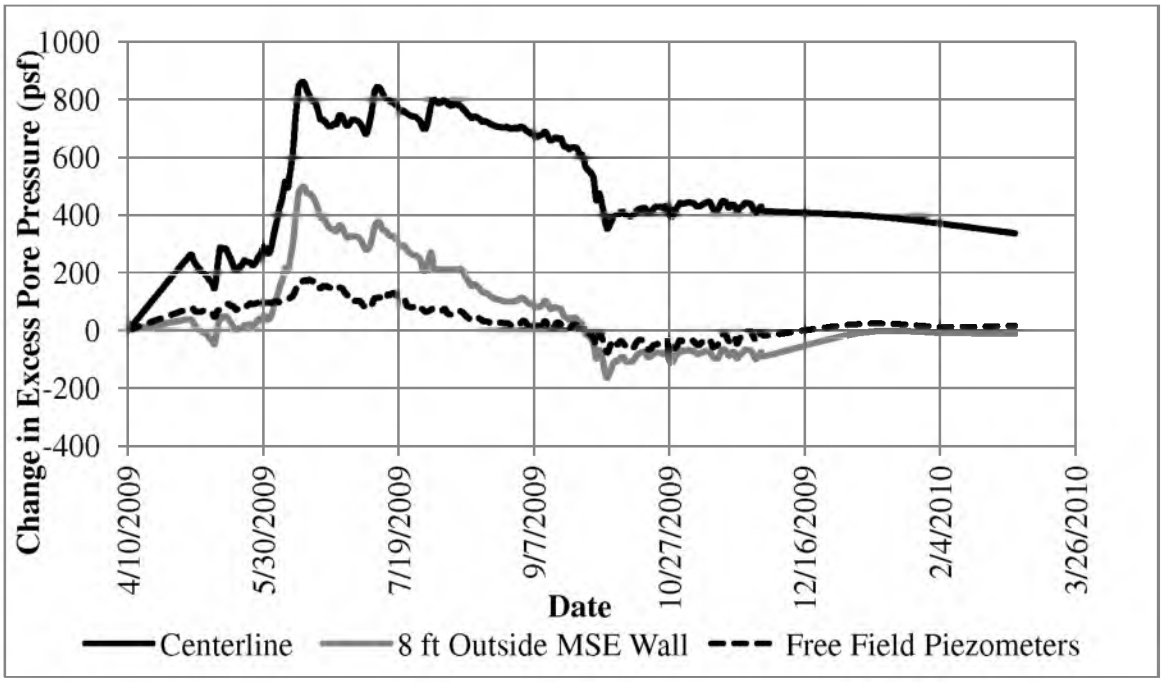

Figure 5-16. Change in excess pore pressure with time at a depth of 78 ft below the original ground surface.

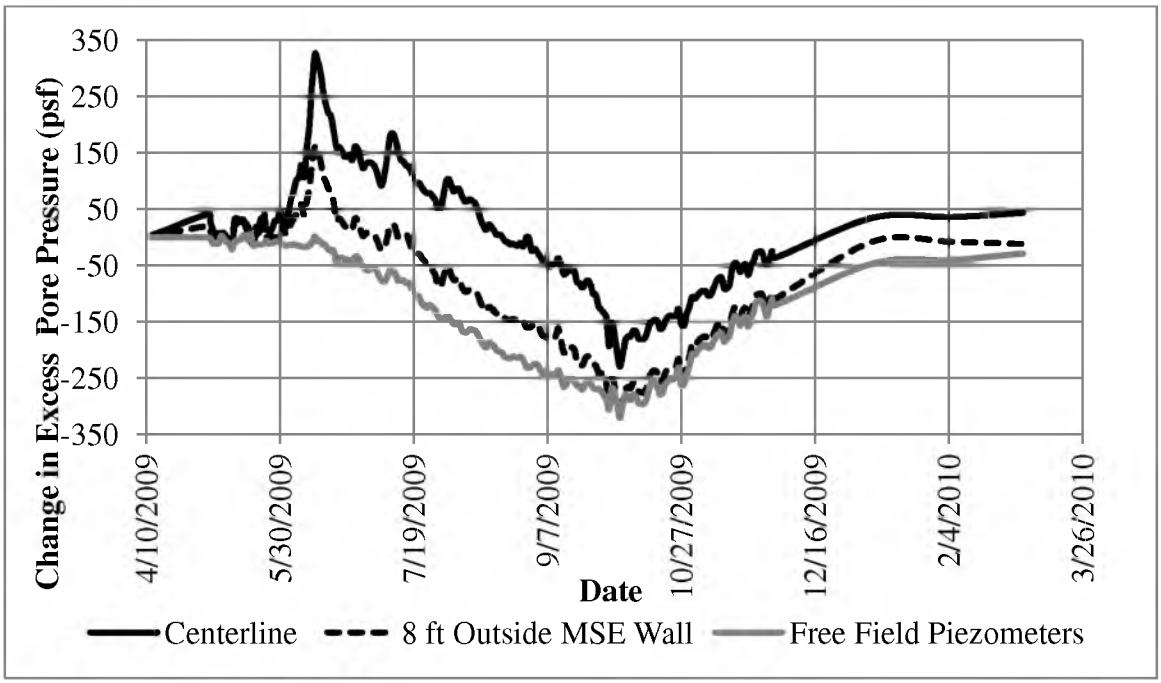

Figure 5-17. Change in excess pore pressure with time at a depth of 118 ft below the original ground surface.

Results obtained from data provided by the piezometers verify that excess pore pressures were generated during placement of fill, and dissipation of excess pore pressures during times that fill placement stopped during and after construction. The greatest amount of sustained excess pore pressure generation occurred within Layer 7 at a depth of 78 ft at the centerline. Results indicate the excess pore pressures generated within Layer 7 had not yet fully dissipated upon removal of surcharge. Large excess pore pressures developed at a depth of 5.75 ft but dissipated quickly.

Knowledge of the steady state pore pressures are vital to monitoring excess pore pressures developed during construction. Knowing the pore pressures during steady state conditions allows one to see the increase in excess pore pressure during and after loading. The excess pore water pressure caused by construction of the embankment is calculated

as the change measured within the bearing soil affected by the construction minus any change in the free field value during the same time period.

Excess pore pressures for five different depths are compared at three different horizontal locations (shown in Figure 5-13 through Figure 5-17). Horizontal locations where excess pore pressures were measured are: (1) Underneath the centerline of the embankment, (2) 8 ft outside the MSE wall, and (3) the free field.

Plots for each different vertical depth show the excess pore pressures developed during construction were greatest at the centerline of the embankment. The next greatest amount of excess pore pressures occurred 8 ft outside the MSE wall. The least amount of excess pore pressures developed was in the free field. The excess pore pressures in the free field were the smallest as expected, because they were outside the zone of influence of the construction activity. This pattern was consistent at the five different vertical locations.

5.5 Settlement

Settlement caused by constructing and surcharging the embankment and then removing the surcharge was measured by settlement manometers, settlement cells, magnet extensometers, and a horizontal inclinometer. Settlement results from the previously mentioned instrumentation will be discussed in this section.

5.5.1 Settlement Manometers

Settlement manometers were used to measure settlement at the following locations at Station 32+25: (1) Centerline of the embankment, (2) 30 ft south of

centerline, and (3) 8 ft inside the south MSE wall. Settlement readings from the manometers are shown in Figure 5-18.

Final readings for total settlement were obtained on April 29, 2010. On this date a total of 12.5 in of settlement was measured at the centerline of the embankment; 10.9 in of settlement was measured 30 ft south of the centerline; and 7.50 in of settlement was measured at 8 ft inside the south MSE wall.

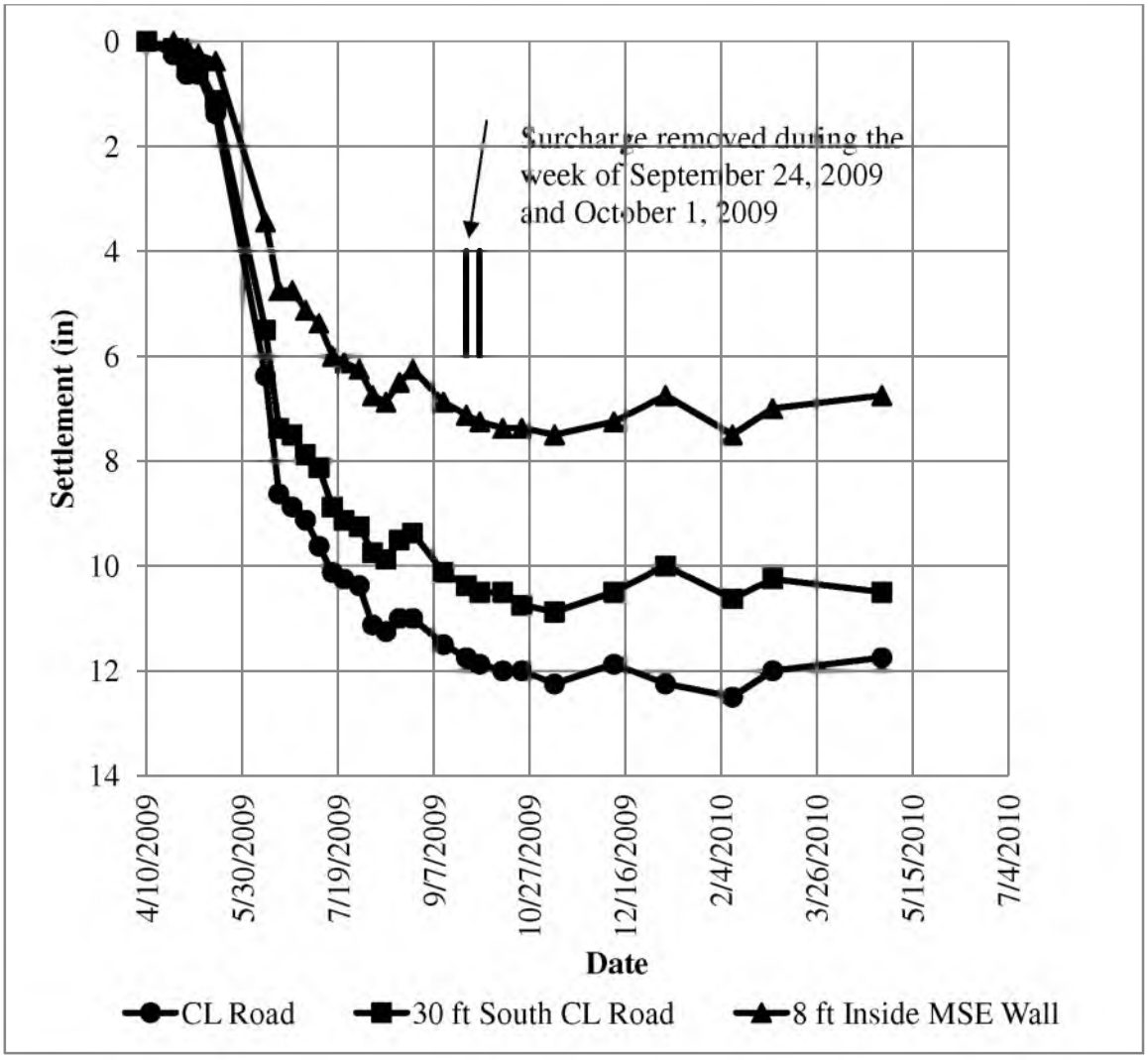

Figure 5-18. Settlement results using manometers at the centerline, 30 ft south of centerline, and 8 ft inside the south MSE wall.

5.5.2 Settlement Cells

Vibrating wire settlement cells were used to measure settlement 4 ft right of centerline, 24 ft right of centerline, and 48 ft right of centerline (see Figure 5-19). Final readings for the vibrating wire settlement cells were obtain on November 26, 2009.

On this date a total of 9.42 in of settlement was measured at 4 ft right of centerline; 6.68 in of settlement was measured at 24 ft right of centerline of the embankment; and 9.00 in of settlement was measured at 48 ft right of centerline of the embankment.

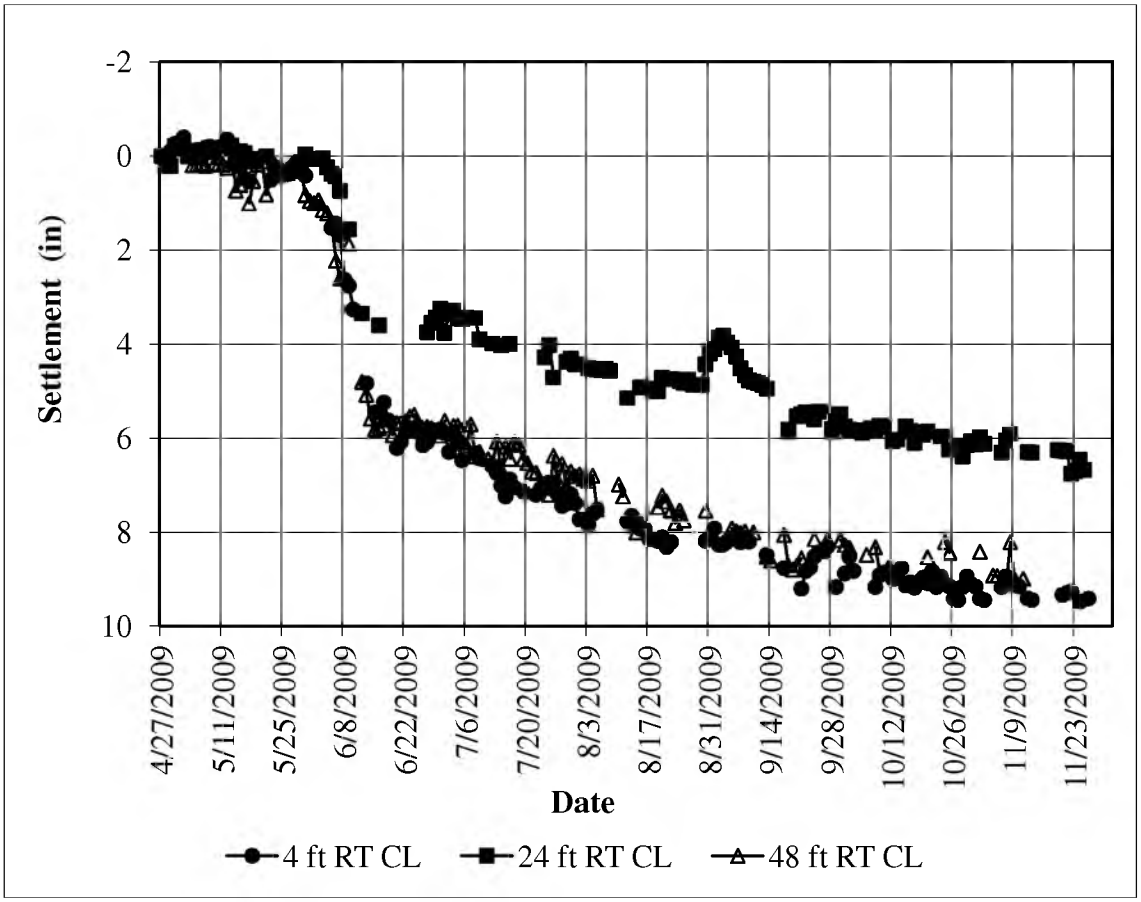

Figure 5-19. Results measured by the vibrating wire settlement cells at 4 ft right of centerline, 24 ft right of centerline, and 48 ft right of centerline.

5.5.3 Magnet Extensometers

Magnet extensometers were installed to measure the settlement of the foundation soil at two locations - at centerline of the embankment and 7 ft outside (south of) the south MSE wall. Individual layers and their respective ranges of depths are identified in Table 5-1.

Initial baseline elevations for the centerline magnet extensometer were taken March 19, 2009. Resulting settlement of the foundation was measured relative to the initial elevations for each of the magnets. Readings were obtained by first measuring the top elevation of the 1 in PVC pipe by surveying from a bench mark outside the zone of settlement caused by construction of the embankment, and then measuring the depths of the individual magnets by lowering a probe down the PVC pipe. During construction, the elevation of the PVC pipe was extended upward as the height of the embankment increased. Each time the PVC pipe was extended upward, the elevation of the top of the

Table 5-1. Layers corresponding to their respective depths used for measuring settlement from data obtained by the magnet extensometer.

Layer	Depth to Top of Layer[a] (ft)	Depth to Bottom of Layer[a] (ft)
1	3	8
2	8	14
3	14	20
4	20	29
5	29	45
6	45	54
7	54	88
8	88	105
9	105	108
10	108	120

[a] Depths are from the original ground surface

pipe was measured for each set of readings and incorporated into the calculations for settlement.

Four cohesive layers were designated as Layer 1 (3 to 8 ft), Layer 3 (14 to 20 ft), Layer 5 (29 to 44 ft) and Layer 7 (54 to 88 ft). These layers were delineated from the CPT logs (tip resistance, sleeve resistance, friction ratio, cone pore pressure, and soil behavior type) and from results of CRS tests. The boundaries for each layer are shown on a plot of CPT tip resistance versus depth below the original ground surface in Figure 5-20. The other layers were determined to be granular. Cohesive and granular layers were also verified using CRS test results. As previously mentioned in Section 0, CRS tests were performed at depths within each type of layer to determine σ'_p, virgin compression and recompression indices, c_v as a function of effective stress, and permeability as function stress. CRS tests results also verified which depths were cohesive and which depths were granular by excess pore pressure developed during testing. For cohesive soils, CRS test results yielded c_v as a function of effective stress and build up of pore pressures during the test. CRS test results for granular soils yielded no results for c_v and pore pressures did not build up during the test. CRS tests performed at 10.3, 20.4, 25.5, 45.3, 50.3, 90.5, 95.4, 100.3, and 100.5 ft yielded no values for c_v and exuded no build of pore pressure during CRS testing.

Settlement measured from the centerline magnet extensometer for individual layers and accumulative settlement are shown in Table 5-2, Figure 5-21, and Figure 5-22.

The foundation for the embankment settled 13.3 in at the centerline. Layers 1, 3, 5, 7, and 10 were cohesive layers, where settlement occurred slowly throughout

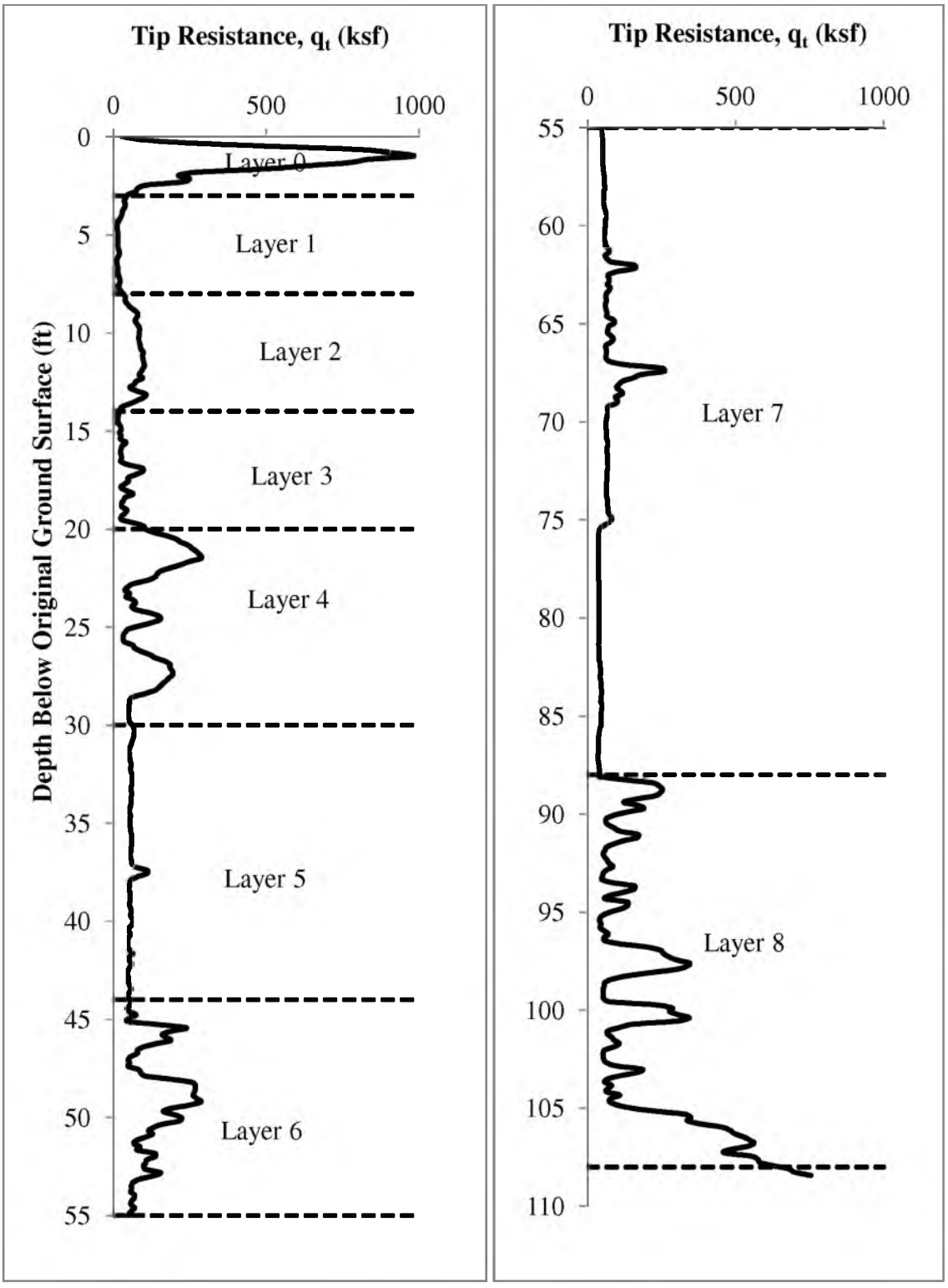

Figure 5-20. Designated layers within the foundation soils for the embankments used to measure change in layer heights using the magnet extensometer.

Table 5-2 Summary of settlement that occurred within the individual layers near the centerline of the embankment as of July 1, 2010.

Layer	Settlement (in)
1	4.80
2	3.21
3	1.54
4	0.28
5	0.59
6	0.04
7	1.40
8	1.46
9	0.26
10	-0.20
Total	13.37

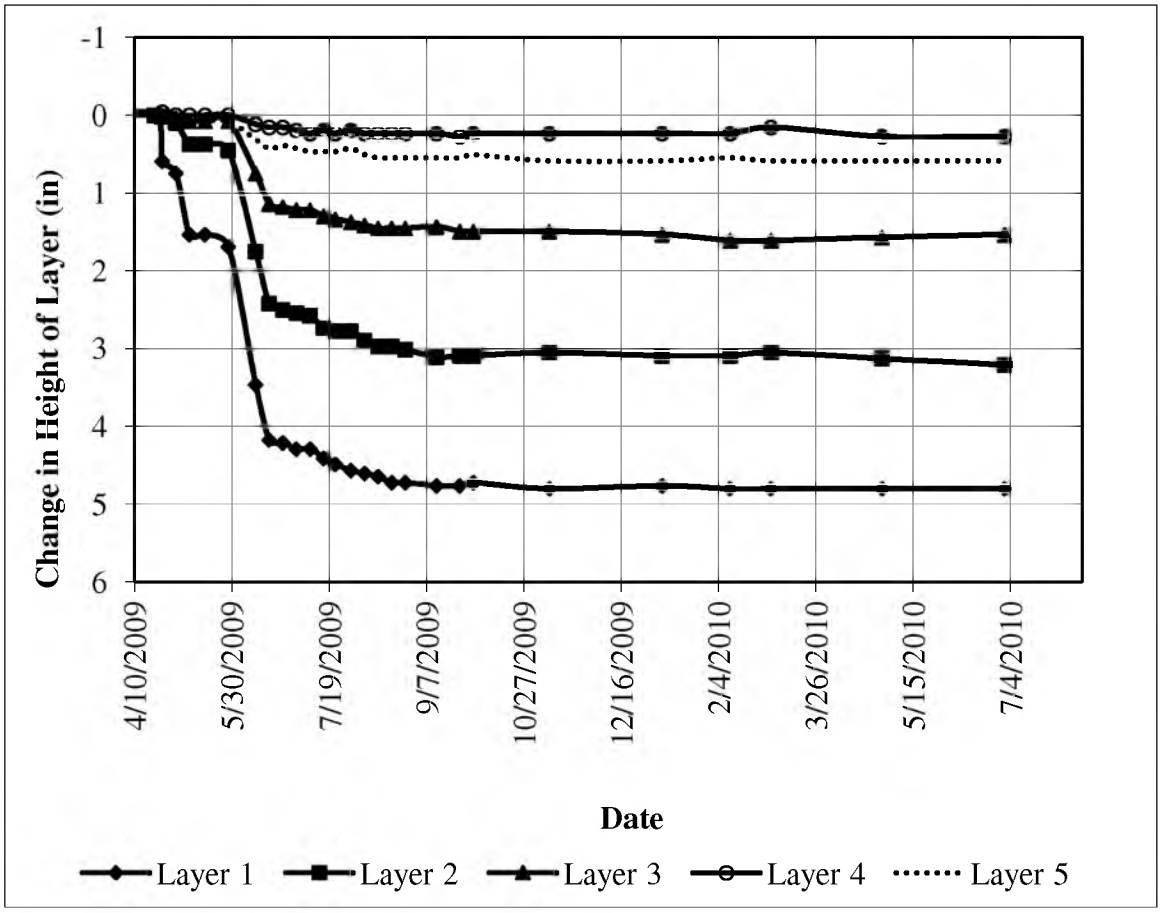

Figure 5-21. Changes in layer heights for Layers 1 - 5 for spider magnets 7 ft right of centerline.

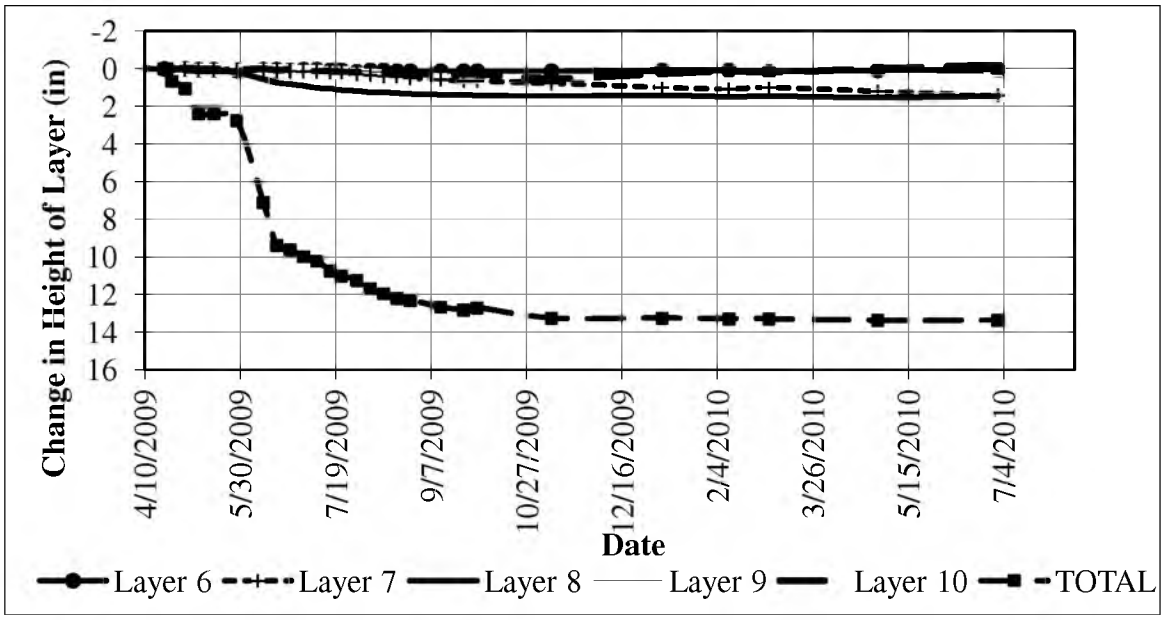

Figure 5-22. Changes in layer heights for Layers 6 – 10, and the total change in height for spider magnets 7 ft right of centerline.

construction. A majority of the settlement occurred between the months of April and October.

Resulting settlement measured by the magnet extensometers 7 ft outside the south MSE wall are shown in Figure 5-23, Figure 5-24, and Table 5-3. On March 3, 2010, a total settlement of 3.03 in occurred at this location.

5.5.4 Horizontal Inclinometers

Readings taken for the horizontal inclinometer were used to measure the settlement occurring across the width of the embankment at station 32+25. Settlement that occurred while the embankment was being constructed and surcharged, and during and after the surcharge removal can be seen in Figure 5-25. Settlement results provided in Figure 5-25 show settlement as a function of time when the vertical stress acting on the

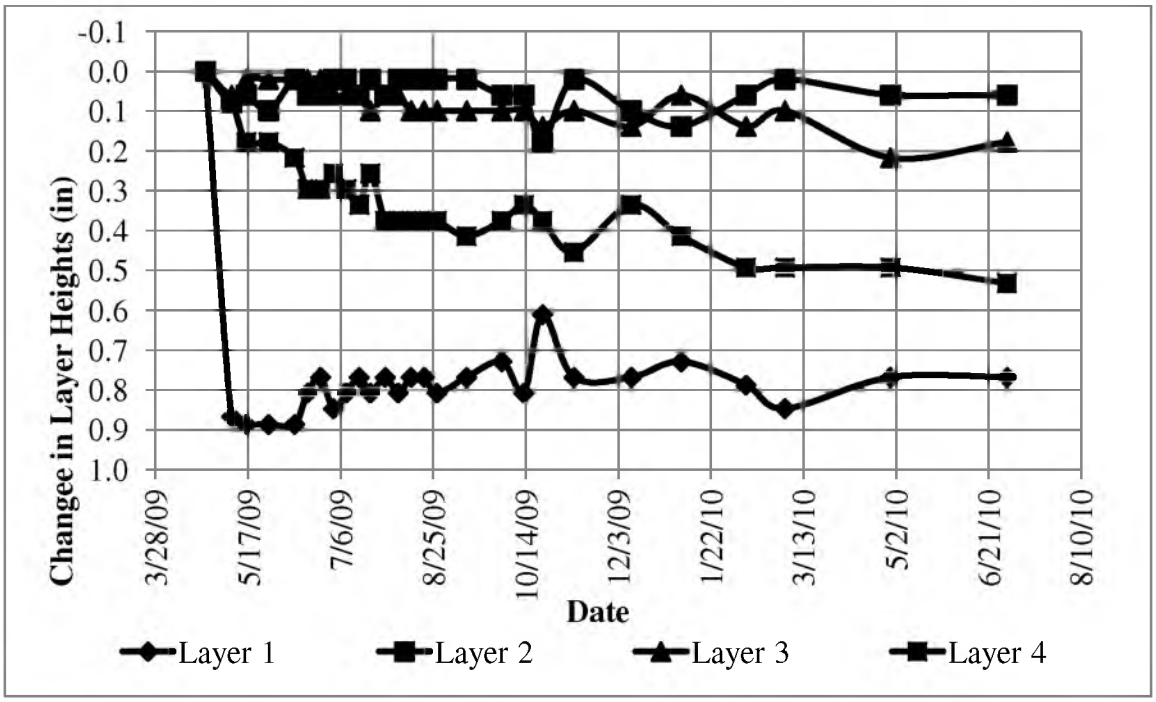

Figure 5-23. Changes in layer heights between spider magnets 7 ft outside (south) of the MSE wall.

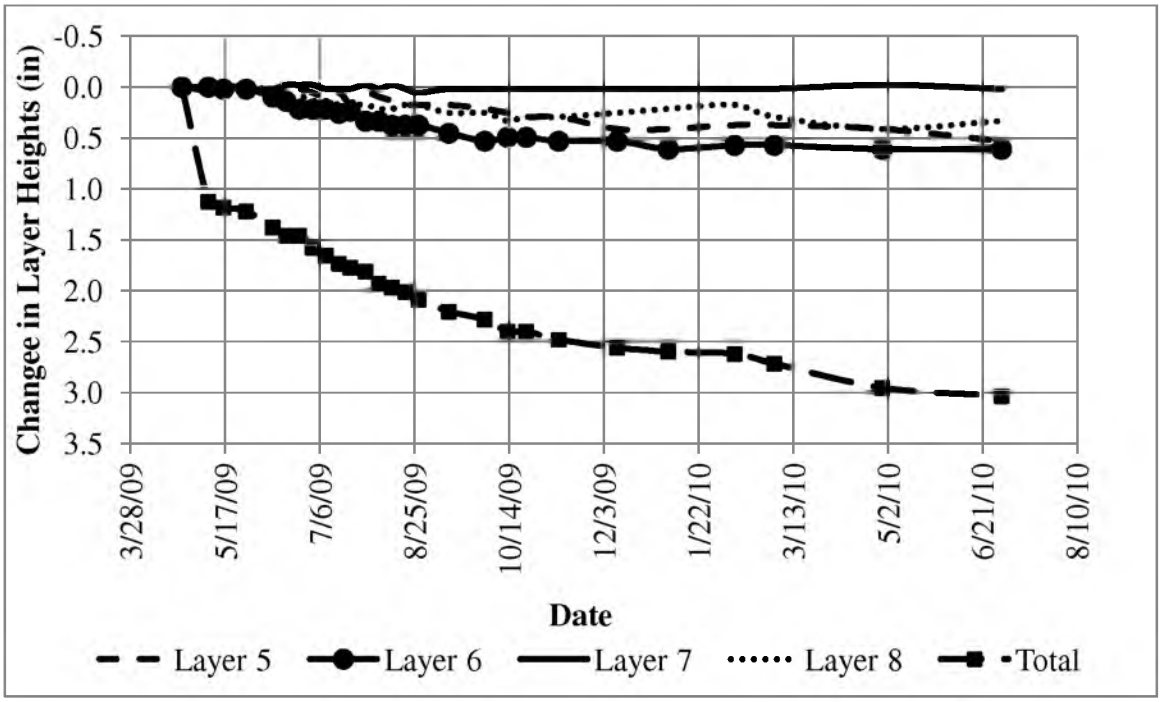

Figure 5-24. Changes in layer heights between spider magnets 7 ft outside the south MSE wall.

Table 5-3 Summary of settlement that occurred within the individual layers 7 ft outside the south MSE wall as of July 1, 2010.

Layer	Settlement (in)
1	0.77
2	0.06
3	0.18
4	0.53
5	0.53
6	0.61
7	0.02
8	0.33
Total	3.03

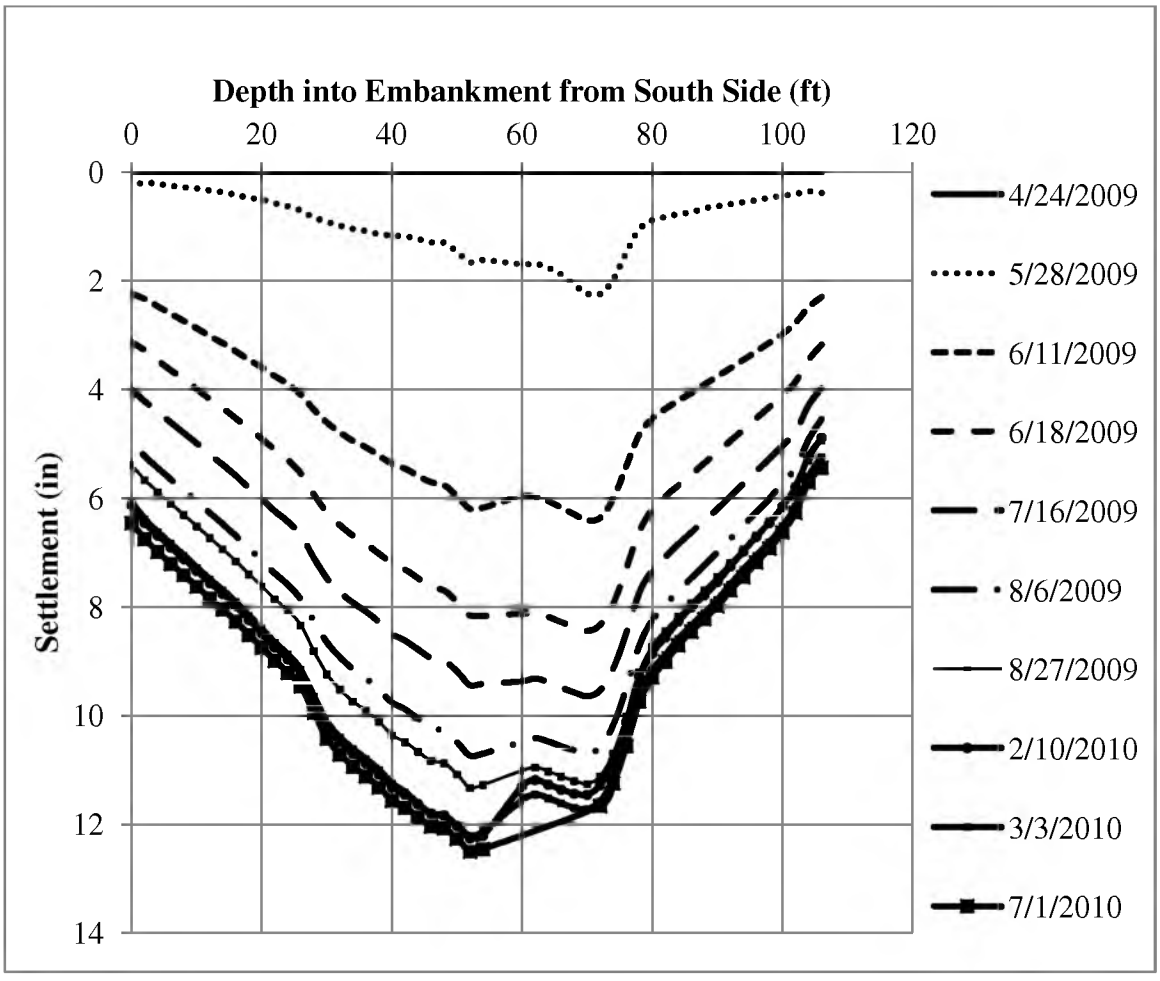

Figure 5-25. Cross section of settlement measured from the horizontal inclinometer at station 32 + 25 as of July 1, 2010.

foundation increased or decreased. Vertical stress increased during the construction of the embankment and placement of surcharge. Vertical stress decreased during removal of surcharge. The width of the embankment was 106 ft. During construction of the embankment, a portion of the casing was crushed between 54 and 60 ft into the embankment from the south side. Due to crushing of the casing at this location within the embankment, readings were obtained from both the south and north sides of the embankment. Readings were obtained from the south side to 54 ft into the embankment. Readings were obtained from the north side to 60 ft into the embankment. Final readings for total settlement were obtained on July 1, 2010. For this date, settlement results near the centerline of the embankment, 30 ft right of centerline, and 48 ft right of centerline from the magnet extensometer, vibrating wire settlement sensor, settlement manometers, and horizontal inclinometer are found in Table 5-4. Graphical results of the settlement at these locations are shown in Figure 5-26 through Figure 5-28. At the centerline of the embankment the greatest amount of settlement (13.37 in) was measured using the magnet extensometer with 13.37 in. Thirty ft right of centerline, the greatest amount of settlement was recorded from the settlement manometers with 10.50 in. Forty-eight ft right of centerline, the greatest amount of settlement recorded by the settlement sensor was 9.00 inches.

Settlement behavior during the SR 77 embankment construction was measured via four different methods: (1) Settlement manometers, (2) vibrating wire settlement cells, (3) magnet extensometer, and (4) horizontal inclinometer. Each of these methods produced data which was reliable and valuable in determining the amount of settlement that had occurred. However, improvements for each method could be made in order to

Table 5-4. Summary of maximum settlement results for July 1, 2010 from the magnet extensometer, vibrating wire settlement sensors, and horizontal inclinometer at the centerline of embankment, 30 ft right of centerline of embankment, and 48 ft right of centerline of embankment.

Location	Settlement (in) as of July 1, 2010		
	Near Centerline	30 ft Right	48 ft Right
Magnet Extensometer	13.37	NA	NA
Vibrating Wire Settlement Sensor	9.42	6.46	9.00
Settlement Manometer	12.50	10.50	6.75
Horizontal Inclinometer	12.51	8.58	6.16

NA = Not Available

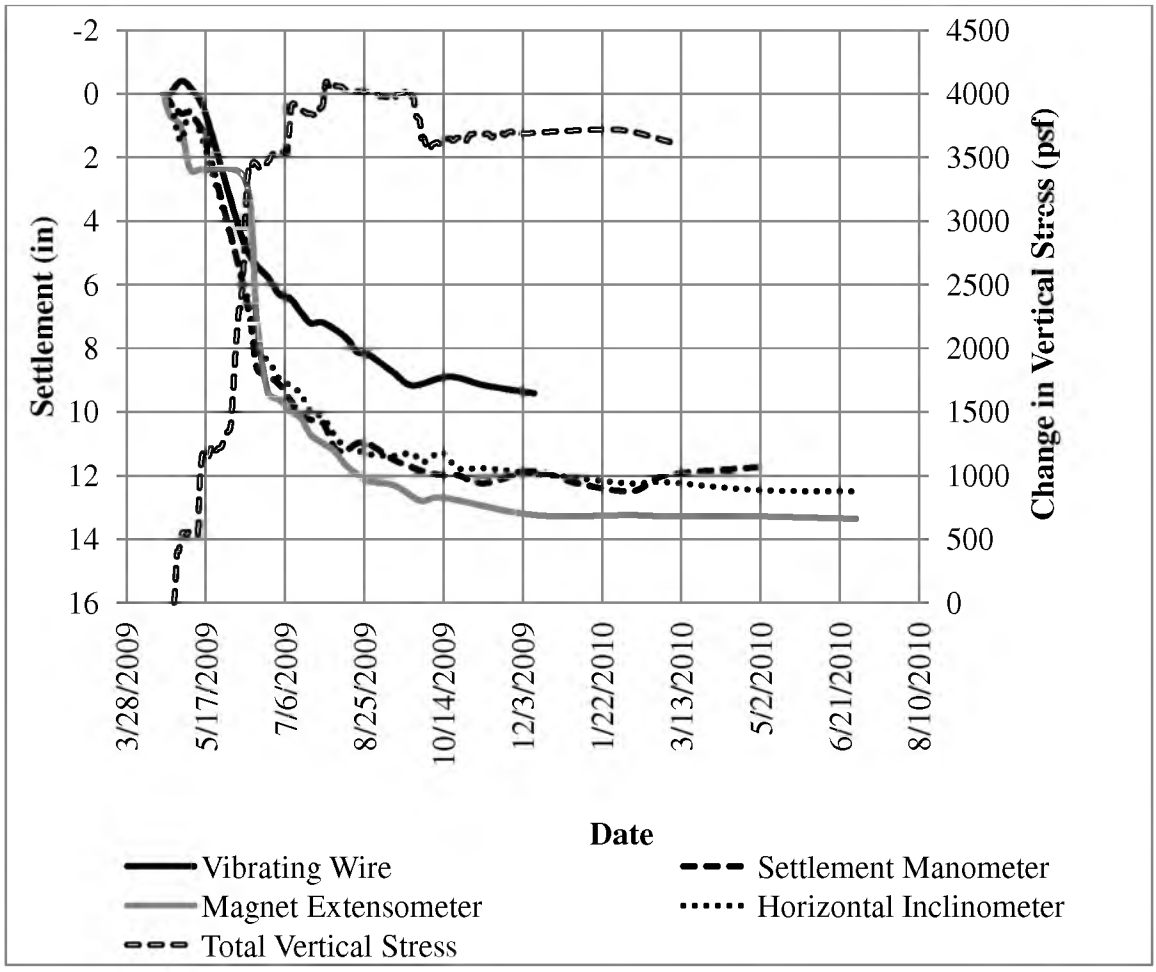

Figure 5-26. Settlement results near the centerline from the vibrating wire settlement cells, settlement manometers, magnet extensometer, and horizontal inclinometer with the change in vertical stress as a function of time.

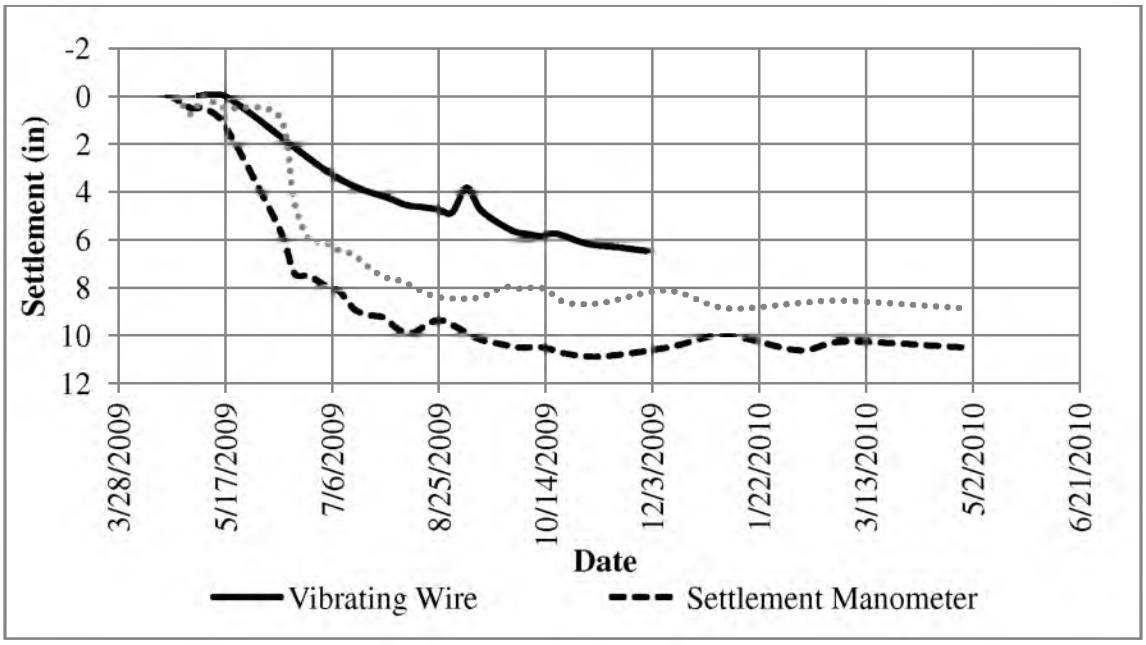

Figure 5-27 Settlement results from the vibrating wire settlement cell located 30 ft right of centerline, settlement manometer located at 30 ft right of centerline, and horizontal inclinometer located 30 ft right of centerline.

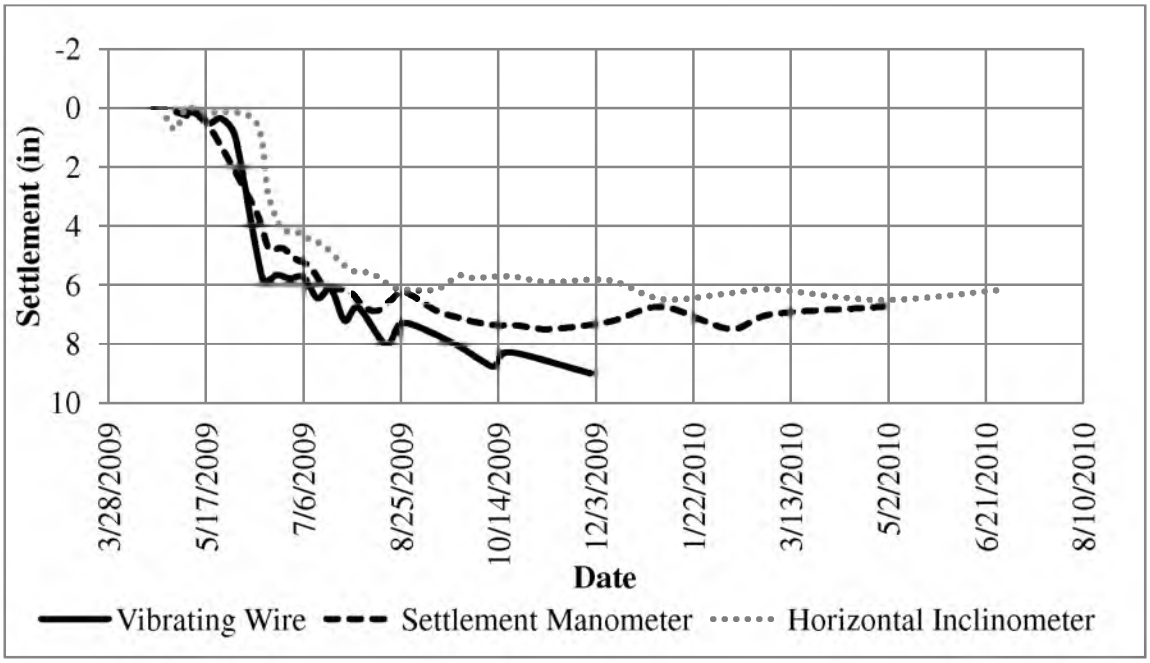

Figure 5-28. Settlement results from the vibrating wire settlement cells, settlement manometer, and horizontal inclinometer located 48 ft right of centerline.

understand settlement results. For example, settlement manometers provided settlement as the fluid level decreased in both tubes due to the decrease in fluid level at the settlement platform underneath the embankment, but they were located in the zone where settlement occurred causing the settlement manometer box to settle. The actual settlement occurring underneath the embankment would then become greater than the settlement measured. Vibrating wire settlement cells measured the least amount of settlement. Readings obtained via the vibrating wire settlement cells had a great amount of variability in the readings causing some settlement data to be erroneous. Readings that were erroneous needed to be taken out and discarded. The resulting readings then yielded a reasonable settlement trend. As long as vibrating wire settlement cells are logged continuously, readings for settlement results will be reliable and reasonable. The magnet extensometer was the only method to provide changes in layer heights between the different layers underneath the embankment while measuring settlement. The settlement results obtained by way of the magnet extensometer were reliable in determining the settlement that had occurred in the cohesive layers and that showed each individual cohesive layer was consolidating at a different rate. Readings from the magnet extensometer were very reliable because the elevations for each set of readings at the top of the PVC came from surveying a point that was located outside the zone of influence. The magnitude of settlement measured via the magnet extensometer was reasonable when compared to the other methods of instrumentation. However, errors in slope can be introduced and can cumulate with time with other slope readings. Overall, all four methods provided reasonable results.

5.6 Lateral Deformation

The instrumentations used at the SR 77 embankment research site to measure and monitor lateral deformation were a vertical inclinometer and two ShapeAccelArray (SAA). The vertical inclinometer is a common method used to measure lateral deformation. The purpose of using the SAA was to monitor the lateral deformation of the foundation soil using a different method and to compare the results of the SAA with those of the vertical inclinometer to determine if the SAA gives reliable results.

5.6.1 Vertical Inclinometer

The vertical inclinometer was installed to monitor the lateral stability of the foundation soil during construction of the embankment. Data collection for the vertical inclinometer began on April 24, 2009 and continued through July 1, 2010. Results for lateral deformation obtained via the vertical inclinometer are shown in Figure 5-29. Due to a significant amount of data collected, lateral deformation shown in Figure 5-29 is displayed only for critical weeks, where significant amounts of lateral deformation occurred.

A significant amount of lateral deformation occurred early on in the construction project as backfill was being placed upon the foundation between April 24, 2009 and June 18, 2009. There was 0.18 in of lateral deformation that was measured on June 11, 2009 at a depth of 4 ft below the ground surface. On, June 18, 2009, 0.38 inches of lateral deformation was measured at the same depth below the ground surface. The maximum amount of lateral deformation measured was 0.710 in and occurred on August 6, 2009 at a depth of

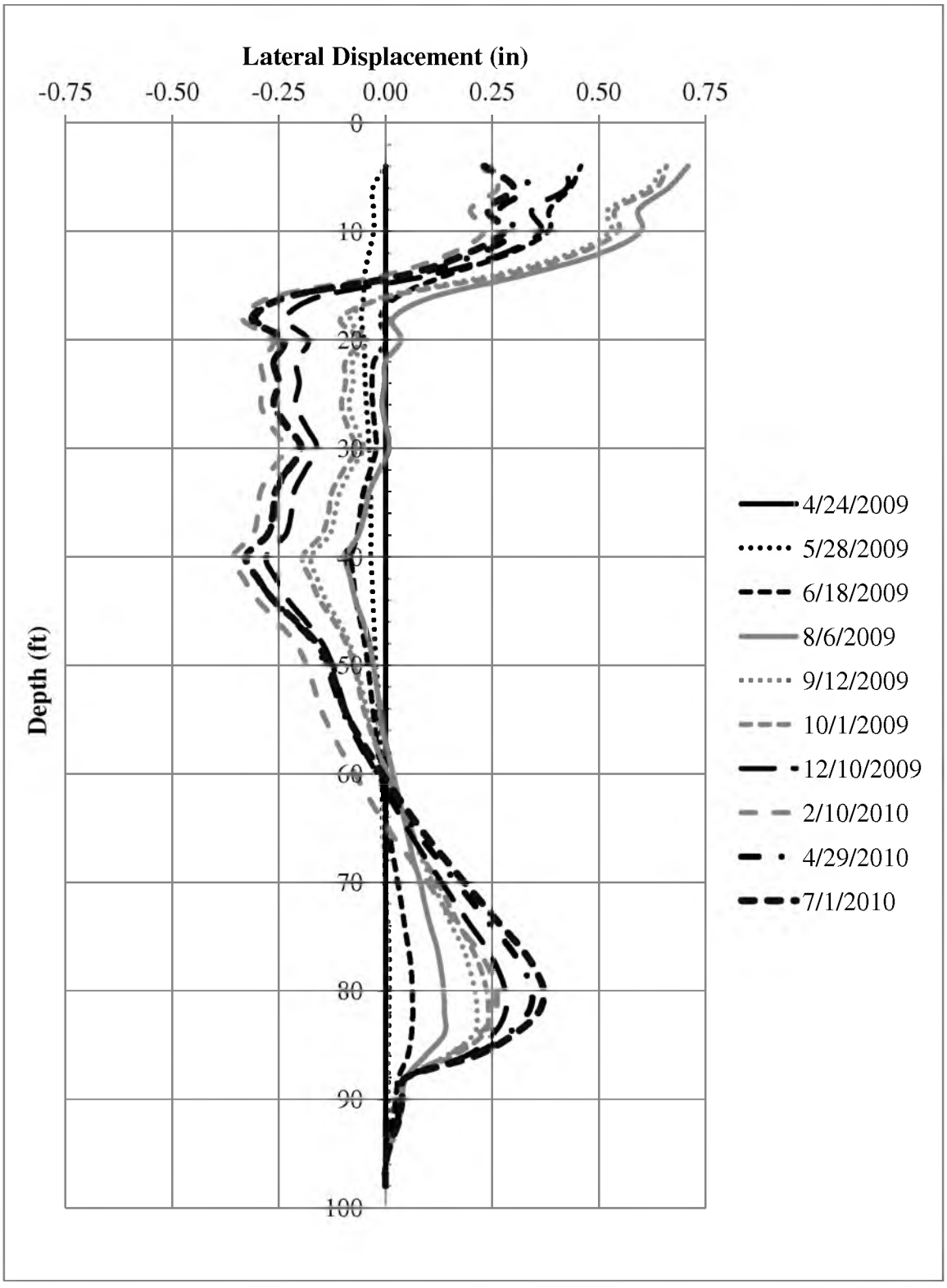

Figure 5-29. Results from vertical inclinometer located 8 ft outside the south MSE wall.

4 ft below the ground surface. The magnitude of lateral deformation obtained via readings from the vertical inclinometer at a depth of 4 ft below the ground surface on July 1, 2009 was 0.232 in at the same depth. The increased amount of lateral displacement between weeks was an indication of impending failure. A detailed analysis of the squeezing beneath the edge of the embankment is being performed by others and will not be presented here.

5.6.2 ShapeAccelArray

Two SAAs were installed to depths of 96 ft below the original ground surface with the purpose of monitoring the stability and lateral deformation of SR 77 embankment's foundation. These SAAs were located 20 ft inside the south MSE wall and 8 ft outside the MSE wall near the vertical inclinometer. The SAA located 8 ft outside the MSE wall near the vertical inclinometer was positioned there to determine the reliability of lateral deformation readings obtained by the SAA when compared to the vertical inclinometer outside the MSE wall near the vertical inclinometer. Results for lateral deformation obtained via SAA located 20 ft inside the south MSE wall for May 26, 2009; May 28, 2009; June 18, 2009; August 6, 2009; and December 2, 2009 are shown in Figure 5-30. Results for lateral deformation obtained via the SAA located 8 ft inside the south MSE wall for the same dates are shown in Figure 5-31.

5.6.3 Comparison

Both methods of measuring lateral deformation show a significant amount of movement in the upper 10 ft of their respective profiles. In terms of soil layering and the

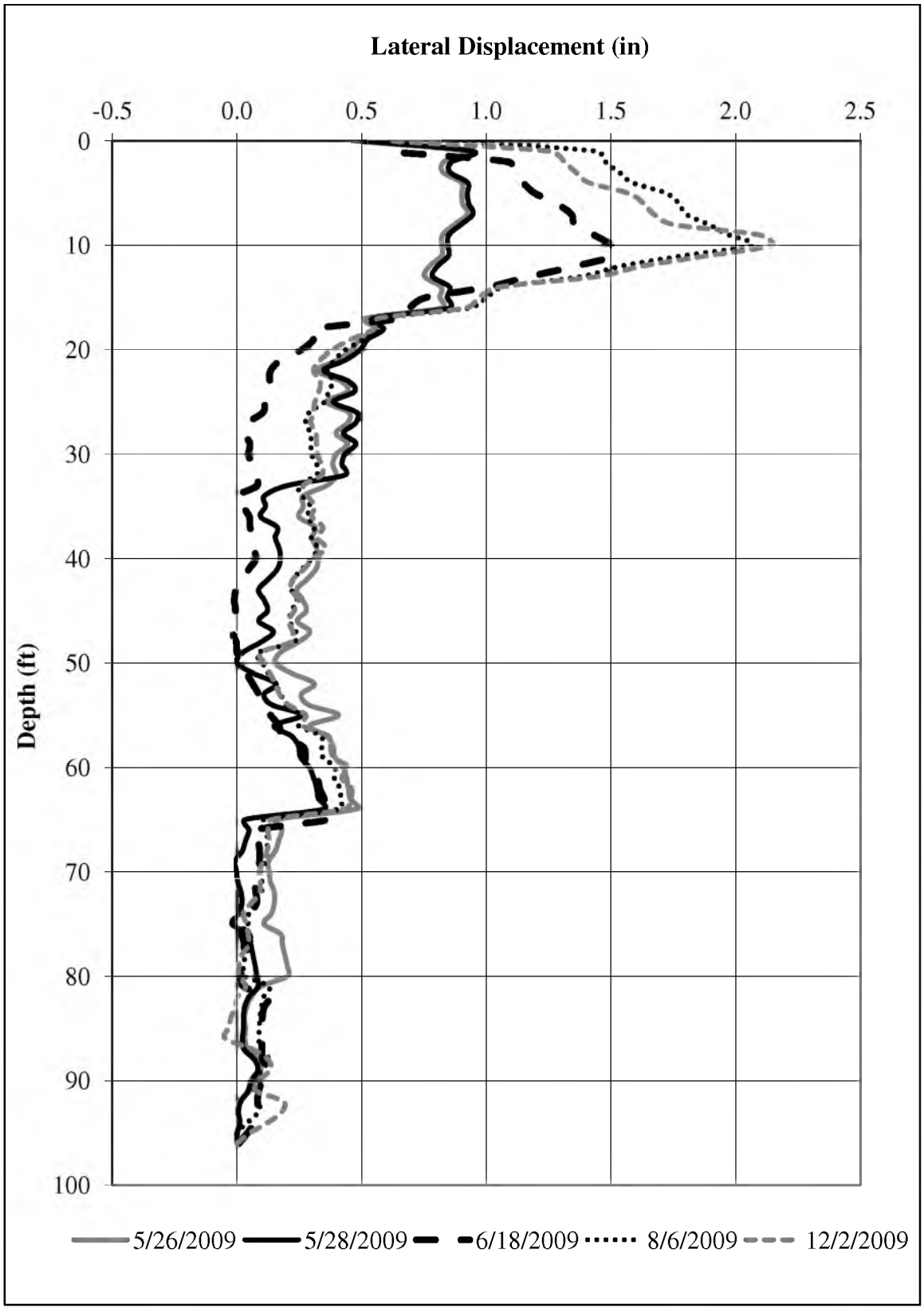

Figure 5-30. Results from SAA located 20 ft inside the south MSE wall.

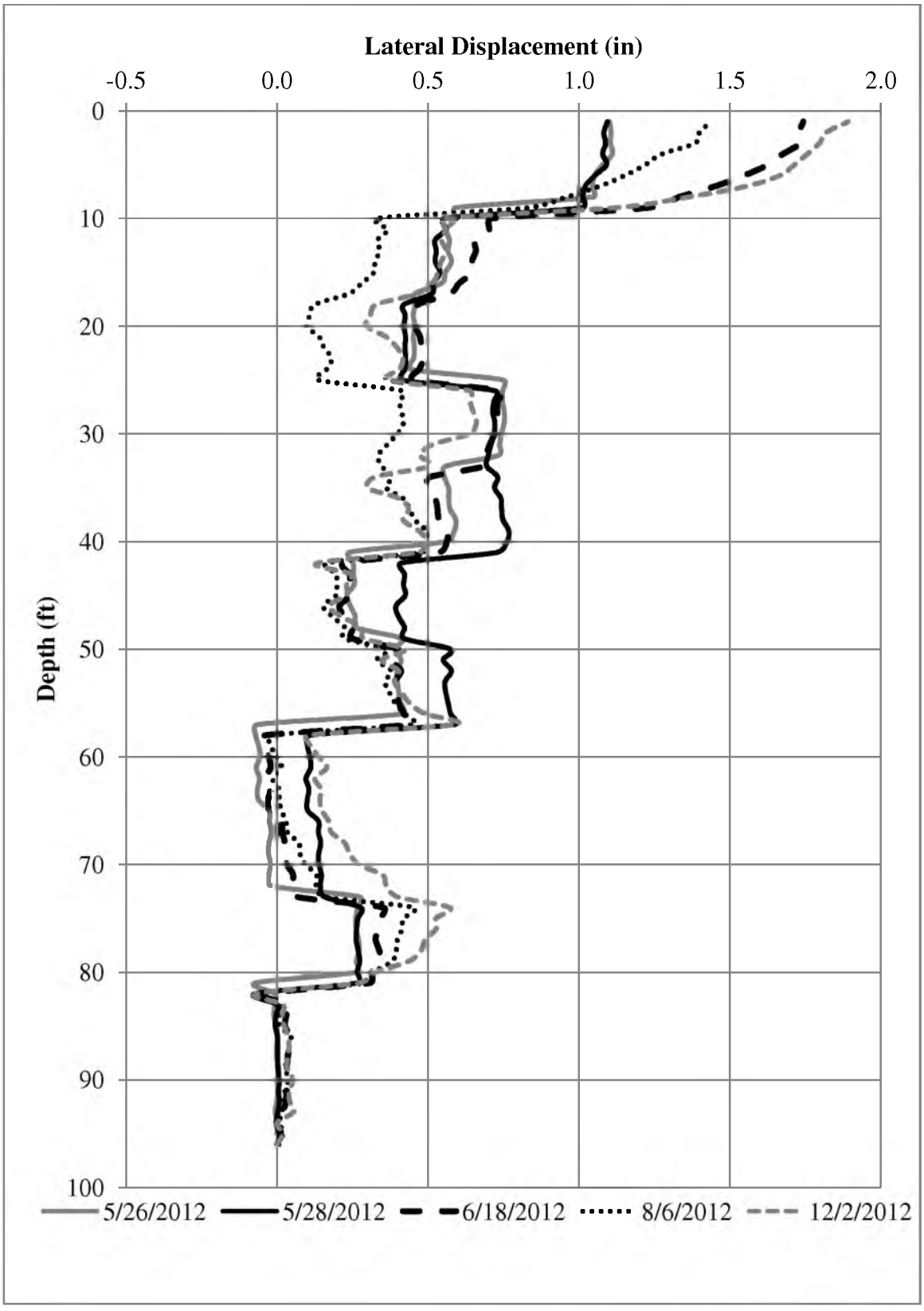

Figure 5-31. Results from SAA located 8 ft outside the south MSE wall.

CPT results (see Figure 4-1 and Figure 4-2) this makes sense due to a soft layer of soil at 3 to 8 ft below the original ground surface between two hard layers located between 0 to 3 ft below the original ground surface, and 8 to 14 ft below the original ground surface. Lateral deformation measured by the SAA, located within the embankment's foundation at a depth of 10 ft, was 2.37 inches at the end of the project. The lateral deformation measured by the SAA, located 8 ft outside the south MSE wall at the same depth was 1.41 inches. Due the amount of readings collected by the data collector, lateral deformation readings for the beginning of the project, at the date of drop in horizontal pressure determined by the push-in cells, middle of the project, and end of the project for both locations are shown in Figure 5-30 and Figure 5-31.

Lateral deformation measured by the vertical inclinometer probe and the SAA throughout the construction of the embankment are compared and shown in Figure 5-32 through Figure 5-35 at four distinct dates: (1) Beginning of construction, (2) drop in horizontal pressure determined from Figure 5-5, (3) middle of construction, and (4) the end of construction. At all four time periods, lateral deformation measured by the SAA exceeds lateral deformation measured by the vertical inclinometer probe.

Lateral deformation measured by SAA is more defined and more realistic in shape and relative magnitude than the lateral deformation measured by the vertical inclinometer due to the flexibility of the SAA, the spacing of the joints connecting the rigid segments in the SAA, and the continuous real time logging of SAA data readings. The flexible joints are spaced at every 1 ft interval allowing deformation readings to be obtained at these joints. Real time data was collected using the Campbell Scientific data logger, which allowed for sudden movements to be obtained during the construction and removal

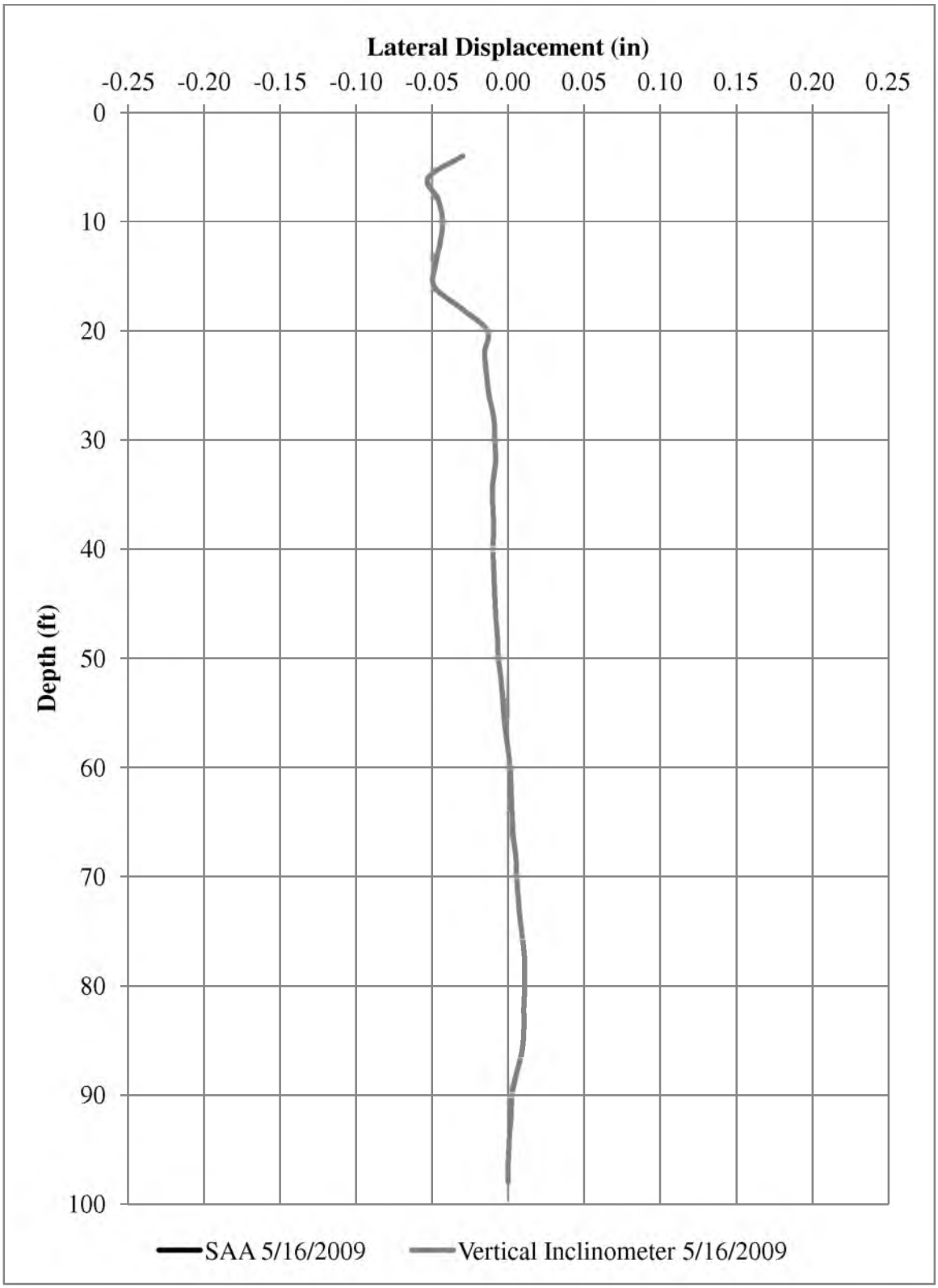

Figure 5-32. Measured lateral deformation from traditional vertical inclinometer and SAA located 8 ft outside the south MSE at the beginning stages of the project on May 16, 2009.

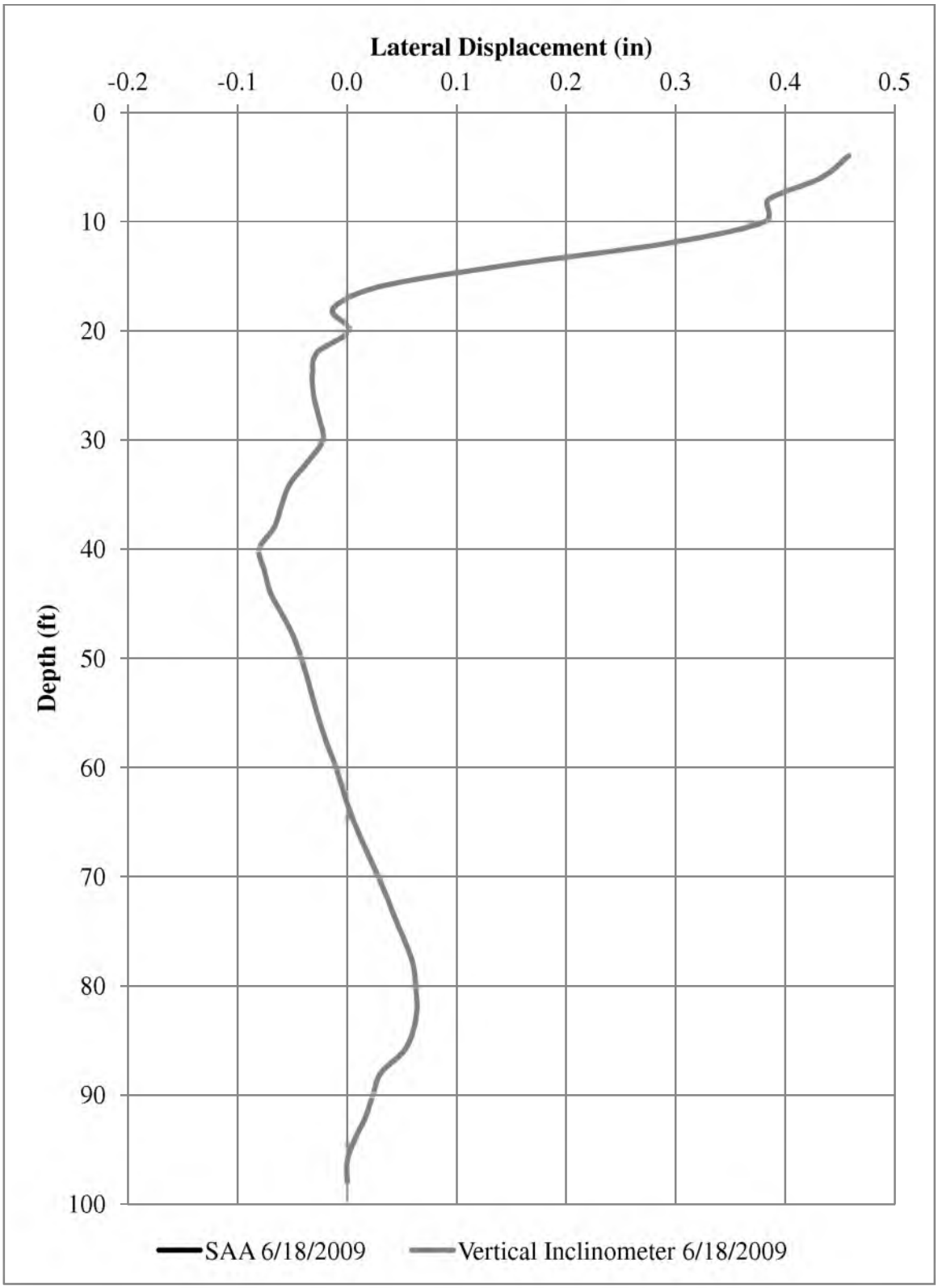

Figure 5-33. Measured lateral deformation from traditional vertical inclinometer and SAA located 8 ft outside the south MSE on June 18, 2009.

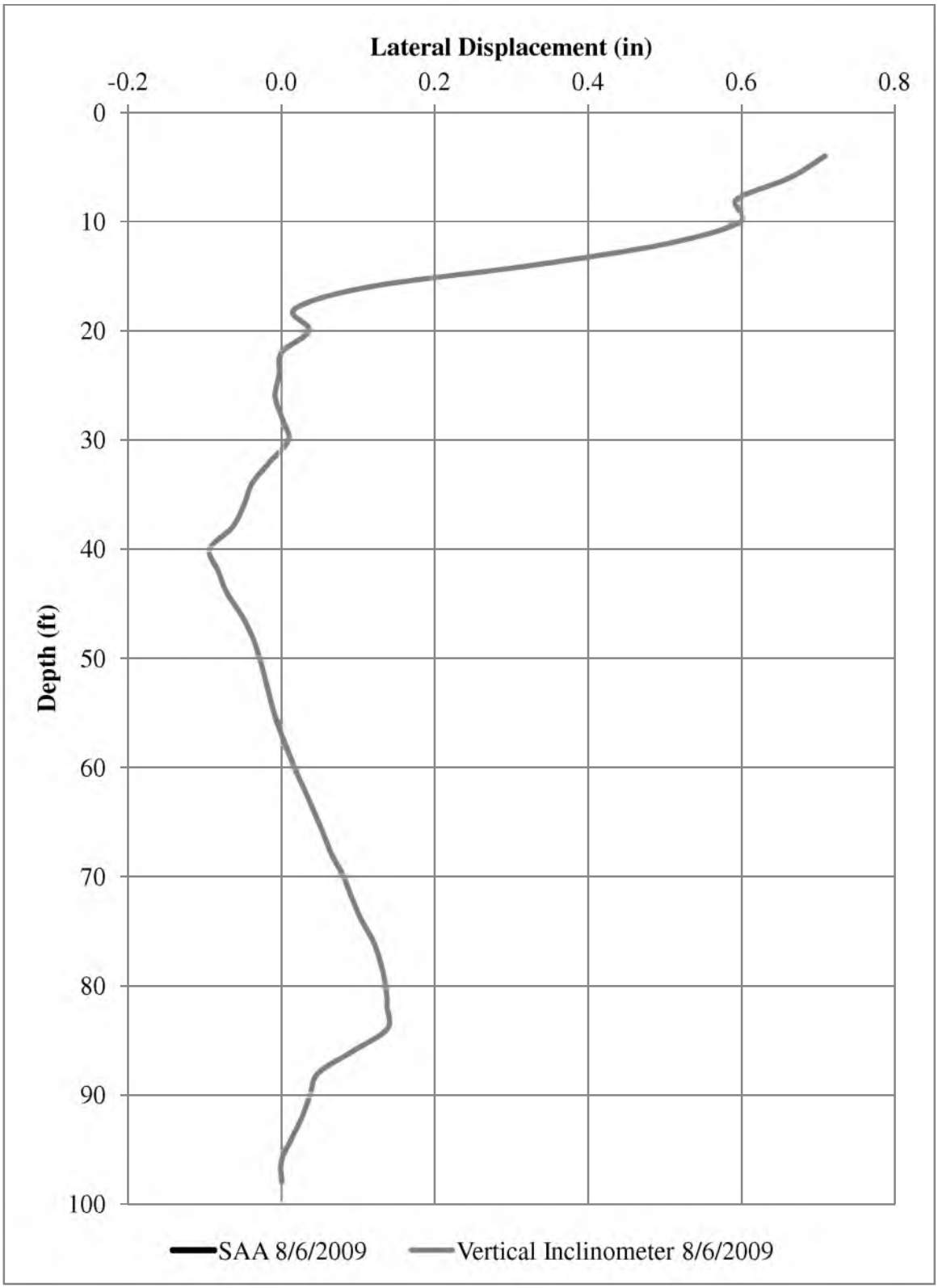

Figure 5-34. Measured lateral deformation from traditional vertical inclinometer and SAA located 8 ft outside the south MSE on August 6, 2009.

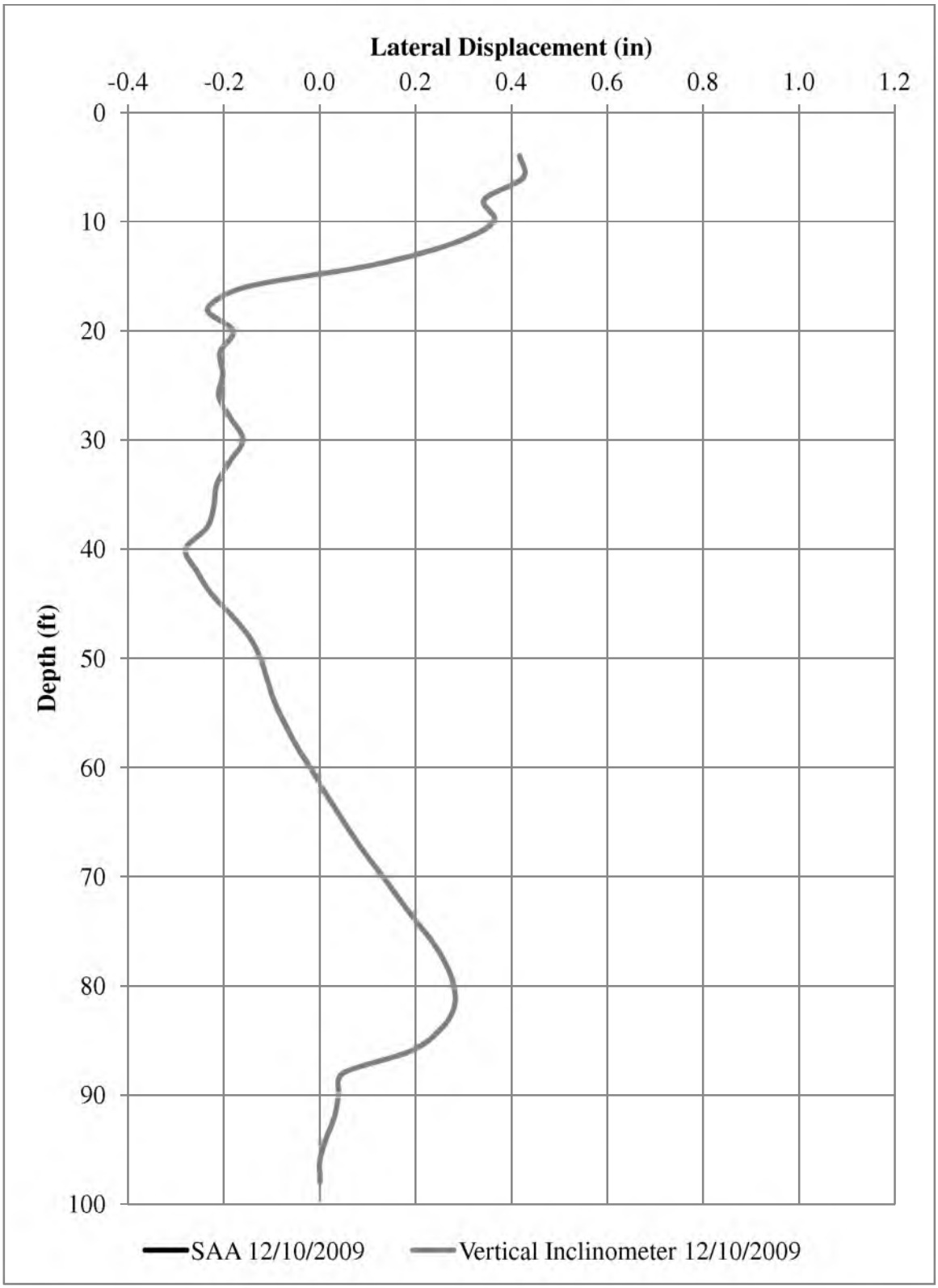

Figure 5-35. Measured lateral deformation from traditional vertical inclinometer and SAA located 8 ft outside the south MSE on December 10, 2009.

of the surcharge. In contrast, measurements obtained via the vertical inclinometer are constrained by the PVC pipe, are measured at an interval of 2 ft, and were obtained on a weekly schedule throughout construction.

Movement of the lateral deformation using the vertical inclinometer and SAA were previously shown in Figure 5-29 and Figure 5-31. Lateral deformation during construction and placement of surcharge was expected to move away from the wall. This was not the case for most of the movement recorded by the vertical inclinometer (see Figure 5-29). Lateral deformation recorded by the SAA shows movement, as expected, moving away from the wall (see Figure 5-31).

6 ANALYSIS OF RESULTS FROM INSTRUMENTATION

The following section discusses several methods of analyses used to predict magnitude and time rate of primary consolidation settlement. Primary consolidation settlement analysis, including a comparison of prediction of primary consolidation at time with the measured settlement obtained using the magnet extensometer, will be discussed in Section 6.1. Magnitude and time rates of the primary consolidation settlement using Terzaghi's method and Davis and Raymond's method for prediction of excess pore pressure dissipation for individual cohesive layers will be discussed in Section 6.2. The prediction of primary consolidation settlement and time for surcharge removal will be analyzed using two methods: (1) Asaoka's method, and (2) individual layer method and a comparison between the two methods also will be discussed with in Section 6.3.

6.1 Ultimate Primary Consolidation Settlement

The ultimate consolidation settlements for the permanent embankment load predicted within the cohesive layers at the SR 77 research embankment were calculated using results for soil parameters obtained from CRS testing. The ultimate primary consolidation settlement for individual sublayers within the cohesive layers was determined using Eq. 6-1 and 6-2.

$$S_{c,ult} = C_{r\varepsilon} \log \frac{\sigma'_{v,i,j}}{\sigma'_{v,i,j=0}} \Delta z \quad (6\text{-}1)$$

$$\sigma'_{v,i,j} = \sigma'_{v,i,j=0} + \Delta\sigma_{v,i,j} - \Delta u_{ss} \quad (6\text{-}2)$$

where:

$\sigma'_{v,i,j=0}$ = initial effective vertical stress (before embankment is constructed)

$\sigma'_{v,i,j}$ = final effective vertical stress (after permanent embankment is constructed)

$\Delta\sigma_{v,i,j}$ = change in total vertical stress at original ground surface as measured by the centerline pressure plates

$\Delta u_{ss} = u_{i,j} - u_{i,j=0}$ = change excess pore pressure at steady state conditions measured by the free field piezometers

For $\Delta\sigma_{v,i}$, at all depths to be equal to $\Delta\sigma_{v,i,}$ at ground surface, one-dimensional conditions were assumed due to the geometry of the embankment (the length of the embankment being much greater than the width of the loaded area).

It needs to be noted that, $C_{r\varepsilon}$ was used in place of $C_{c\varepsilon}$ for ultimate primary consolidation settlement, because $\sigma'_{v,i,j}$ was less than σ'_p.

A sample calculation of predicted primary consolidation settlement for a sublayer at a depth of 16.5 ft in Layer 3 for July 1, 2010 is as follows:

z_{gwt} = depth of groundwater table relative to the original ground surface = 4.0 ft

γ_w = unit weight of water = 62.4 pcf (assumed)

Total unit weight and thickness of all layers down to the desired depth:

γ_1 = 126.90 psf, t_1 = 3 ft

$\gamma_2 = 112.78$ psf, $t_2 = 5$ ft

$\gamma_3 = 126.90$ psf, $t_3 = 6$ ft

$\gamma_4 = 125.15$ psf, $t_4 = 2.5$ ft

$C_{c\varepsilon} = 0.0451$

$\Delta h = 1$ ft

Calculated effective overburden stress at depth of 16.5 ft, prior to construction of the embankment:

$$\sigma_{v,i,j=0} = \sum_{k=1}^{k=n} \gamma_k t_k = (126.90)(3) + (112.78)(5) + (126.90)(6) + (125.15)(2.5) = 2018.88 \text{ psf}$$

Assuming that the pore water was in equilibrium at the time construction of the embankment began:

$u_{i,j=0} = u_{ss,I} = \gamma_w(z_i - z_{gwt}) = 62.4(16.5\text{-}4.0) = 780$ psf

$\sigma'_{v,i,j=0} = \sigma_{v,i,j=0} - u_{i,j=0} = 2018.88 - 780 = 1238.88$ psf

The value of change in total vertical stress for time j=0 to July 1, 2010 was obtained from readings of the pressure plates as:

$$\Delta\sigma_{v,(i,j=0\rightarrow j)} = 360279 \text{ psf}$$

The value of change in steady state pore pressures for time j=0 to July 1, 2010 was obtained from readings of the free field piezometers as:

$$\Delta u_{ss} = -28.74 \text{ psf}$$

The change in effective stress as defined in Eq. 6-2:

$$\sigma'_{v,i,j} = \sigma'_{v,i,j=0} + \Delta\sigma_{v,i,j} - \Delta u_{ss}$$

$$\sigma'_{v,i,j} = 1{,}238.88 + 360279 - (-28.74) = 4870.41 \text{ psf}$$

The ultimate primary consolidation settlement is now calculated using Eq. 6-1:

$$S_{c,ult} = C_{r\varepsilon} \log \frac{\sigma'_{v,i,j}}{\sigma'_{v,i,j=0}} \Delta z = 0.0451 \log\left(\frac{4870.41}{1238.88}\right) 1 = 0.322 \text{ in}$$

The ultimate primary consolidation using 1-ft sublayers within Layer 3, for July 1, 2010 is shown in Table 6-1.

The ultimate primary consolidation settlement for Layer 3 is the summation of all the settlement occurring in the sublayers:

$$S_{c,ult} = \sum_{i=1}^{i=n} S_{ci,ult} = 1.909 \text{ in}$$

Results for predicted primary consolidation settlement for July 1, 2010 within each cohesive layer are summarized in Table 6-2.

The best estimate of ultimate primary consolidation results using Eq. 6-1 and Eq. 6-2 for July 1, 2010 were compared with measured settlement obtained via the magnet extensometer for July 1, 2010 and are presented in Table 6-3

To determine if the predicted ultimate primary consolidation settlement results obtained from Eq. 6-1 and Eq. 6-2 for July 1, 2010 are reasonable, the percent difference was calculated using Eq. 6-3. The measured primary consolidation settlement obtained via the magnet extensometers for July 1, 2010 was the target value used for calculations.

$$\left[\frac{S_{c,measured} - S_{c,ult}}{S_{c,measured}}\right] 100 \qquad (6\text{-}3)$$

Table 6-1. Ultimate primary consolidation settlement using 1-ft sublayers within Layer 3, for July 1, 2010.

Sublayer	Depth to Top of Sublayer (ft)	Depth to Bottom of Sublayer (ft)	Depth to Mid Height of Sublayer (ft)	Δz (ft)	$\sigma'_{v,i,j=0}$ (psf)	$\Delta\sigma_v$ (psf)	Δu_{ss} (psf)	$\sigma'_{v,i,j}$ (psf)	$S_{c,ult}$ (in.)
1	14	15	14.5	1	1113.38	3602.79	-28.75	4744.91	0.341
2	15	16	15.5	1	1176.13	3602.79	-28.75	4807.66	0.331
3	16	17	16.5	1	1238.88	3602.79	-28.75	4870.41	0.322
4	17	18	17.5	1	1301.63	3602.79	-28.75	4933.16	0.313
5	18	19	18.5	1	1364.38	3602.79	-28.75	4995.91	0.305
6	19	20	19.5	1	1427.13	3602.79	-28.75	5058.66	0.297
								Total	1.909

Table 6-2 Predicted ultimate consolidation settlement for each layer for July 1, 2010 using soil parameters obtained from CRS tests.

Layer	$S_{c,ult}$ (in)
1	1.536
3	1.909
5	0.922
7	1.182

Table 6-3. Magnitudes of predicted utlimate primary consolidation settlement results for July 1, 2010 using Eq. 6-1 and Eq. 6-2 and measured settlement from the magnet extensometer.

Settlement for July 1, 2010 (in)		
Layer	$S_{c,ult}$	Magnet Extensometer
1	1.536	4.803
3	1.909	1.535
5	0.922	0.591
7	1.182	1.398

where:

$S_{c,measured}$ = measured settlement obtained via magnet extensometer readings

$S_{c,ult}$ = best estimate of ultimate primary consolidation settlement determined from Eq. 6-1 and Eq. 6-2. Percent differences for each layer are found in Table 6-4.

The differences between the predicted primary consolidation settlement for July 1, 2010 and measured settlement using the magnet extensometers at the same time are shown in Table 6-3 and Table 6-4.

Predicted ultimate primary consolidation settlement at time for Layers 1 and 7 were underestimated when compared to the measured value at time. Predicted primary consolidation settlements for Layers 3, and 5 were overestimated when compared to the measured value at time for these layers.

These discrepancies, shown in Table 6-3 and Table 6-4, for predicting primary consolidation settlement at time with measured values at the same time reveal that improvements need to be made in predicting settlement with time.

Table 6-4. Percent difference for each layer using the predicted utlimate primary consolidation settlement and measured settlement using the magnet extensometer for July 1, 2010.

Layer	% Difference
1	212.67
3	19.59
5	35.89
7	18.23

6.2 Time Rate of Primary Consolidation Settlement

Time rate of primary consolidation settlement analyses using the measured excess pore pressures obtained via vibrating wire piezometers located at the centerline of the embankment and the predicted excess pore pressures using Terzaghi's method and Davis and Raymond's method was performed for cohesive layers for the SR 77 research embankment project. Properties and locations of cohesive layers where excess pore pressures developed were analyzed and will be discussed in Section 6.2.1. A comparison of predicted and measured excess pore pressures for July 1, 2010 will be analyzed in Section 6.2.2. To conclude the discussion of time rate of consolidation settlement, a comparison of predicted and measured primary consolidation settlement will be discussed in Section 6.2.3. The purpose of Section 6.2 is to show the effect of excess pore pressure dissipation, whether measured or predicted, on the time rate of primary consolidation settlement.

6.2.1 Properties and Locations of Cohesive Soil Layers

The magnitude of primary consolidation settlement within the cohesive layers at the SR 77 research embankment site were predicted as a function of time using

Terzaghi's method and Davis and Raymond's method, in conjunction with the finite difference method. Details of these analyses, as well as results from them will be discussed in this section.

As mentioned previously, there were four significant cohesive layers within the foundation beneath the SR 77 research embankment. The interfaces between the cohesive and granular layers were assumed to be free drainage boundaries for the predictions of primary consolidation settlement for each layer or sublayer as a function of time.

The following parameters were needed for each cohesive layer to perform the predictions of time rate of primary consolidation settlement: Total vertical stress (σ_v) acting on the foundation caused by construction of the embankment; the total unit weight (γ) of each layer; the elevation of the ground water table; and the initial height (h_0), the coefficient of consolidation (c_v), the coefficient of permeability (k), the preconsolidation pressure (σ'_p), and the recompression and/or virgin compression indices ($C_{r\varepsilon}$ and/or $C_{c\varepsilon}$) for each cohesive layer.

Values of σ_v acting on the surface of the foundation soil beneath the embankment were obtained from the average value of the readings taken for the two vibrating wire pressure plates located 4 ft south of the centerline of the embankment (see Figure 5-3). One-dimensional strain conditions were assumed, which allows the calculation of $\Delta\sigma_v$ at any depth beneath the centerline to be set equal to σ_v acting on the surface. This assumption is reasonably valid since the width of the loaded area (the width of the embankment) is relatively large in comparison to the thickness of the zone where most of the settlement occurred. As previously mentioned in Section 3.3, vibrating wire readings

were obtained on an hourly basis from the beginning of construction until December 1, 2009. Because of the extremely large number of readings collected, the change in vertical stress needed to be consolidated into time steps that were large enough that the finite difference method was stable. As previously mentioned in Section 2.4.2, a value of α less than 1/2 is required for the finite difference method to be stable and a value of 1/6 is optimal. α is a function of C_v, Δt, and Δz (see Eq. 2-14). To determine an appropriate value for α for each layer or sublayer, the following parameters were considered and analyzed: Boundary conditions, drainage paths, variation of C_v and k with effective stress, and selection of appropriate values of Δt and Δz. The layering of the soils and the determination of the type of each soil (granular or cohesive) was described previously in Section 5.5.3. It was assumed that each interfaces between a cohesive layer and the adjacent granular layer was a free drainage boundary, which to be valid requires that two requirements be met (Seed and Booker 1976): (1) The ratio of permeability of the granular soil to the permeability of the cohesive soil ($k_{granular}/k_{cohesive}$) be greater than about 200; and (2) the granular soil have sufficient pore capacity to handle the flow of water from the cohesive soil. Both these requirements were met for the soils analyzed at this site. Based on the results from CRS tests, it was determined that C_v varied with depth within Layers 1, 3, 5, and 7, and that each depth C_v also varied with change in effective vertical stress. To account for the variation of C_v (and hence, k) as a function of σ'_v at each depth where a CRS test was performed, a second order polynomial regression analysis was performed yielding an equation for $C_v = f(\sigma'_v)$ (see Appendix B). This variation of C_v with depth within the cohesive layers, required that values of Δt and Δz for each cohesive layer or sublayer be different. The interval for Δt that stabilized the finite

difference program for each layer was determined through a trial and error process. The trial and error process involved writing a macro within Microsoft Excel to consolidate the vertical stresses into averages for every 3, 4, 6, and 8 hours, while keeping in mind that Δt needed to be a multiple of a certain value so that direct comparisons of settlement at any given time could be made. The interval of Δt selected for this process was 1/8 day. In general, if C_v was greater than 1.0 ft^2/day within a cohesive layer, Δt for that layer needed to be 0.125 days and Δz needed to be greater than Δt. If C_v was smaller than 1.0 ft^2/day, then Δt needed to be 0.25 days and Δz needed to be larger than 0.25 ft.

To maintain α below 1/2, Δt, Δz, and the initial values of C_v that were used in the predictions of primary consolidation settlement are summarized in Table 6-5 for each layer and sublayer. These values were selected after careful consideration to ensure that the value of α for each layer and sublayer was less than 1/2 and as close to 1/6 as possible. The logic used to select appropriate values of Δt and Δz for two of the cohesive layers is discussed in the paragraphs below.

Layer 1, with a depth range from 3 to 8 ft below the original ground surface, consisted primarily of clayey silt (see Figure 4-1 and Table 4-1 for details). The initial value of C_v at a depth of 5 ft was determined from the regression equation shown in Figure 6-1 is as follows:

$\sigma'_{v0} = 0.563$ ksf

$$C_v = 0.0009207\,1(\sigma'_{v0})^2 - 0.009794(\sigma'_{v0}) + 2.751$$

$$C_v = 0.0009207\,1(0.563)^2 - 0.009794(0.563) + 2.751 = 2.70\,\frac{ft^2}{day}$$

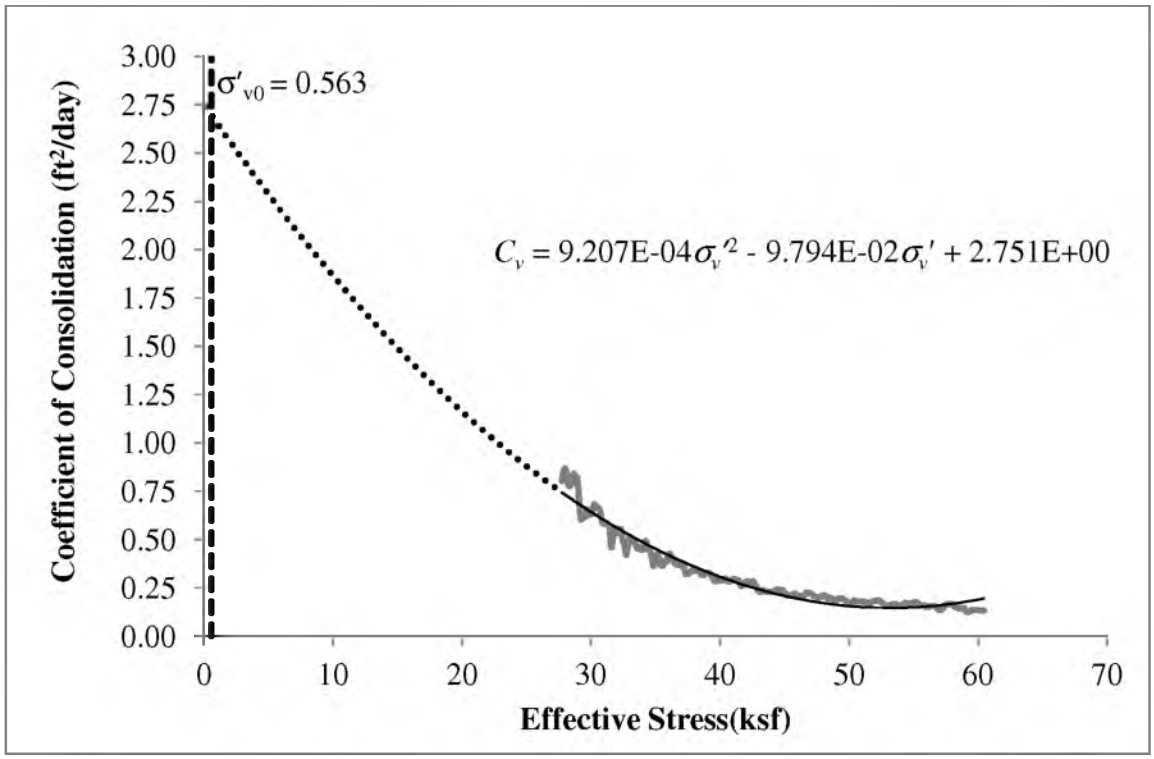

Figure 6-1. Regression plot for determining C_v with effective stress at 5 ft.

Because of the high value of C_v, the time for complete pore pressure dissipation was expected to be rapid. To stabilize the finite difference program for Layer 1 with the high value of C_v using Eq. 2-14, Δt needed to be a multiple of 0.125. The value of Δt used to stabilized Eq. 2-14 was determined to be 0.125.

The depth increment, Δz, needed to be a number that would divide Layer 1 into equal sublayers using Eq. 6-4.

$$\Delta z = \frac{H_t}{N} \tag{6-4}$$

where:

H_t = total height of the layer

N = number of sublayers

Layer 1 had a total height of 5 ft. Rearranging Eq. 2-14 and solving for the Δz is shown in Eq. 6-5.

$$\Delta z = \sqrt{\frac{C_v \Delta t}{\alpha}} \tag{6-5}$$

Assuming α to be 1/2 and using the initial value for C_v and the chosen Δt, Δz is calculated as follows:

$$\Delta z = \sqrt{\frac{C_v \Delta t}{\alpha}} = \sqrt{\frac{(2.71)(0.125)}{0.5}} = 0.82 \text{ ft}$$

Assuming α = 1/6 and using the initial value for C_v and the chosen value of Δt, Δz is calculated as follows:

$$\Delta z = \sqrt{\frac{C_v \Delta t}{\alpha}} = 1.42 \text{ ft}$$

Rearranging Eq. 6-4 and solving for the number of sublayers using the calculated values of Δz are as follows:

$$N = \frac{H_t}{\Delta z} = \frac{5}{0.82}$$

$$N = \frac{H_t}{\Delta z} = \frac{5}{0.82} = 6.1 \text{ for } \alpha = ½$$

$$N = \frac{H_t}{\Delta z} = \frac{5}{1.42} = 3.5 \text{ for } \alpha = 1/6$$

To keep α between 1/6 and 1/2, the number of sublayers must be between 3.5 and 6.1. However, the values for Δz cannot be used because the number of sublayers needed

to be a whole integer number. Using Eq. 6-4 and Eq. 2-14 with the number of sublayers equal to 4, 5, and 6, the corresponding values for Δz and α are as follows:

For N = 4, $\Delta z = 5 / 4 = 1.25$ ft and $\alpha = \frac{c_v \Delta t}{\Delta z^2} = \frac{(2.70)(0.125)}{(1.25)^2} = 0.216$

For N = 5, $\Delta z = 5 / 5 = 1$ ft and $\alpha = \frac{c_v \Delta t}{\Delta z^2} = \frac{(2.70)(0.125)}{(1)^2} = 0.338$

For N = 6, $\Delta z = 5 / 6 = 0.833$ ft and $\alpha = \frac{c_v \Delta t}{\Delta z^2} = \frac{(2.70)(0.125)}{(0.833)^2} = 0.486$

N = 4 would have given a value of α closest to 1/6. However, it was also desired to keep $\Delta z \leq 1.0$ ft whenever possible, so $N = 5$ was chosen with $\alpha = 0.338$ as shown above.

Layer 7, with a depth range from 55 to 88 ft below the original ground surface, consisted of primarily of clay (see Figure 4-1 and Table 4-1 for details). Layer 7 was divided into six depth ranges consisting of sublayers with varying values of C_v as shown in Table 6-5 (interactions of sublayers within depth ranges will be discussed shortly hereafter). The initial value of C_v at a depth of 75.6 ft was determined from the regression equation shown in Figure 6-2 as follows:

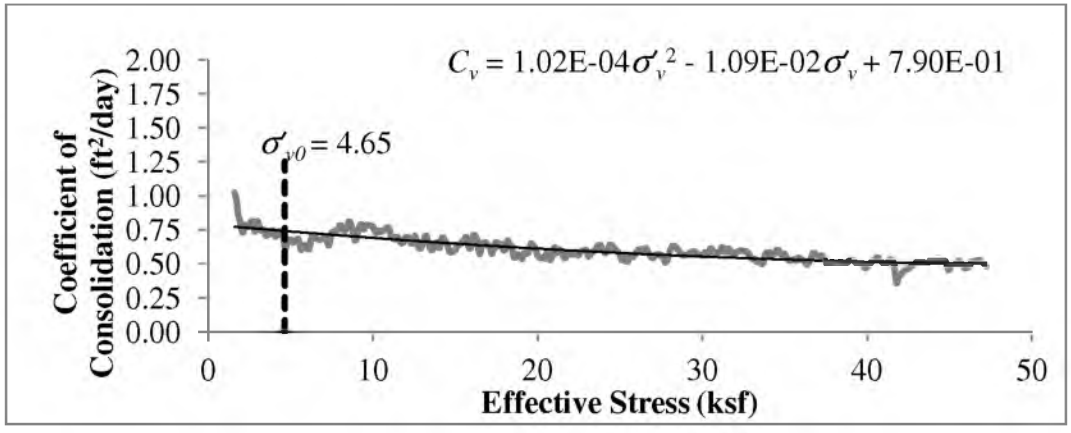

Figure 6-2. Regression plot for determining C_v with effective stress at 75.6 ft

$\sigma'_{v0} = 4.65$ ksf

$C_v = 0.000102\sigma'^{2}_{v} - 0.0109\sigma'_{v} + 0.790$

$$C_v = 0.000102(4.65)^2 - 0.0109(4.65) + 0.7415 \ \frac{\text{ft}^2}{\text{day}}$$

Because of the low value of C_v, the time for complete pore pressure dissipation was expected to be time consuming. To stabilize the finite difference program for Layer 7 at depth range of 72.25 to 78.25 ft with a low value of C_v, using Eq. 2-14, Δt needed to be a multiple of 0.125 as previously stated. The value of Δt used to stabilize Eq. 2-14 was determined to be 0.25.

The sublayer at a depth range of 72.25 ft to 78.25 ft had a total of 6 ft. The depth increment, Δz, needed to be a number that would divide this depth range into sublayers of equal heights while stabilizing the finite difference method and was determined using Eq. 6-4.

Assuming α to be 1/2 and using the initial value of C_v and the chosen Δt for this sublayer, it is calculated as follows:

$$\Delta z = \sqrt{\frac{(0.742)(0.25)}{1/2}} = 0.61 \text{ ft}$$

Assuming $\alpha = 1/6$ and using the initial value of C_v and the chosen Δt for this layer, it is calculated as follows:

$$\Delta z = \sqrt{\frac{(0.742)(0.25)}{1/6}} = 1.05 \text{ ft}$$

Rearranging Eq. 6-4 and solving for the number of sublayers using the calculated values of Δz are as follows:

$$N = \frac{H_t}{\Delta z} = \frac{6}{0.6} = 9.8 \text{ for } \alpha = ½$$

$$N = \frac{H_t}{\Delta z} = \frac{6}{1.05} = 5.7 \text{ for } \alpha = 1/6$$

To keep α between 1/6 and 1/2, the number of sublayers needed to be between 5.7 and 9.8. As previously stated, the values for Δz cannot be used because the number of sublayers needed to be a whole integer number. Using Eq. 6-4 and Eq. 2-14 with the number of sublayers equal to 6, 7, 8, and 9, the corresponding values for Δz and α are as follows:

For $N = 6$, $\Delta z = 6 / 6 = 1$ ft and $\alpha = \frac{c_v \Delta t}{\Delta z^2} = \frac{(0.7415)(0.25)}{(1)^2} = 0.19$

For $N = 7$, $\Delta z = 6 / 7 = 0.857$ ft and $\alpha = \frac{c_v \Delta t}{\Delta z^2} = \frac{(0.7415)(0.25)}{(0.857)^2} = 0.25$

For $N = 8$, $\Delta z = 6 / 8 = 0.75$ ft and $\alpha = \frac{c_v \Delta t}{\Delta z^2} = \frac{(0.7415)(0.25)}{(0.75)^2} = 0.33$

For $N = 9$, $\Delta z = 6 / 9 = 0.667$ ft and $\alpha = \frac{c_v \Delta t}{\Delta z^2} = \frac{(0.7415)(0.25)}{(.667)^2} = 0.42$

$N = 6$, gives us a value of α closest to 1/6. It also satisfied one criterion presented during the discussion of Layer 1, which stated if possible to keep $\Delta z \leq$ to 1 ft. $N = 6$ was chosen with $\alpha = 0.19$. Values of Δt, Δz, initial C_v, and α used in the finite difference calculations for excess pore pressures within the cohesive layers and sublayers are presented in Table 6-5.

The next step was to determine the parameter β using Eq. 2-15 at the interfaces of sublayers within Layers 5 and 7. Layer 5 had one interface at a depth of 37.3 ft. Layer 7, the most complicated layer, had four interfaces. Depths of interfaces, along with their

Table 6-5. Values of Δt, Δz, initial C_v, and α used in the finite difference calculations for excess pore pressures within the cohesive layers and sublayers.

Layer	Top of Depth (ft)	Bottom of Layer (ft)	Depth of Interface (ft)	Δt (days)	Δz (ft)	Initial C_v (ft^2/day)	α
1	3	8	-	0.125	1	2.7	0.34
3	14	20	-	0.125	1	3.49	0.44
5	30.25	37.25	37.25	0.25	1	0.47	0.12
5	37.25	44.92	-	0.25	0.33	0.09	0.21
7	55	57.5	57.5	0.25	0.5	0.44	0.44
7	57.5	67.5	65.5	0.25	1	1.05	0.26
7	70.25	78.25	78.25	0.25	1	0.74	0.19
7	78.25	82.75	82.75	0.25	0.5	0.4	0.4
7	82.75	88	-	0.25	0.25	0.09	0.35

initial values of k and β at depths i-1 and i+1, are shown in Table 6-6. A sample calculation of β for the interface at a depth of 37.25 ft is as follows:

The initial effective overburden stress:

$\sigma'_{v0} = 2.55$ ksf

The coefficient of permeability, k, at node i-1, located just above a depth of 37.25 ft below the original ground surface was determined from a regression equation shown in in Figure 6-3 as follows:

Table 6-6. Initial values of β used in the finite difference calculations for excess pore pressures adjacent to the interfaces of the cohesive layers and sublayers.

Depth of Interface (ft)	k_{i-1} (cm/s)	k_{i+1} (cm/s)	Δz_{i-1} (ft)	Δz_{i+1} (ft)	β
37.25	4.43E-08	1.87 E-08	1.00	0.33	1.27
57.50	5.83E-08	6.62E-08	0.50	1.00	0.57
65.50	5.70E-08	6.49E-08	1.00	0.75	1.52
78.25	5.50E-08	6.31E-08	1.00	0.50	2.29
82.50	5.43E-08	6.26E-08	0.50	0.25	2.31

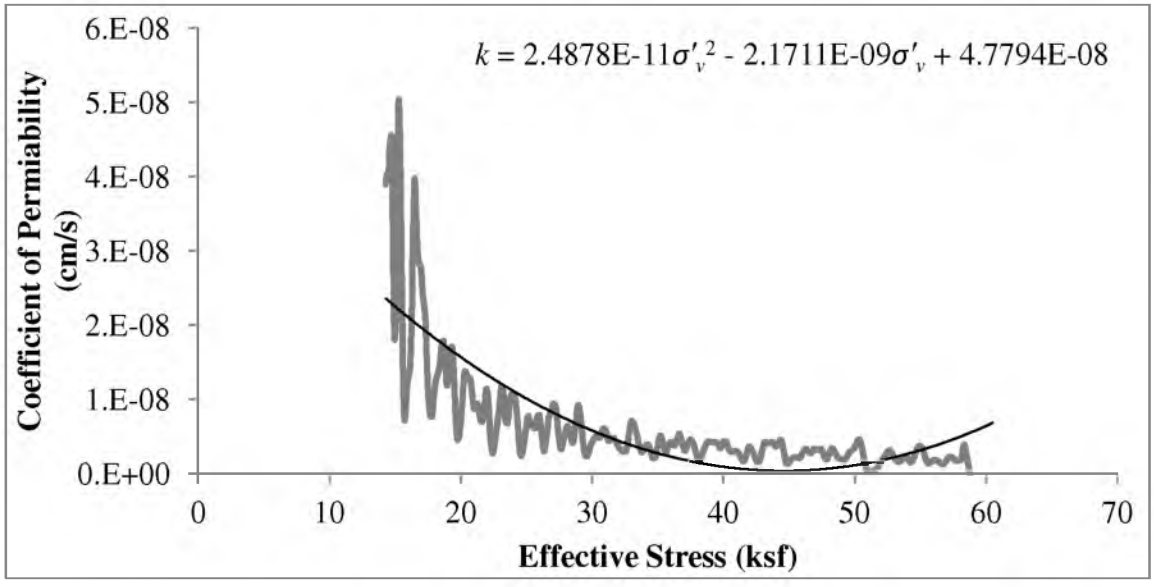

Figure 6-3. Regression plot for determining k with effective stress at 30.5 ft.

$$k_{i-1} = 2.4878\text{E-}11\sigma'^{2}_{v} - 2.1711\text{E-}9\sigma'_{v} + 4.7794\text{E-}08$$

$$k_{i-1} = 2.4878\text{E-}11(2.55)^{2} - 2.1711\text{E-}9(2.55) + 4.7794\text{E-}08 = 4.430E-8\frac{cm}{\text{sec}}$$

The coefficient of permeability, *k*, at node i+1, located just below a depth of 37.25 ft below the original ground surface was determined from a regression equation shown in in Figure 6-4 as follows:

$$k_{i+1} = 1.1972E-11\sigma'^{2}_{v} - 9.8745E-9\sigma'_{v} + 2.1166E-8$$

$$k_{i+1} = 1.1972E-11(2.55)^{2} - 9.8745E-9(2.55) + 2.1166E-8 = 1.868E-8\frac{cm}{\text{sec}}$$

The depth intervals, Δz, above and below node i:

$\Delta z_{i-1} = 1$ ft

$\Delta z_{i+1} = 1/3$ ft

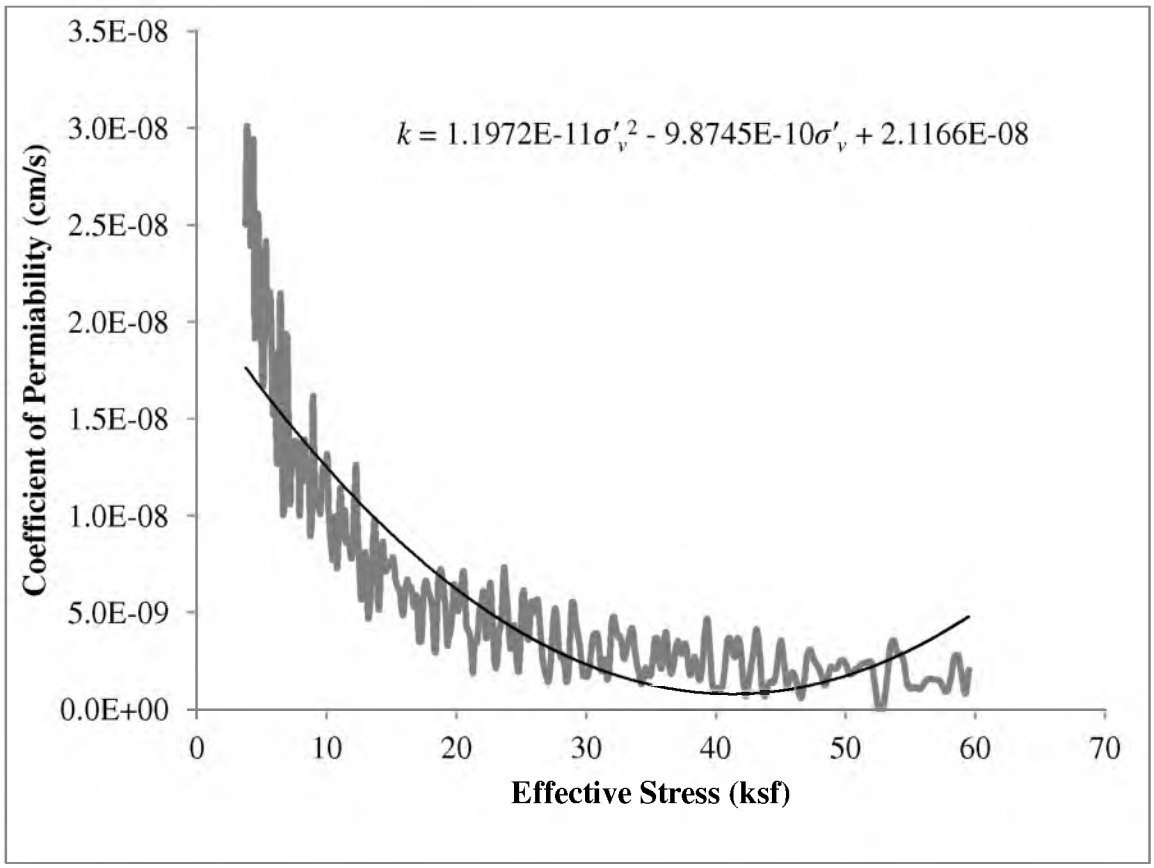

Figure 6-4. Regression plot for determining *k* with effective stress at 39.75 ft.

The initial value of β, located at a depth of 37.25 ft below the original ground surface using Eq. 2-18 from Section 2 is as follows:

$$\beta = \frac{k_{i+1}\Delta z_{i-1}}{k_{i-1}\Delta z_{i+1}} = \frac{1.868E-8(1)}{4.43E-8(\frac{1}{3})} = 1.265$$

After values of α or β were determined, excess pore pressures were estimated as a function of time during the construction period and using Terzaghi's method (Eq. 2-13) and Davis and Raymond's Method (Eq. 2-23). Detailed sample calculations are provided in Appendix C.

6.2.2 Comparison of Predicted and Measured Excess Pore Pressures

Development of excess pore pressures within cohesive soils underlying an embankment occur with the application of load being placed upon the embankment's foundation. To monitor excess pore pressures and their increase upon application of load, piezometers were placed at depths of 5.75, 16.5, 33, 37.25, 41, 58, 64, and 78 ft below the original ground surface within Layers 1, 3, 5, and 7 (see Figure 5-20). As previously stated, the purpose of the piezometers was to measure the change in pore pressures due to placement of fill upon the embankment's foundation from the beginning of construction on April 10, 2009.

A comparison of measured and predicted excess pore pressures at the centerline of the embankment, for depths where piezometers were located, within Layers 1, 3, 5, and 7 was made. Predicted excess pore pressures were analyzed using Terzaghi's method and Davis and Raymond's method while assuming a $\Delta u/\Delta\sigma_v$ ratio of 1. Values of k_{i-1}, k_{i+1}, Δz_{i-1}, Δz_{i+1} , and initial β values used in the finite difference calculations for excess

pore pressures at the interfaces within the cohesive layers and sublayers were presented in Table 6-6.

Results for measured and predicted excess pore pressures are shown in Figure 6-5 through Figure 6-12. Layers 1 and 3 (see Figure 6-5 and Figure 6-6), having a high value for C_v, dissipated rapidly and the excess pore pressures are shown for December 1, 2009. The excess pore pressures at depths located within Layers 5 and 7 (see Figure 6-7 through Figure 6-12), having low values of C_v, dissipated slower than the excess pore pressures in Layers 1 and 3 and are shown for March 3, 2010.

An assumption that many geotechnical engineers make to predict the development of excess pore pressures is: once the induced vertical stress is applied, the change in induced vertical stress ($\Delta\sigma_v$) is instantaneously absorbed by the pore pressure, or simply stated, Δu is equal to $\Delta\sigma_v$ once $\Delta\sigma_v$ is applied. The purpose of this assumption is to assist in estimating the magnitudes of excess pore pressures developed during loading. In order to better predict the magnitude of excess pore pressures developed during placement of fill or increase in vertical stress, the normalized pore pressure ratio,($\Delta u/\Delta\sigma_v$), for depths where vibrating wire piezometers were located was calculated. As previously shown in Chapter 5, results for σ_v were measured by the vibrating wire pressure plates and results for u were measured by the vibrating wire piezometers. The $\Delta\sigma_v$ is defined by Eq. 6-4 and the Δu is defined by Eq. 6-5.

$$\Delta\sigma_{vi} = \sigma_{vi,j} - \sigma_{vi,j-1} \tag{6-4}$$

where:

$\sigma_{vi,j}$ = the vertical stress at time j

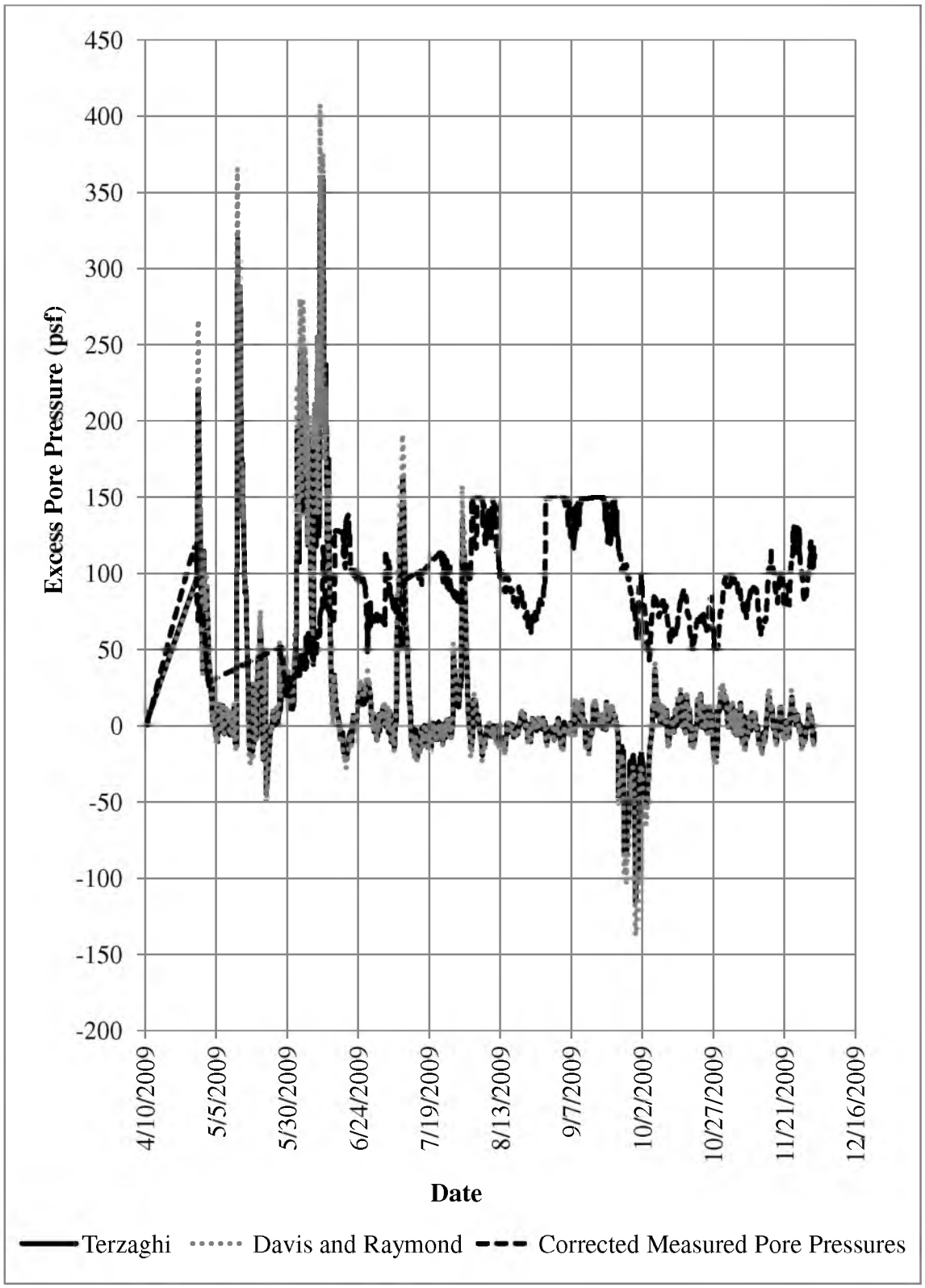

Figure 6-5. Measured and predicted excess pore pressures assuming a value of C equal to 1within Layer 1 at a depth of 5.75 ft below the original ground surface at the centerline of the embankment.

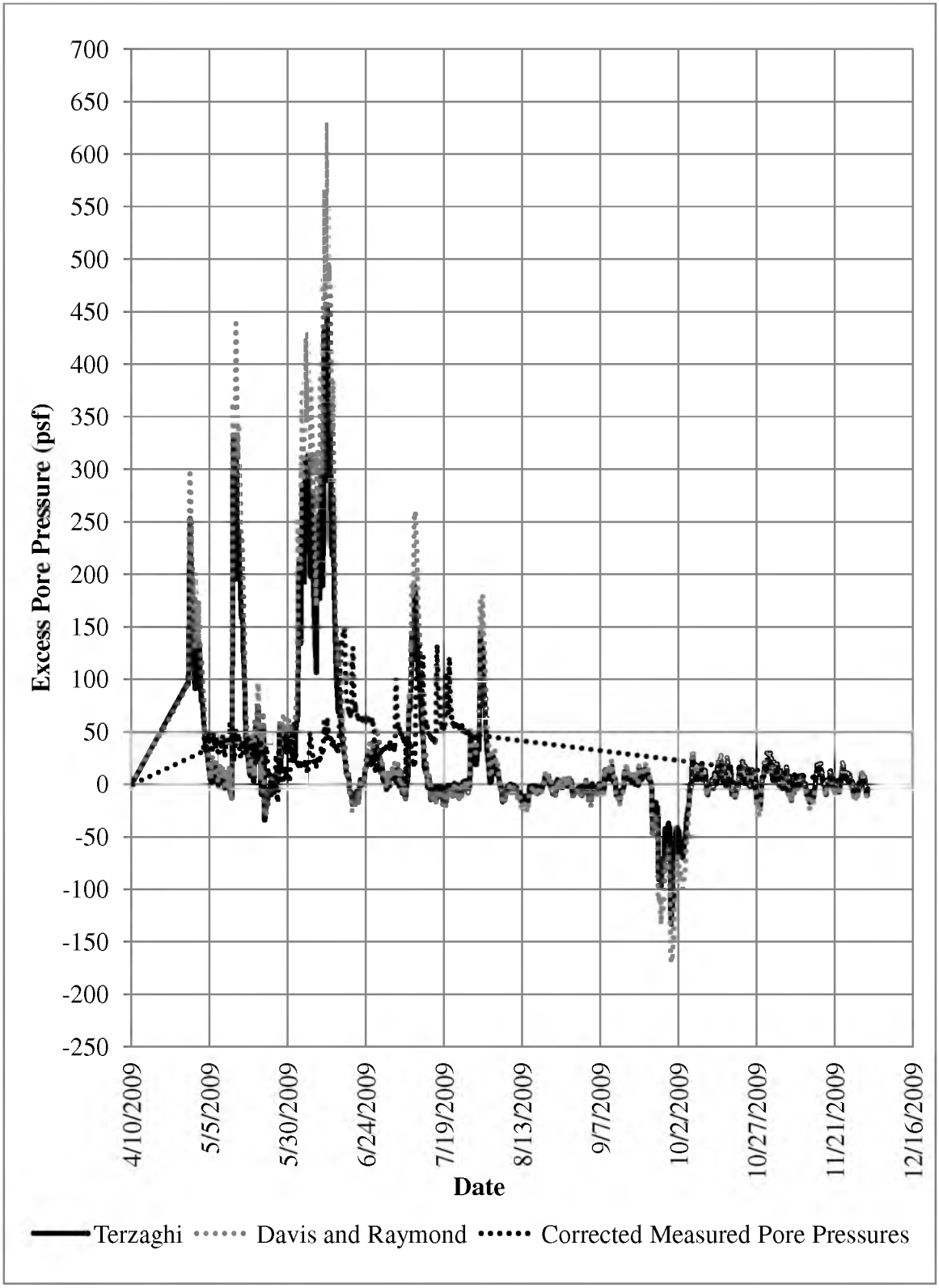

Figure 6-6. Measured and predicted excess pore pressures assuming a value of C equal to 1 within Layer 3 at a depth of 16.5 ft below the original ground surface at the centerline of the embankment.

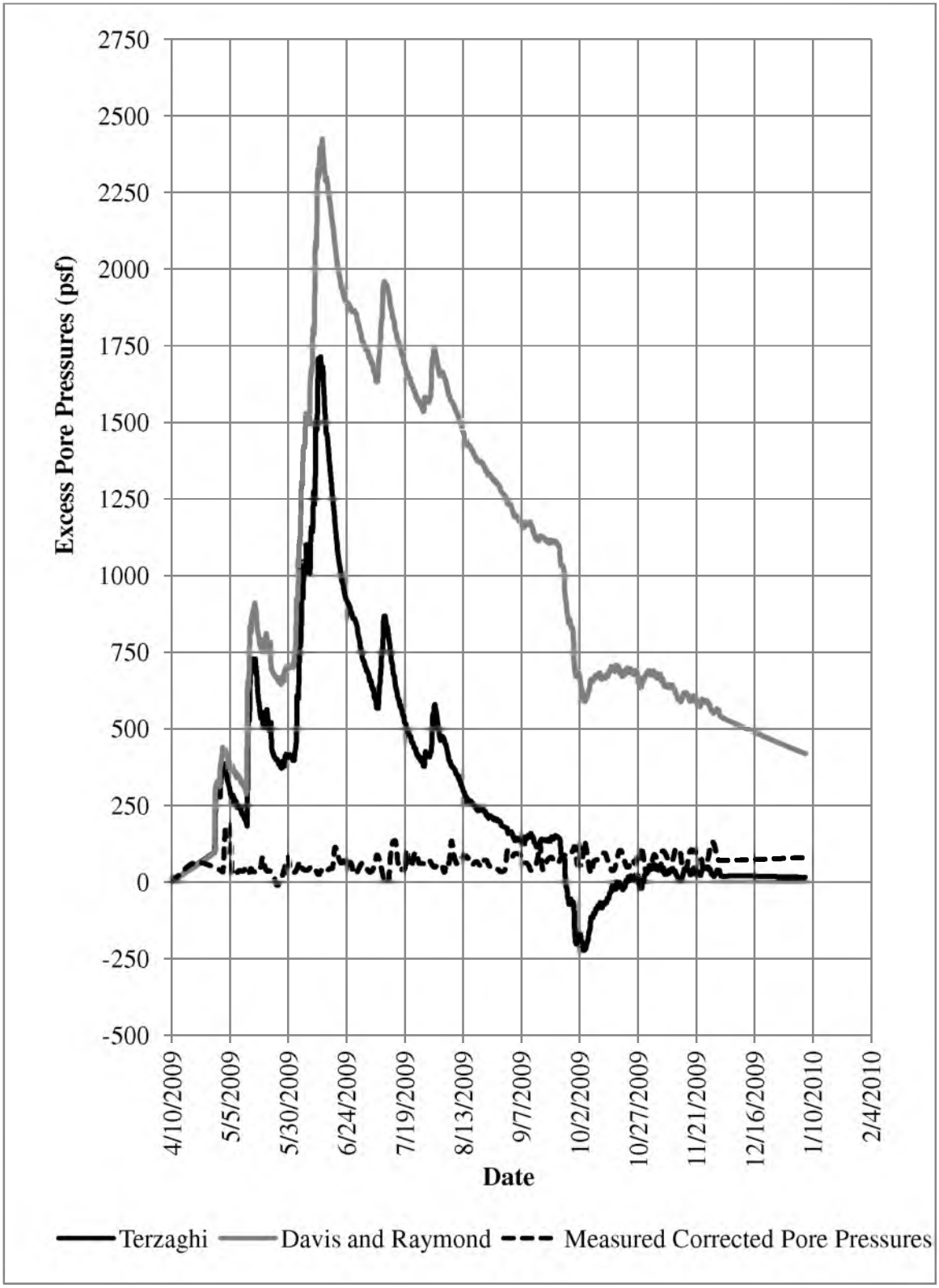

Figure 6-7. Measured and predicted excess pore pressures assuming a value of C equal to 1 within Layer 5 at a depth of 33 ft below the original ground surface at the centerline of the embankment.

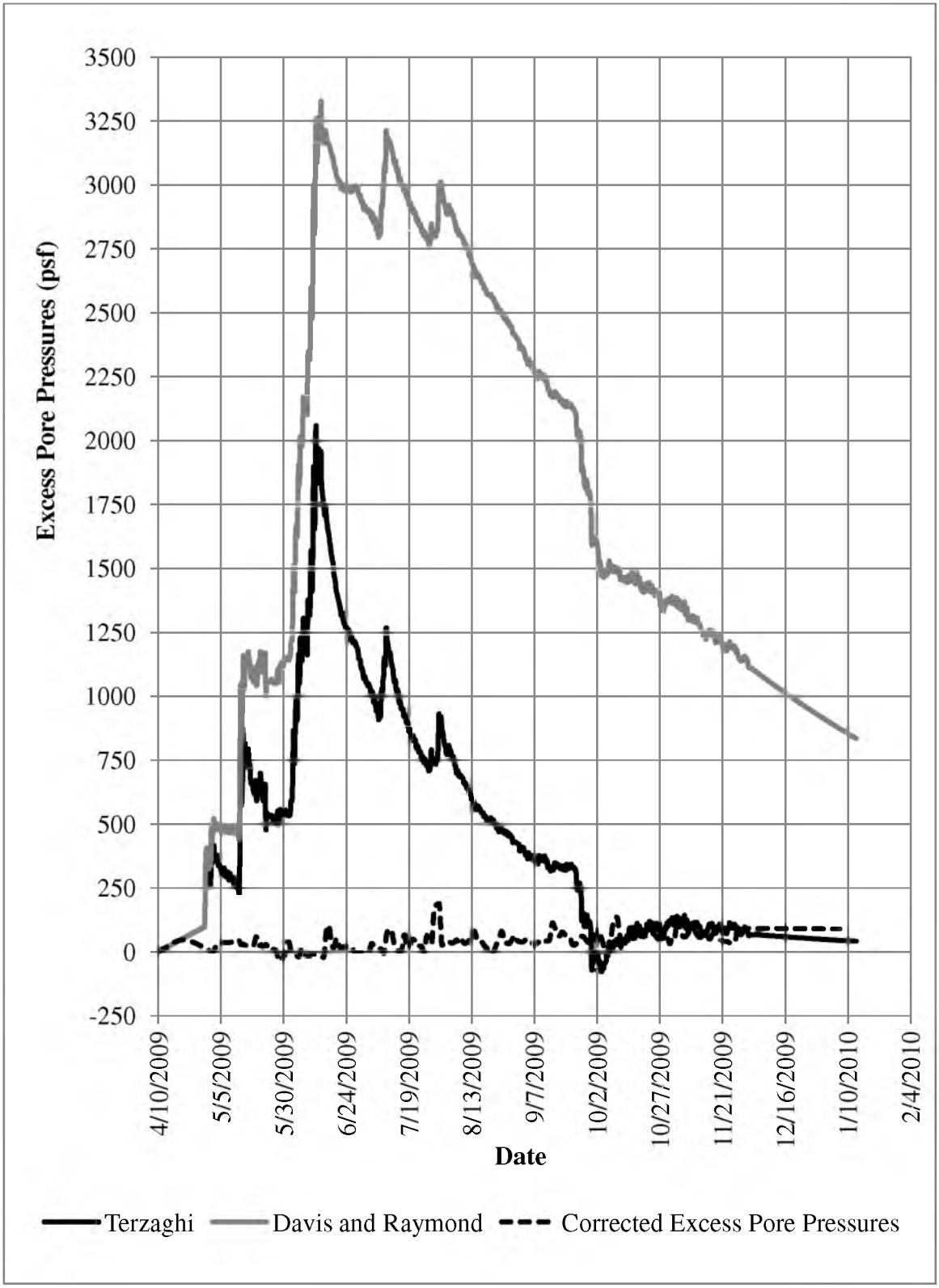

Figure 6-8. Measured and predicted excess pore pressures assuming a value of C equal to 1 within Layer 3 at a depth of 37.5 ft below the original ground surface at the centerline of the embankment.

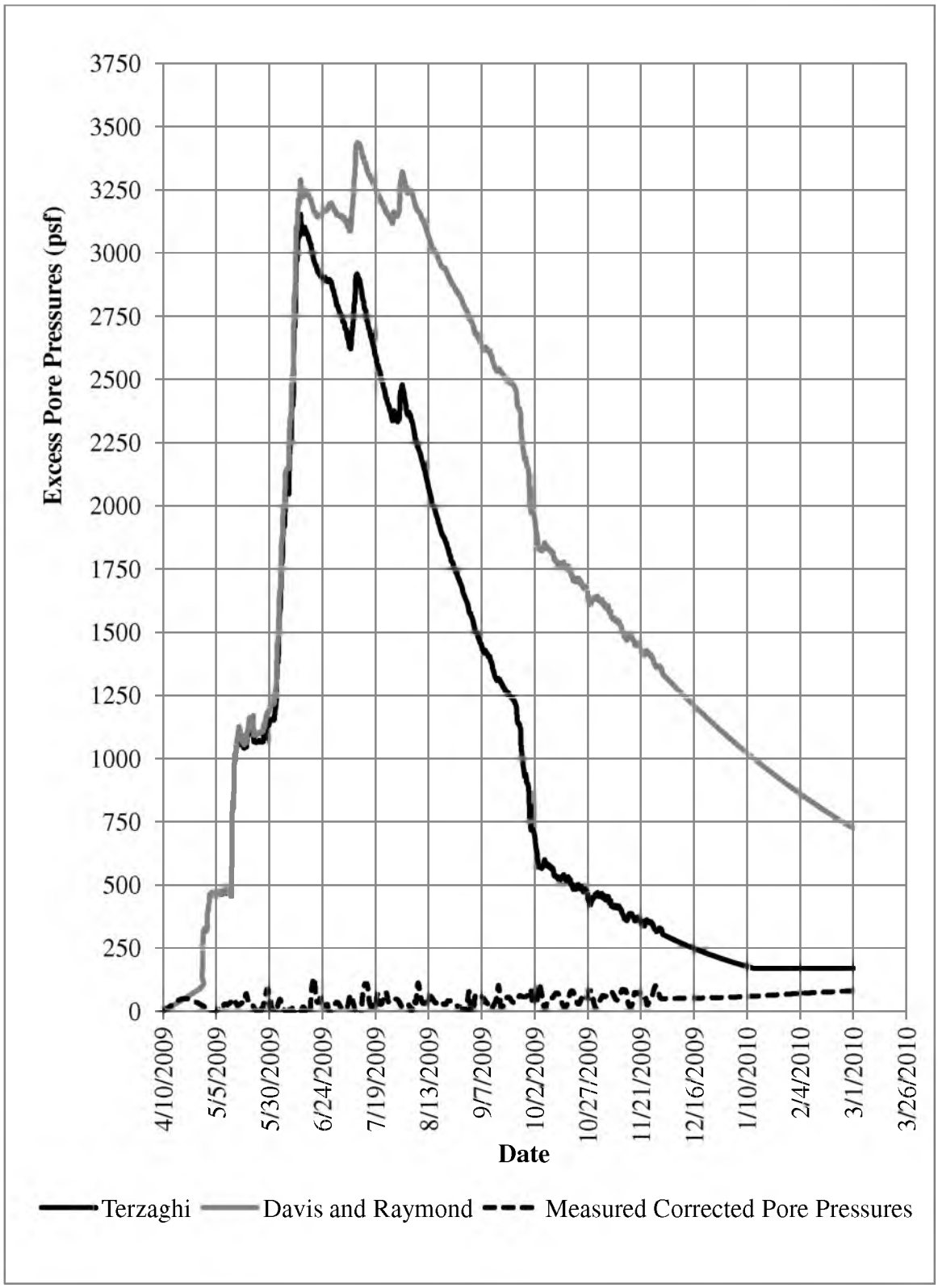

Figure 6-9. Measured and predicted excess pore pressures assuming a value of C equal to 1 within Layer 3 at a depth of 41 ft below the original ground surface at the centerline of the embankment.

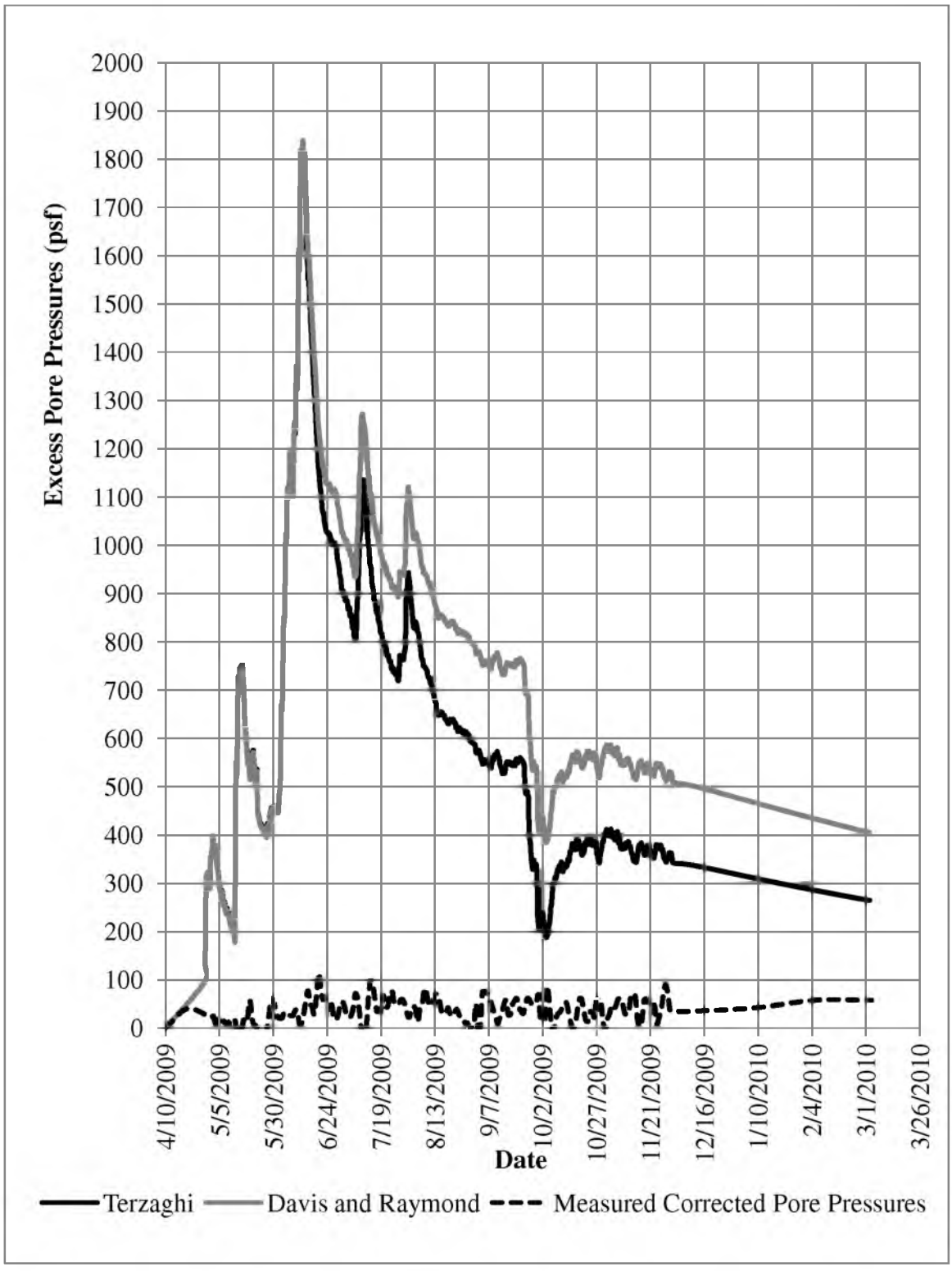

Figure 6-10. Measured and predicted excess pore pressures assuming a value of C equal to 1within Layer 7 at a depth of 58 ft below the original ground surface at the centerline of the embankment.

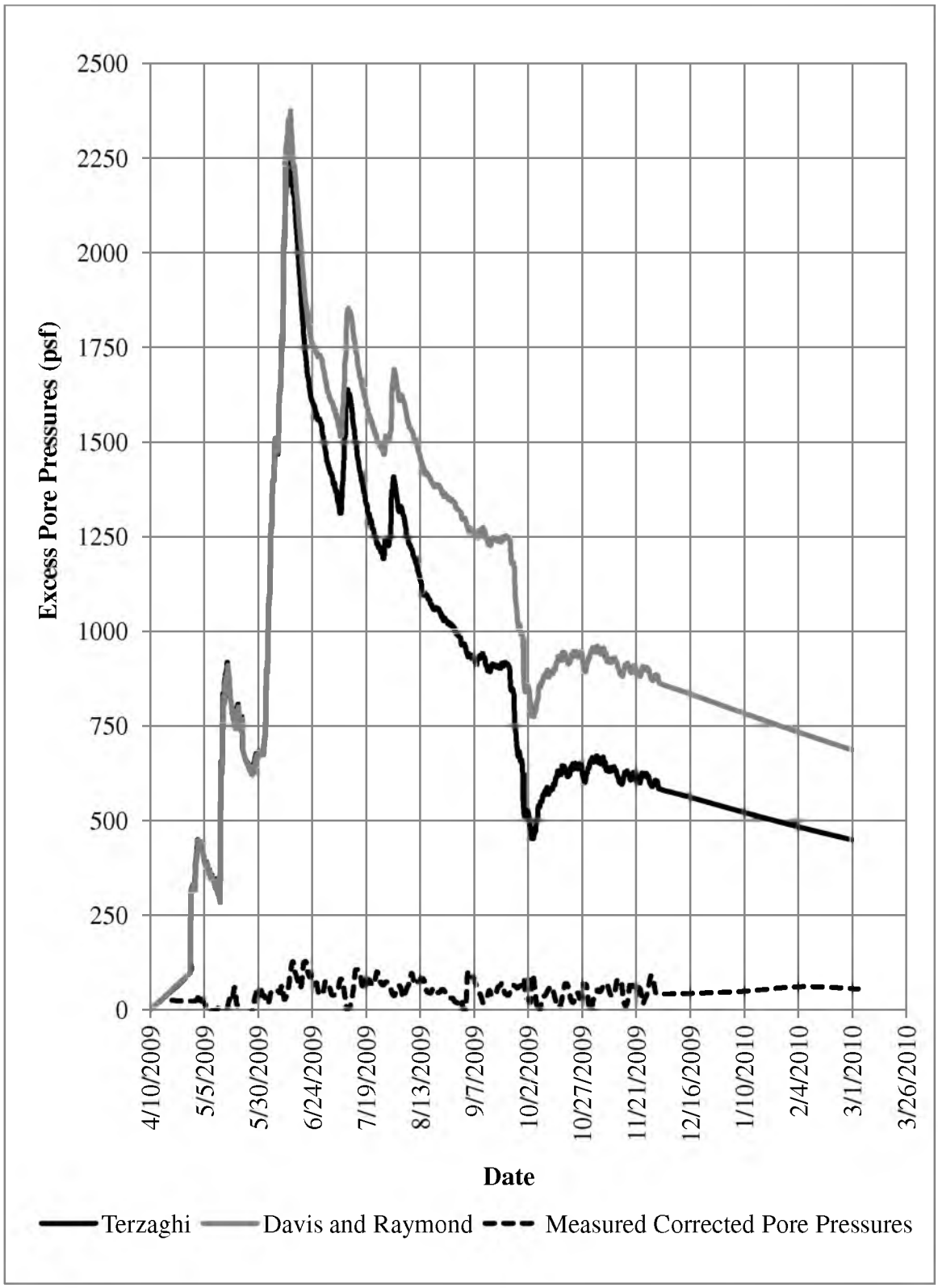

Figure 6-11. Measured and predicted excess pore pressures assuming a value of C equal to 1 within Layer 7 at a depth of 64 ft below the original ground surface at the centerline of the embankment.

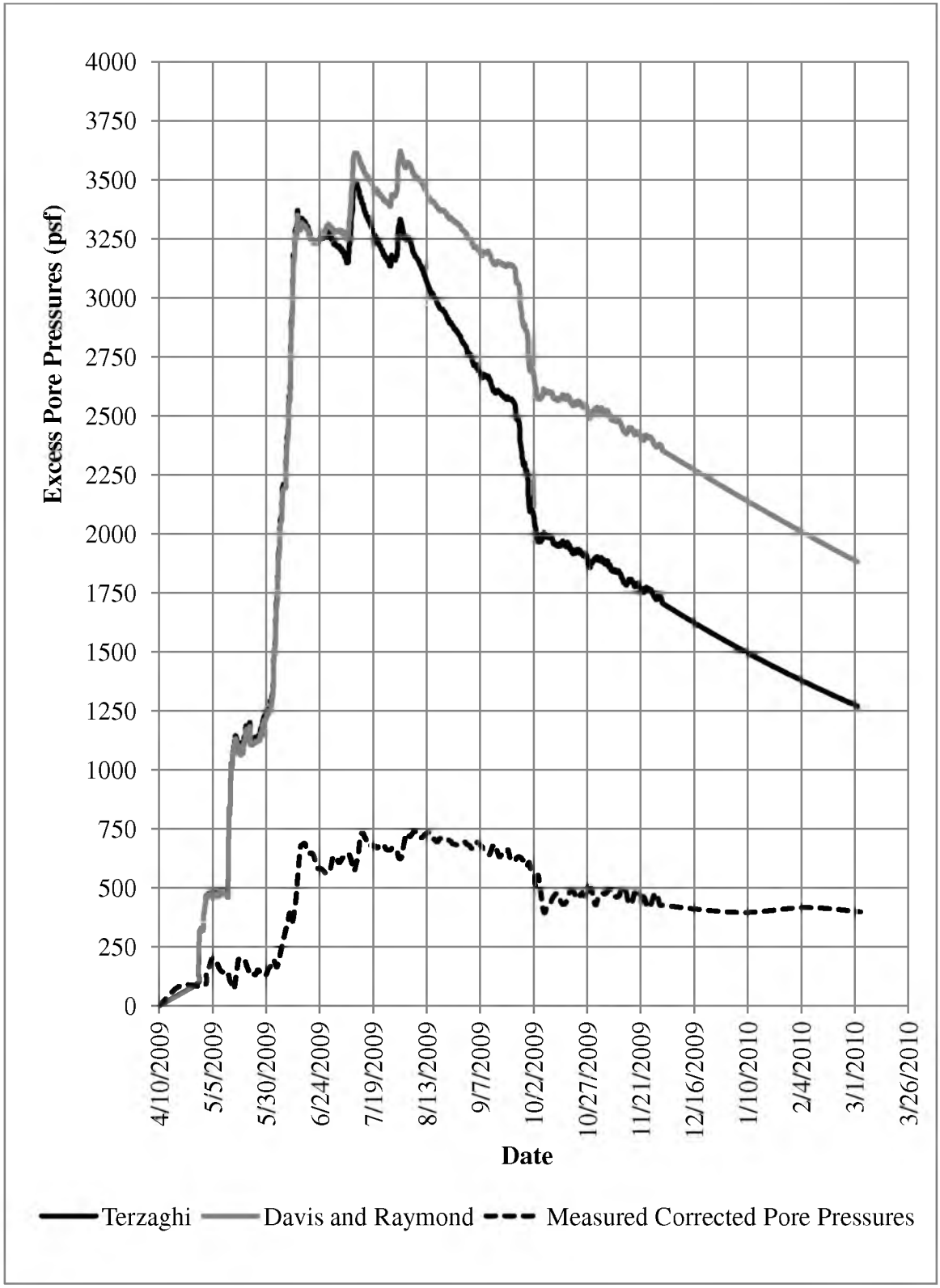

Figure 6-12. Measured and predicted excess pore pressures assuming a a value of C equal to 1 within Layer 7 at a depth of 78 ft below the original ground surface at the centerline of the embankment.

$\sigma_{vi,j-1}$ = the vertical stress at time j-1

$$\Delta u = u_{i,j} - u_{i,j-1} \tag{6-5}$$

where:

$u_{i,j}$ = the pore pressure at time j

$u_{i,j-1}$ = the pore pressure at time j-1

That normalized pore pressure ratio ($\Delta u/\Delta\sigma_v$), denoted by the letter *C*, is defined by Eq. 6-6:

$$C = \frac{\Delta u}{\Delta \sigma_v} \tag{6-6}$$

To better predict the development of excess pore pressures that were to occur, the normalized pore pressure ratio, *C*, at the centerline of the embankment was determined for dates when rapid placement of fill occurred. Dates pertaining to rapid placement of fill at the centerline of the embankment were chosen using Figure 5-2 and Figure 5-3. The following dates where rapid placement of fill occurred causing an increase in the induced vertical stress at the centerline of the embankment are as follows: May 13, 2009 – May 14, 2009; June 2, 2009 – June 8, 2009; June 9, 2009 – June 12, 2009; and July 8, 2009 – July 10, 2009. Results for the value of C for the four different time periods are shown in Figure 6-13 through Figure 6-19 for depths of 16.5, 33, 37.25, 41, 58, 64, and 78 ft.

The average normalized pore pressure ratios, C_{ave}, are shown in Table 6-7.

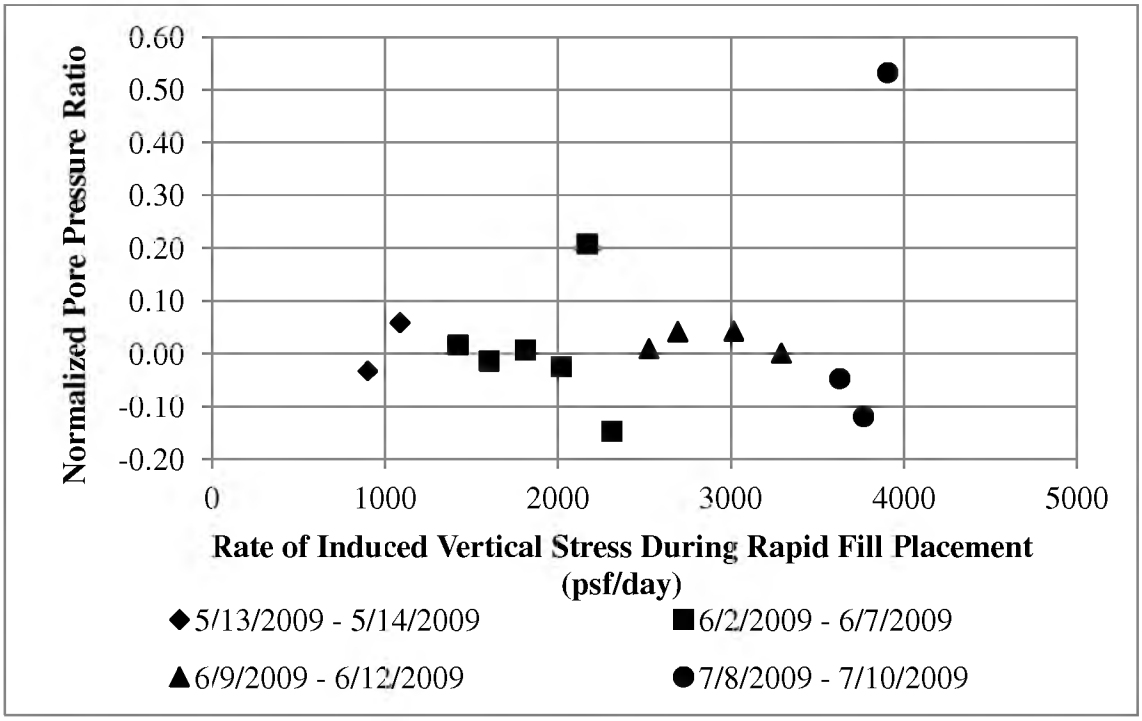

Figure 6-13. The normalized pore pressure ratio, *C*, at a depth of 16.5 ft below the original ground surface located at the centerline of the embankment for dates when rapid placement of fill occurred between April 10, 2009 to July 31, 2009.

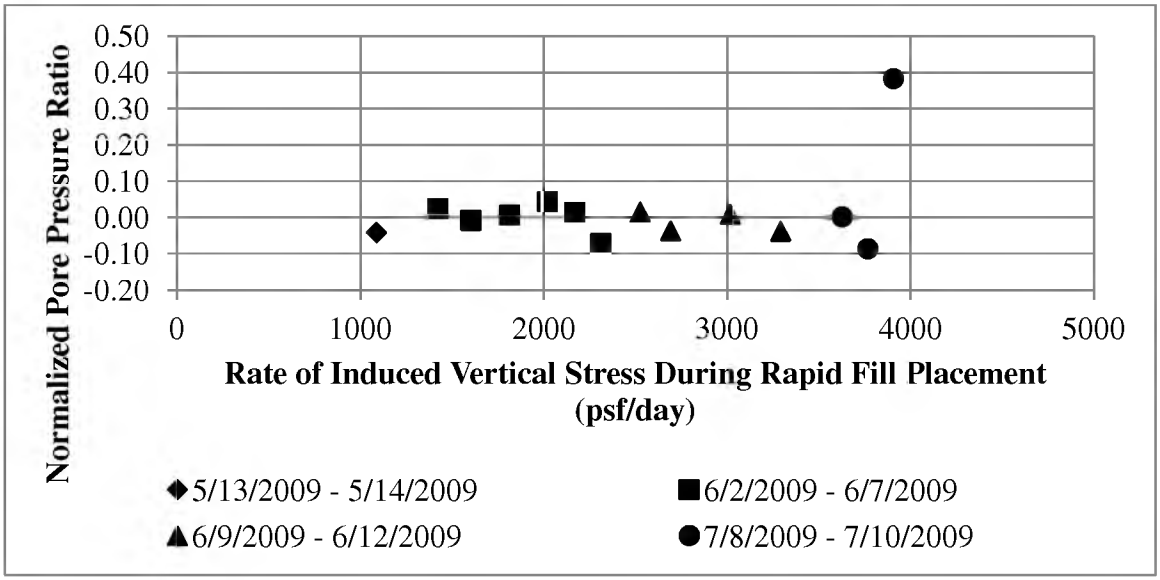

Figure 6-14. The normalized pore pressure ratio, *C*, at a depth of 33 ft below the original ground surface located at the centerline of the embankment for dates when rapid placement of fill occurred between April 10, 2009 to July 31, 2009.

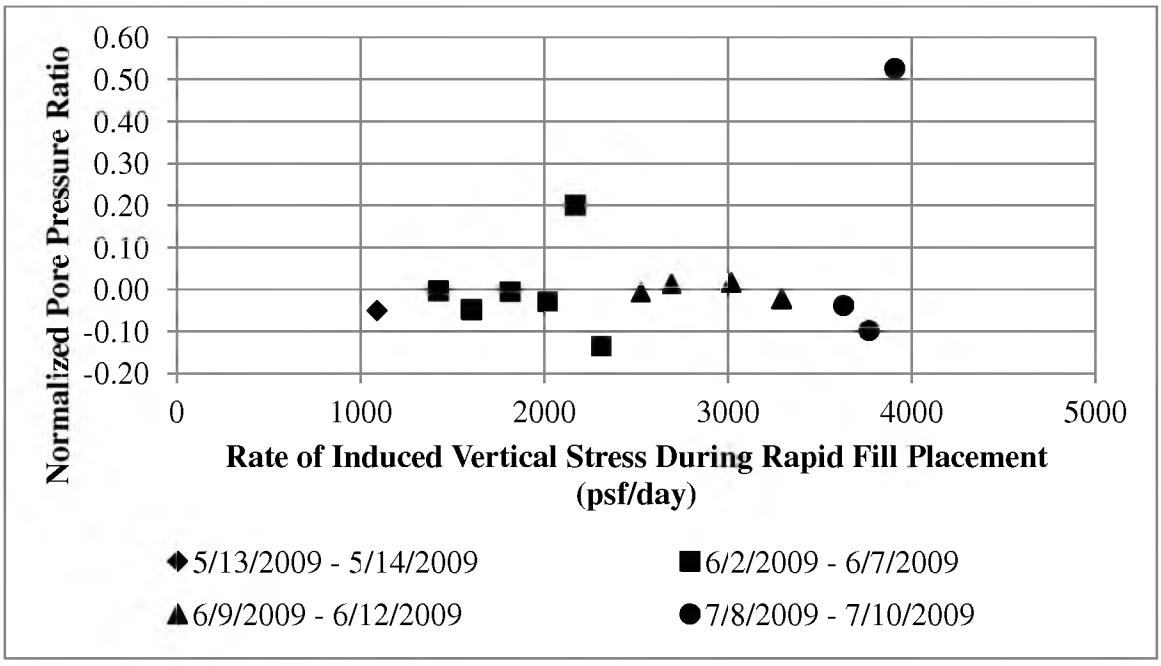

Figure 6-15. The normalized pore pressure ratio, *C*, at a depth of 37.25 ft below the original ground surface located at the centerline of the embankment for dates when rapid placement of fill occurred between April 10, 2009 to July 31, 2009.

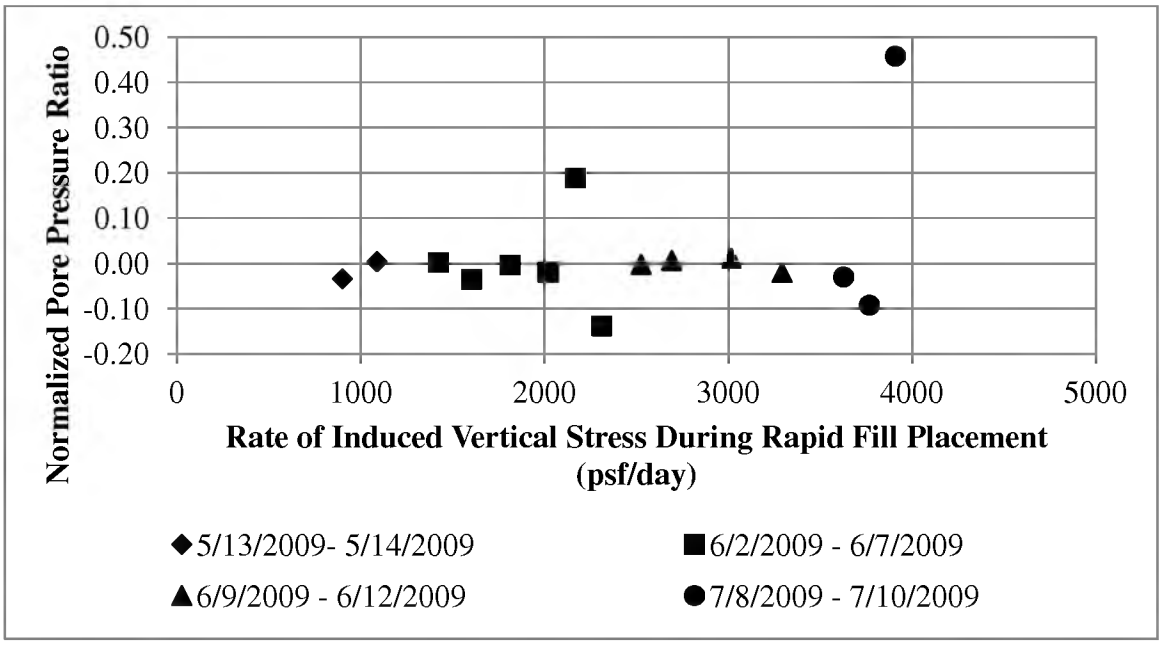

Figure 6-16. The normalized pore pressure ratio, *C*, at a depth of 41 ft below the original ground surface located at the centerline of the embankment for dates when rapid placement of fill occurred between April 10, 2009 to July 31, 2009.

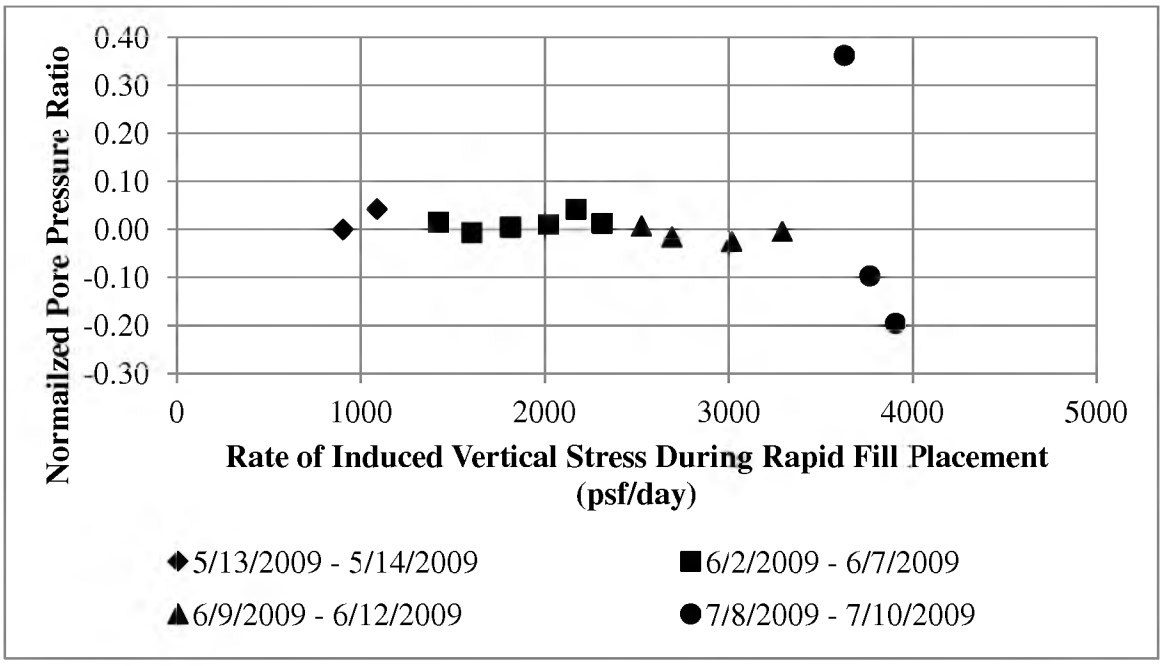

Figure 6-17. The normalized pore pressure ratio, *C*, at a depth of 58 ft below the original ground surface located at the centerline of the embankment for dates when rapid placement of fill occurred between April 10, 2009 to July 31, 2009.

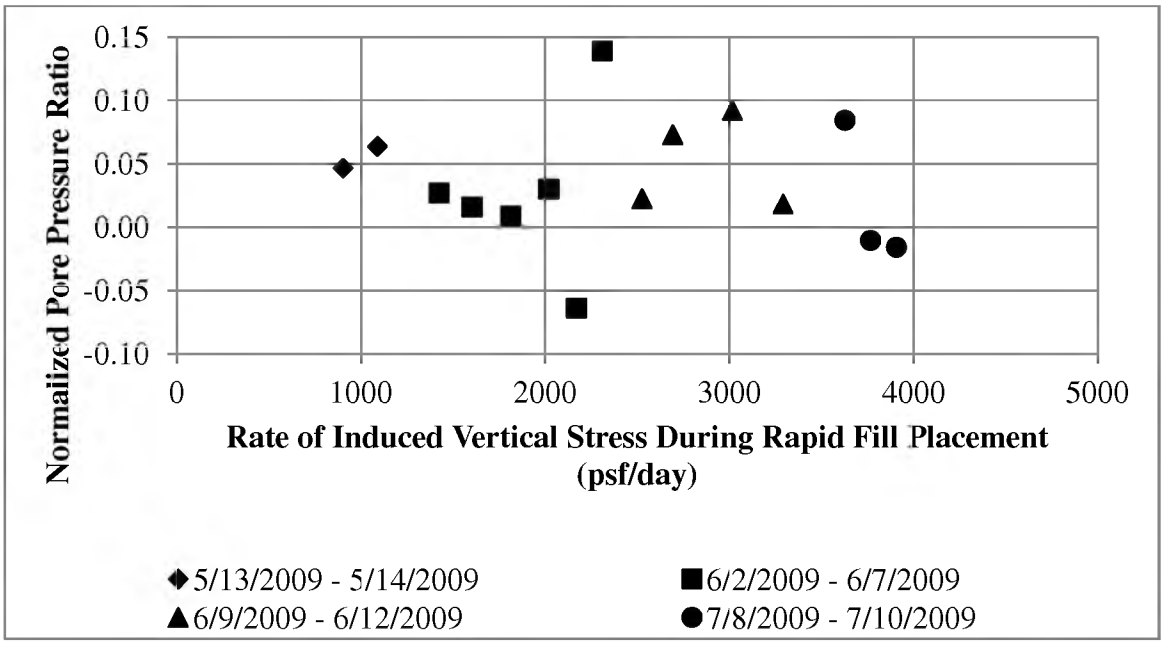

Figure 6-18. The normalized pore pressure ratio, *C*, at a depth of 64 ft below the original ground surface located at the centerline of the embankment for dates when rapid placement of fill occurred between April 10, 2009 to July 31, 2009.

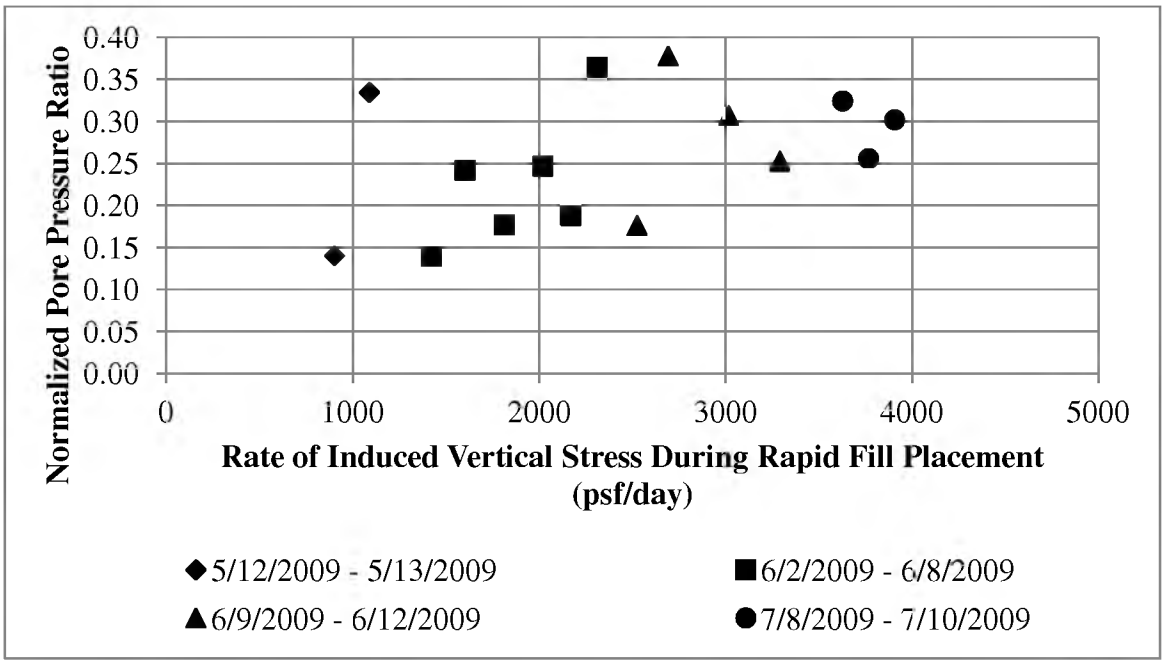

Figure 6-19. The normalized pore pressure ratio, *C*, at a depth of 78 ft below the original ground surface located at the centerline of the embankment for dates when rapid placement of fill occurred between April 10, 2009 to July 31, 2009.

Table 6-7. The average normalized pore pressure ratios, C_{ave}, for depths below the original ground surface at the centerline line of the embankment located within the cohesive layers.

Layer	Depth Below Original Ground Surface ft	C_{ave}
1	5.75	N/A
3	16.5	0.04
5	33	0.02
5	37.25	0.02
5	41	0.02
7	58	0.01
7	64	0.04
7	78	0.26

A comparison of measured and predicted excess pore pressures at the centerline of the embankment for depths where piezometers were located within layers 1, 3, 5, and 7 was made using C_{ave}. Predicted excess pore pressures were analyzed using Terzaghi's method and Davis and Raymond's method as was a value of C equal to C_{ave} for each depth where a piezometer was located.

Results for measured and predicted excess pore pressures using the C_{ave} are shown in Figure 6-20 through Figure 6-26. Layer 3 (see Figure 6-20), having a high value for C_v dissipated rapidly and the excess pore pressures are shown for December 1, 2009.

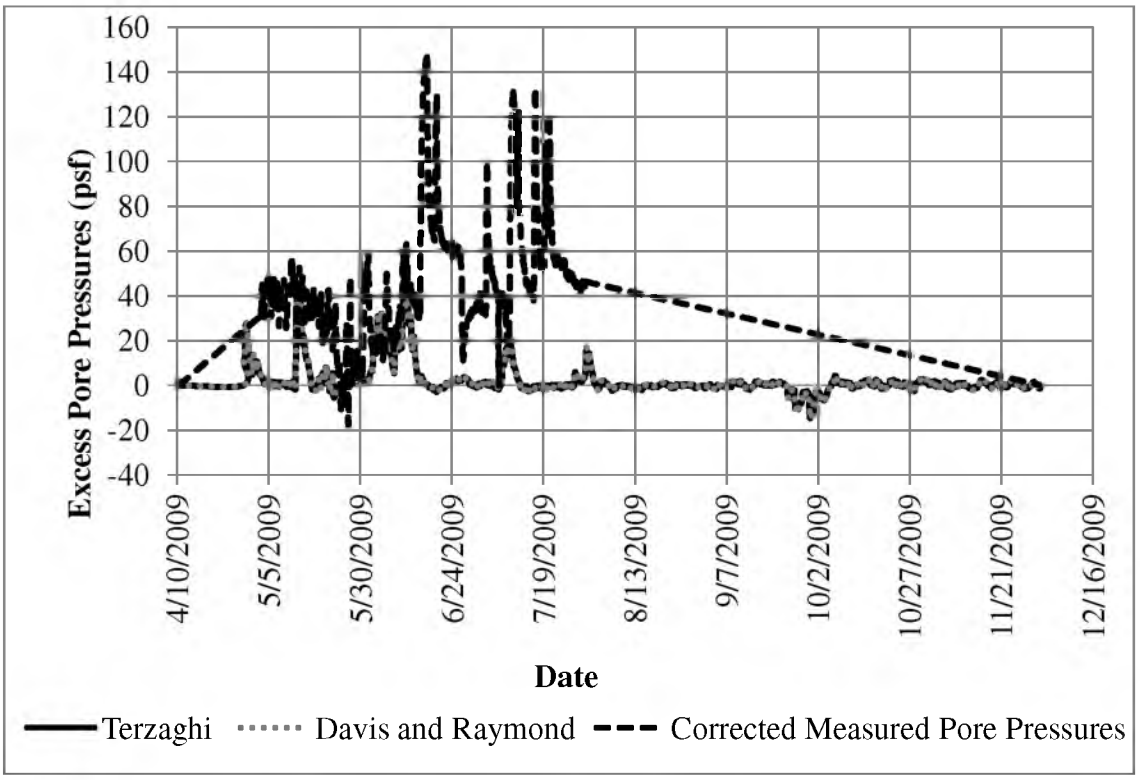

Figure 6-20. Predicted excess pore pressures using C_{ave} = 0.04 and measured excess pore pressures at the centerline of the embankment at a depth of 16.5 ft below the original ground surface.

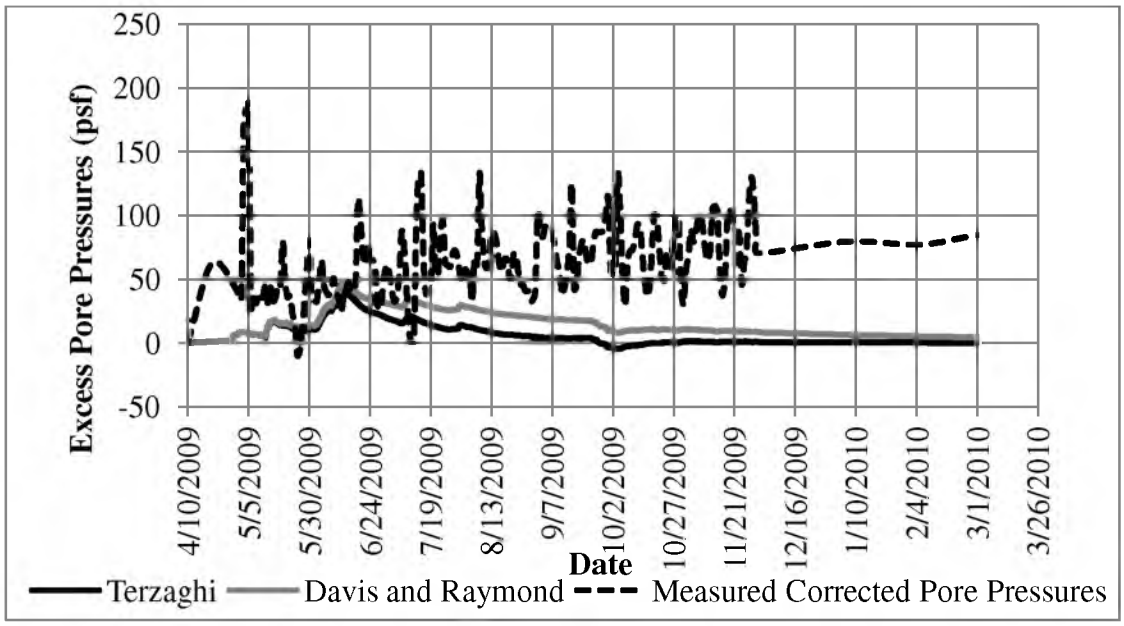

Figure 6-21. Predicted excess pore pressures using C_{ave} = 0.02 and measured excess pore pressures at a depth of 33 ft below the original ground surface at the centerline of the embankment for March 1, 2010.

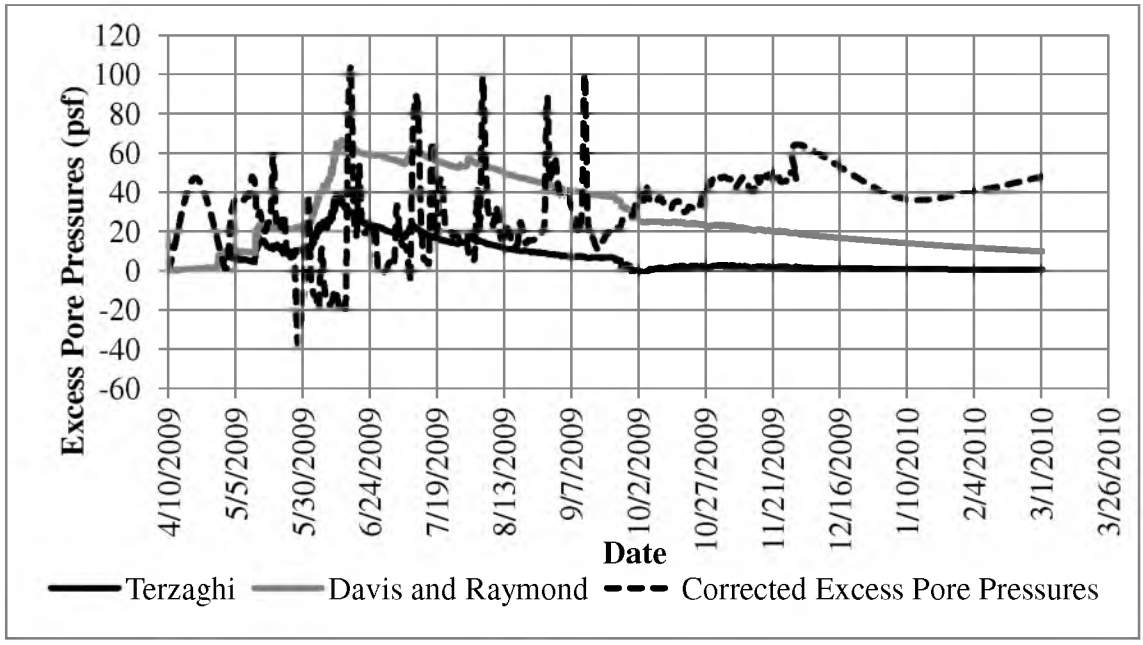

Figure 6-22 Predicted excess pore pressure using C_{ave} = 0.02 and measured excess pore pressures at a depth of 37.25 ft below the original ground surface at the centerline of the embankment for March 1, 2010.

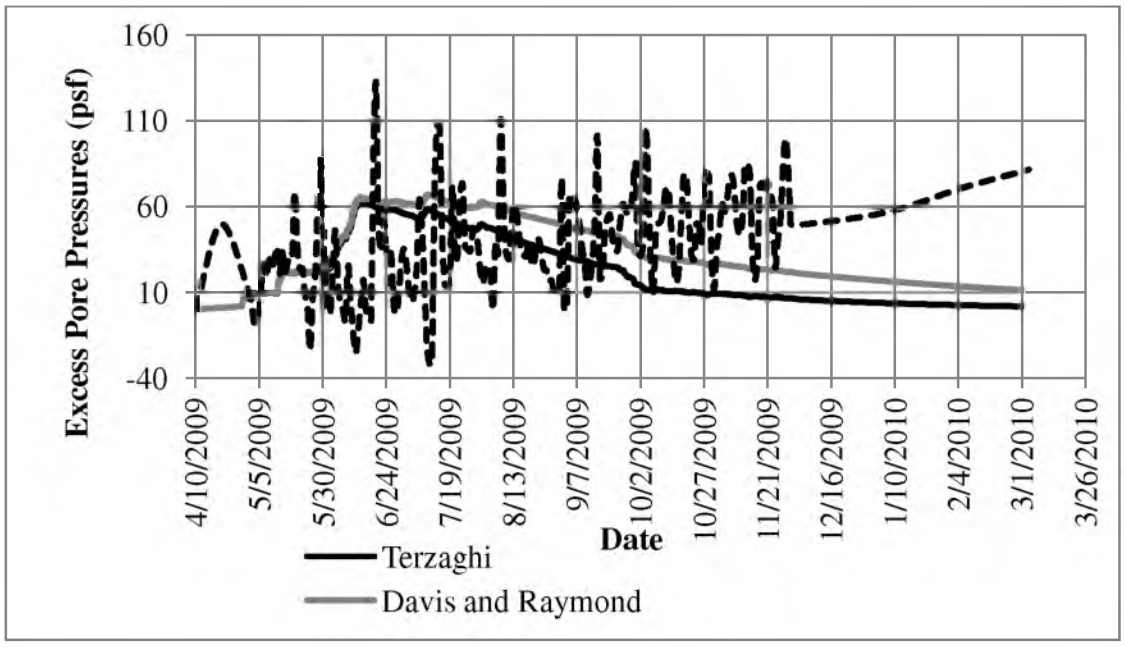

Figure 6-23. Predicted excess pore pressure using C_{ave} = 0.02 and measured excess pore pressures at a depth of 41 ft below the original ground surface at the centerline of the embankment for March 1, 2010.

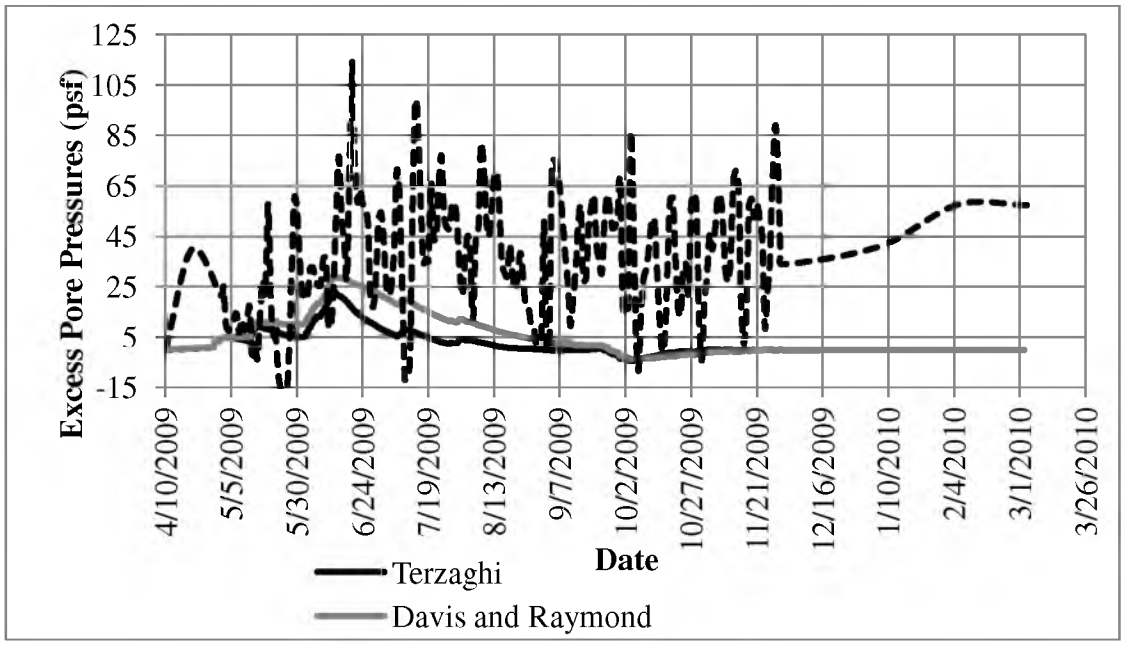

Figure 6-24. Predicted excess pore pressure using C_{ave} = 0.01 and measured excess pore pressures at a depth of 58 ft below the original ground surface at the centerline of the embankment for March 1, 2010.

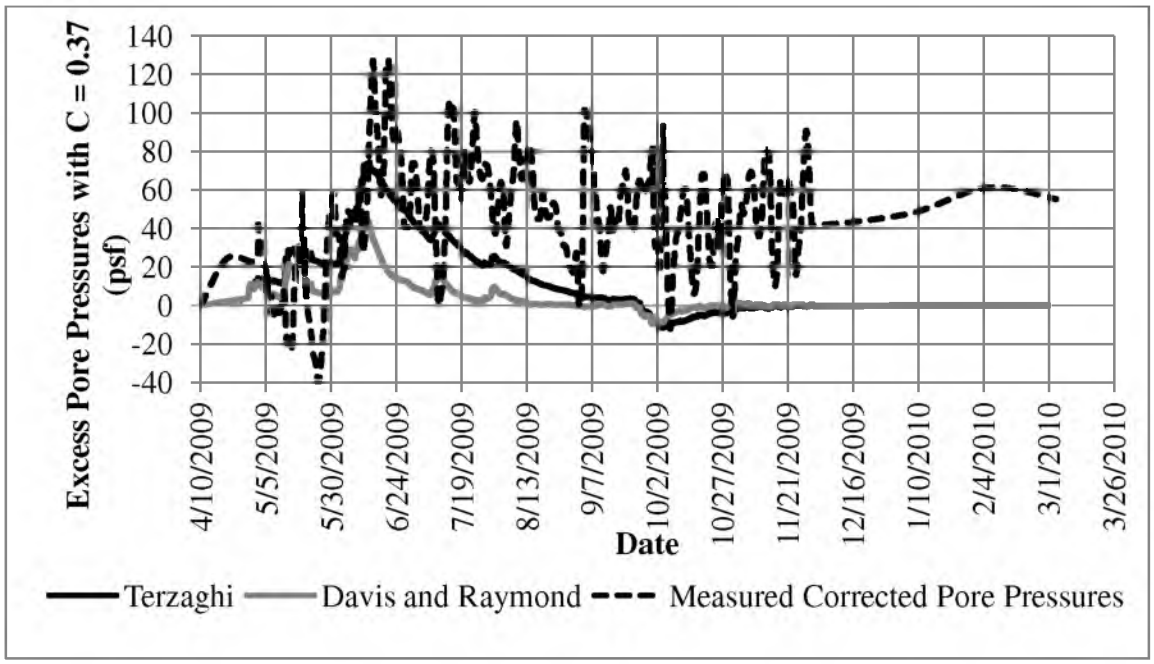

Figure 6-25. Predicted excess pore pressure using C_{ave} = 0.04 and measured excess pore pressures at a depth of 64 ft below the original ground surface at the centerline of the embankment for March 1, 2010.

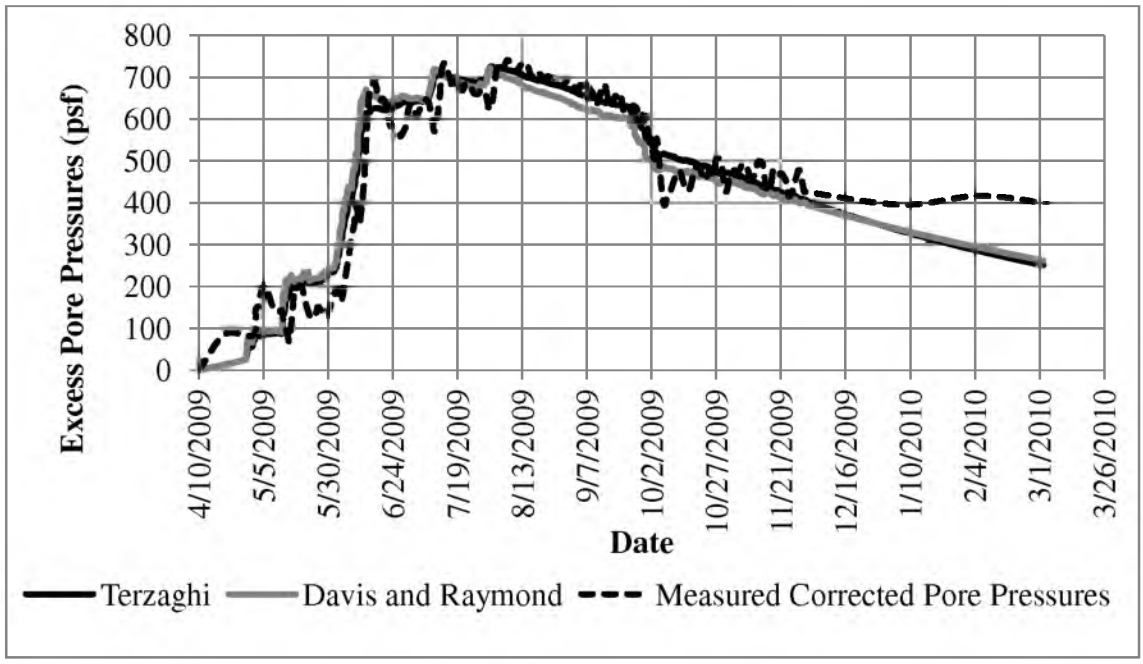

Figure 6-26. Predicted excess pore pressure using C_{ave} = 0.26 and measured excess pore pressures at a depth of 78 ft below the original ground surface at the centerline of the embankment for March 1, 2010.

The excess pore pressures at depths located within layers 5 and 7 (see Figure 6-21 through Figure 6-26), having low values of C_v, dissipated slower than the excess pore pressures in Layers 1 and 3 and are shown for March 3, 2010. The predicted excess pore pressures for Layers 1 and 3, having initial high values of C_v and being comprised of clayey silt, yielded complete excess pore pressure dissipation upon removal of surcharge on September 24, 2009 (see Figure 6-5 and Figure 6-6). The predicted excess pore pressures for Layers 5 and 7, having low initial values of c_v and being comprised fat and lean clay, produced excess pore pressures and were still dissipating upon removal of surcharge. The excess pore pressures within layers 5 and 7 were still dissipating for March 3, 2010, 160 days since removal of surcharge (see Figure 6-7 through Figure 6-12).

Predicted excess pore pressures at the centerline of the embankment using both methods and a value of C equal to 1, yielded excess pore pressures greater than what was measured by the vibrating wire piezometers. A more realistic prediction of excess pore pressures is to determine the C_{ave}, using Eq. 6-6 for each depth at the centerline of the embankment where a piezometer was located.

Using the C_{ave} with Terzaghi's method and Davis and Raymond's method in conjunction with the finite difference method yielded predicted excess pore pressures closer to the measured excess pore pressures (see Figure 6-20 through Figure 6-26).

The predicted excess pore pressures and time for complete dissipation of excess pore pressures with time is different for Terzaghi's method than the predicted excess pore pressures using Davis and Raymond's method. Predicted excess pore pressures were greater using Davis and Raymond's method than Terzaghi's method. The difference of excess pore pressures from Terzaghi's method and Davis and Raymond's method stems

from the assumption that the change in void ratio is proportional to the change in effective stress. The correct assumption is that the change in void ratio is proportional to the change in the logarithm of effective stress. This assumption was made by Davis and Raymond in their nonlinear approach to determining excess pore pressures. As a result, the excess pore pressures are a function of the effective stress at depth.

6.2.3 Comparison of Predicted and Measured Primary Consolidation Settlement

Primary consolidation settlement is a result of excess pore pressures dissipating with time. The magnitude of primary consolidation settlement is a function of the effective vertical stress acting within the soil. Predicted and measured primary consolidation settlement at the centerline of the embankment using predicted excess pore pressures results from Terzaghi's method and Davis and Raymond's method will be compared with the measured settlement obtained via the magnet extensometers readings for Layers 1, 3, 5, and 7.

Effective stresses were calculated using the pore pressures predicted from the finite difference method, and for settlement analysis purposes, were assumed to have a value of C equal to 1. Assuming a value of C equal to 1 produces the change in effective stress as defined by Eq. 6-7.

$$\Delta\sigma_v' = \Delta\sigma_v - \Delta u \tag{6-7}$$

where:

$\Delta\sigma_v$ = the change in vertical stress

Δu = the change in pore pressure.

Δu in Eq. 6-5 occurs in two manners: (1) As a result of excess pore pressure dissipation from time j to time j+1 which was predicted by Terzaghi's method or Davis and Raymond's method, Δu_d and (2) assuming a value of C equal to 1 to which the $\Delta\sigma_v$ is equal to Δu, Δu_t.

Δu_d used in pore pressure analysis is the change in excess pore pressure predicted from the finite difference solution using either Eq. 2-10 (Terzaghi's method) or Eq. 2-20 (Raymond and Davis' method) and is defined by Eq. 6-8.

$$\Delta u_d = u_{j+1} - u_j \tag{6-8}$$

Δu_t used in pore pressure analysis was determined by the increase of total vertical stress due to the placement or removal of fill during construction and is defined by Eq. 6-9. When C =1, as is commonly assumed in geotechnical engineering practice, $\Delta u_t = \Delta\sigma_{vt}$.

$$\Delta u_t = C \cdot \Delta\sigma_{vt} \tag{6-9}$$

Substituting Eqs. 6-8 and 6-9 into Eq. 6-7, the change in effective stress is defined in Eq. 6-10.

$$\Delta\sigma'_v = \Delta\sigma_v - \left(\Delta u_t - \Delta u_D\right) \tag{6-10}$$

When C = 1, $\Delta u_t = \Delta\sigma_{vt}$, the applied load is offset by the change in pore pressures and the change in effective stress is then defined by Eq. 6-11.

$$\Delta\sigma'_v = \Delta u_D \tag{6-11}$$

The effective stress for a given depth i at the end of the time increment (time j+1) was calculated using Eq. 6-12.

$$\sigma'_{vi,\,j+1} = \sigma'_{vi,\,j} + \Delta\sigma'_{v} \tag{6-12}$$

Effective stresses used in primary consolidation settlement analysis were calculated using a value of *C* equal to 1 and an average value of *C*. The importance of the value of *C* in pore pressure prediction was previously discussed and shown in Section 6.2.2.

The σ'_p is the parameter that determines whether the underlying cohesive soils or sublayers within the cohesive layers are in recompression or virgin compression during primary consolidation settlement. Soils underlying the SR 77 embankment were found to be in recompression due to σ'_v being less than the σ'_p for all cohesive layers.

The ultimate primary consolidation settlements within individual cohesive layers were determined using predicted excess pore pressures from Terzaghi's method, Davis and Raymond's method, and predicted excess pore pressures at the interfaces. Primary consolidation settlement for Layers 1 and 3 will be shown for February 10, 2010, due to their high values of C_v. Primary consolidation settlement for Layers 3 and 5 will be shown for July 1, 2010, due their low values of C_v. An analysis of predicted primary consolidation settlement using Terzaghi's method and Davis and Raymond's method was performed while assuming a value of *C* equal to 1. Sample calculations for primary consolidation settlement using Terzaghi's method and Davis and Raymond's method for a depth of 33.25 ft below the original ground surface at time of 100 days are provided in

Appendix C. Settlement versus time plots for Layers 1, 3, 5, and 7 at the centerline of the embankment are shown in Figure 6-27 through Figure 6-30.

Using Terzaghi's method for one-dimensional consolidation with the finite difference method and assuming a value of *C* equal to 1, predicted primary consolidation settlements in Layers 1, 3, 5, and 7 were 1.613, 1.925, 0.954, and 0.931 in. Using Davis and Raymond's method for one-dimensional consolidation with the finite difference method and assuming a value *C* equal to 1, yielded predicted settlements of 1.602, 1.650, 0.836, and 0.839 in.

Settlement measured by the magnet extensometer for the individual cohesive Layers 1, 3, 5, and 7 were 4.803, 1.535, 0.591, and 1.398 in. Primary consolidation settlement using Terzaghi's method, Davis and Raymond's method, and magnet extensometer is shown in Table 6-8.

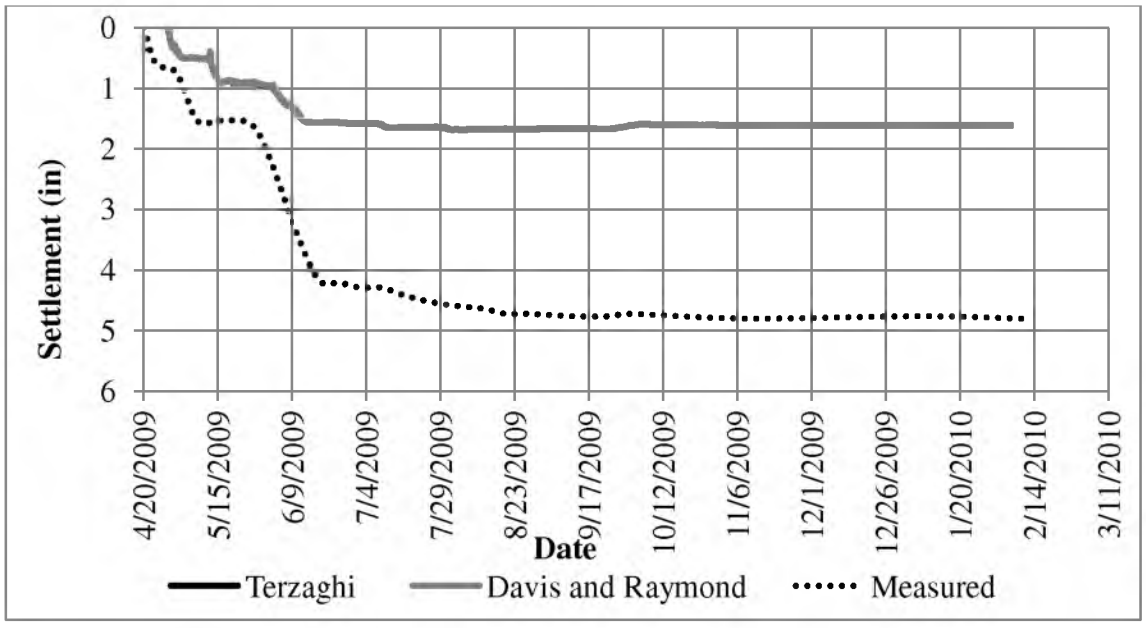

Figure 6-27. Comparison of primary consolidation settlement for Layer 1, depth range of 3 to 8 ft below the original ground surface at the centerline of the embankment for February 10, 2010 using a *C* equal to 1.

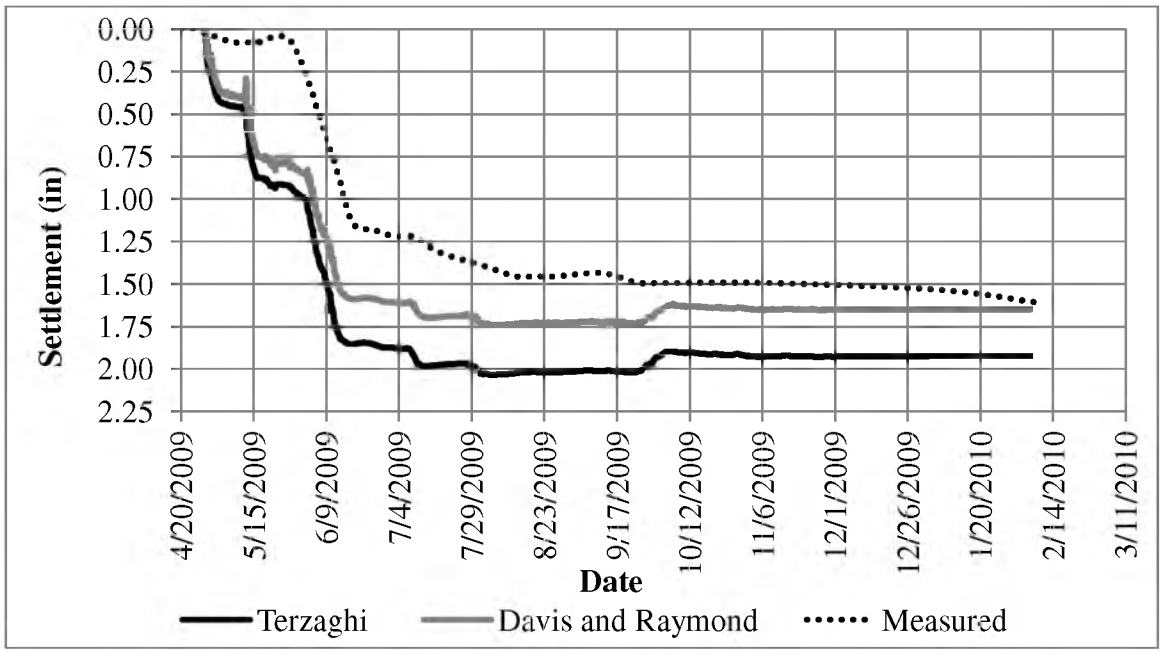

Figure 6-28. Comparison of primary consolidation settlement for Layer 3, depth range of 14 to 20 ft below the original ground surface at the centerline of the embankment for February 10, 2010 using a *C* equal to 1.

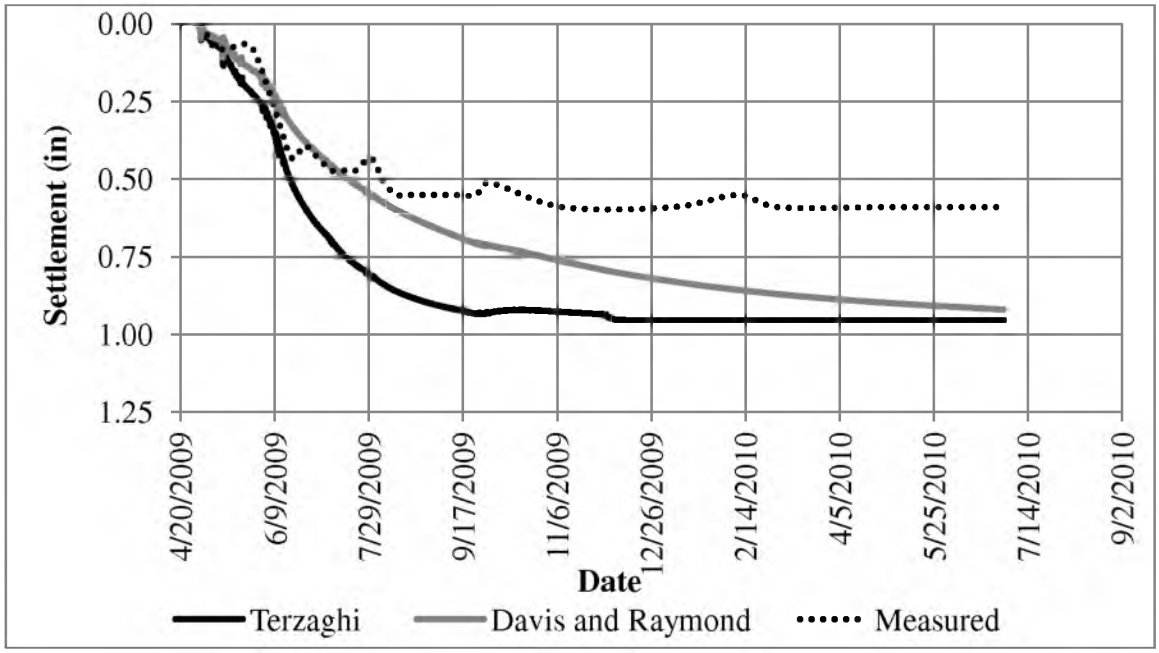

Figure 6-29. Comparison of primary consolidation settlement for Layer 5, depth range of 30 to 44.92 ft below the original ground surface at the centerline of the embankment for July 1, 2010 using a *C* equal to 1.

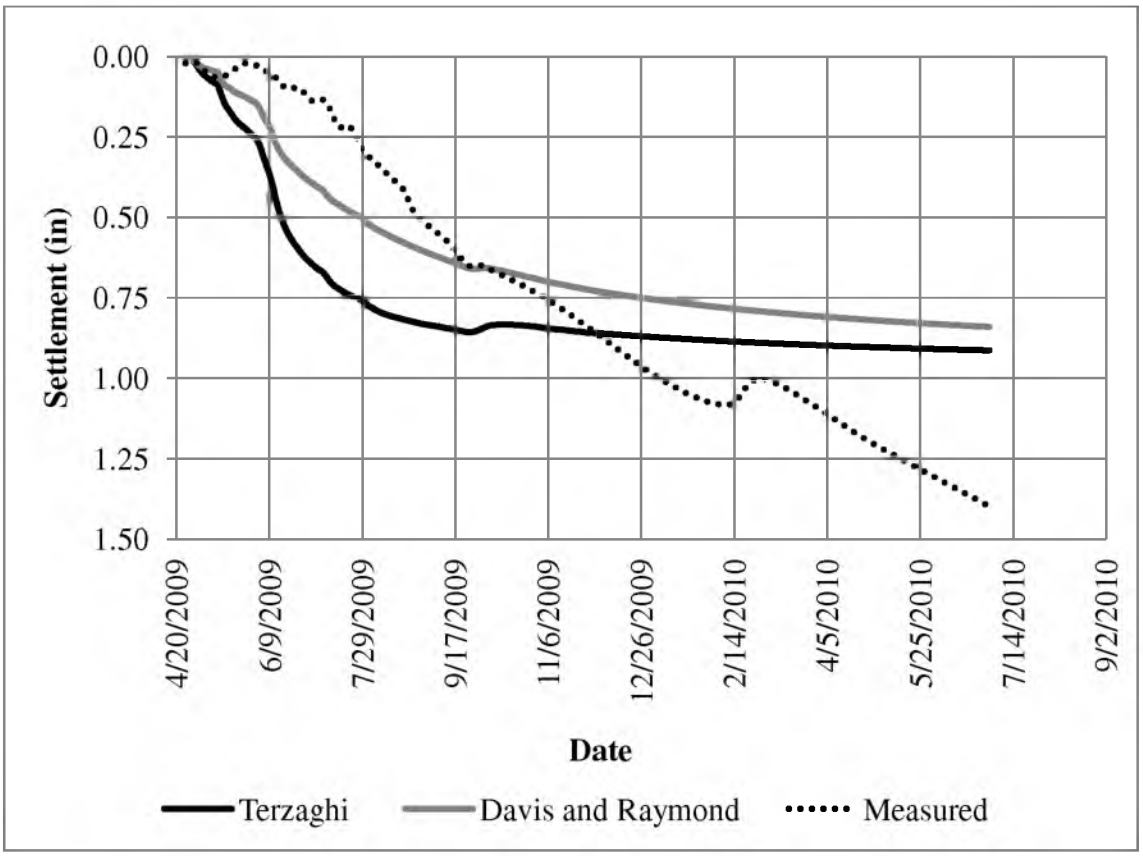

Figure 6-30. Comparison of primary consolidation settlement for Layer 7, depth range of 55 to 88 ft below the original ground surface at the centerline of the embankment for July 1, 2010 using a *C* equal to 1.

Table 6-8. Predicted primary consolidation settlement using Terzaghi's one-dimensional primary consolidation theory, Davis and Raymond's one-dimensional primary consolidation theory, and a C value of 1, and measured settlement obtained by way of the magnet extensometers for July 1, 2010.

Settlement (in)			
Layer	Terzaghi C = 1	Davis and Raymond C =1	Magnet Extensometer
1	1.613	1.602	4.803
3	1.925	1.650	1.535
5	0.954	0.836	0.591
7	0.913	0.839	1.398

Primary consolidation settlement in Layer 7 for July 1, 2010 was still occurring as seen by excess pore pressures dissipating in Figure 6-24 through Figure 6-26. The excess pore pressures within layer 7 had not fully dissipated, causing the primary consolidation settlement to take place past the completion date of construction.

An analysis of primary consolidation settlement at the centerline of the embankment was performed using Terzaghi's method and Davis and Raymond's method, as well as for the average value of *C* for depths below the original ground surface where vibrating wire piezometers were located within layers 3, 5, and 7.

The normalized pore pressure ratio of *C* indicates how much of the vertical load is initially carried by the pore pressures without dissipation of pore pressures. The assumption that the entire load is carried by the pore pressure indicates that the ratio of *C* is equal to 1. A value of *C* less than 0.1 indicates consolidation will take place quickly (Learoueil, Tavenas, Mieussens, & Peifnaud, 1978) .

The average value of *C* within Layer 3 was 0.04. The average value of *C* combined with the high value of C_v for Layer 3 indicate that this layer had the majority of the settlement occurring rapidly, as shown in Figure 6-32. Predicted primary consolidation settlements using Terzaghi's method and Davis and Raymond's method in conjunction with the average value of *C* for each layer was compared to the settlement measured by the magnet extensometer. Excess pore pressure values were determined using the same procedure outlined in Sections 2.4 and 6.2.2, except initial Δu values used in the finite difference method were multiplied by *C*, defined in Eq. 6-9. The change in effective stresses calculation is defined in Eq. 6-13.

$$\Delta\sigma_v' = \Delta\sigma_v - \Delta u \tag{6-13}$$

where:

Δu = the total change in pore pressure determined by the finite difference method using Terzaghi's method or Davis and Raymond's method and the average value of C.

Predicted results for primary consolidation settlement using these methods and C_{ave} for each cohesive layer, indicated small amounts of change in primary consolidation settlement for each cohesive layer and are shown in Figure 6-31 through Figure 6-34.

Results for primary consolidation settlement using Terzaghi' Method and C equal to 1, Terzaghi's method with C equal to C_{ave}, Davis and Raymond's method with C equal to 1, Davis and Raymond's method with C equal to C_{ave}, and magnet extensometer readings are shown in Table 6-9.

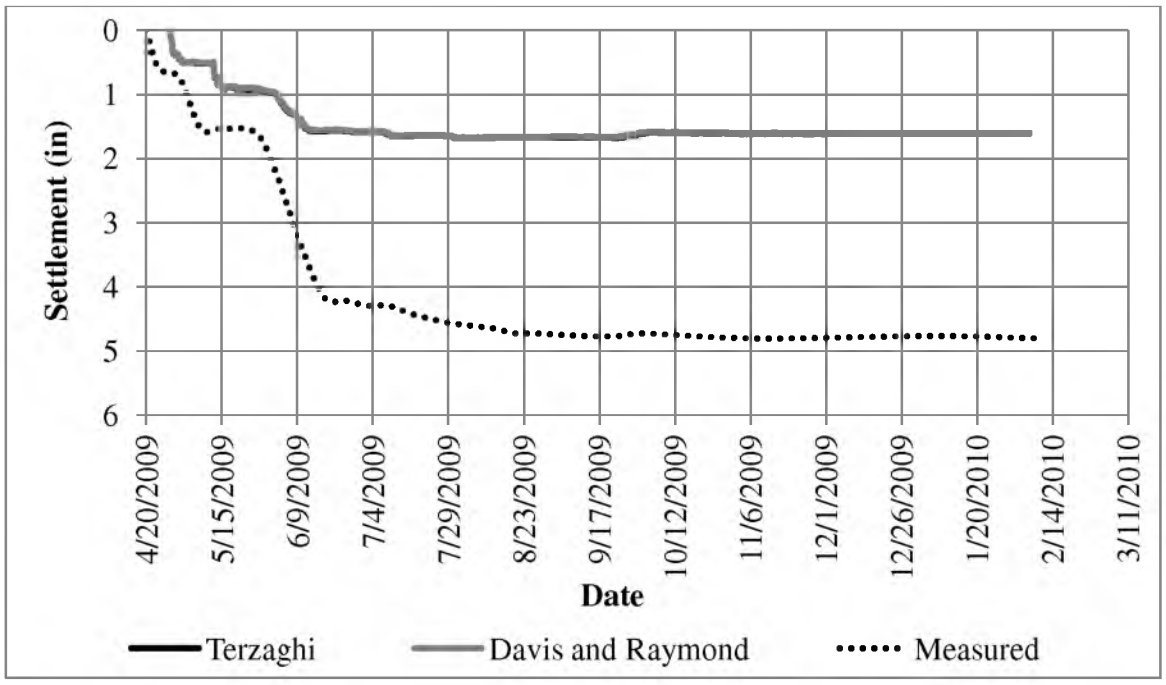

Figure 6-31. Comparison of primary consolidation settlement for Layer 1, depth range of 3 to 8 ft below the original ground surface at the centerline of the embankment for February 10, 2010 using C_{ave} equal to 0.12.

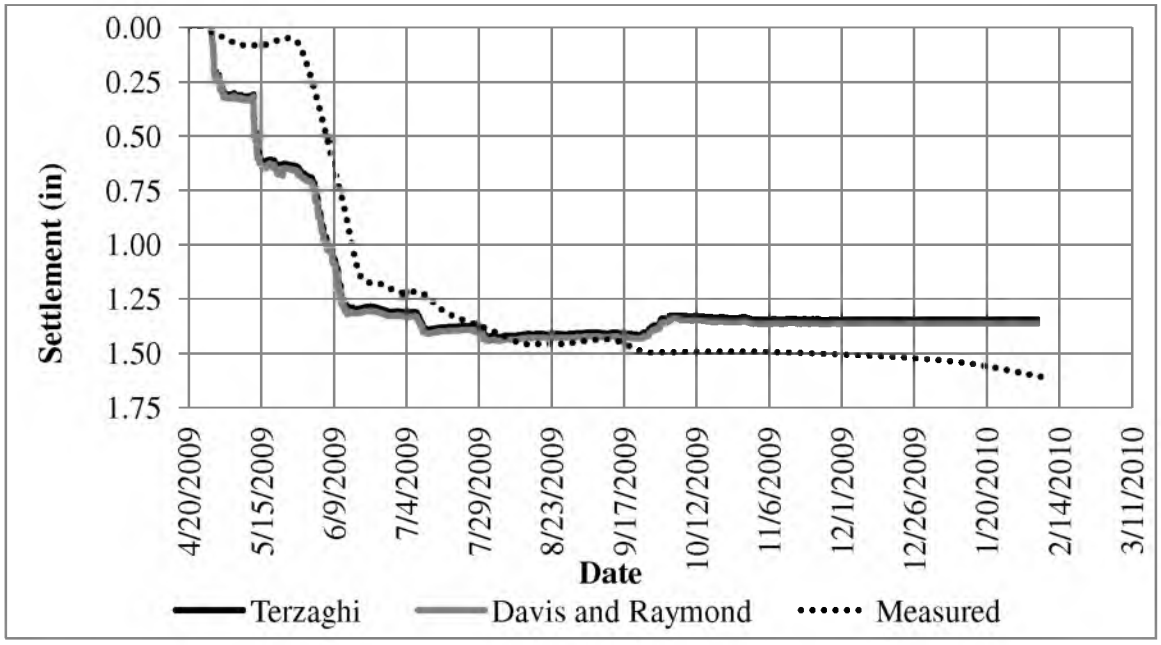

Figure 6-32. Comparison of primary consolidation settlement for Layer 1, depth range of 14 to 20 ft below the original ground surface at the centerline of the embankment for February 10, 2010 using C_{ave} equal to 0.04.

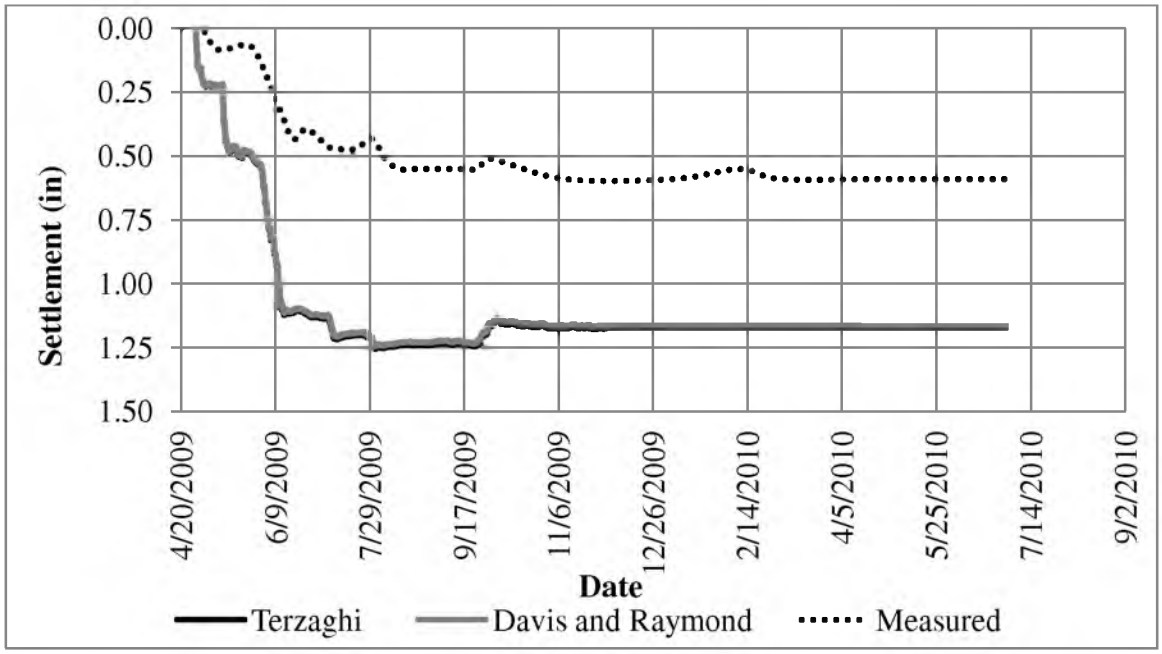

Figure 6-33. Comparison of primary consolidation settlement for Layer 5, depth range of 30 to 44.92 ft below the original ground surface at the centerline of the embankment for July 1, 2010 using a C_{ave} equal to 0.02, 0.02, 0.02.

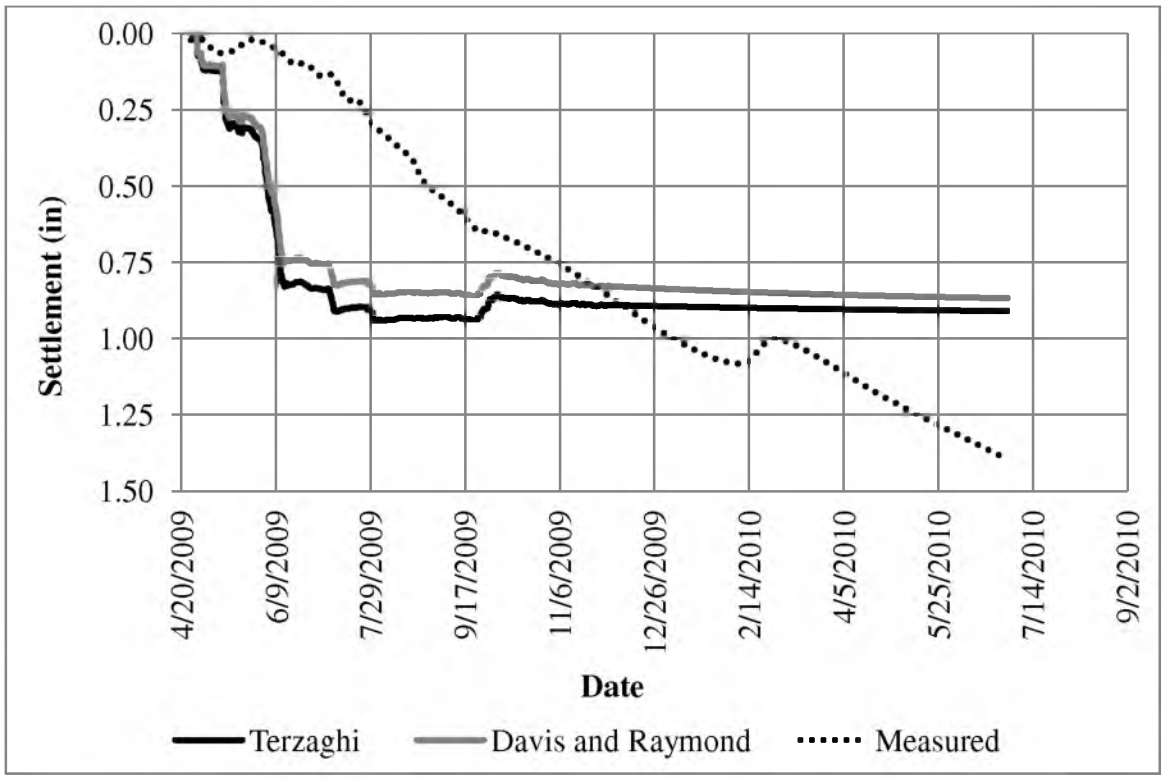

Figure 6-34. Comparison of primary consolidation settlement for Layer 7, depth range of 55 to 88 ft below the original ground surface at the centerline of the embankment for July 1, 2010 using a C_{ave} equal to 0.01, 0.04, 0.25.

Table 6-9. Primary consolidation settlement results using Terzaghi's method, Terzaghi's method with associated C_c, Davis and Raymond's method, Davis and Raymond's method with associated C_{ave}, and measured settlement using readings from the magnet extensometer for each layer.

	Settlement (in)				
Layer	Terzaghi $C_c = 1$	Terzaghi C_{ave}	Davis and Raymond $C_c = 1$	Davis and Raymond C_{ave}	Magnet Extensometer
1	1.613	1.613	1.602	1.602	4.724
3	1.925	1.552	1.650	1.465	1.535
5	0.954	0.954	0.836	0.932	0.630
7	0.931	0.909	0.839	0.866	1.398

Predicting primary consolidation settlement with time using Terzaghi's method and Davis and Raymond's method in conjunction with the finite difference method yield settlement results for a value of C equal to 1 and an average value C equal to C_{ave}, as determined within Layers 1,3, 5, and 7 produced reasonable settlement results. In order to achieve settlement results, many of the assumptions that geotechnical engineers usually make were not made. Assuming the soil is homogenous can lead to erroneous results when calculating settlement. A more correct procedure is to determine the cohesive layers and their corresponding geotechnical parameters and perform settlement analysis using geotechnical parameters within their respective layers using interfaces within sublayers if necessary. There were four distinct cohesive layers underneath the embankment as determined by the initial CPT. The distinctions between cohesive and granular layers were verified through laboratory testing by performing Atterberg limits and CRS tests at depths within the embankment's foundation. Each cohesive layer had a different c_v value determined from CRS testing. The C_v value changes as the effective stress changes, in particular, once the preconsolidation stress is reached. The C_v will drastically decrease once the preconsolidation stress is reached. The preconsolidation stress is also different within each cohesive layer. Since the preconsolidation stress was never reached in the cohesive layers, the soil was in recompression and the coefficients of consolidation had to be greater than if the soil was in virgin compression.

A major part of the underestimation of the total primary consoldiation settlement was due to the underestimation of the settlement that occurred in Layer 1. The underestimation of settlement within Layer 1 was due to sampling. A block sample was taken 8 ft outside of the north MSE wall at a depth of 5 ft below the ground surface. The location of this sample was different than the location of the rest of the Shelby tube

samples. Initial sampling started at a depth of 10 ft below the ground surface and at the centerline of the embankment. The importance of quality samples for laboratory testing is imperitive to quality settlement analysis.

6.3 Prediction of Surcharge Removal

Surcharging compressible soils is one method to accelerate the primary consolidation settlement and is accomplished by placing additional load beyond the final load in order to achieve the final effective stress. The time at which the surcharge is left on and consequently removed depends on the underlying soil and the dissipation of excess pore pressures developed in the underlying soils during the loading process. Asaoka's method for predicting ultimate primary consolidation settlement using total settlement of the original ground surface, as well as predictions for ultimate primary consolidation settlement using primary consolidation settlement of individual cohesive layers will be discussed in Section 6.3.1 . An individual layer method using distinct geotechnical parameters determined from field and laboratory testing to predict the average degree of consolidation (U_{avg}) will be discussed in Section 6.3.2. Measured settlement since removal of surcharge will be provided in Section 6.3.3

6.3.1 Asaoka's Method

The predicted ultimate primary consolidation settlement and time for surcharge removal were analyzed using Asaoka's method. Time sensitivity in selecting the time increment for use in analysis purposes will be discussed in Section 0. Results for ultimate primary consolidation settlement at time at which the surcharge was removed will be compared with the actual time at which the surcharge was removed (September 24, 2009

– October 1, 2009) using settlement of the original ground surface readings obtained via the magnet extensometer, settlement manometer, vibrating wire settlement cells, and horizontal inclinometer and will be discussed in Section 0. Ultimate primary consolidation settlement predictions for cohesive layers (Layers 1, 3, 5, and 7, see Figure 4-1 and Table 4-1) using settlement readings obtained by way of the magnet extensometer at the centerline of the embankment will be presented and discussed in Section 0

6.3.1.1 Sensitivity to selected time increment. An issue in estimating ultimate primary consolidation settlement based on measured values of ultimate primary consolidation settlement using Asaoka's method is that of time sensitivity. If the time increment is carelessly applied during analysis, erroneous settlement estimations can be calculated. The influence of selected time increment on the estimation of ultimate settlement, settlement at removal of surcharge, and time of surcharge are presented in Table 6-10.

Table 6-10 – Influence of selected time increments on predicted primary consolidation settlement using Asaoka's method and measured data from the vibrating wire settlement sensors.

Δt (Days)	Asaoka Settlement (in)	Settlement at Removal of Surcharge (in)	Time of Surcharge (Days)	Date for Removal of Surcharge
3	9.00	8.75	140	9/7/2009
7	9.32	8.75	167	10/4/2009
10	9.38	8.75	174	10/11/2009
20	9.41	8.75	178	10/14/2009

6.3.1.2 Predictions based on total settlement of original ground surface. To provide better estimates of the time for completion of primary consolidation settlement and time for removal of surcharge using Asaoka's method, settlement data obtained from the different types of field instrumentation were analyzed and compared to actual primary consolidation settlements for dates on which surcharge was removed (September 24 through October 1). Settlement results from the following field instruments were used in this comparison: (1) Magnet extensometer, (2) settlement manometer, (3) settlement cells, and (4) horizontal inclinometer.

The value of Δt chosen for predicting ultimate primary consolidation settlement was based on what value of Δt provided the most accurate value of predicted primary consolidation settlement to the settlement value obtained for each instrument. Asaoka's method equaled the measured primary consolidation settlement obtained from readings for each instrumentation. The values of Δt used for prediction of surcharge removal are shown in Table 6-11.

Asaoka's method for prediction of ultimate primary consolidation settlement and time for removal of surcharge requires that field data be obtained during constant time intervals. During this project, settlement data were not obtained during constant time intervals due to scheduling conflicts. To enable us to use Asaoka's method, a best fit

Table 6-11. Final time steps selected for settlement prediction using Asaoka's method for different types of instrumentation.

Instrumentation	Δt (days)
Magnet Extensometer	7
Settlement Manometers	7
Settlement Sensors	20
Horizontal Inclinometer	20

regression line was fitted through the field settlement data for each type of instrument. The procedure used to predict primary consolidation settlement and time for removal of surcharge using Asaoka's method is as follows:

1. Develop the settlement with time curve using measured settlement data obtained from field instruments with the fill height of the embankment with time on the same plot, as shown in Figure 6-35.
2. Develop the ultimate primary consolidation settlement at time using Asaoka's method, by plotting (S_t) versus the settlement from the previous time step (S_{t-1}) as seen in Figure 2-16 based on constant time intervals to determine the magnitude of ultimate primary consolidation settlement.

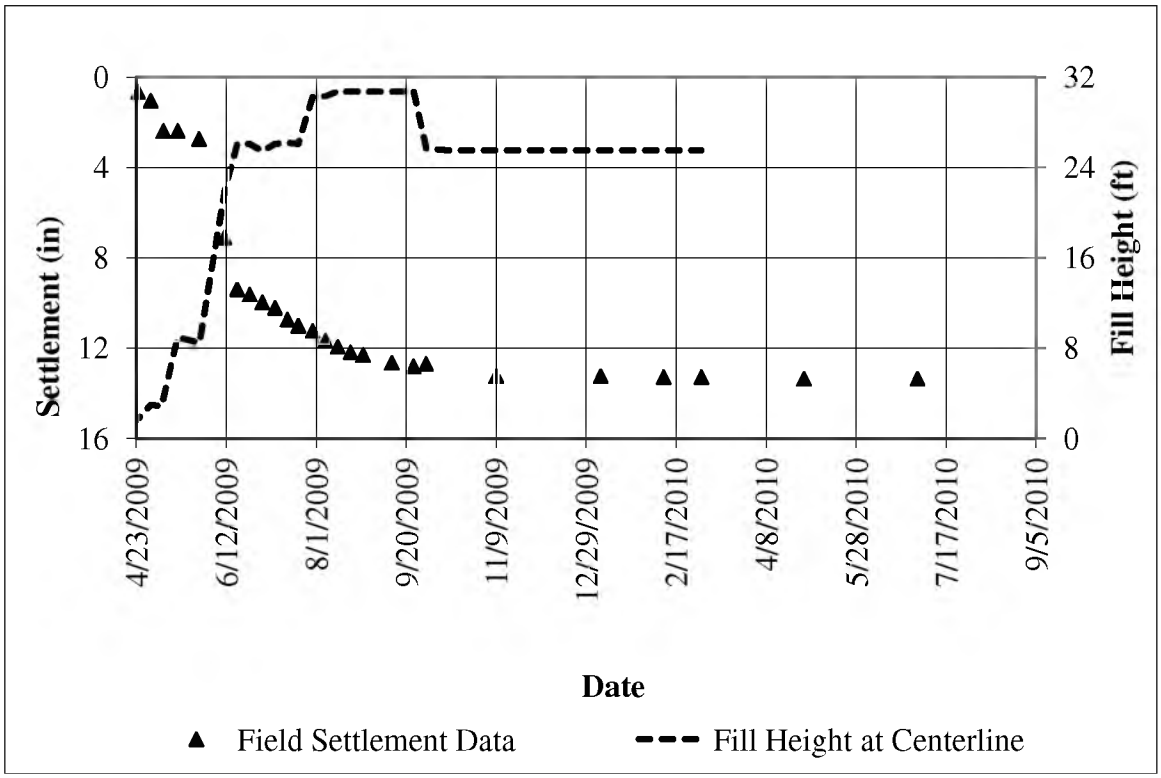

Figure 6-35. Example of the settlement with time curve plotted with the fill height of the embankment with time.

3. Determine the best fit settlement data line that fits the measured settlement data by estimating the settlement that occurs with time as a function of ultimate primary consolidation settlement and the average degree of consolidation, $S_{ci} = S_{c,ult}(U_{avg})$, Eq. 2-23, and determining most appropriate time step (Δt) and c_v/H^2_{dr}, as shown in Figure 6-36.

However, it needs to be reiterated here that a percentage of final settlement is not equal to the average degree of consolidation (typically called U_{avg}). U_{avg} represents the average degree of dissipation of excess pore pressure (and hence the average degree of change in effective vertical stress), not the average degree of settlement, because primary

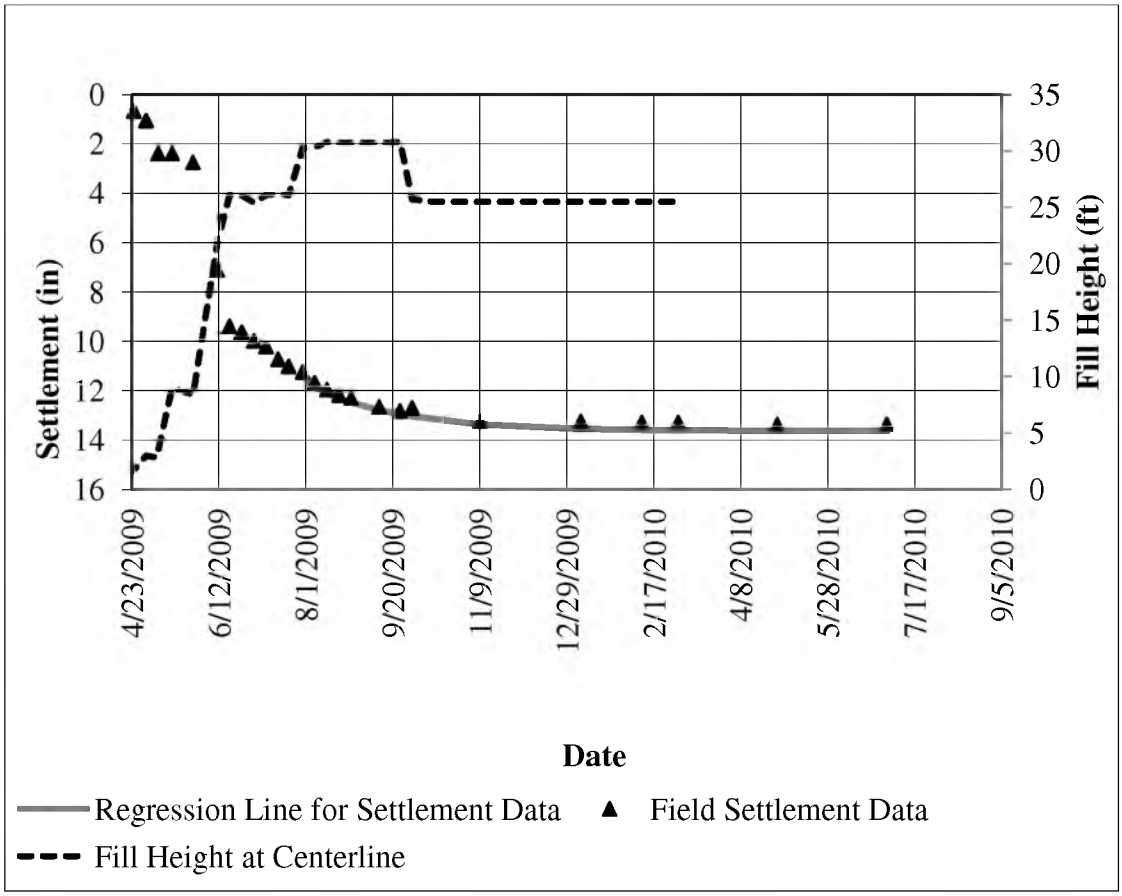

Figure 6-36. A best fit regression model using field settlement data from the magnet extensometer to determine the settlement with time.

consolidation settlement is not proportional to the change in the effective vertical stress, as discussed in Section 2.4.1.2.

4. Extrapolate the time at which a certain amount of primary consolidation settlement is to occur by using Eq. 2-23 and Figure 6-36.

Ultimate primary consolidation settlements using Asaoka's method in conjunction with measured surface settlements obtained via the magnet extensometer, settlement manometer, settlement cells, and horizontal inclinometer are provided in Figure 6-37 through Figure 6-44. Using the field data obtained by the aforementioned field instruments, predicted ultimate primary consolidation settlements were different for field data obtained from each field instrument. The greatest amount of predicted ultimate primary consolidation settlement was 13.6 inches using field data obtained from the magnet extensometer. The least amount of predicted ultimate primary consolidation settlement was 9.40 inches using field data obtained from the vibrating wire settlement cells.

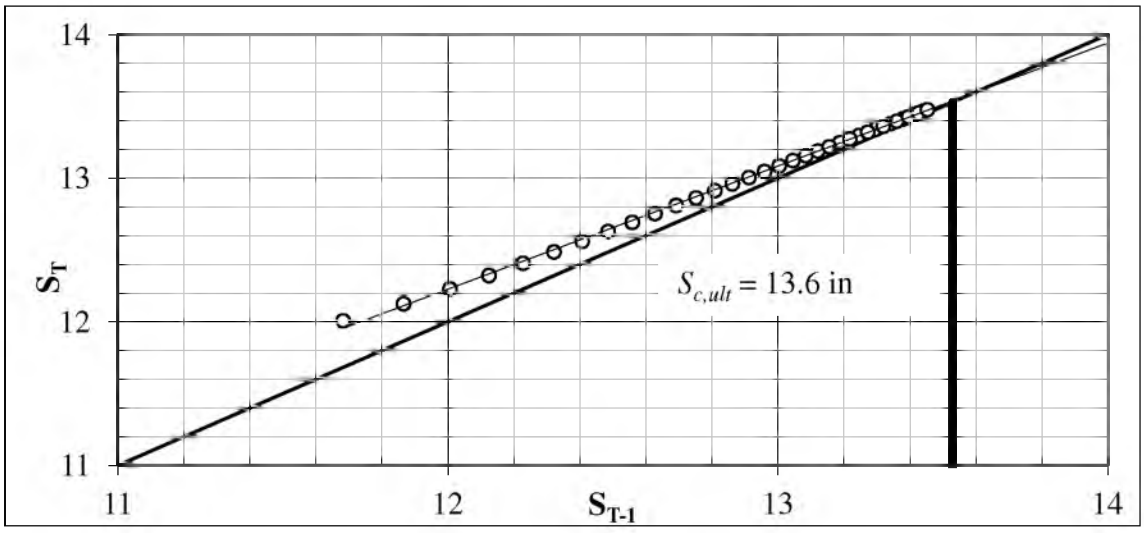

Figure 6-37 Prediction of ultimate primary consolidation settlement using measured data from magnet extensometer and Asaoka's method.

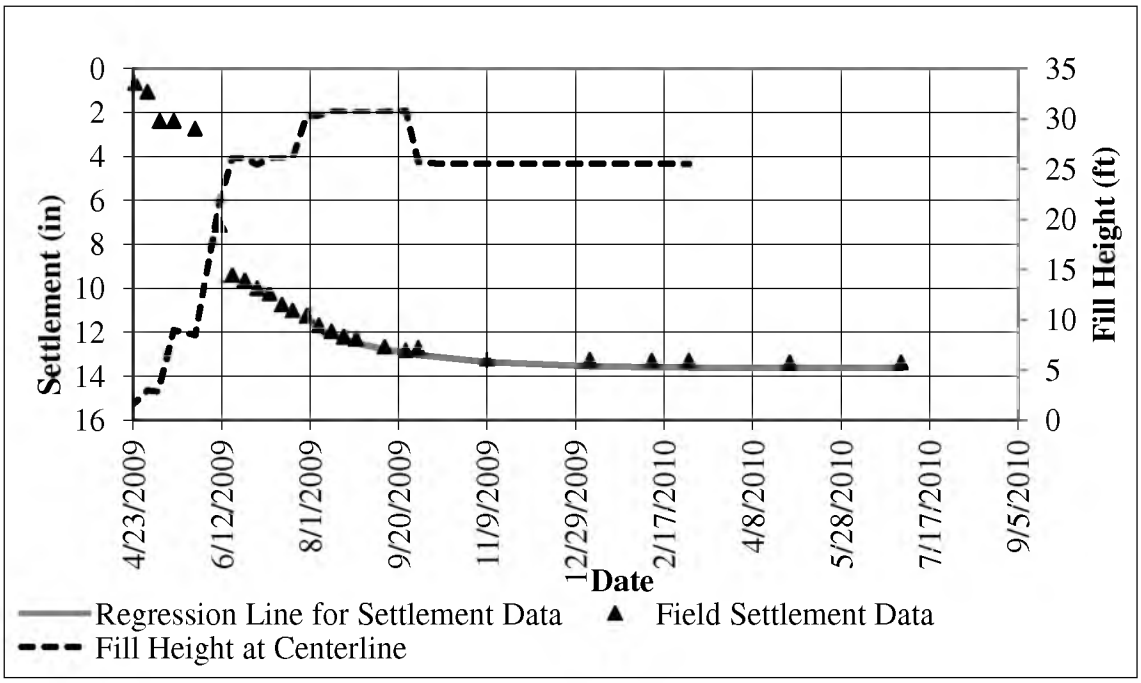

Figure 6-38. Magnet extensometer settlement field data, best fit regression line for settlement data, and fill height for estimated elapsed time for surcharge removal.

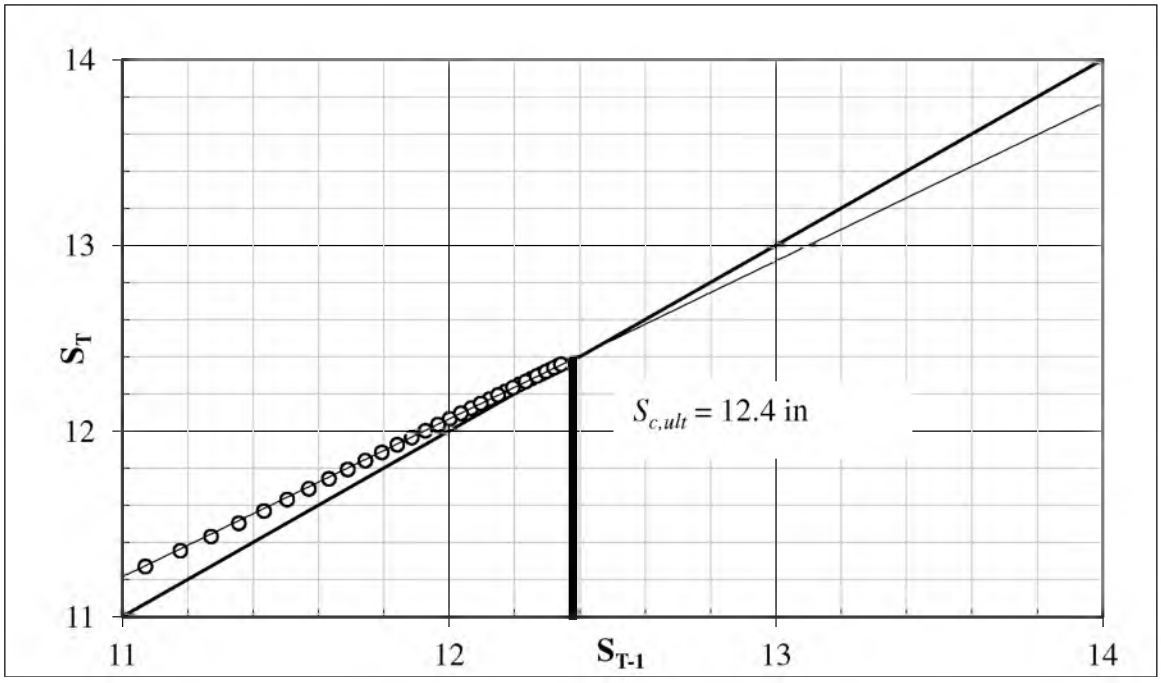

Figure 6-39. Prediction of ultimate primary consolidation settlement using measured data from settlement manometers and Asaoka's method.

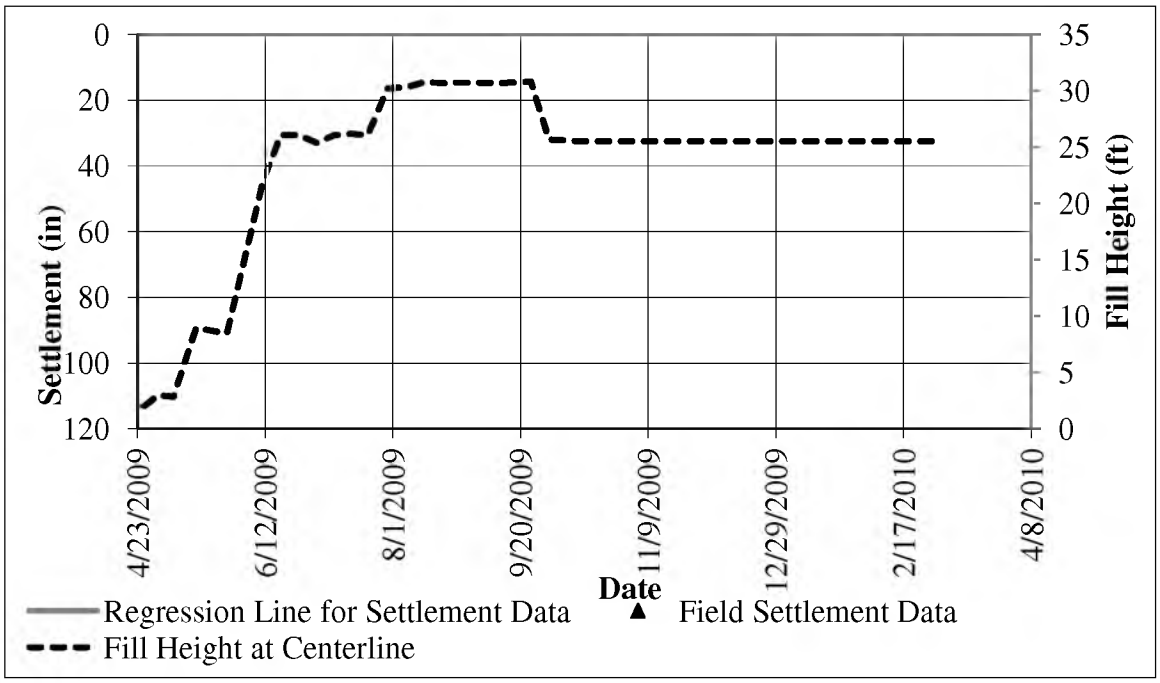

Figure 6-40. Settlement manometer field data for settlement, best fit regression line for settlement data, and fill height for estimated elapsed time for surcharge removal.

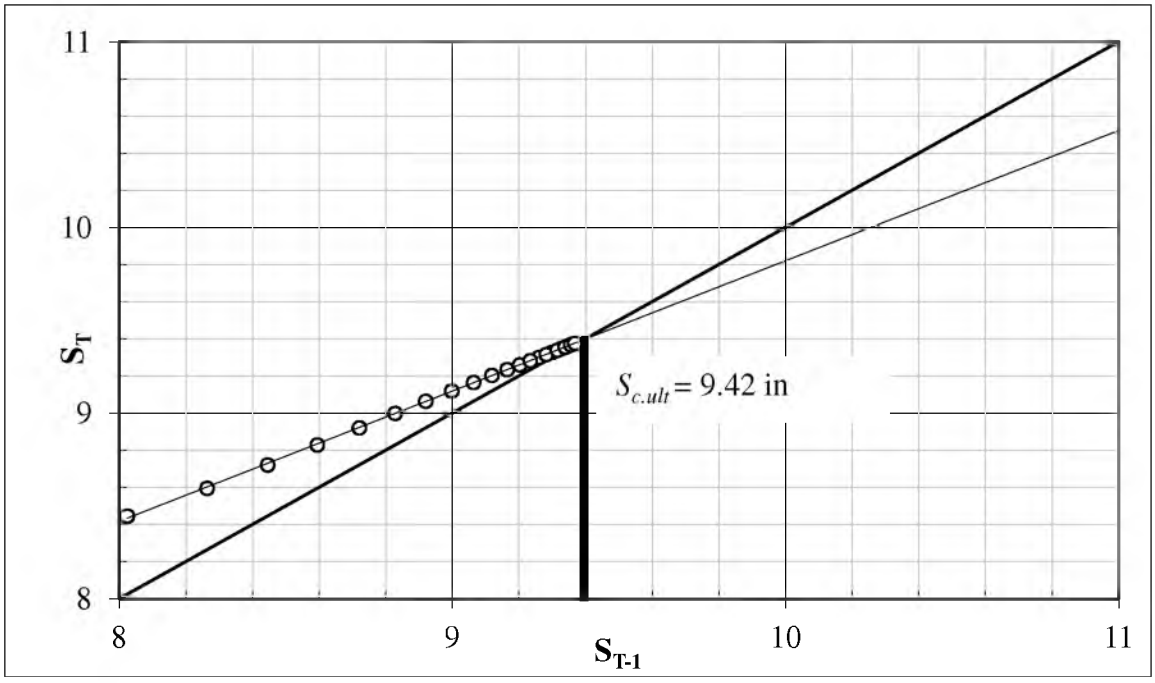

Figure 6-41. Prediction of ultimate primary consolidation settlement using measured data from settlement cells and Asaoka's method.

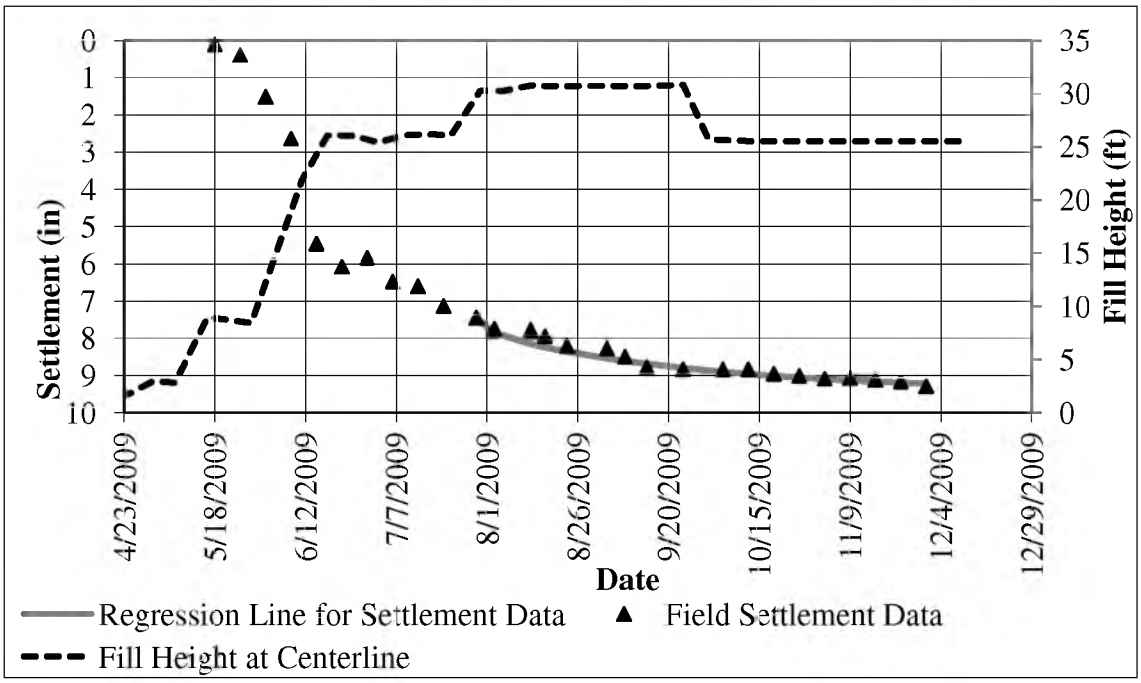

Figure 6-42. Settlement cells field data for settlement, best fit regression line for settlement data, and fill height for estimated elapsed time for surcharge removal.

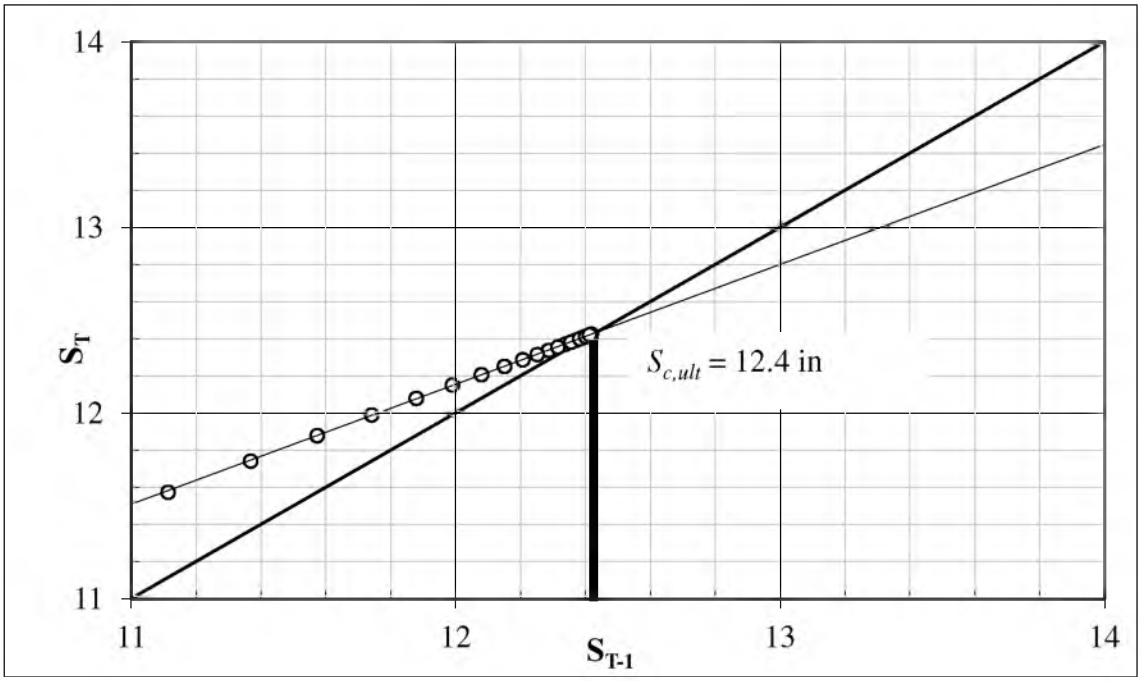

Figure 6-43. Prediction of ultimate primary consolidation settlement using measured data from horizontal inclinometers and Asaoka's method.

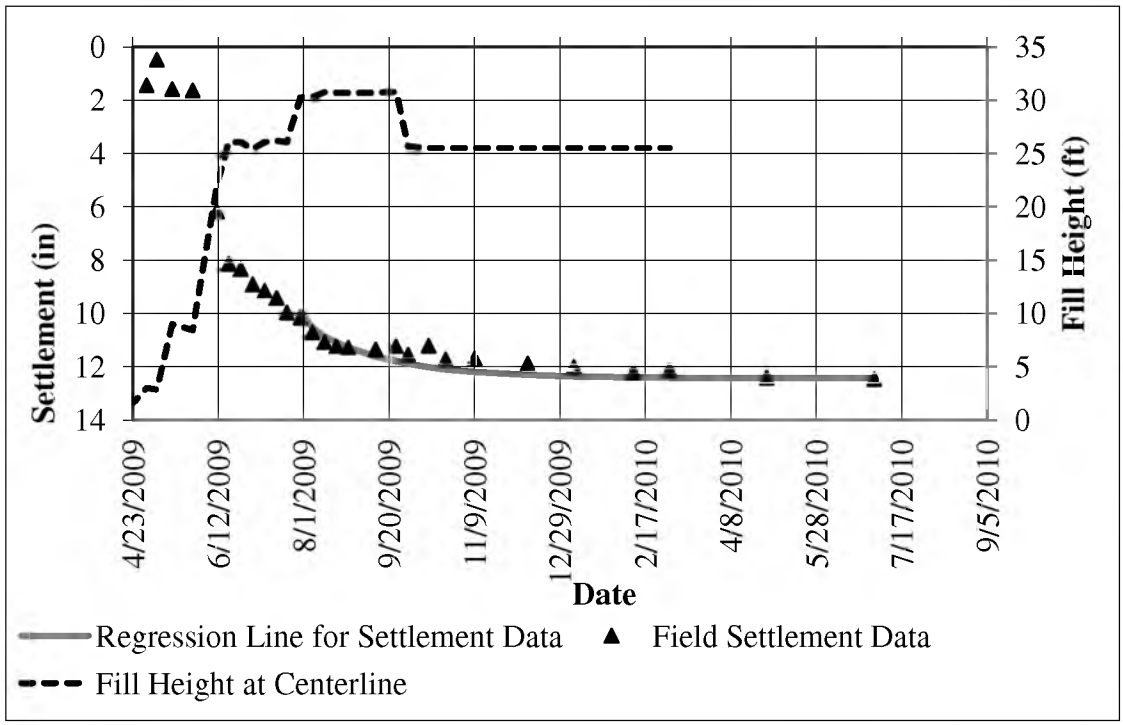

Figure 6-44. Horizontal inclinometer settlement field data, best fit regression line for settlement data, and fill height for estimated elapsed time for surcharge removal.

The ultimate primary consolidation settlement results using Asaoka's method and field data obtained from each field instrument were used in back calculating the predicted dates for removal of surcharge. Three dates for removal of surcharge were back calculated using settlements that were 90%, 95%, and 98% of the ultimate primary consolidation settlement. Using data obtained from the magnet extensometer as an example, the dates for removal of surcharge using the ultimate primary consolidation settlement are as follows:

where:

$S_{c,ult}$ = 13.6 inches

$S_{c,90\%} = (0.9)S_{c,ult} = 0.9(13.6) = 12.2$ inches

$S_{c,95\%} = (0.95)S_{c,ult} = 0.95(13.6) = 12.9$ inches

$S_{c,98\%} = (0.98)S_{c,ult} = 0.98(13.6) = 13.3$ inches

Using Figure 6-38 to extrapolate the dates from the settlement versus time plot, for $S_{c,90\%}$, $S_{c,95\%}$, and $S_{c,98\%}$ were determined. The removal dates for these three percentages of settlements are: August 13, 2009, October 1, 2009, and January 6, 2010. Resulting settlements for 90%, 95%, and 98% of ultimate primary consolidation settlement with surcharge removal dates corresponding to the percentage of ultimate primary consolidation settlement using data obtained from each field instrument is presented in Table 6-12.

Because of the varying results for ultimate primary consolidation settlements and variation in the dates for surcharge removal, improvements to existing methods needed to occur. Using the Asaoka method, ultimate primary consolidation settlement was analyzed using measured settlement data for individual cohesive layers.

6.3.1.3 Predictions based on settlement of individual cohesive layers. To better estimate the primary consolidation settlement occurring underneath the embankment, and the time for removal of surcharge, primary consolidation settlement within Layers 1, 3, 5, and 7 were analyzed using settlement readings obtained via the magnet extensometers, Asaoka's method, U_{avg} (Eq. 2-23), the time at which surcharge was removed (September 24, 2009 – October 1, 2009), and the procedure that was outlined in Section 0. Ultimate primary consolidation settlement results for individual cohesive layers using Asaoka's method and settlement versus time plots for each cohesive layer are shown in Figure 6-45 through Figure 6-52.

Ultimate primary consolidation settlements for individual cohesive layers were analyzed in the same manner as the ultimate primary consolidation settlement of the original ground surface. Results for individual cohesive layers are presented in

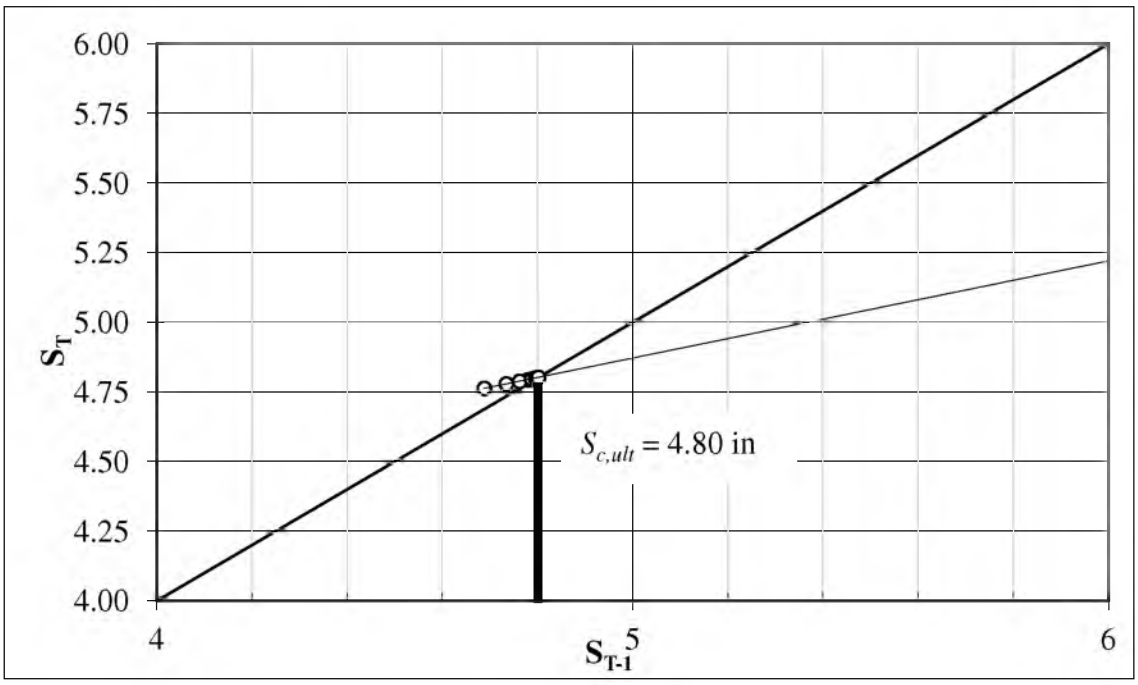

Figure 6-45. Prediction of ultimate primary consolidation settlement using measured data from magnet extensometer and Asaoka's method for Layer 1.

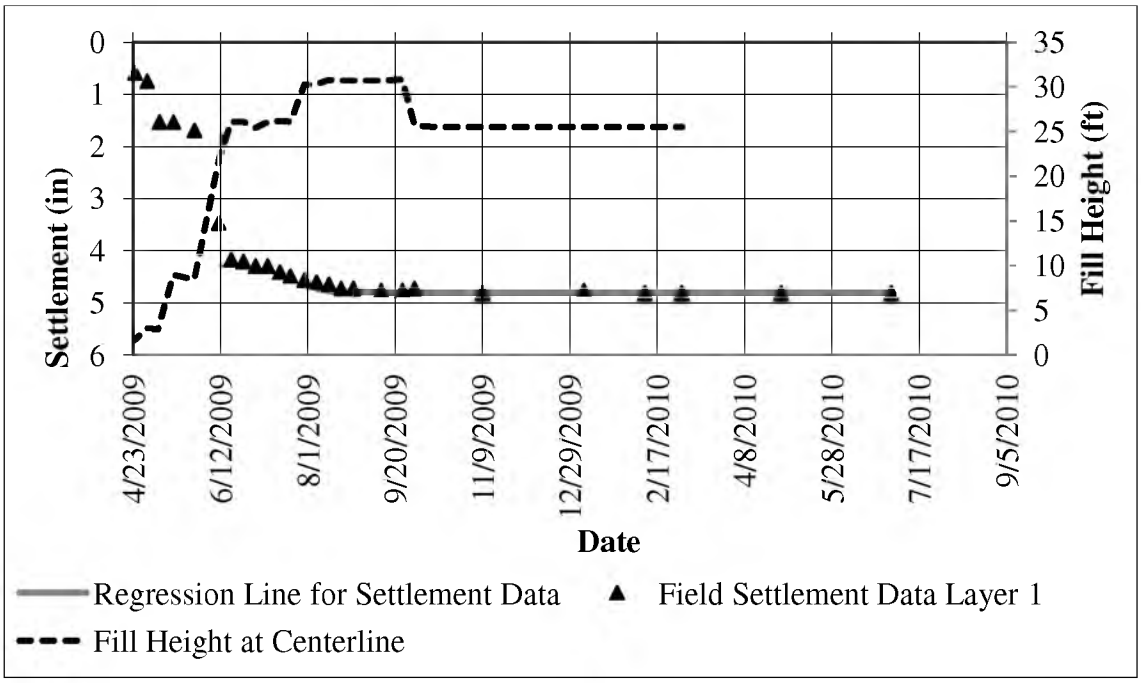

Figure 6-46. Magnet extensometer settlement field data for Layer 1, best fit regression line for settlement data, and fill height for estimated elapsed time for surcharge removal.

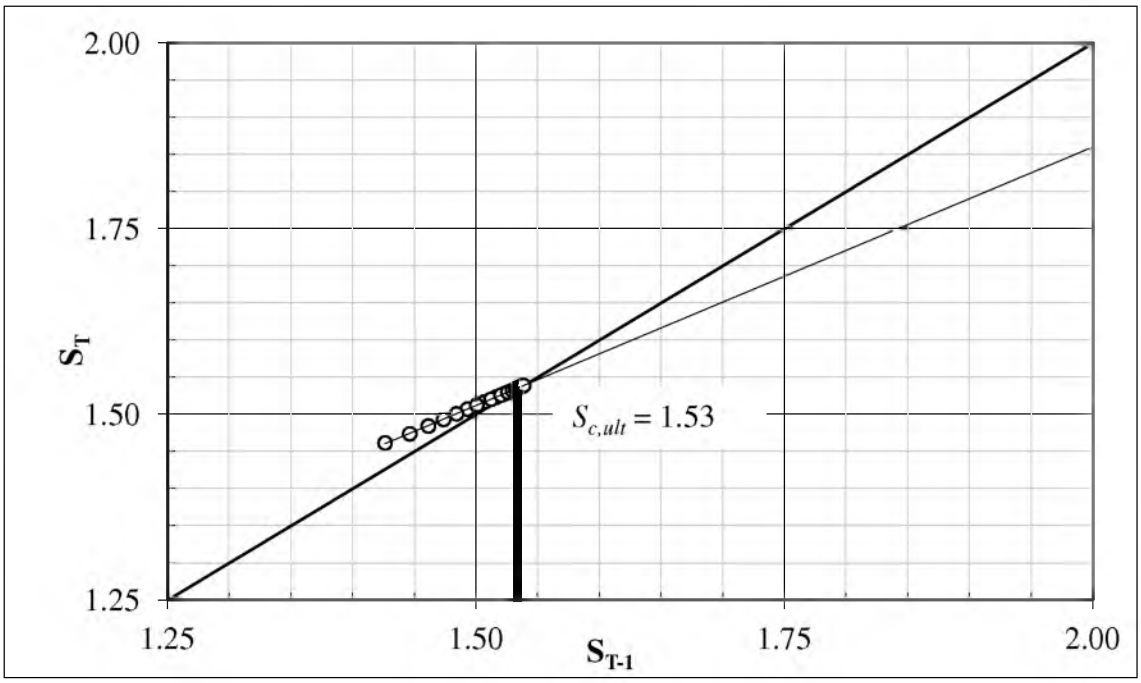

Figure 6-47. Prediction of ultimate primary consolidation settlement using measured data from magnet extensometer and Asaoka's method for Layer 3.

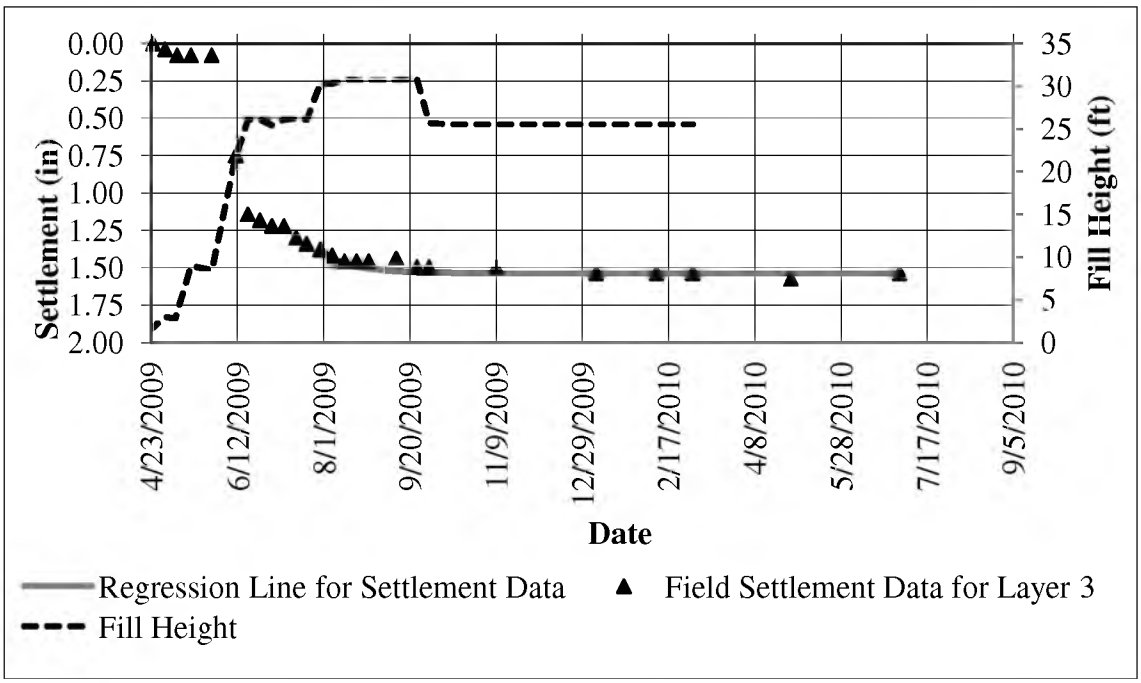

Figure 6-48. Magnet extensometer settlement field data for Layer 3, best fit regression line for settlement data, and fill height for estimated elapsed time for surcharge removal.

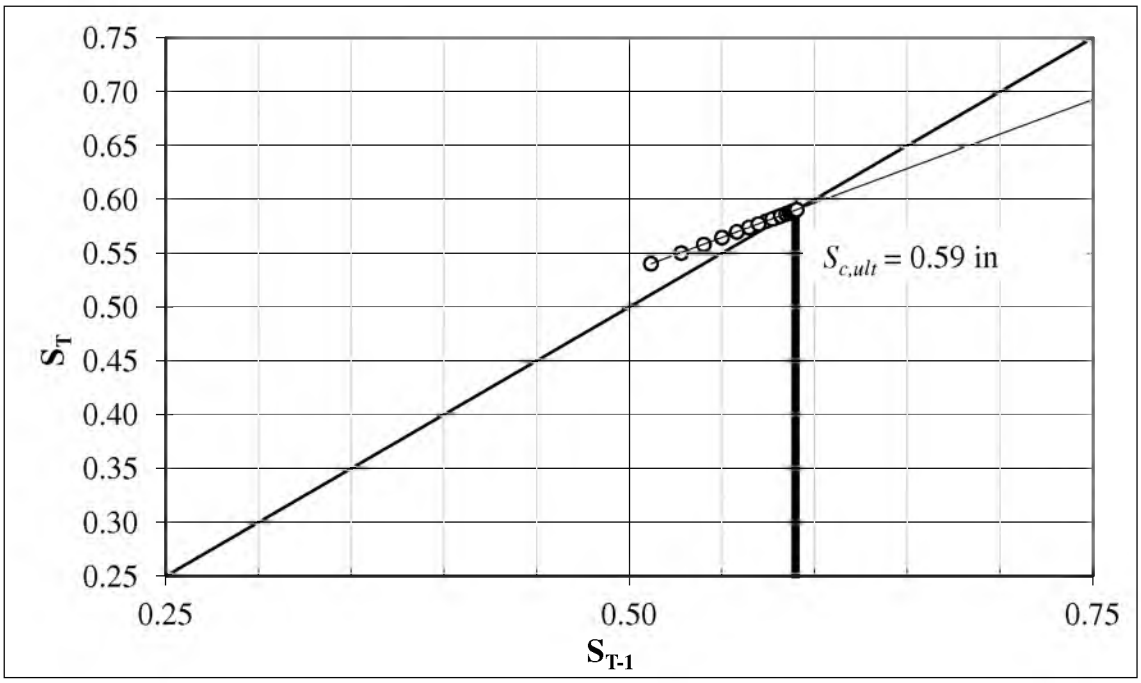

Figure 6-49. Prediction of ultimate primary consolidation settlement using measured data from magnet extensometer and Asaoka's method for Layer 5.

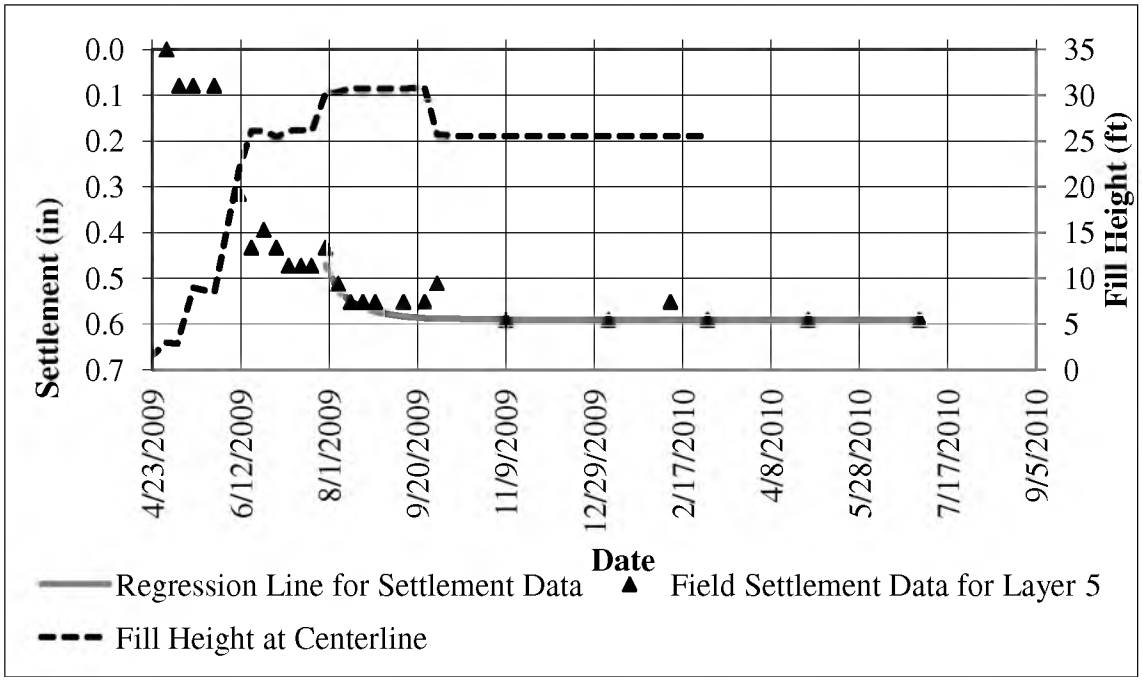

Figure 6-50. Magnet extensometer settlement field data for Layer 5, best fit regression line for settlement data, and fill height for estimated elapsed time for surcharge removal.

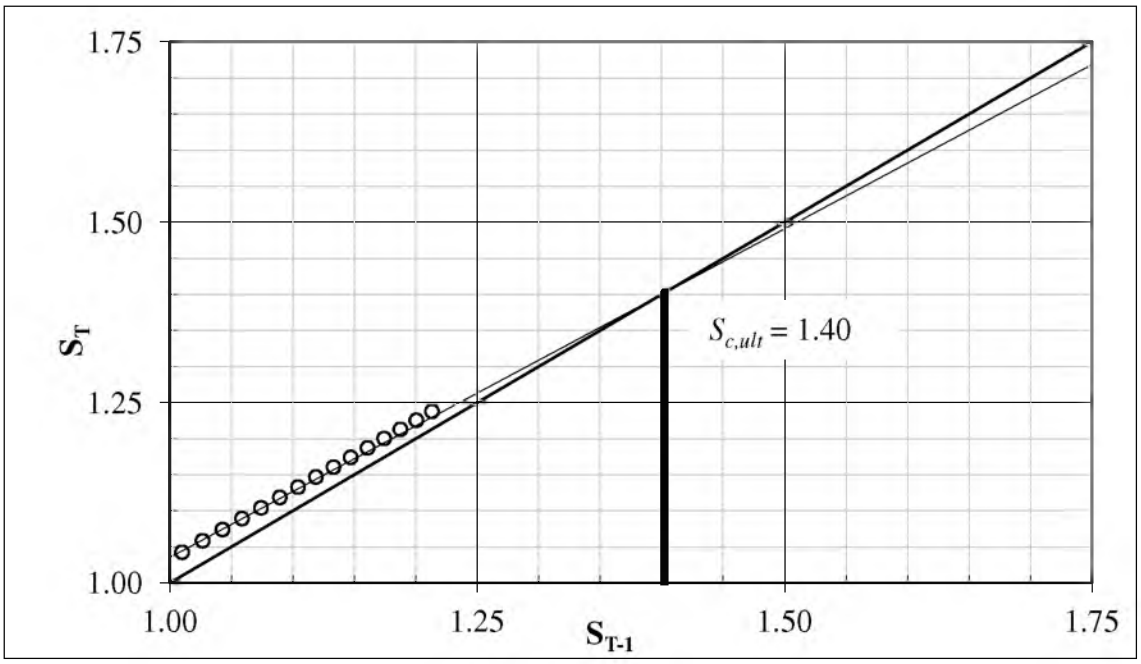

Figure 6-51. Prediction of ultimate primary consolidation settlement using measured data from magnet extensometer and Asaoka's method for Layer 7.

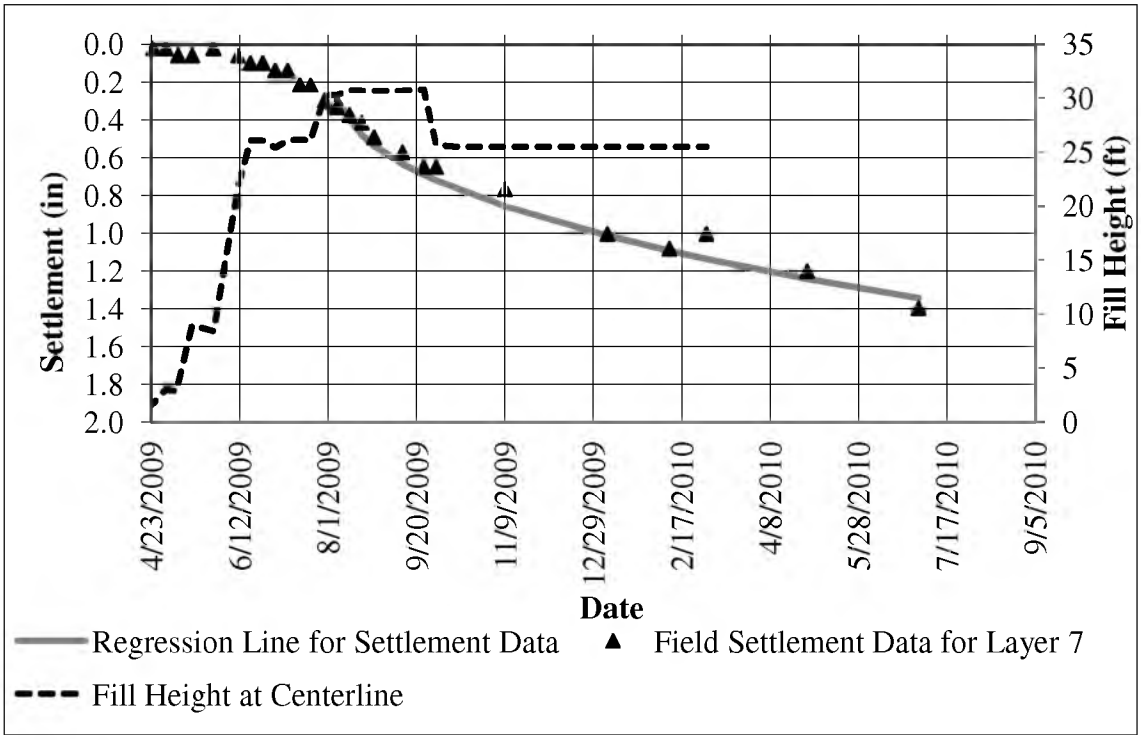

Figure 6-52. Magnet extensometer settlement field data for Layer 7, best fit regression line for settlement data, and fill height for estimated elapsed time for surcharge removal

Table 6-12. Resulting settlements for 90%, 95%, and 98% of ultimate primary consolidation settlement with surcharge removal dates corresponding to the percentage of ultimate primary consolidation settlement using data obtained from each field instrument.

	$S_{c,ult}$	$S_{c,90\%}$	Surcharge Removal	$S_{c,95\%}$	Surcharge Removal	$S_{c,98\%}$	Surcharge Removal
Instrument	(in.)	(in.)	Date	(in.)	Date	(in.)	Date
Magnet Extensometer	13.6	12.2	8/13/2009	12.9	10/1/2009	13.3	1/6/2010
Settlement Manometer	12.4	11.2	8/27/2009	11.8	9/24/2009	12.2	12/10/2009
Settlement Cells	9.4	8.5	9/3/2009	8.9	10/12/2009	9.2	11/23/2009
Horizontal Inclinometer	12.4	11.2	8/13/2009	11.8	11/9/2009	12.2	1/6/2010

Table 6-13 for September 24, 2009.

The primary consolidation settlements for Layers 1, 3, and 5, along with their respected values of estimated U_{avg} are reasonable for the time at which surcharge was removed. However, an estimated value of U_{avg} for Layer 7 indicated that settlement was still occurring within Layer 7 at the time at which surcharge was removed.

Complete dissipation of excess pore pressures had not occurred at the time surcharge was removed. The low values of C_v within Layer 7, combined with the height of the longest drainage path, allowed for dissipation of excess pore pressures within Layer 7 to be time consuming.

6.3.2 Individual Layer Method

An individual layer method was applied to Layers 1, 3, 5, and 7 using distinct geotechnical parameters determined by field and laboratory testing. U_{avg} determined by Sivaram and Swamee (1977) Eq. 2-23 and Eq. 2-24, for a U_{avg} varying from 0 to 100% (Das 1993) was determined using: (1) The height of the longest drainage path (H_{dr}), (2) the initial value of C_v obtained from the CRS test results at the appropriate range in effective stress, (3) the elapsed time from beginning of construction until removal of surcharge, t_c (April 10, 2009 to September 24, 2009).

Using Eq. 2-23 and Eq. 2-24 from Section 2.5.1, a sample calculation of U_{avg} for Layer 1 is provided and is calculated as follows:

where:

H_{dr} = 2.5 ft

C_v = 2.71 ft^2/day

$$\frac{C_v}{H_{dr}^2} = \frac{2.71}{2.5^2} = 0.434$$

t_c= September 24, 2009 – April 10, 2009 = 167 days

$$T_v = \frac{c_v}{H_{DR}^2}(t_c) = 0.434(167) = 72.4$$

$$U_{avg} = \frac{(4T_v/\pi)^{0.5}}{\left[1 + (4T_v/\pi)^{2.8}\right]^{0.179}} = \frac{(4(72.4)/\pi)^{0.5}}{\left[1 + (4(72.4)/\pi)^{2.8}\right]^{0.179}} = 99.5$$

Results for predicted ultimate primary consolidation settlement for individual cohesive layers using Asaoka's method when compared to the measured primary consolidation settlement for removal of surcharge and the estimated U_{avg} at time for removal of surcharge are presented in Table 6-13.

Results using distinct geotechnical parameters obtained from field and laboratory testing for each cohesive layer are shown in Table 6-14. Treating the subsurface soils as a

Table 6-13. Predicted ultimate primary consolidation settlement for individual cohesive layers using Asaoka's method compared to the primary consolidation settlement for removal of surcharge and the estimated U_{avg} at time of removal of surcharge using Eq. 2-23 under a constant load for September 24, 2009.

Layer	Predicted Settlement (in)	Settlement at Removal of Surcharge (in)	Estimate U_{avg} (%)
1	4.80	4.76	99.5
3	1.53	1.50	94.5
5	0.59	0.55	96.8
7	1.40	0.65	23.9

Table 6-14. Average degree of consolidation calculated for each layer using the height of the longest drainage path, coefficient of consolidation, and time factor for each cohesive layer.

Layer	H_{dr}	c_v	c_v/H^2_{DR}	T_v	U_{avg}

	(ft)	(ft^2/day)			
1	2.5	2.71	4.34E-01	72.4	99
3	3.0	3.59	3.99E-01	66.6	99
5	7.0	0.13	2.57E-03	0.43	72
7	16.5	0.38	1.39E-03	0.23	54

homogeneous material is an incorrect assumption as previously mentioned. It has been shown in Section 4, during the geotechnical investigation, that the subsurface soils were comprised of four distinct cohesive layers with varying geotechnical properties. Using the distinct properties for each individual cohesive layer, U_{avg} was determined to show the excess pore pressures had not fully dissipated within layers 5 and 7 when surcharge was removed. U_{avg} for individual layers 1, 3, 5, and 7 when surcharge was removed were 99, 99, 72, and 54. Thus, indicating primary consolidation settlement was not complete at the time for which surcharge was removed.

6.3.3 Settlement Since Removal of Surcharge

As previously shown using Terzaghi's method and Davis and Raymond's method in conjunction with the finite difference method, excess pore pressure dissipation was still occurring within Layer 5 and Layer 7 upon removal of surcharge and placement of final pavement, causing postconstruction settlement to occur. Both, the finite difference method and the vibrating wire piezometers determined excess pore pressures were still dissipating in layers 5 and 7, thus causing post construction settlement to occur. Post-construction settlement results were taken from when the final pavement was placed on October 23, 2009 to July 1, 2010. As of July 1, 2010, the settlement manometers and vibrating wire settlement sensors were no longer active.

The settlement manometer's last reading was taken on April 29, 2010 and yielded -0.25 in of settlement. The last reading for the vibrating wire settlement sensor was taken on November 30, 2009 and yielded 0.35 in of settlement. Postconstruction settlement from magnet extensometer and horizontal inclinometer was measured and recorded on July 1, 2010. Postconstruction settlement for each instrument is shown in Table 6-15. It is also important to remember that as of September 27, 2011, the excess pore pressures from underneath the centerline of the embankment at a depth of 78 ft below the original ground surface had not fully dissipated as shown in Figure 6-53 and quite possibly, more settlement would have occurred between July 1, 2010 and September 2011.

Table 6-15. Postconstruction settlement determined from the various types of instrumentation for date of each instruments availability.

	Date	Postconstruction Settlement (in)
Magnet Extensometer	July 1, 2010	0.67
Settlement Manometer	April 29, 2010	-0.25
Vibrating Wire Settlement Sensors	November 30, 2010	0.35
Horizontal Inclinometer	July 1, 2010	0.74

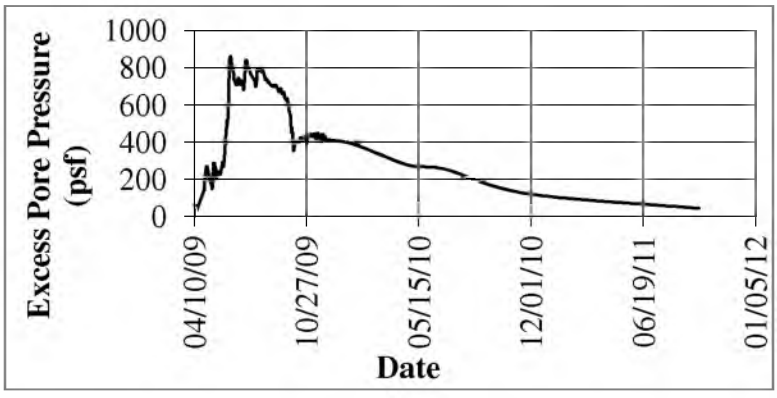

Figure 6-53. Change in pore water pressures at 3:00 AM on September 27, 2011 beneath the centerline of the embankment at a depth of 78ft below the original ground surface.

7 SUMMARY AND CONCLUSIONS

Reconstruction on Interstate 15/State Route 77 began during the fall of 2008, and was completed in the fall of 2009. Part of this project included constructing a bridge over railroads tracks located ¼ mile east of Interstate 15/State Route 77 intersection. The bridge spanned 425-ft in length and was supported by an embankment of 106-ft wide and 30-ft tall at its highest point. An MSE located on the north and south wall, with vertical slopes supported the embankment laterally.

The SR 77 embankment was built upon four thick compressible cohesive layers located at depths of 3-8, 14-20, 30-45, and 55-88-ft. Due to the thick compressible cohesive layers, the embankment was susceptible to settlement during the construction process. In order to monitor the behavior of the thick compressible clay layers, field instrumentation was placed in the ground.

The goals of the research presented in this thesis were as follows: (1) Monitor actual settlement by way of field instrumentation, (2) estimate settlement using a finite difference model to solve Terzaghi's (1942) equation and Davis and Raymond's (1965) equation for excess pore pressure dissipation, (3) estimate settlement by modifying the coefficient of consolidation with a change in effective stress during excess pore pressure dissipation process, (4) estimate settlement by implementing an average $\Delta\sigma u/\Delta\sigma_v$ ratio

during the loading, and (5) determine the end of primary consolidation settlement using Asaoka's method and individual layer method.

The first assignment undertaken to achieve these objectives was to perform a preliminary geotechnical field investigation to determine the location of the thick compressible cohesive layers. Shelby tube samples were taken within the cohesive layers for constant rate of strain testing (performed at University of Utah geotechnical laboratory). Parameters determined from the constant rate of strain tests were preconsolidation stress, coefficient of recompression, and coefficient of consolidation.

Knowledge of these parameters led to appropriate settlement modeling using the finite difference method to solve for the rate of excess pore pressure dissipation. The rate of excess pore pressure dissipation and magnitude of settlement was determined for each individual layer for modifications to Terzaghi's equation and Davis and Raymond's equation. The resulting settlement from each modification was compared to actual settlement obtained from the field instrumentations.

The settlements calculated from Terzaghi's equation and Davis and Raymond's equation with an average $\Delta\sigma u/\Delta\sigma_v$ ratio, and with a $\Delta\sigma u/\Delta\sigma_v$ ratio of 1 produced different results for each cohesive layer. Yet, neither ratio yielded conclusive results as to which method is more productive.

The Asaoka method is an approach in which removal of surcharge is determined and the magnitude of primary consolidation to occur is determined. When using this method, primary consolidation settlement is predicted by assuming the excess pore pressures generated underneath a homogeneous foundation will dissipate at a constant rate. Analysis of the individual cohesive layers illustrate these layers dissipate at

different rates and complete, full dissipation of each individual layer occurs at different times. Data show Layers 5 and Layers 7 were still dissipating upon removal of surcharge, and full primary consolidation settlement had not occurred. Furthermore, the average degrees of consolidation at 33 and 78 ft, located in Layers 5 and 7, determined from the vibrating wire piezometer, demonstrate these layers were still dissipating when surcharge was removed.

In order to better understand the behavior of soft cohesive layers from embankment construction a number of recommendations can be made to future research. Recommendations are as follows:

a. **Improvement to laboratory testing.** Laboratory testing should be performed before any construction project to determine the insitu soil parameters. Insitu soil parameters are constantly changing. The intervals at which soil parameters change need to be identified in an effective yet efficient manner. Identification of change in soil parameters can be determined from the constant rate of strain test which better estimates soil behavior.

b. **Different geotechnical modeling.** Terzaghi's 1942 method is the most commonly used method for estimating or predicting primary consolidation settlement. Terzaghi used various assumptions in determining his solution for rate of excess pore pressure. With knowledge and technology improving, other solutions or methods developed for determining the rate of excess pore pressure dissipation and/or primary consolidation settlement needs to be implemented in order to validate their accuracy.

c. **Three-dimensional effects of primary consolidation theory.** Preloading a soft soil foundation causes distortion in three dimensions. Measuring and estimating one-

dimensional primary consolidation settlement was the major focus of this thesis. In application of preloading, distortion of the soil matrix occurs in three dimensions. The three-dimensional effects should be accounted for when estimating primary consolidation settlement.

d. **Future research sites for instrumentation to verify the proposed methods work.** SR 77 research embankment provided insight into different methods for determining time rate and magnitude of primary consolidation settlement and excess pore pressure dissipation. Excess pore pressure dissipated at different rates within the four cohesive layers. Treating subsurface soil conditions as homogenous can lead to erroneous time rate and magnitude of primary consolidation settlement estimations. Further research studying the rate of excess pore pressure dissipation within cohesive soils underlying an application of loading using the individual layer method is needed to further validate the proposed method.

e. **Instrumentation of future research embankments to monitor the magnitude of secondary compression and the effects preloading.** Field instrumentation is used with the major emphasis of measuring the primary consolidation settlement, while oftentimes not used for measuring secondary compression and the long term effects caused by preloading. Future research sites should include instrumentation used for: (1) Obtaining data for measuring secondary compression, (2) long term settlement effects caused by preloading, and (3) obtaining data in order to verify methods developed for estimating secondary compression settlement.

f. **Correlation between σ_v and $\Delta\sigma u/\Delta\sigma_v$.** Correlations between different soil parameters is a practice geotechnical engineers use during design and analysis in order to

become more efficient in predicting engineering behavior. The $\Delta\sigma u/\Delta\sigma_v$ ratio was determined in three distinct cohesive layers at the SR 77 embankment research site. To better understand the effects $\Delta\sigma u/\Delta\sigma_v$ ratio and primary consolidation settlement, correlating the $\Delta\sigma u/\Delta\sigma_v$ ratio and σ_v parameters should be researched.

In summary, this research project has been successful in identifying the problems associated with geotechnical modeling and geotechnical methods. Correct modeling includes a change of the coefficient of consolidation with change in effective stress and a correct $\Delta\sigma u/\Delta\sigma_v$ ratio for each cohesive layer. This research also identified the problems of using Asaoka's method for determining the end of primary consolidation and removal of surcharge, when cohesive layers are not homogenous.

APPENDIX A

STRESS STRAIN RESULTS FROM CONSTANT RATE OF STRAIN TESTS

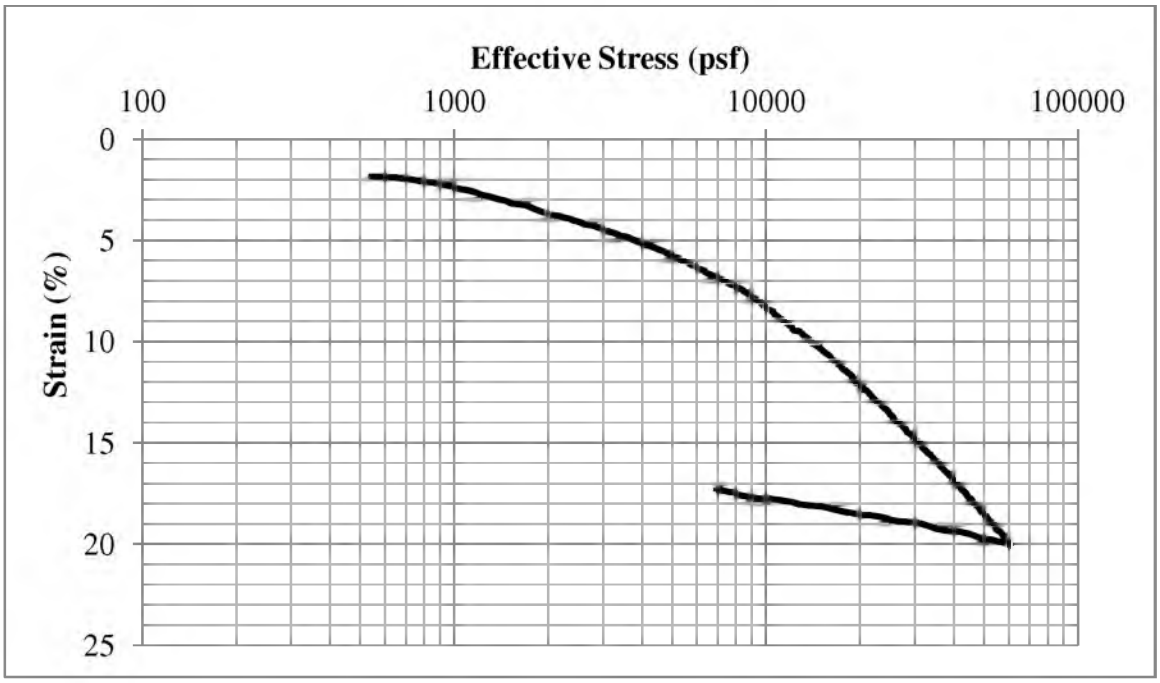

Figure A-1. Stress-strain results from constant rate of strain test at a depth of 5 ft below the original ground surface.

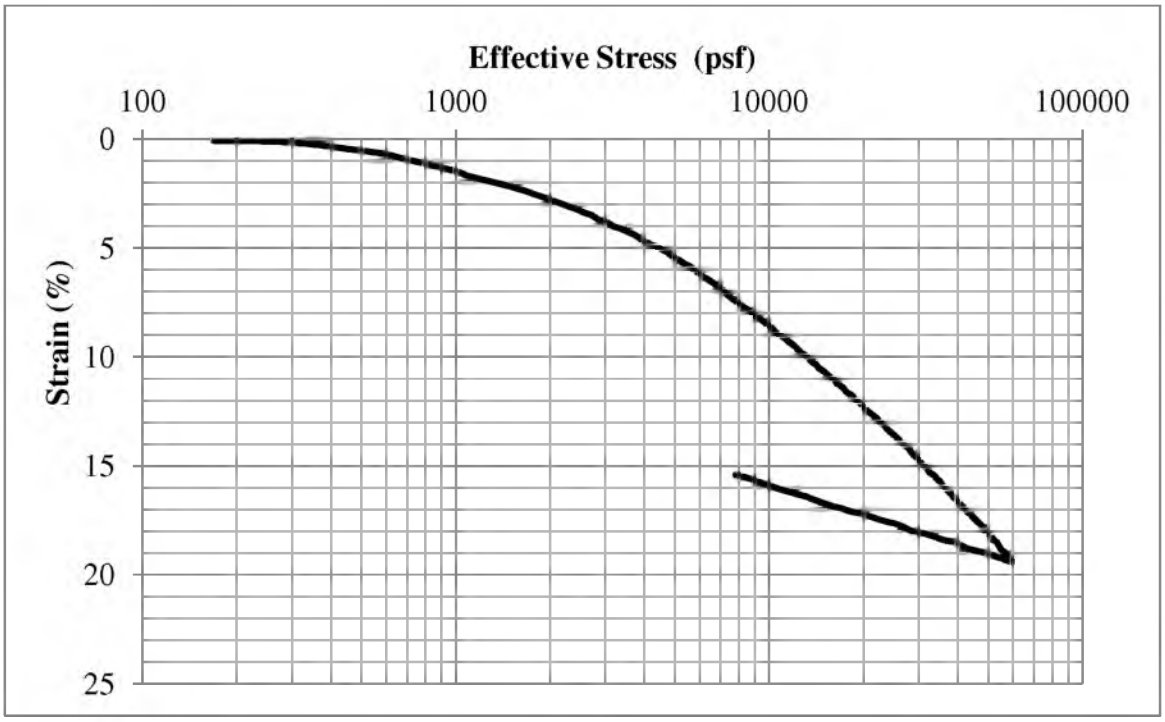

Figure A-2. Stress-strain results from constant rate of strain test at a depth of 15.25 ft below the original ground surface.

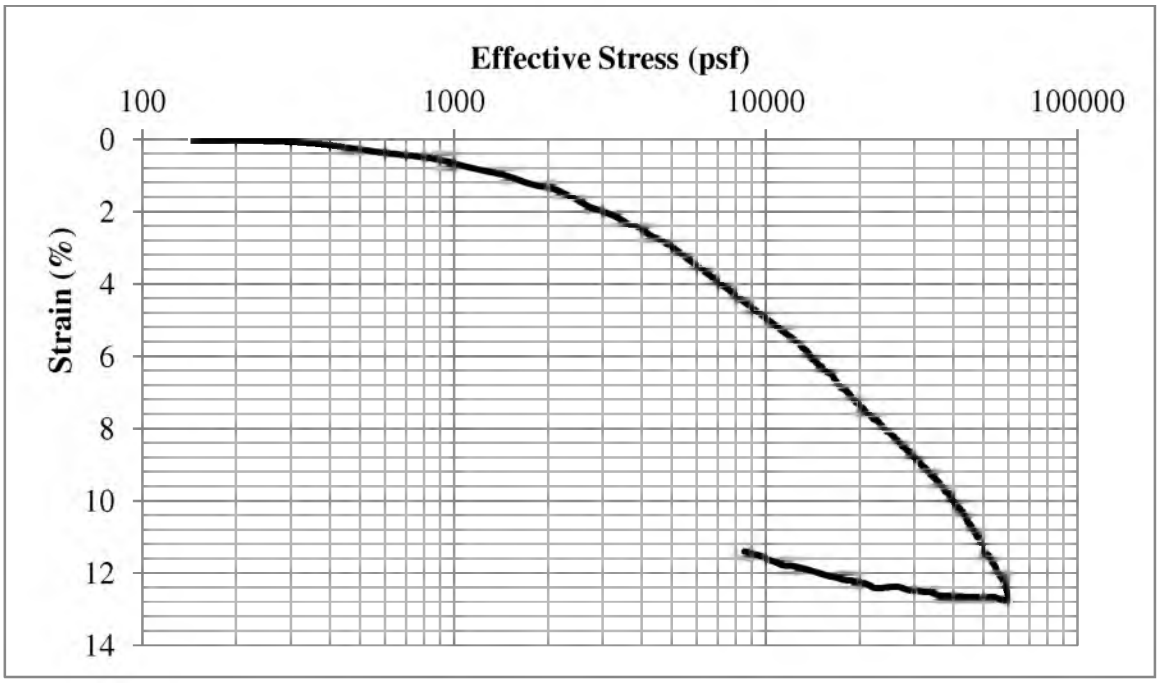

Figure A-3. Stress-strain results from constant rate of strain test at a depth of 30.5 ft below the original ground surface**.**

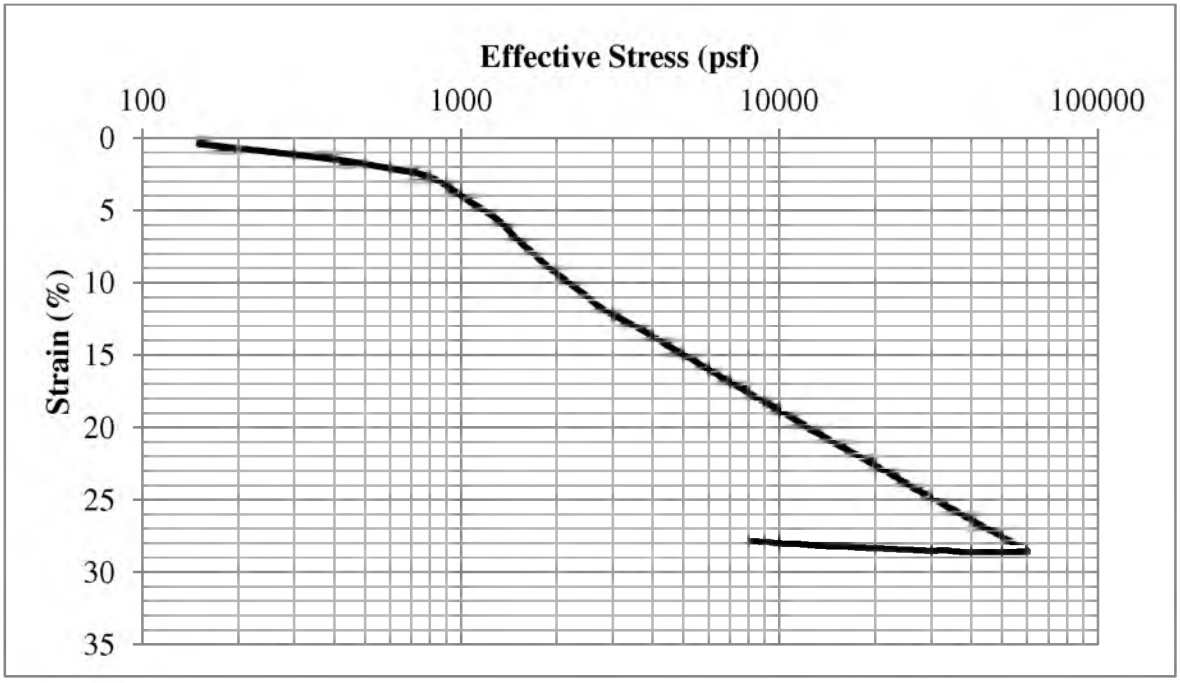

Figure A-4. Stress-strain results from constant rate of strain test at a depth of 39.75 ft below the original ground surface.

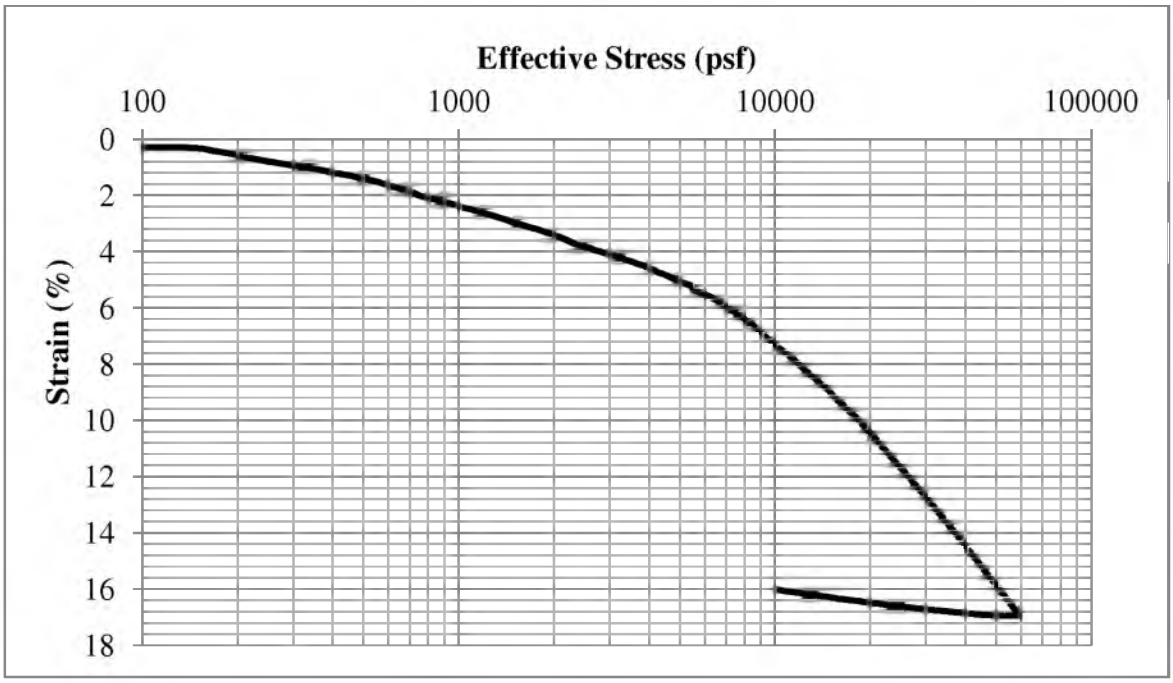

Figure A-5. Stress-strain results from constant rate of Strain test at a depth of 55.5 ft below the original ground surface.

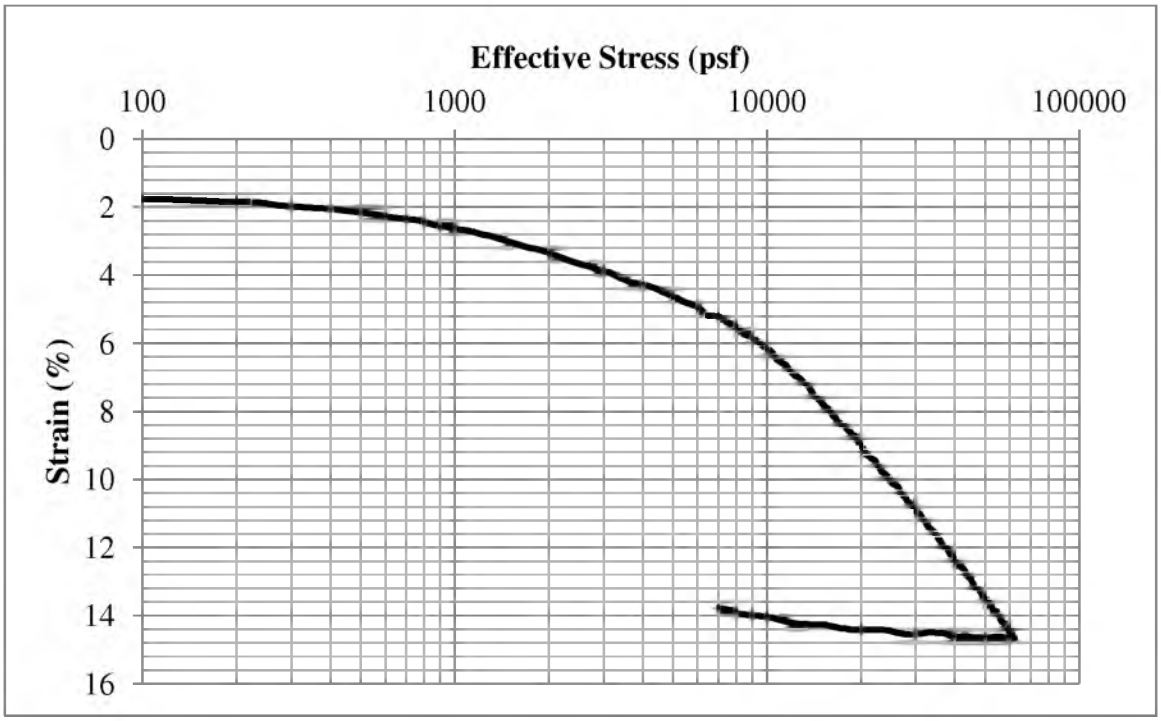

Figure A-6. Stress-strain results from constant rate of strain test at a depth of 60.5 ft below the original ground surface.

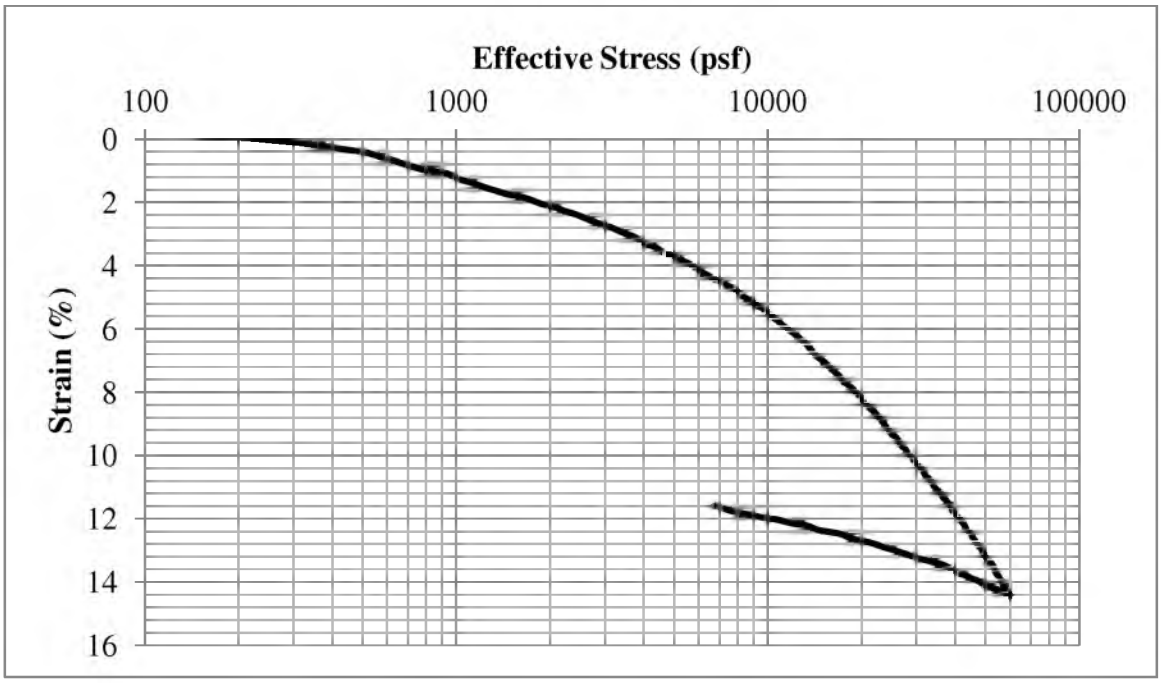

Figure A-7. Stress-strain results from constant rate of strain test at a depth of 65.5 ft below the original ground surface.

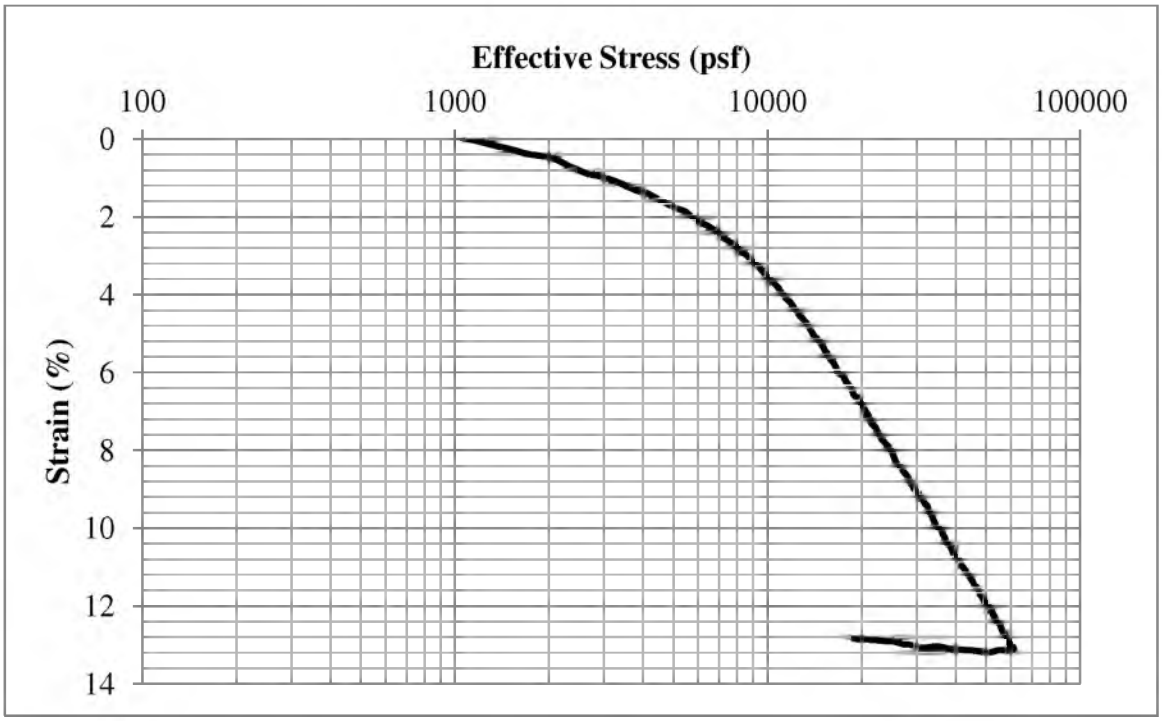

Figure A-8. Stress-strain results from constant rate of strain test at a depth of 70.375 ft below the original ground surface.

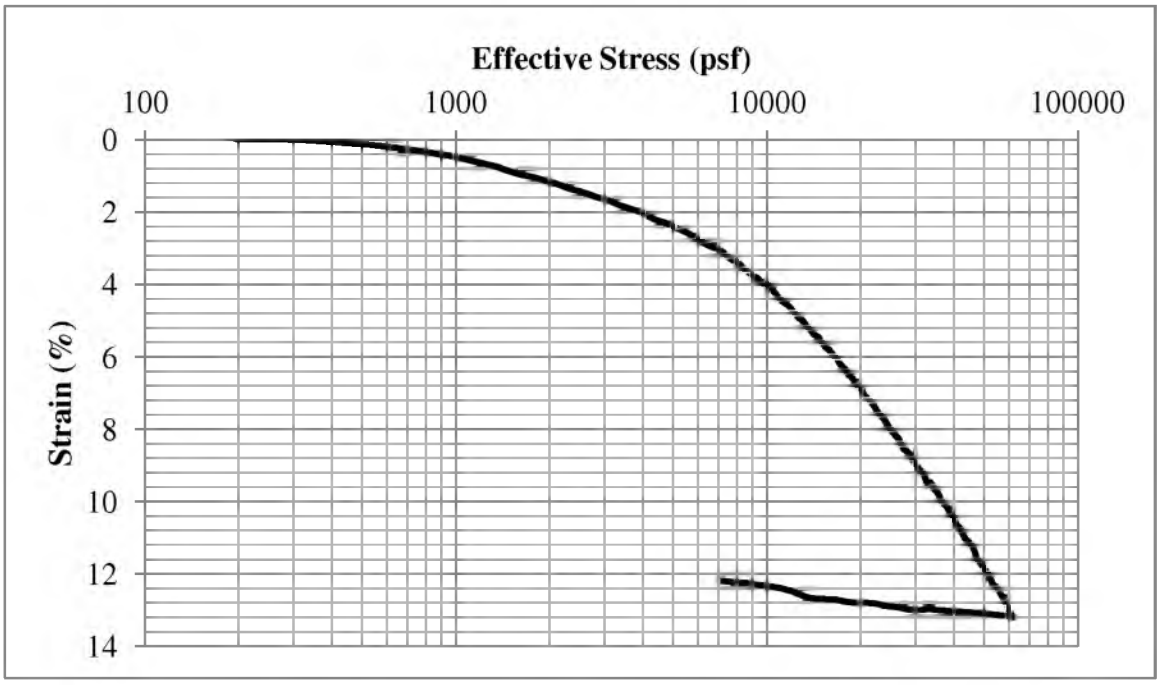

Figure A-9. Stress-strain results from constant rate of strain test at a depth of 75.6 ft below the original ground surface.

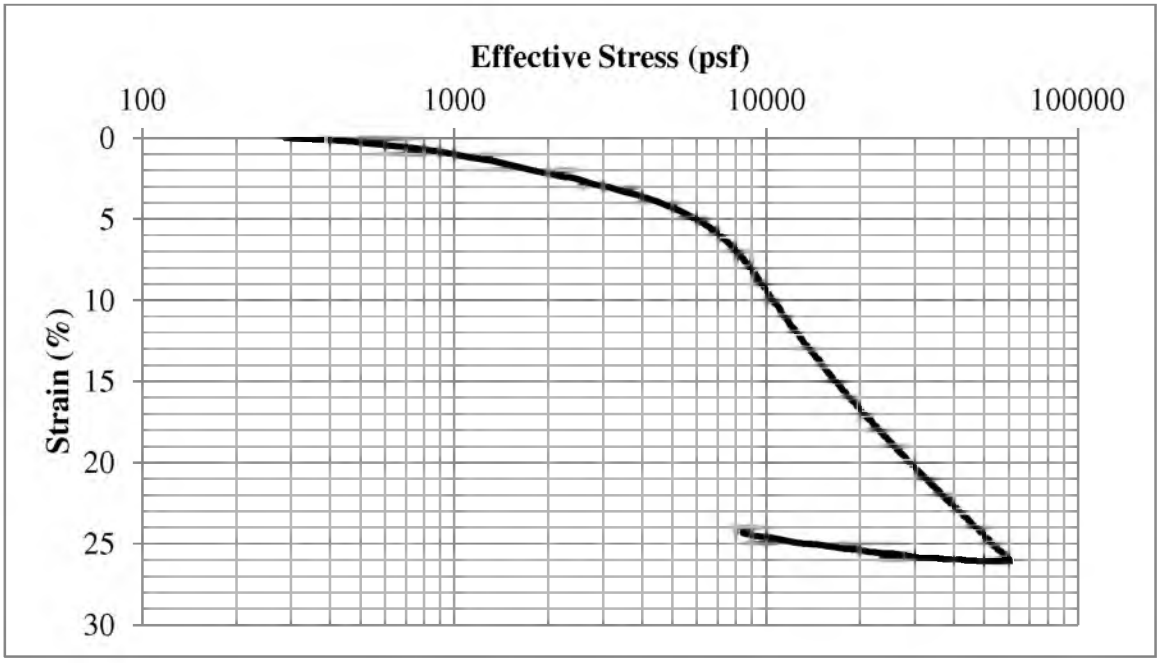

Figure A-10. Stress-strain results from constant rate of strain test at a depth of 80.5 ft below the original ground surface.

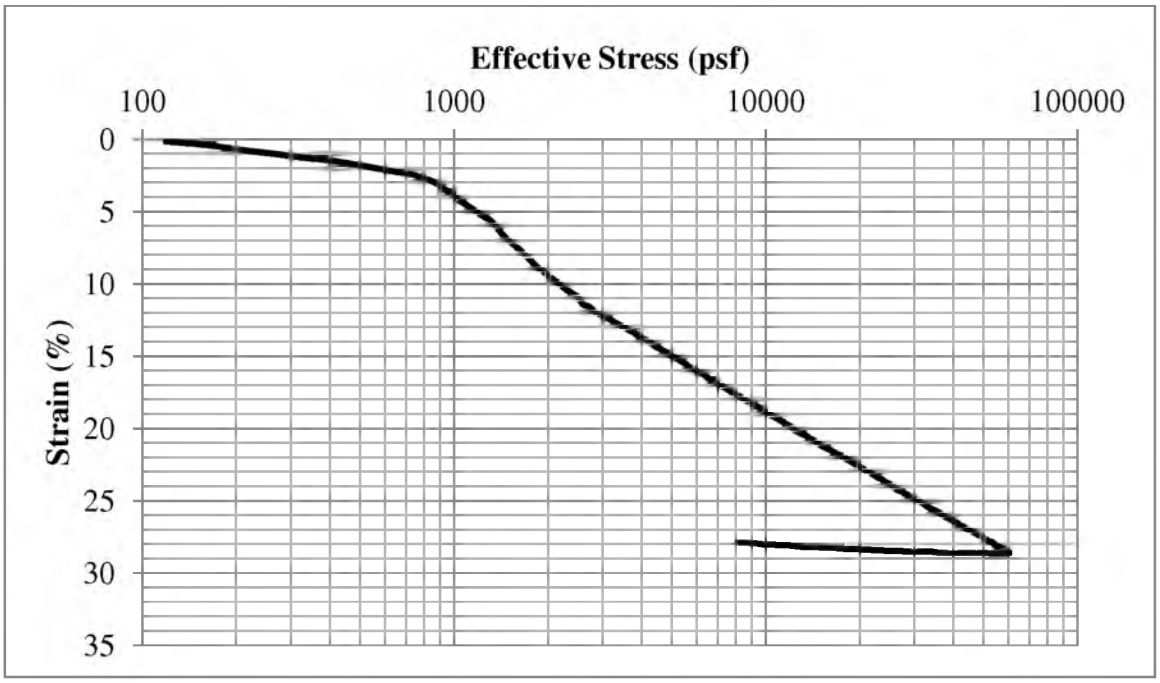

Figure A-11. Stress-strain results from constant rate of strain test at a depth of 85.33 ft below the original ground surface.

APPENDIX B

PLOTS DEVELOPED FOR REGRESSION EQUATIONS

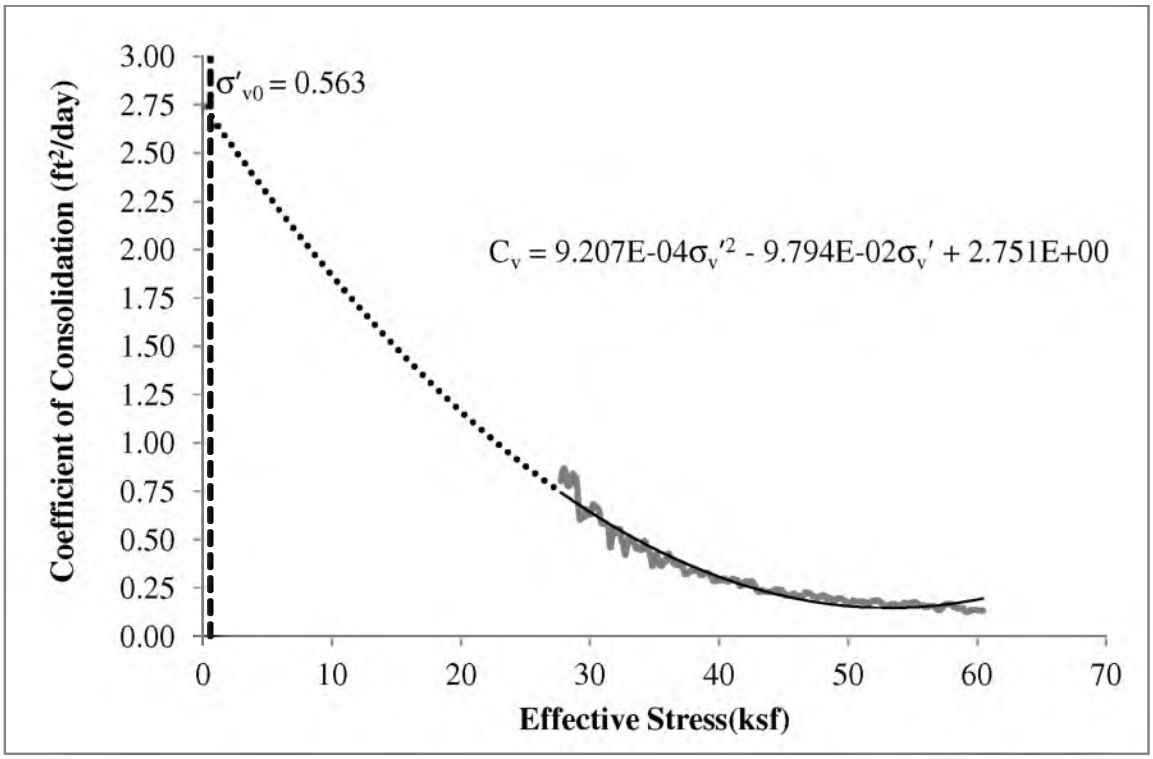

Figure B-1. Regression plot for determining C_v with effective stress at 5 ft.

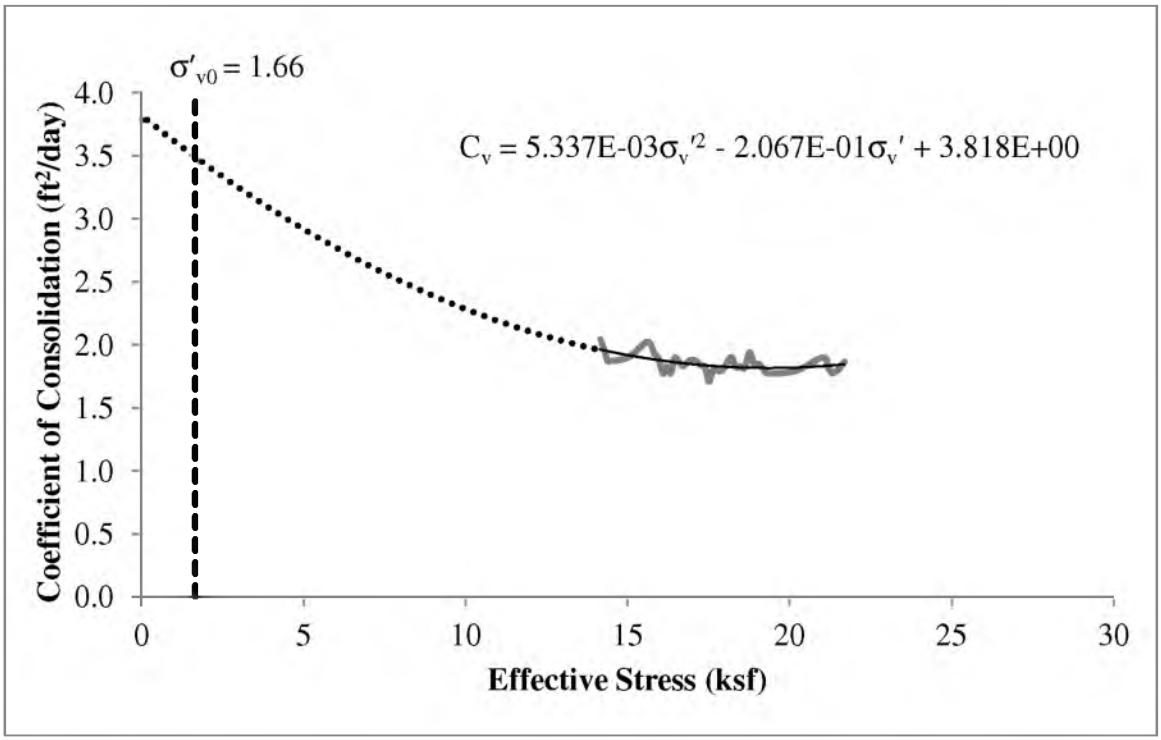

Figure B-2. Regression plot for determining C_v with effective stress at 16.5 ft.

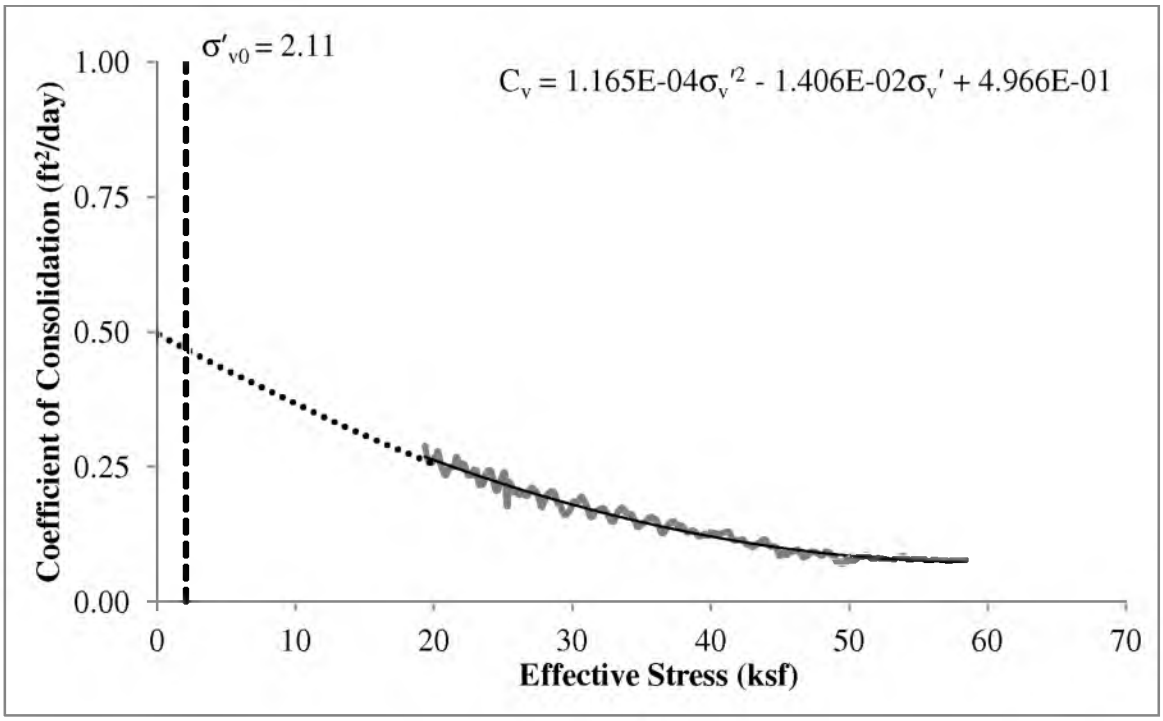

Figure B-3. Regression plot for determining C_v with effective stress at 30.5 ft.

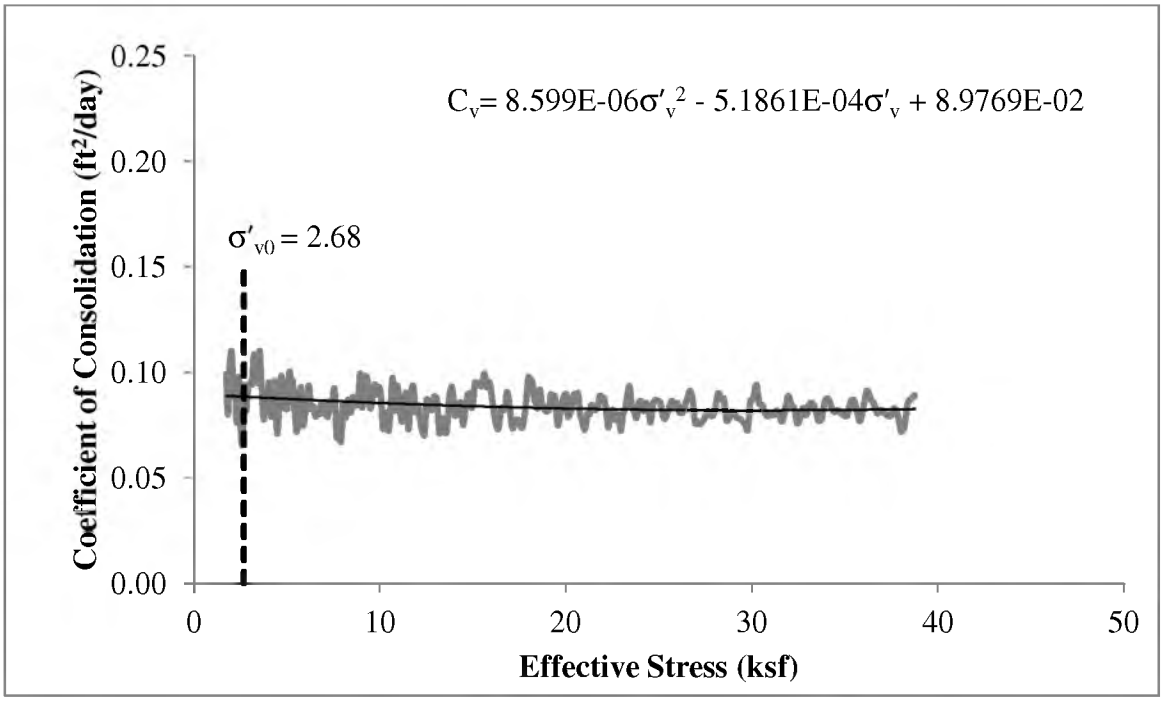

Figure B-4. Regression plot for determining C_v with effective stress at 39.75 ft.

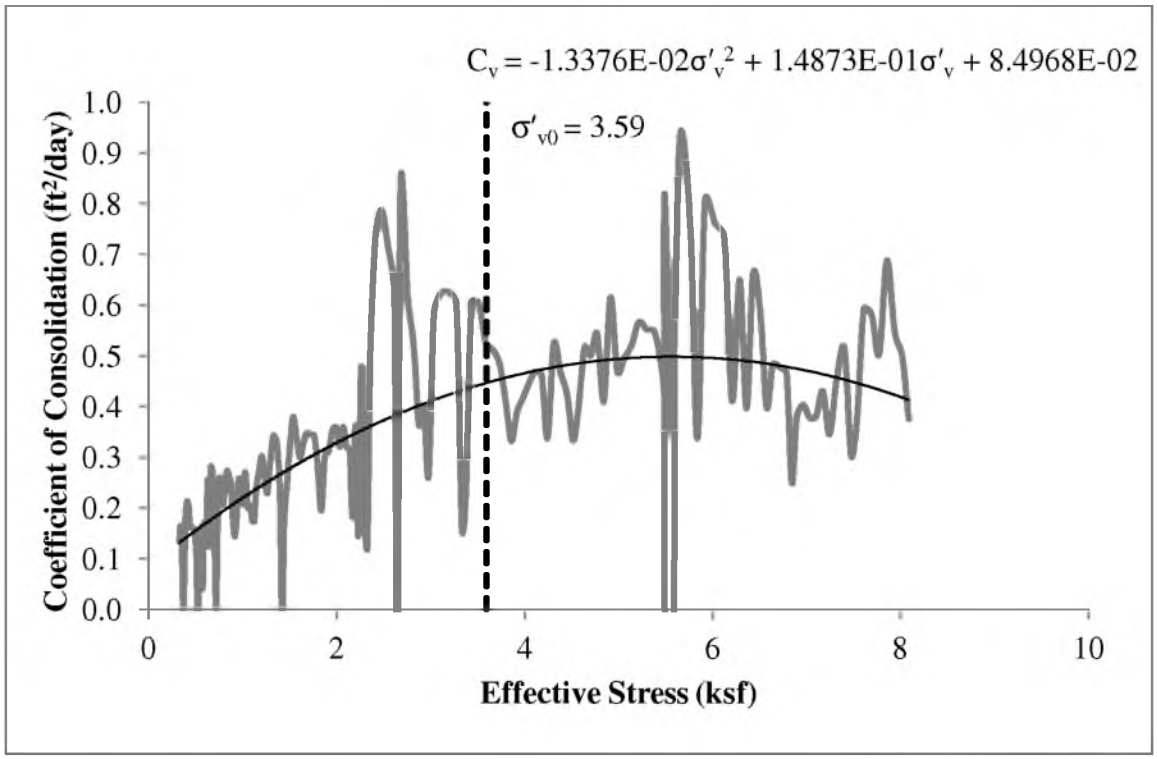

Figure B-5. Regression plot for determining C_v with effective stress at 55.5 ft.

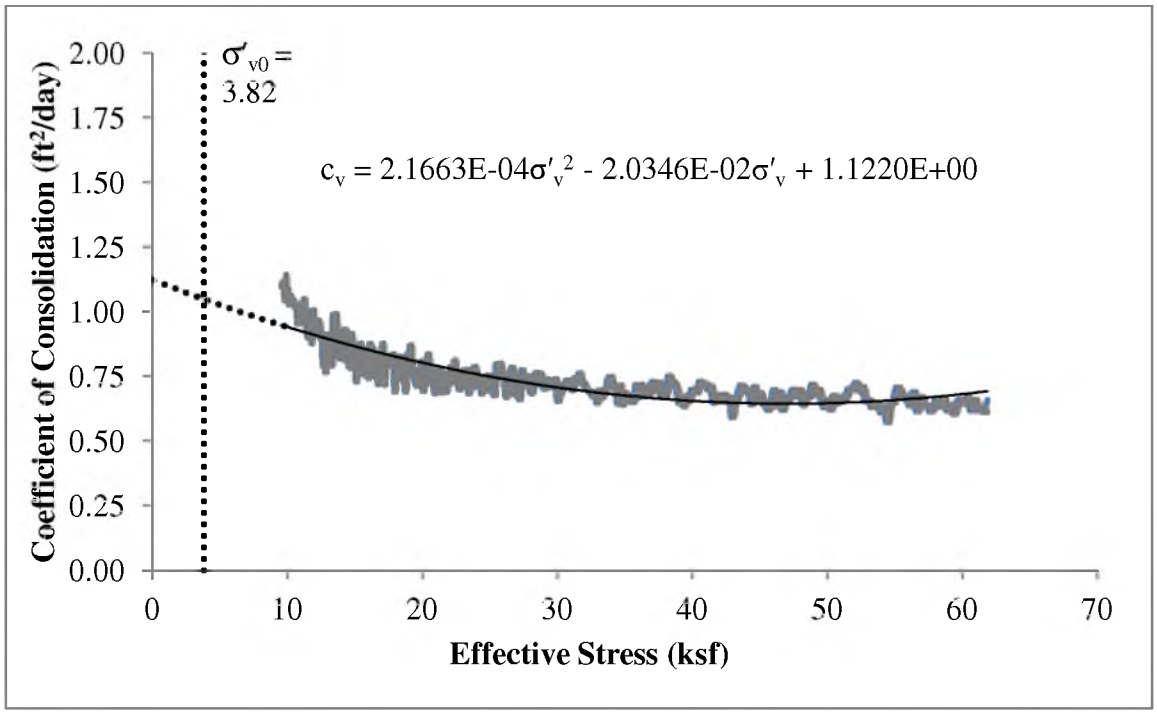

Figure B-6. Regression plot for determining C_v with effective stress at 60.5 ft.

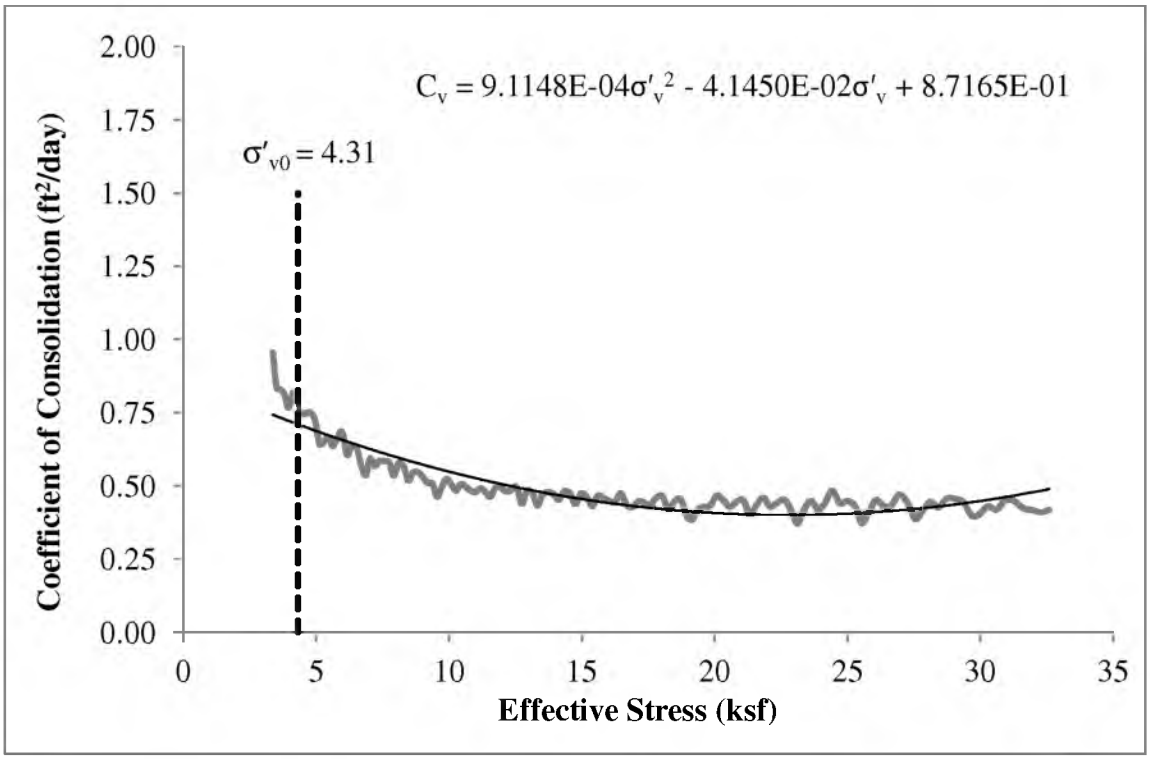

Figure B-7. Regression plot for determining C_v with effective stress at 70.4 ft.

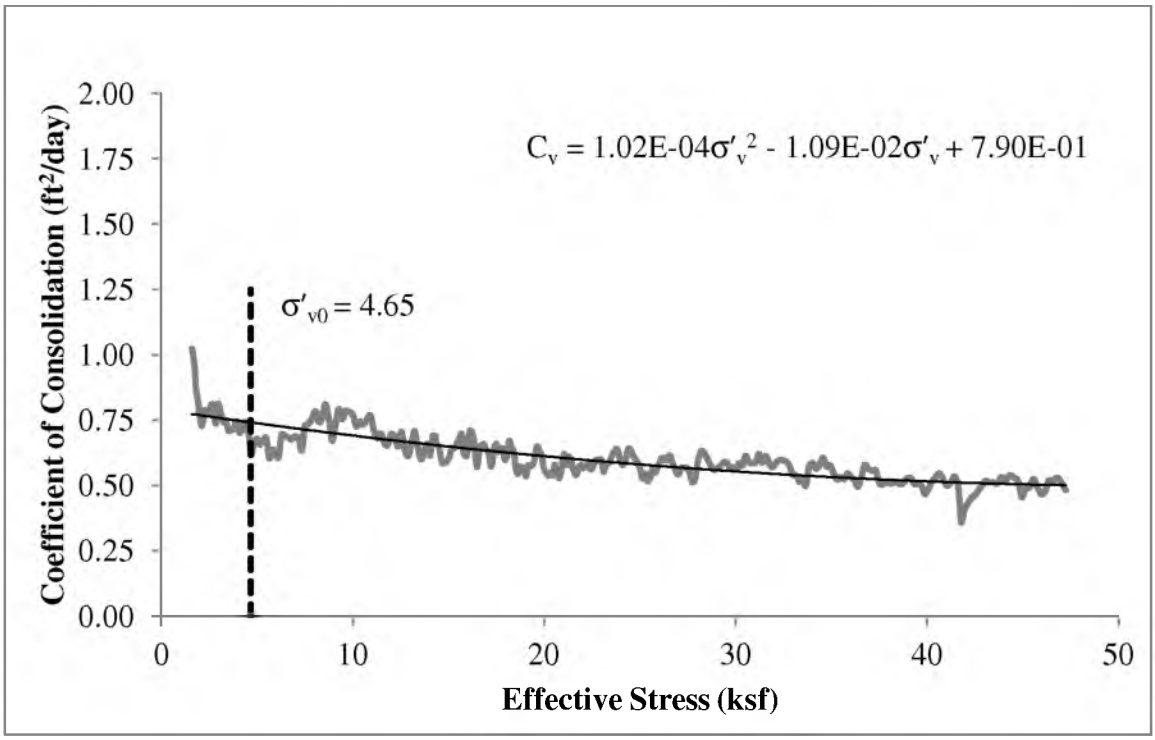

Figure B-8. Regression plot for determining C_v with effective stress at 75.6 ft.

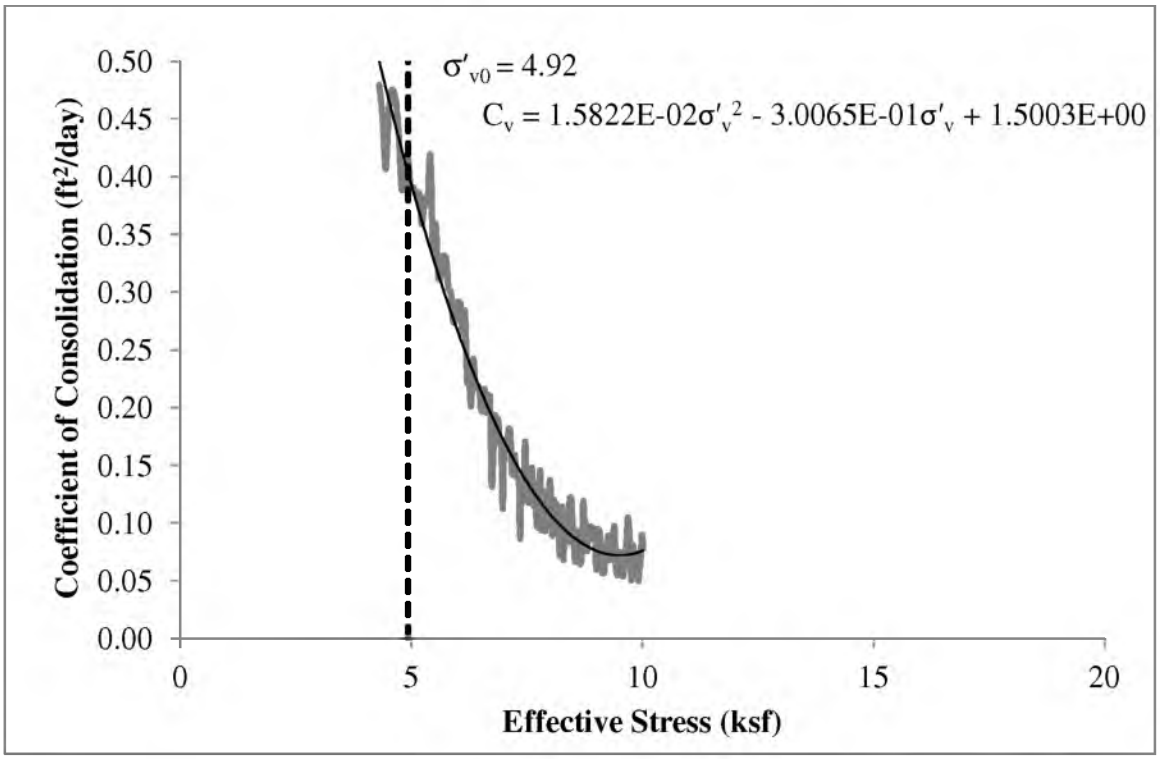

Figure B-9. Regression plot for determining C_v with effective stress at 80.5 ft.

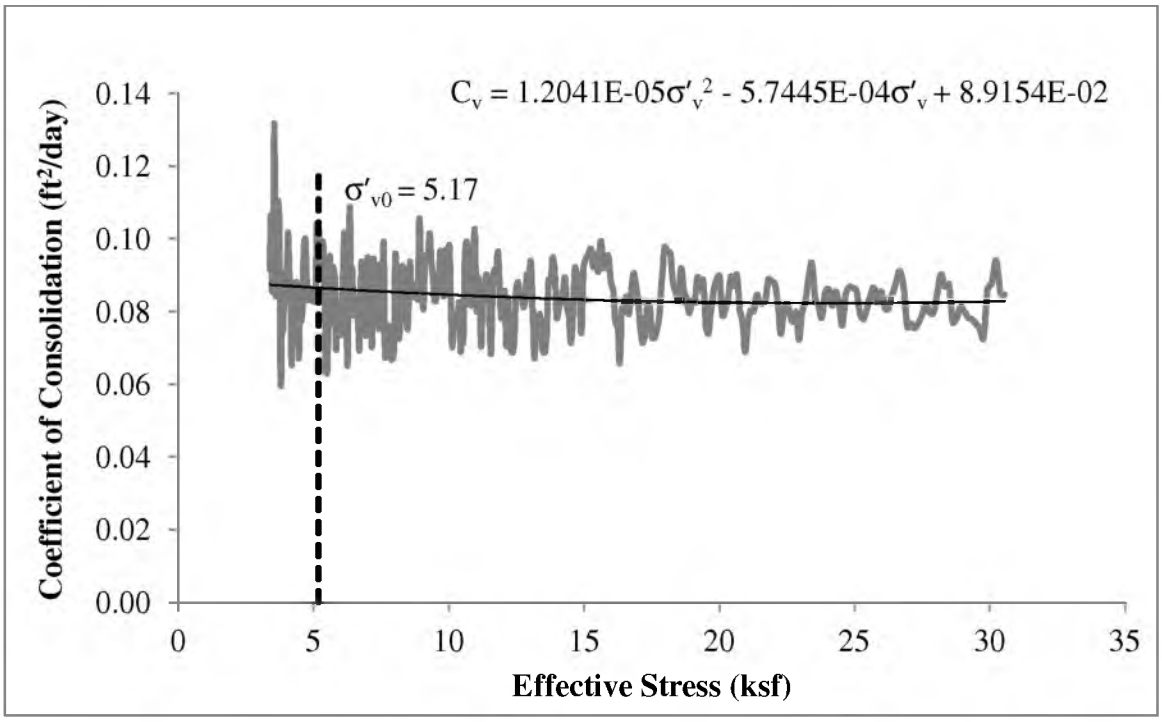

Figure B-10. Regression plot for determining C_v with effective stress at 85.3 ft.

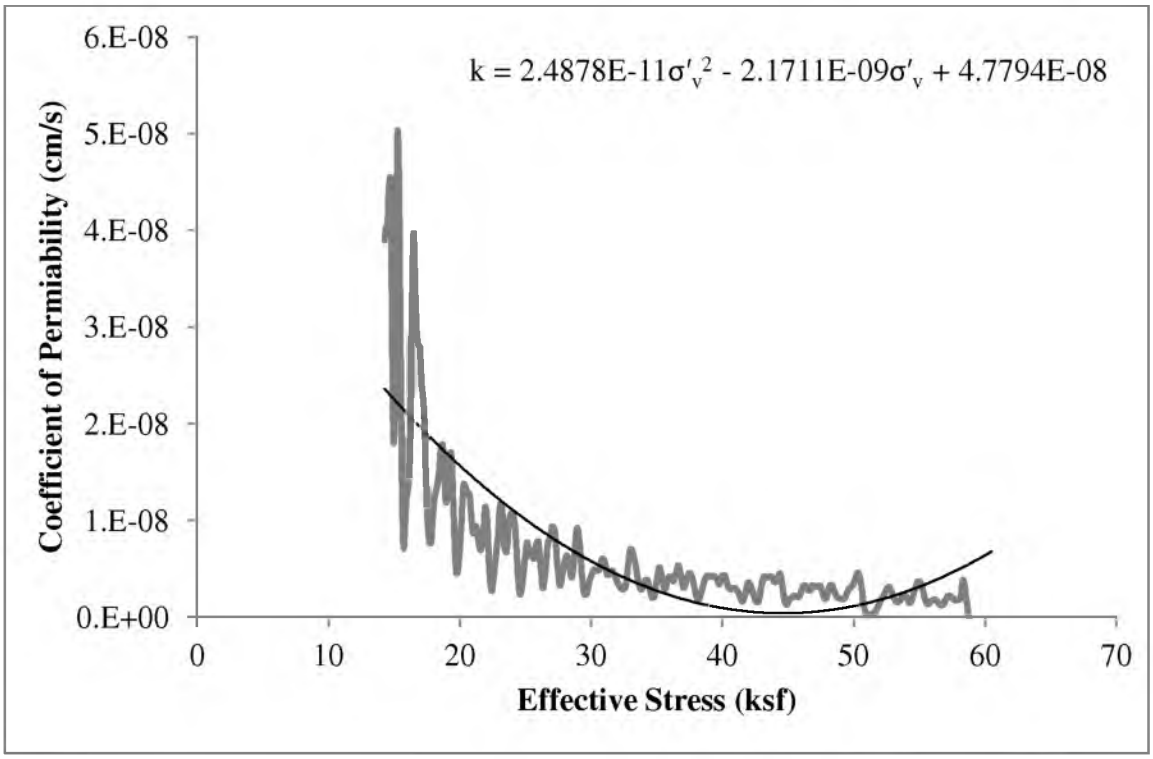

Figure B-11. Regression plot for determining *k* with effective stress at 30.5 ft.

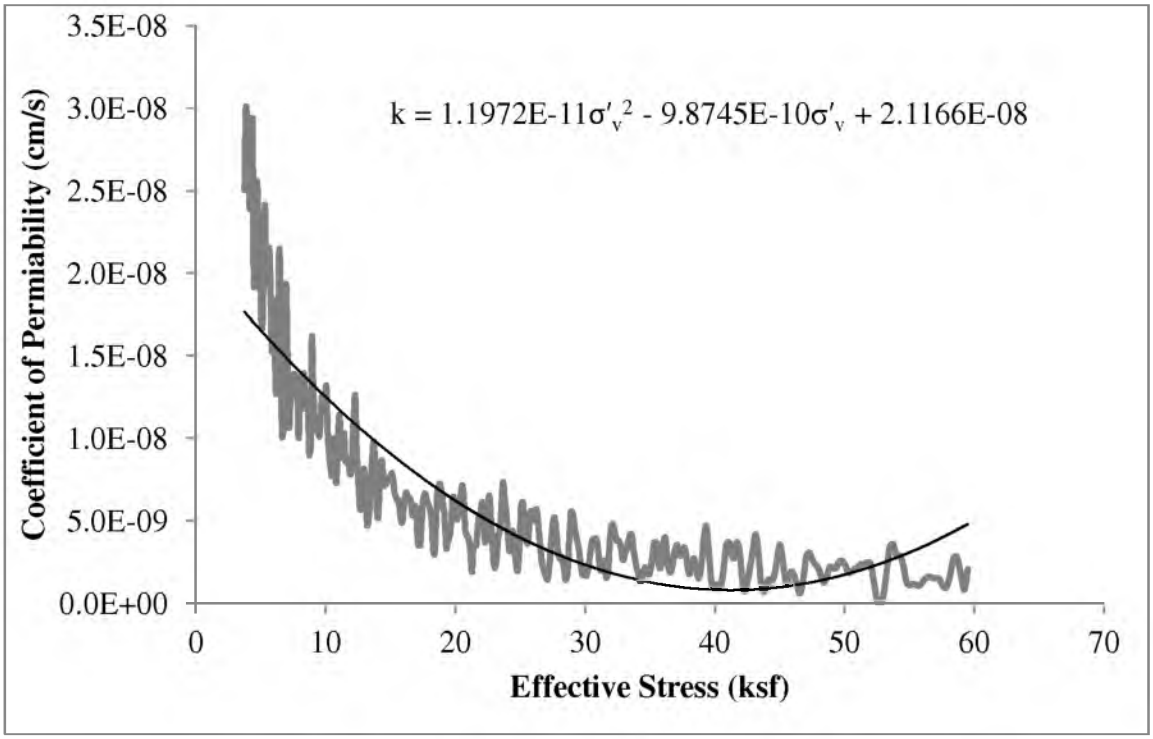

Figure B-12. Regression plot for determining *k* with effective stress at 39.75 ft.

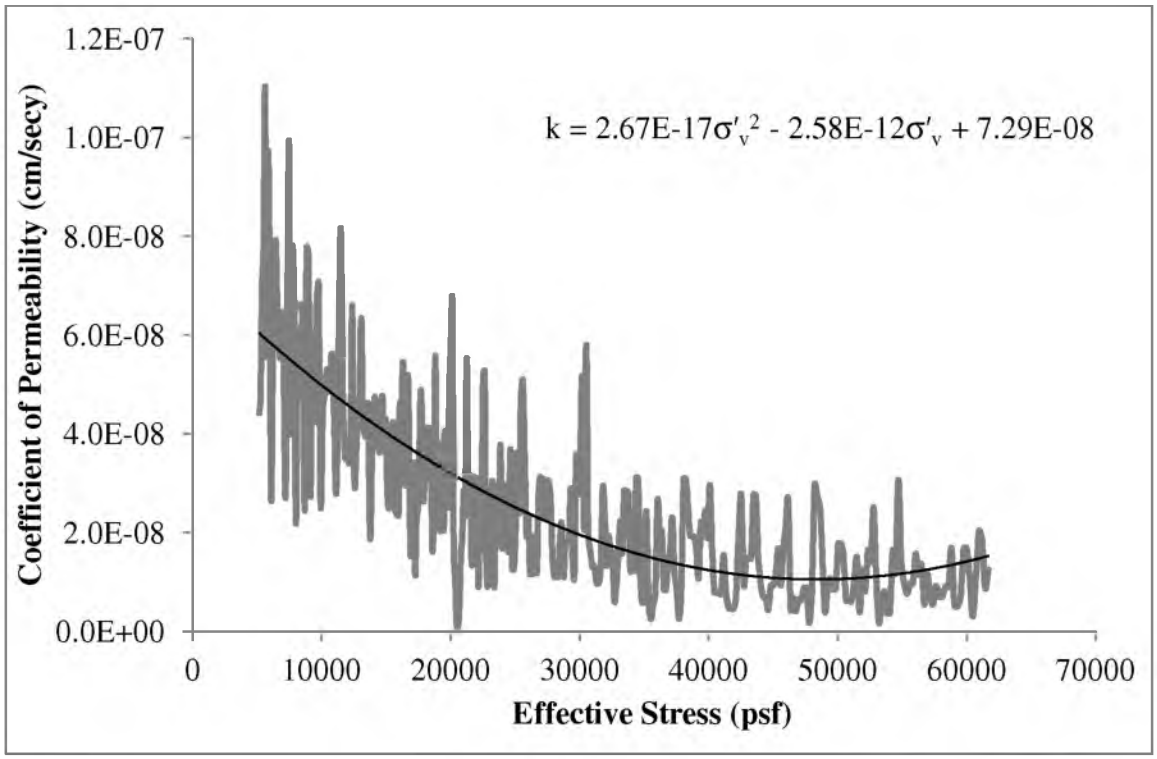

Figure B-13. Regression plot for determining *k* with effective stress at 55.5 ft.

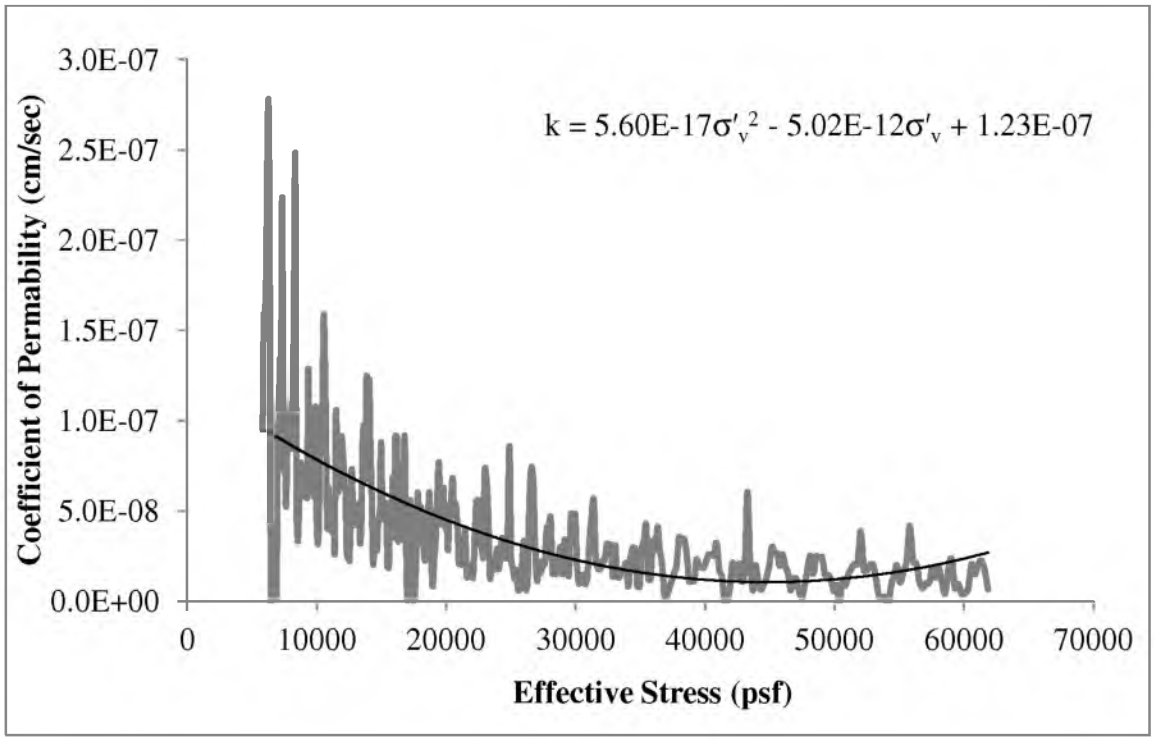

Figure B-14. Regression plot for determining *k* with effective stress at 60.5 ft.

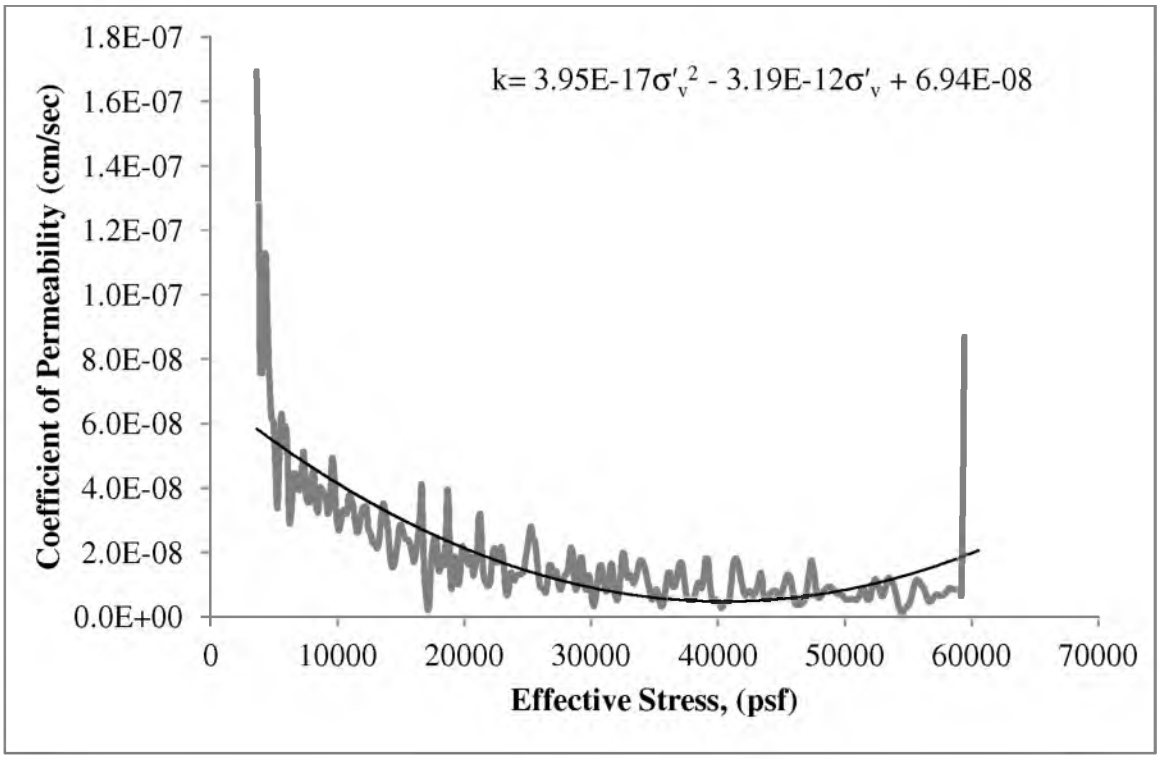

Figure B-15. Regression plot for determining *k* with effective stress at 70.4 ft.

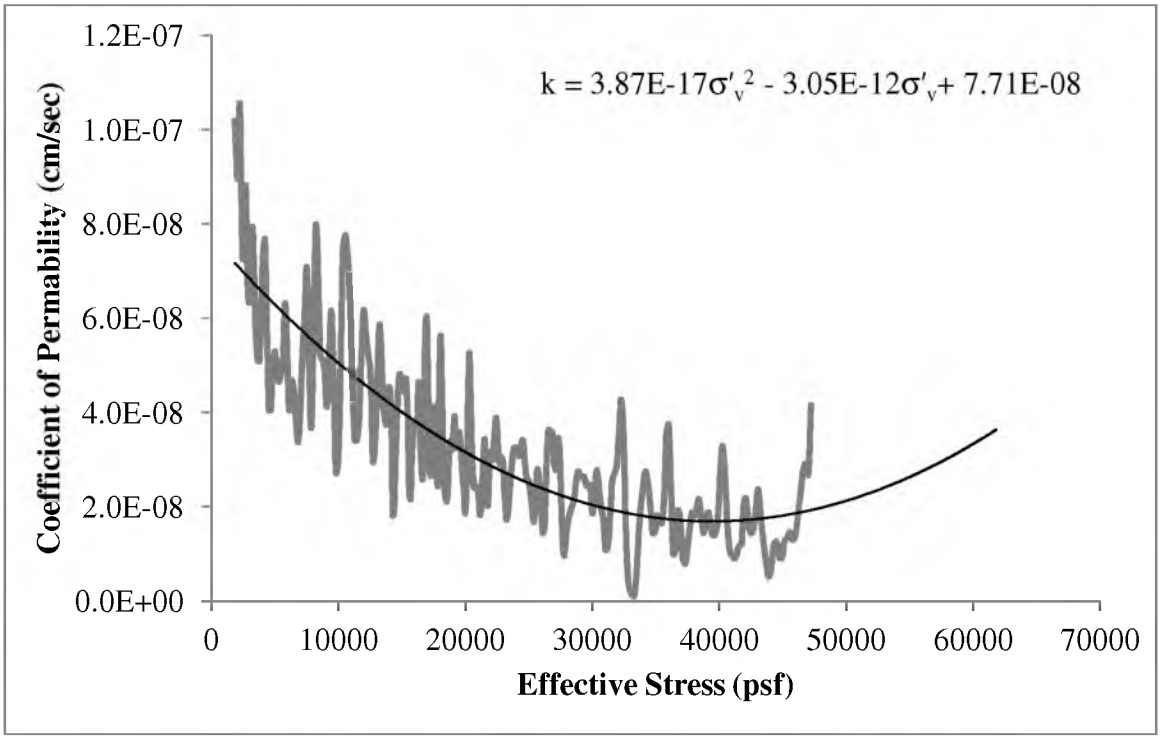

Figure B-16. Regression plot for determining *k* with effective stress at 75.6 ft.

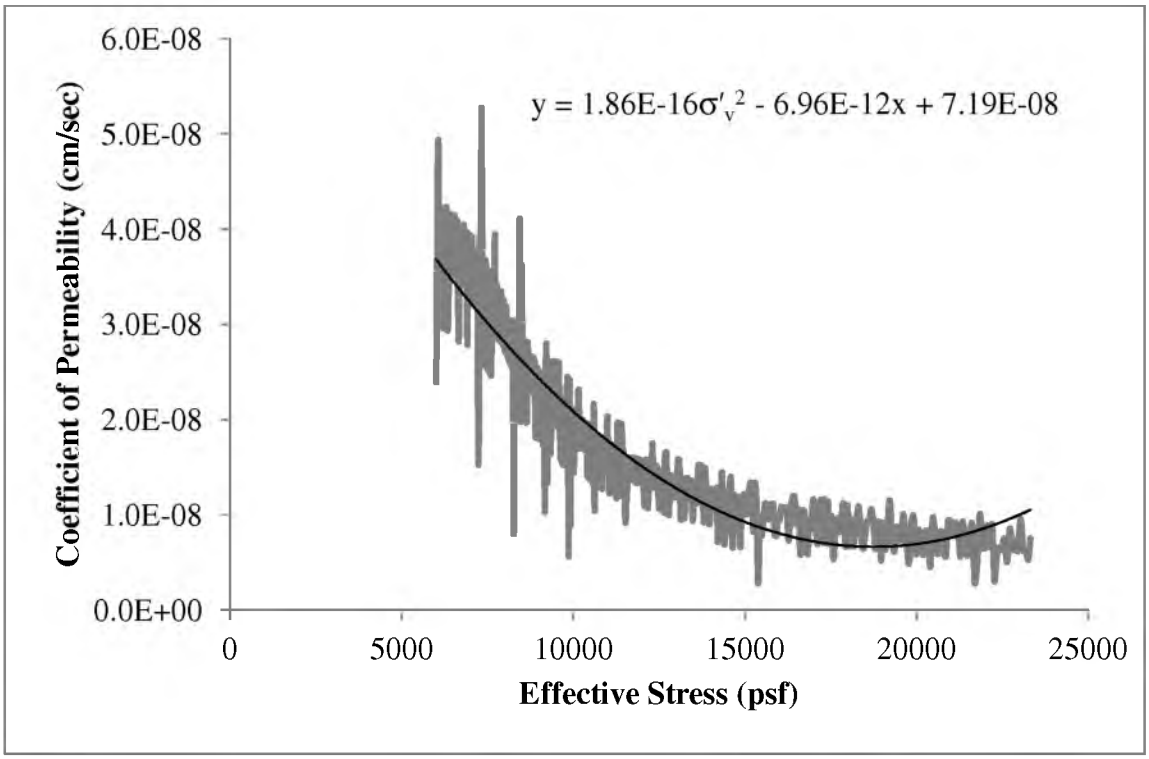

Figure B-17. Regression plot for determining *k* with effective stress at 80.5 ft.

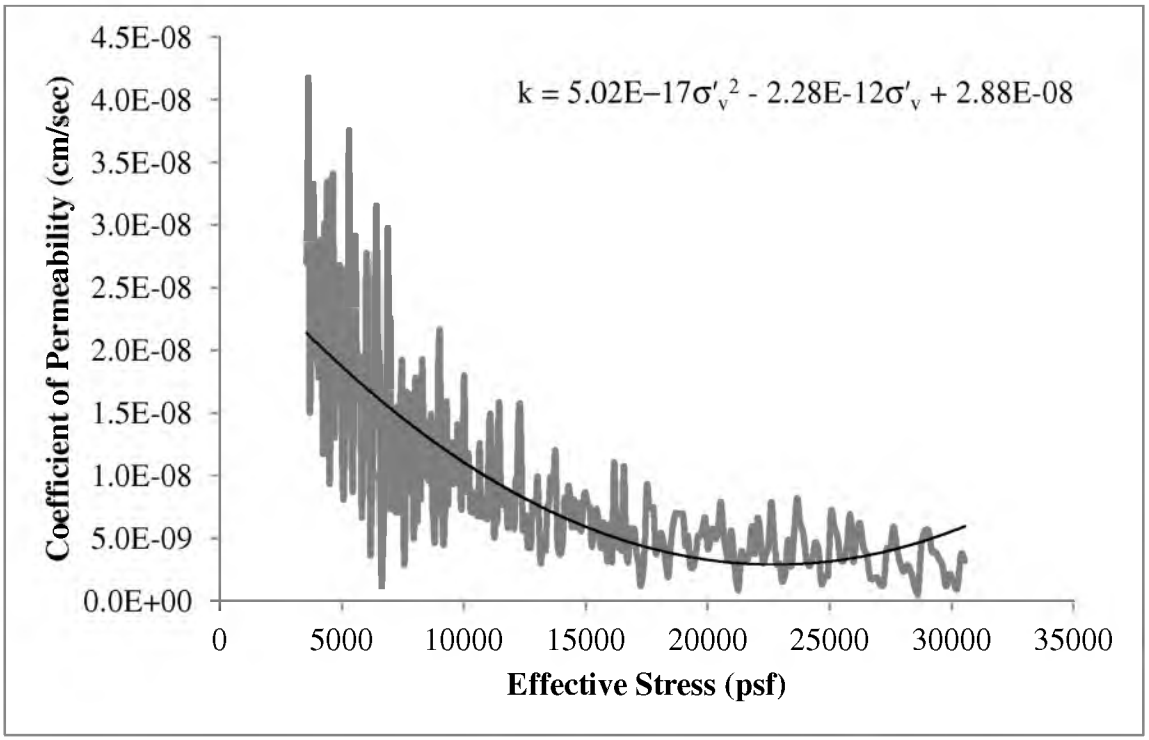

Figure B-18. Regression plot for determining *k* with effective stress at 85.3 ft.

APPENDIX C

SAMPLE CALCULATIONS FOR EXCESS PORE PRESSURE AND PRIMARY CONSOLIDATION SETTLEMENT

C.1 Calculation of Excess Pore Pressure

Equations were derived and presented in Section 2.4 to predict excess pore pressure using Terzaghi's method and Davis and Raymond's method in conjunction with the finite difference technique. Sample calculations of excess pore pressure at one selected depth are provided in Section C.1.1 and Section C.1.2 using the finite difference equations developed for both Terzaghi's method and Raymond and Davis' method. At the end of Section C.1.3, an example calculation is provided for excess pore pressure along the interface of two sublayers with different values of C_v. In the next section of this appendix, sample calculations for primary consolidation settlement of one sublayer are presented based in part on the values of excess pore pressure calculated in this section.

C.1.1 Excess Pore Pressure Using Terzaghi's Method

Excess pore pressure will be calculated using the finite difference solution to Terzaghi's equation for a time t = 100 days after embankment construction began at a depth z = 33.25 ft below the original ground surface. From Eq. 2-13 in Section 2.4:

$$u_{i,j+1} = \alpha u_{i-1,j} + (1 - 2\alpha)u_{i,j} + \alpha u_{i+1,j} \tag{2-13}$$

where the coefficient α is defined in the following equation:

$$\alpha = \frac{C_v \Delta t}{(\Delta z)^2} \tag{2-14}$$

α must be less than 0.5 for stability to occur and the calculated value of $u_{i,j+1}$ is most accurate when α= 1/6. Based on the value of C_v for the soil at the depth of interest, values of time step Δt and depth increment Δz must be carefully selected so that α is as close as possible to 1/6 within the constraints of the problem be solved.

Davis and Raymond's equation is defined as:

$$-C_v\left[\frac{\partial^2 u}{\partial z^2}-\left(\frac{1}{\sigma'}\right)^2 * \frac{\partial u}{\partial z} * \left(\gamma_{sat}-\frac{\partial u}{\partial z}\right)\right]=\frac{\partial u}{\partial t} \tag{2-7}$$

Davis and Raymond's one dimensional consolidation theory for excess pore pressure prediction was solved using Eq. 2-19 through 2-22 previously defined in Section 2.4.2 and shown below.

$$\frac{\partial^2 u}{\partial z^2}=\frac{u_{i-1,j}-2u_{i-1,j}+u_{i+1,j}}{\Delta z^2} \tag{2-19}$$

$$\frac{\partial u}{\partial z}=\frac{u_{i+1,j}-u_{i-1,j}}{2\Delta z} \tag{2-20}$$

$$\frac{\partial u}{\partial t}=\frac{u_{i+1,j}-u_{i-1,j}}{\Delta t} \tag{2-21}$$

$$\sigma'_{i,j}=(\sigma'_{ss})_{i,j}-u_{i,j} \tag{2-22}$$

Excess pore pressure from Davis and Raymond's one dimensional consolidation theory was defined as Eq. 2-25.

$$u_{i,j+1} = C_v \cdot \Delta t \left[\frac{u_{i-1,j} - 2u_{i-1,j} + u_{i+1,j}}{\Delta z^2} - \frac{1}{(\sigma'_{ss})_{i,j} - u_{i,j}} \cdot \left(\frac{u_{i+1,j} - u_{i-1,j}}{2\Delta z} \right) \cdot \left(\gamma_{sat} + \frac{u_{i+1,j} - u_{i-1,j}}{2\Delta z} \right) + u_{i,j} \right] \quad \text{.....(2-25)}$$

Along the interface of two cohesive layers (valid for both Terzaghi's method and Davis and Raymond's method):

$$u_{i,j} = \frac{1}{1+\beta} * u_{i-1,j} + \frac{\beta}{1+\beta} * u_{i+1,j} \quad (2\text{-}17)$$

$$\beta = \frac{k_2 \Delta z_1}{k_1 \Delta z_2} \quad (2\text{-}18)$$

Geotechnical Input Parameters:

z_{gwt} = depth of groundwater table relative to the original surface = 4.0 ft

γ_w = unit weight of water = 62.4 pcf (assumed)

Total unit weight and thickness of all layers down to the desired depth:

γ_1 = 126.90 psf, t_1 = 3 ft

γ_2 = 112.78 psf, t_2 = 5 ft

γ_3 = 126.90 psf, t_3 = 6 ft

γ_4 = 125.15 psf, t_4 = 5 ft

$\gamma_5 = 124.56$ psf, $t_5 = 11.25$ ft

$\gamma_6 = 127.77$ psf, $t_6 = 3$ ft

Calculated effective overburden stress at node i, depth of 33.25 ft, prior to construction of the embankment:

$$\sigma_{v,i,j=0} = \sum_{k=1}^{k=n} \gamma_k t_k = (126.90)(3) + (112.78)(5) + (126.90)(6) + (125.15)(5) +$$

$$(124.56)(11.25) + (127.77)(3) = 4{,}116.36 \text{ psf}$$

Assuming that the pore water was in equilibrium at the time construction of the embankment began:

$u_{i,j=0} = u_{ss,I} = \gamma_w(z_i - z_{gwt}) = 62.4(33.25\text{-}4.0) = 1{,}825.20$ psf

$\sigma'_{v,i,j=0} = \sigma_{v,i,j=0} - u_{i,j=0} = 4116.36 - 1825.20 = 2{,}291.16$ psf

The excess pore water pressures for the three nodes above, at, and below the desired depth for the current time $j = 99.75$ days:

$u_{i\text{-}1,j} = 427.74$ psf ($z = 32.25$ft)

$u_{i,j} = 586.00$ psf ($z = 33.25$ ft)

$u_{i+1,j} = 696.25$ psf ($z = 34.25$ ft)

Δt_i = time step from time $j = 99.75$ days to $j+1 = 100$ days = 0.25 day

Δz_i = depth increment for this cohesive layer = 1.0 ft

$\sigma'_{v,i,j} = 5.70354$ ksf

$$C_{v,i,j} = (1.17 \times 10^{-4})(5.70354)^2 - (1.41 \times 10^{-2})(5.70354) + (4.97 \times 10^{-1}) = 0.420 \frac{ft^2}{day}$$

$$\alpha = \frac{C_v \Delta t}{\Delta z^2} = \frac{(0.420)(0.25)}{1^2} = 0.105$$

Terzaghi's equation is based on the assumption that total vertical stress acting on the soil does not change. In this case the total vertical stress has changed as some surcharge was removed. Therefore, Eq. 2-13 must be modified to account for the effect of this change in total vertical stress on the excess pore pressure. The change in pore pressure as a function of the change in total vertical stress was given previously as Eq. 6-12:

$$C = \frac{\Delta u}{\Delta \sigma_v} \tag{6-12}$$

which can be rearranged to solve for Δu as follows:

$$\Delta u = C \cdot \Delta \sigma_v$$

Adding this component to Eq. 2-13 yields:

$$u_{i,j+1} = \alpha u_{i-1,j} + (1 - 2\alpha) u_{i,j} + \alpha u_{i+1,j} + C \cdot \Delta \sigma_v$$

The value of change in total vertical stress for this time increment was obtained from readings of the pressure plates as:

$$\Delta \sigma_{v,j \to j+1} = -5.24 \text{psf}$$

Assuming that $C = 1$, the excess pore pressure at the end of the time step is calculated as:

$$u_{i,j+1} = \alpha u_{i-1,j} + (1 - 2\alpha) u_{i,j} + \alpha u_{i+1,j} + \Delta \sigma_v$$

$u_{i,j+1}$ = (0.105)(427.74)+(1-2(0.105))(586.00)+(0.105)(696.25)+(-5.24) = 575.72 psf

C.1.2 Excess Pore Pressure Using Davis and Raymond's Method

Excess pore pressure will be calculated using the finite difference solution to Raymond and Davis' equation for the same time and depth for the previous calculation based on Terzhagi's method. From Eq. 2-25 in Section 2.4.2:

$$u_{i,j+1} = C_v \cdot \Delta t \left[\frac{u_{i-1,j} - 2u_{i-1,j} + u_{i+1,j}}{\Delta z^2} - \frac{1}{(\sigma'_{ss})_{i,j} - u_{i,j}} \cdot \left(\frac{u_{i+1,j} - u_{i-1,j}}{2\Delta z} \right) \cdot \left(\gamma_{sat} + \frac{u_{i+1,j} - u_{i-1,j}}{2\Delta z} \right) + u_{i,j} \right] \quad (2\text{-}25)$$

The steady state effective vertical stress is given by the following equation:

$$\sigma'_{ss,i,j} = \sigma'_{v,i,j=0} + q_{i,j}$$

where $q_{i,j}$ is the increase in total vertical stress at depth i and time j from constructing the embankment and is found from readings of the pressure plates.

Geotechnical input parameters: all geotechnical parameters are the same as the geotechnical parameters shown previously with the addition of the saturated unit weight (γ_{sat}) and the embankment load (q) in the excess pore pressure calculation using Terzaghi's one-dimensional consolidation theory

γ_{sat} = 127.77 psf

q = 3602.79 psf

Calculated effective overburden stress at node i, depth of 33.25 ft, prior to construction of the embankment is the same as previously calculated:

$$\sigma_{v,i,j=0} = \sum_{k=1}^{k=n} \gamma_k t_k = (126.90)(3) + (112.78)(5) + (126.90)(6) + (125.15)(5) +$$

(124.56)(11.25) + (127.77)(3) = 4,116.36 psf

Assuming that the pore water was in equilibrium at the time construction of the embankment began:

$u_{i,j=0} = u_{ss,I} = \gamma_w(z_i - z_{gwt})$ = 62.4(33.25-4.0) = 1,825.20 psf

$\sigma'_{v,i,j=0} = \sigma_{v,i,j=0} - u_{i,j=0}$ = 4116.36 -1825.20 = 2,291.16 psf

The excess pore water pressures for the three nodes above, at, and below the desired depth for the current time j = 99.75 days:

$u_{i-1,j}$ = 1,161.78 psf (z = 32.25ft)

$u_{i,j}$ = 1,627.51 psf (z = 33.25 ft)

$u_{i+1,j}$ = 2,022.62 psf (z = 34.25 ft)

Δt_i = time step from time j = 99.75 days to $j+1$ = 100 days = 0.25 day

Δz_i = depth increment for this cohesive layer = 1.0 ft

The steady state effective stress for the desired depth of 33.25 ft:

$\sigma'_{ss,i,j} = q + \sigma'_{v,i,j=0}$ = 3,602.79+2,291.16 = 5,893.21 psf

$\sigma'_{v,i,j}$ = 4,668.68 psf = 4.66868 ks

$$C_{v,i,j} = (1.17 \times 10^{-4})(4.66868)^2 - (1.41 \times 10^{-2})(4.66868) + (4.97 \times 10^{-1}) = 0.4338 \frac{ft^2}{day}$$

Davis and Raymond's equation is based on the assumption that total vertical stress acting on the soil does not change. In this case the total vertical stress has changed as some surcharge was removed. Therefore, Eq. 2-13 must be modified to account for the effect of this change in total vertical stress on the excess pore pressure. The change in pore pressure as a function of the change in total vertical stress was given previously as Eq. 6-12:

$$C = \frac{\Delta u}{\Delta \sigma_v} \tag{6-12}$$

which can be rearranged to solve for Δu as follows:

$$\Delta u = C \cdot \Delta \sigma_v$$

Adding this component to Eq. 2-23 yields:

$$u_{i,j+1} = C_v \cdot \Delta t \left[\frac{u_{i-1,j} - 2u_{i-1,j} + u_{i+1,j}}{\Delta z^2} - \frac{1}{(\sigma'_{ss})_{i,j} - u_{i,j}} \cdot \left(\frac{u_{i+1,j} - u_{i-1,j}}{2\Delta z} \right) \cdot \left(\gamma_{sat} + \frac{u_{i+1,j} - u_{i-1,j}}{2\Delta z} \right) + \Delta u \right]$$

The value of change in total vertical stress for this time increment was obtained from readings of the pressure plates as:

$$\Delta \sigma_{v,j \to j+1} = -5.24 \text{ psf}$$

Assuming that $C = 1$, the excess pore pressure at the end of the time step is calculated as:

$$u_{i,j+1} = C_v \cdot \Delta t \left[\frac{u_{i-1,j} - 2u_{i-1,j} + u_{i+1,j}}{\Delta z^2} - \frac{1}{(\sigma'_{ss})_{i,j} - u_{i,j}} \cdot \left(\frac{u_{i+1,j} - u_{i-1,j}}{2\Delta z} \right) \cdot \left(\gamma_{sat} + \frac{u_{i+1,j} - u_{i-1,j}}{2\Delta z} \right) + (C * \Delta \sigma_v) \right]$$

Incorporating the additional change in pore pressure resulting from the change in total stress that occurred during the time step and assuming that C = 1, the excess pore pressure at the end of the time step is calculated as:

$$u_{i,j+1} = 0.4338 * 0.25\left[\frac{1{,}161.78 - 2(1{,}627.51) + 2{,}022.62}{1^2} - \frac{1}{5{,}893.21 - 1{,}627.51} \cdot \left(\frac{2{,}022.62 - 1{,}161.78}{2(1)}\right) \cdot \left(127.77 + \frac{2{,}022.62 - 1{,}161.78}{2(1)}\right) + \left(-5.24_v\right)\right]$$

$u_{i,j+1}$ = 1,617.92 psf

C.1.3 Excess Pore Pressure Along Interface of Two Sublayers with Different Values of C_v

The calculations in the previous two sections were performed at a node located along the interface of two sublayers consisting of the same soil (C_v is the same for both layers). In this section, sample calculations are provided for excess pore pressure along the interface of two different soils (C_v is different for the two adjacent sublayers). A different approach is required for this case, as described in Section 2.4.2.

The calculations shown below are for excess pore pressures along the interface of the two sublayers within Layer 5, 100 days after the embankment construction started at a depth of 37.25 ft below the original ground surface. Subscript $_1$ refers to the sublayer above the interface, and subscript $_2$ refers to the sublayer below the interface. The subscript for time is shown as $j+1$ to be consistent with the subscripts used from t = 100 days in the previous two sections.

Δz = 1 ft

Δz = 1/3 ft

The permeability for sublayers with different values for C_v were determined by developing regression models of permeability as a function of the effective stress from CRS test results.

$k_1 = 2.49\text{E-}17\,\sigma'^{\,2}_{v,i,j} - 2.17\text{E-}12\,\sigma'_{v,i,j} + 4.78\text{E-}08$

$k_1 = (2.49\text{E-}17)(5{,}797.94^2) - (2.17\text{E-}12)(5{,}797.94) + 4.78\text{E-}08 = 3.61\text{E-}08\ \frac{cm}{\text{sec}}$

$k_2 = 2.16\text{E-}17\,\sigma'^{\,2}_{v,i,j} - 1.66\text{E-}12\,\sigma'_{v,i,j} + 3.07\text{E-}08$

$k_2 = (2.16\text{E-}17)(5{,}797.94)^2 - (1.66\text{E-}12)(5{,}797.94) + 3.07\text{E-}08 = 2.18\text{E-}08\ \frac{cm}{\text{sec}}$

$$\beta = \frac{k_2 \Delta z_1}{k_1 \Delta z_2} = \frac{\left(2.18 \times 10^{-8}\right) \cdot 1}{\left(4.78 \times 10^{-8}\right) \cdot \frac{1}{3}} = 1.81$$

$u_{\text{i-1,j+1}} = 749.85$ psf

$u_{i+1,j+1} = 693.78$ psf

$\Delta\sigma_{v,j\to j+1} = -5.24$ psf

$$u_{i,j+1} = \frac{1}{1+\beta} \cdot u_{i-1,j} + \frac{\beta}{1+\beta} \cdot u_{i+1,j} + \Delta\sigma_v$$

$$u_{i,j+1} = \frac{1}{1+1.81}(749.95) + \frac{1.81}{1+1.81}(693.78) + \left(-5.24\right) = 708.49\ \text{psf}$$

C.2 Calculation of Primary Consolidation Settlement

Sample calculations using Terzaghi's method and Davis and Raymond's method for settlement at time of 100 days and in the sublayer below node i, located at a depth of 33.25 ft are presented in Section C.2.1 and C.2.2. Excess pore pressures and average effective stresses were determined at the mid height of the sublayer using Terzaghi's

method and Davis and Raymond's method in conjunction with the finite difference method.

C.2.1 Calculation of Primary Consolidation Settlement Using Terzaghi's Equation

Geotechnical Input Parameters:

z = depth of node relative to original ground surface = 33.25 ft

z_{gwt} = depth of groundwater table relative to the original surface = 4.0 ft

γ_w= unit weight of water = 62.4 pcf (assumed)

$C_{r\varepsilon}$ = 0.0160

Δz = 1 ft

The effective vertical stress prior to construction of the embankment was previously calculated and is presented below:

$\sigma'_{v,i,j=0} = \sigma_{v,i,j=0} - u_{i,j=0}$ = 4116.36 -1825.20 = 2,291.16 psf

Now that the excess pore pressure has been calculated, the effective vertical stress will be calculated at node i and time j+1.

The total vertical stress at node i and time j+1:

$$\sigma_{v,i,j+1} = \sigma_{v,i,j} + \Delta\sigma_{v,(i,j=0\rightarrow j=100days}$$

Calculated effective overburden stress at node i, depth of 33.25 ft, prior to construction of the embankment is the same as previously calculated:

$$\sigma_{v,i,j=0} = \sum_{k=1}^{k=n} \gamma_k t_k = (126.90)(3) + (112.78)(5) + (126.90)(6) + (125.15)(5) +$$

(124.56)(11.25) + (127.77)(3) = 4,116.36 psf

The value of change in total vertical stress for time j=0 to j=100 days was obtained from readings of the pressure plates as:

$\Delta\sigma_{v,(i,j=0\rightarrow j=100days}$ = 3,894.31 psf

The total vertical stress at node i and time j+1:

$\sigma_{v,i,j+1} = \sigma_{v,i,j=0} + \Delta\sigma_{v,(i,j=0\rightarrow j=100days} = 4{,}116.36 \text{ psf} + 3{,}894.31 \text{ psf} = 8{,}010.67 \text{ psf}$

The effective vertical stress at node i and time j+1 is a function of the total vertical stress, as previously calculated, and the pore pressure. The pore pressure at node i and time j+1 is a combination of the steady state pore pressure (u_{ss}) and the predicted excess pore pressure (u_e) determined by Terzaghi's equation or Davis and Raymond's equation and is defined below.

$u_{i,j+1} = u_{zz,I} + u_{e,i,j+1}$

The steady state effective stress is defined as the unit weight of water (γ_w) multiplied by the height of water above node i, ($z - z_{gwt}$), at the desired depth of 33.25 ft.

$u_{ss,i,j+1} = \gamma_w(z - z_{gwt}) = 62.4(33.25 - 4.0) = 1{,}825.5$ psf

The excess pore pressure was previously derived and calculated using Terzaghi's equations and is defined below:

$u_{e,i,j+1} = 575.72$ psf

Now the pore pressure at node i, depth of 33.25 ft, and time j+1 is calculated:

$u_{i,j+1} = u_{zz,I} + u_{e,i,j+1} = 1{,}825.2 \text{ psf} + 575.72 \text{ psf} = 2{,}400.92 \text{ psf}$

The effective vertical stress used in settlement calculations at the end of the time j=100 days is calculated as:

$\sigma'_{v,i,j+1} = \sigma_{v,i,j+1} - u_{i,j+1} = 8{,}010.67 \text{ psf} - 2{,}400.92 \text{ psf} = 5{,}609.75 \text{ psf}$

The average effective vertical stress in the sublayer located between node i and node i+1 is calculated as:

$\sigma'_{v,avg} = ½ (\sigma'_{v,i,j+1} + \sigma'_{v,i+1,j+1})$

The effective vertical stress at node i+1 and time j+1 was calculated in the same manner as the effective vertical stress at node i and time j+1, and the value for effective vertical stress is as follows:

$\sigma'_{v,i+1,j+1} = 5671.96$ psf

Now the average effective vertical stress is as follows:

$\sigma'_{v,avg} = ½ (\sigma'_{v,i,j+1} + \sigma'_{v,i+1,j+1}) = ½(5609.75 + 5671.96) = 5640.86$ psf

The best estimate for preconsolidation pressure for this sublayer was found to be:

$\sigma'_p = 10{,}800$ psf

Since $\sigma'_{v,avg} < \sigma'_p$, the soil is in recompression and the following equation is used to calculate the settlement occurring within the sublayer located between node i and node i+1:

$$S_c = C_{r\varepsilon} \cdot \log \frac{\sigma'_{v,avg}}{\sigma'_{v0}} \cdot \Delta z = 0.016 \cdot \log \frac{5{,}640.86}{2{,}291.16} \cdot 1 = 0.006261 = 0.07513 \text{ in}$$

C.2.2 Calculation of Primary Consolidation Settlement Using Davis and Raymond's Equation

The geotechnical input parameters defined during the calculation of primary consolidation settlement using Terzaghi's method are the same geotechnical parameters that will be used in the calculation of primary consolidation using Davis and Raymond's method.

The effective vertical stress prior to construction of the embankment was previously calculated and is presented below:

$$\sigma'_{v,i,j=0} = \sigma_{v,i,j=0} - u_{i,j=0} = 4{,}116.36 - 1825.20 = 2{,}291.16 \text{ psf}$$

Now that the excess pore pressure has been calculated, the effective vertical stress will be calculated at node i and time j+1.

The total vertical stress at node i and time j+1:

$$\sigma_{v,i,j+1} = \sigma_{v,i,j=0} + \Delta\sigma_{v,(i,j=0\rightarrow j=100days}$$

Calculated effective overburden stress at node i, depth of 33.25 ft, prior to construction of the embankment is the same as previously calculated:

$$\sigma_{v,i,j=0} = \sum_{k=1}^{k=n} \gamma_k t_k = (126.90)(3) + (112.78)(5) + (126.90)(6) + (125.15)(5) +$$

$$(124.56)(11.25) + (127.77)(3) = 4{,}116.36 \text{ psf}$$

The value of change in total vertical stress for time j=0 to j=100 days was obtained from readings of the pressure plates as:

$$\Delta\sigma_{v,(i,j=0\rightarrow j=100days} = 3{,}894.31 \text{ psf}$$

The total vertical stress at node i and time j+1:

$$\sigma_{v,i,j+1} = \sigma_{v,i,j} + \Delta\sigma_{v,(i,j=0\rightarrow j=100days} = 4{,}116.36 \text{ psf} + 3{,}894.31 \text{ psf} = 8{,}010.67 \text{ psf}$$

The effective vertical stresses at node i and time j+1 is a function of the total vertical stress, as at previously calculated, and the pore pressure. The pore pressure at node i and time j+1 is a combination of the steady state pore pressure (u_{ss}) and the predicted excess pore pressure (u_e) determined by Terzaghi's equation or Davis and Raymond's equation and is defined below.

$$u_{i,j+1} = u_{ss,i} + u_{e,i,j+1}$$

The steady state effective stress is defined as the unit weight of water (γ_w) multiplied by the height of water above node i, ($z - z_{gwt}$), at the desired depth of 33.25 ft.

$u_{ss,i,j+1} = \gamma_w(z - z_{gwt}) = 62.4(33.25 - 4.0) = 1{,}825.5$ psf

The excess pore pressure was previously derived and calculated using Davis and Raymond's equation and is defined below:

$u_{e,i,j+1} = 1{,}617.92$ psf

Now the pore pressure at node i, depth of 33.25 ft, and time j+1 is calculated:

$u_{i,j+1} = u_{ss,i} + u_{e,i,j+1} = 1{,}825.2$ psf + 1,617.92 psf = 3,443.12 psf

The effective vertical stress used in settlement calculations at the end of the time j=100 days is calculated as:

$\sigma'_{v,i,j+1} = \sigma_{v,i,j+1} - u_{i,j+1} = 8{,}010.67$ psf – 3,443.12 psf = 4,567.55 psf

The average effective vertical stress between within between node i and node i+1 is calculated as:

$\sigma'_{v,avg} = ½ (\sigma'_{v,i,j+1} + \sigma'_{v,i+1,j+1})$

The effective vertical stress at node i+1 and time j+1 was calculated in the same manner as the effective vertical stress at node i and time j+1 and the value for effective vertical stress is as follows:

$\sigma'_{v,i+1,j+1} = 4339.02$ psf

Now the average effective vertical stress is as follows:

$\sigma'_{v,avg} = ½ (\sigma'_{v,i,j+1} + \sigma'_{v,i+1,j+1}) = ½(4567.55 + 4339.02) = 4453.29$ psf

The best estimate for preconsolidation pressure for this sublayer was found to be:

$\sigma'_p = 10{,}800$ psf

Since $\sigma'_{v,avg} < \sigma'_p$, the soil is in recompression and the following equation is used to calculate the settlement occurring within the sublayer located between node i and node i+1:

$$S_c = C_{r\varepsilon} \cdot \log \frac{\sigma'_{v,avg}}{\sigma'_{v0}} \cdot \Delta z = 0.016 \cdot \log \frac{4{,}453.29}{2{,}291.16} \cdot 1 = 0.004618 = 0.05542 \text{ in}$$

The primary consolidation settlement using the excess pore pressures at the interfaces was calculated in the same manner as Terzaghi's equation and Davis and Raymond's equation.

APPENDIX D

PRECONSOLIDATION STRESS AND COMPRESSION INDICES

D.1 Determination of Preconsolidation Stress

The preconsolidation stress, σ'_p, was estimated using two empirical regression equations based on tip resistance from a cone penetration test (Ozer's 2005 and Kulhawy and Mayne's 1990) and two methods based on stress-strain results from one-dimensional consolidation tests [Casagrande's (1936) graphical procedure and the work method (Becker et al. 1997)] are presented in Section D.1.1 through Section D.1.4. Example calculations and procedures for σ'_p are shown in this appendix at a depth of 75.6 ft below the original ground surface.

D.1.1 Ozer (2005)

Correlating the preconsolidation stress with CPT parameters for Lake Bonneville clay was previously discussed in Section 2.6.1. The empirical correlation for σ'_v, Eq. (2-28) was shown in Section 2.6.1 and has been duplicated below.

$$\frac{\sigma'_p}{P_a} = 0.6323\left(\frac{\sigma_{v,i,j=0}}{P_a}\right)^{0.565} * \left(\frac{q_t - \sigma_{v,i,j=0}}{P_a}\right)^{0.3422} \quad (2\text{-}28)$$

Total unit weight and thickness of all layers down to the desired depth:

$\gamma_1 = 126.90$ psf, $t_1 = 3$ ft

$\gamma_2 = 112.78$ psf, $t_2 = 5$ ft

$\gamma_3 = 126.90$ psf, $t_3 = 6$ ft

$\gamma_4 = 125.15$ psf, $t_4 = 5$ ft

γ_5 = 124.56 psf, t_5 = 11.25 ft

γ_6 = 127.77 psf, t_6 = 7 ft

γ_7 = 113.30 psf, t_7 = 8 ft

γ_8 = 124.48 psf, t_8 = 9.5 ft

γ_9 = 122.08 psf, t_9 = 3 ft

γ_{10} = 121.40 psf, t_{10} = 14.75 ft

γ_{11} = 127.35 psf, t_{11} = 3.1 ft

The load of the embankment determined by readings obtained from the pressure plates:

q = 3,602 psf

Calculated total overburden stress at node i, depth of 75.6 ft:

$$\sigma_{v,i,j=0} = \sum_{k=1}^{k=n} \gamma_k t_k = (126.90)(3) + (112.78)(5) + (126.90)(6) + (125.15)(5) +$$

(124.56)(11.25) + (127.77)(7) + (113.30)(8) + (124.48)(9.5) + (122.08)(3) +

(121.40)(14.75) = (127.35)(3.1) + 3,602 = 12,857.02 psf

The total cone tip resistance (q_t) was obtained from the cone penetration test:

q_t = 41,812 psf

Constants C_1, B_1, and B_2 as determined by Ozer (2005):

c_1 = 0.6323

B_1 = 0.565

B_2 = 0.3423

P_a = 1800 psf

From Eq. 2-28 in Section 2.6.1:

$$\sigma'_p = \left[0.6323\left(\frac{12{,}857.02}{1{,}800}\right)^{0.565} \times \left(\frac{41{,}812 - 12{,}587.02}{1{,}800}\right)^{0.3422}\right] 1{,}800 = 8{,}940 \text{ psf}$$

D.1.2 Kulhawy and Mayne (1990)

Empirical correlation between various geotechnical parameters can be found in almost any geotechnical engineering textbook as discussed in Section 2.6.1. A general correlation for σ'_p developed by Kulhawy and Mayne (1990), Eq. 2-29, based on CPT data from many sites was provided in Section 2.6.1 and has been duplicated below.

$$\sigma'_p = 0.33(q_t - \sigma_{v,i,j}) \tag{2-29}$$

The total cone tip resistance (q_t) was obtained from the cone penetration test:

$q_t = 41{,}812$ psf

The overburden stress previously calculated:

$\sigma_{v,i,j=0} = 12{,}857.02$ psf

From Eq. 2-29 in Section 2.6.1:

$\sigma'_p = 0.33(q_t - \sigma_{v,i,j}) = 0.33(41{,}812 - 12{,}857.02)$

D.1.3 Casagrande's Method

The procedure for using Casagrande's method to determine the preconsolidation stress was discussed and outlined in Section 2.6.2. The following steps were used in determining the preconsolidation stress using Casagrande's method:

1) Choose by eye the point of maximum curvature from the strain versus logarithm of effective stress curve.
2) Extend a horizontal line from the point of maximum curvature.
3) Draw a line tangent to the point of maximum curvature.
4) Bisect the angle created by the horizontal line and the line tangent to the maximum point of curvature.
5) Extend a line from the virgin compression portion of the curve toward the bisector line created in step 4. The stress corresponding to the point of intersection of these two lines provides an estimate of σ'_p.

This procedure was used to best estimate the preconsolidation stress at a depth of 75.6 ft. The plot and result for preconsolidation stress is provided below in Figure D-1.

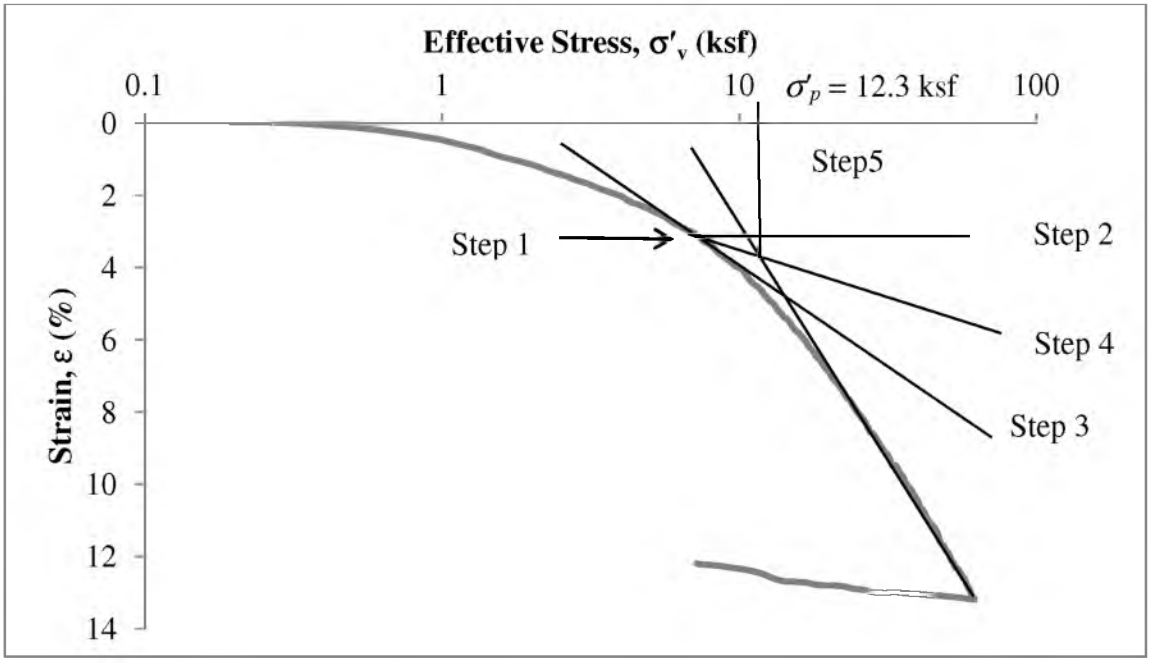

Figure D-1. Casagrande's method for preconsolidation stress at 75.6 ft.

D.1.4 Strain Energy Method

The procedure for using the strain energy method to determine the preconsolidation stress was discussed and outlined in Section 2.6.2. This procedure was used to best estimate the preconsolidation stress at a depth of 75.6 ft. The plot and result for preconsolidation stress is provided below in Figure D-2.

σ'_p was determined using two empirical correlations (Ozer's 2005 and Kulhawy and Mayne's 1990) and two graphical procedures using stress-strain results from one-dimensional consolidation tests [Casagrande's (1936) graphical procedure and the work method (Becker et al. 1997)]. Results from the empirical correlations were not used in settlement calculations because there is great caution in using results from empirical

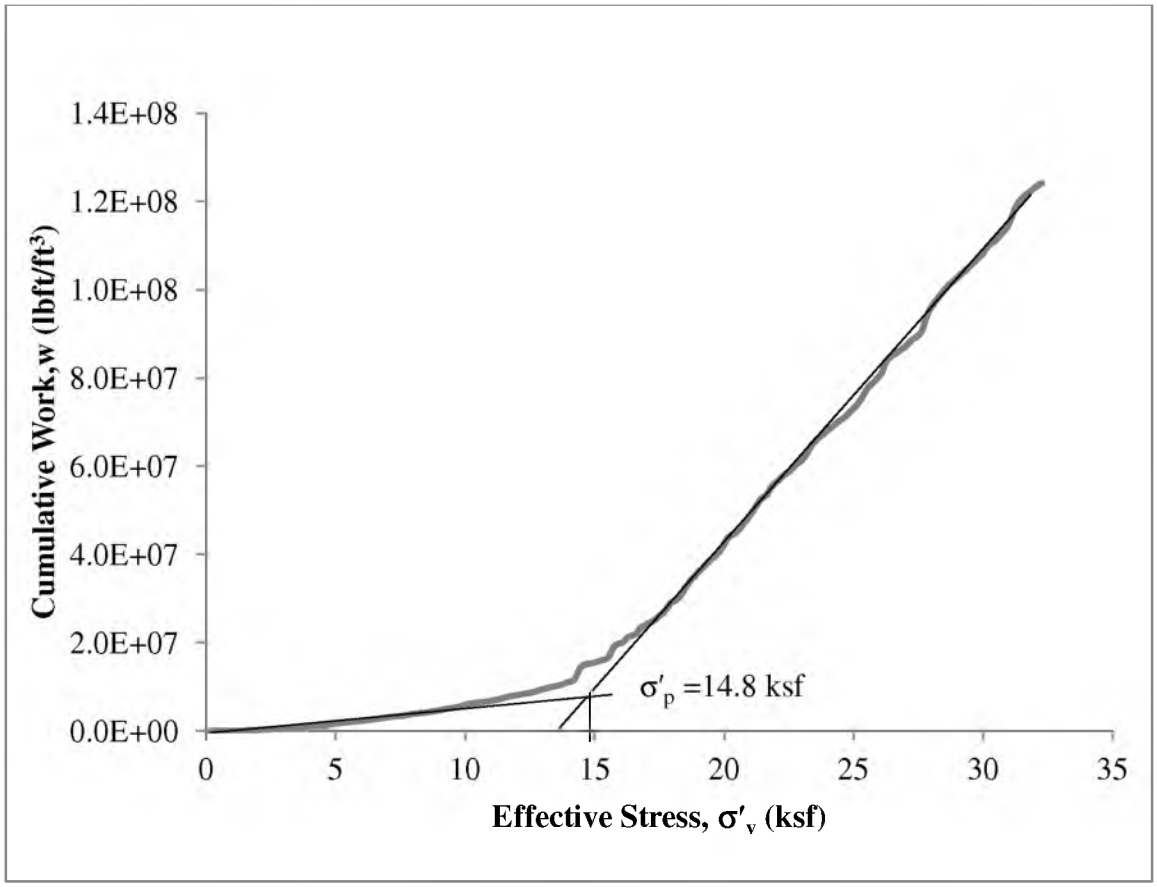

Figure D-2. Strain energy method at 75.6 ft.

correlations. σ'_p results from Casagrande's (1936) and the work method (Becker et al. 1997) were compared. It was determined that the best estimate for σ'_p was determined by the work method for two reasons: (1) Plots developed from the work method show a distinct point of curvature that allowed for a reasonable estimate of σ'_p to be made while the maximum point of curvature was difficult to choose for Casagrande's method due to the smoothness of the stress-strain curve and (2) due to the point of curvature being distinct, plots from the work method yielded more realistic results for determining preconsolidation stress.

D.2 Determination of Compression Indices

The compression index ($C_{c\varepsilon}$) and recompression ratio ($C_{r\varepsilon}$) were determined using stress-strain results from one-dimensional consolidation tests. Procedures and sample calculations for $C_{c\varepsilon}$ and $C_{r\varepsilon}$ are shown in this appendix at a depth of 75.6 ft below the original ground surface.

The following steps were used in determining the compression indices using Schertmanns's (1955) procedure:

1. Determine the initial void ratio.
2. Determine the effective stress of the soil as denoted by the square in D-3.
3. Determine the preconsolidation stress of the soil as denoted by the diamond in Figure D-3.
4. Draw a horizontal line parallel to the abscissa from the initial void ratio the effective stress.
5. Connect σ'_{v0} to σ'_p by the recompression index, C_r or $C_{r\varepsilon}$.

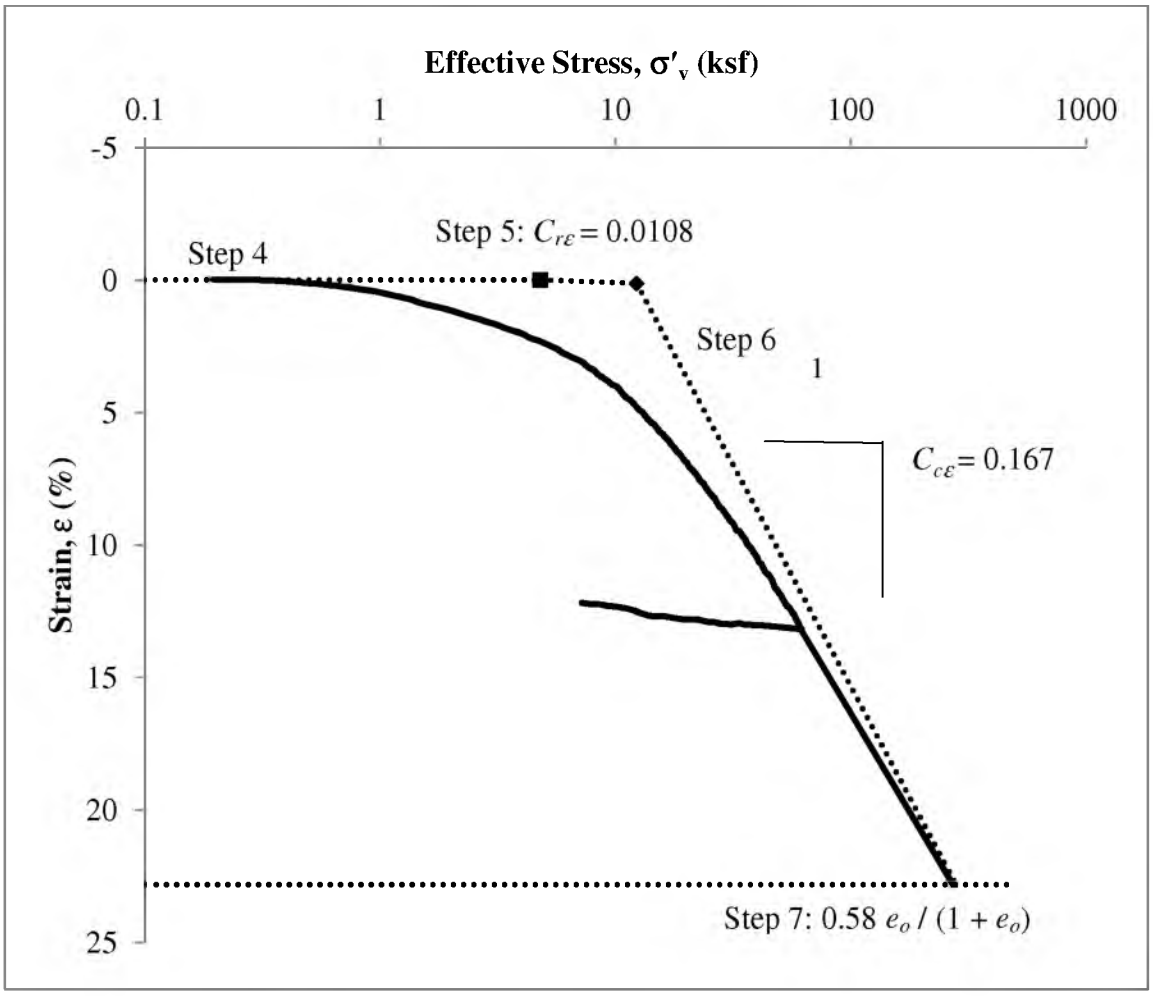

Figure D-3. Schertmann's procedures for compression indices at a depth of 75.6 ft. Using Eq. D-5 from Appendix D.

6. Extend the virgin compression curve to $0.42e_0$ or $0.58e_0/(1+e_0)$.
7. Connect the preconsolidation stress with the intersection point of $0.42e_0$ or $0.58e_0/(1+e_0)$ and the extension of the virgin compression curve.

However, because the one-dimensional consolidation curves were reported in vertical strain, ε, and not void ratio, e, an equivalent term for change in void ratio, Δe, was needed to use Schertmann's procedure. The following equations along with a sample calculation of the equivalent strain were used make Schertmann's procedure applicable.

The final void ratio, e_f, is equal to $0.42e_0$ and is defined as Eq. D-1:

$$e_f = 0.42\ e_o \tag{D-1}$$

The change in void ratio, Δe, is equal to e_0 minus e_f and is defined as Eq. D-2:

$$\Delta e = e_o - 0.42e_o \tag{D-2}$$

Substituting Eq. D-1 into D-2, the change in void ratio is:

$$\Delta e = 0.58e_o \tag{D-3}$$

Strain, ε, defined in terms of void ratio is defined as Eq. D-4

$$\varepsilon = \Delta e\ /\ (1 + e_o) \tag{D-4}$$

Substituting Eq. D-3 into Eq. D-4, the equivalent strain, ε_{58}, used for Schmertmann's procedure is:

$$\varepsilon = 0.58\ e_o\ /\ (1 + e_o) \tag{D-5}$$

The resulting plot using Schmertmann's procedure along with sample calculations for ε_{58}, Cc_{ε}, and $C_{r\varepsilon}$.

Geotechnical Input Parameters:

$e_0 = .6516$

$\gamma_1 = 126.90$ psf, $t_1 = 3$ ft

$\gamma_2 = 112.78$ psf, $t_2 = 5$ ft

$\gamma_3 = 126.90$ psf, $t_3 = 6$ ft

$\gamma_4 = 125.15$ psf, $t_4 = 5$ ft

$\gamma_5 = 124.56$ psf, $t_5 = 11.25$ ft

$\gamma_6 = 127.77$ psf, $t_6 = 7$ ft

$\gamma_7 = 113.30$ psf, $t_7 = 8$ ft

$\gamma_8 = 124.48$ psf, $t_8 = 9.5$ ft

$\gamma_9 = 122.08$ psf, $t_9 = 3$ ft

$\gamma_{10} = 121.40$ psf, $t_{10} = 14.75$ ft

$\gamma_{11} = 127.35$ psf, $t_{11} = 3.1$ ft

z_{gwt} = depth of groundwater table relative to the original surface = 4.0 ft

γ_w = unit weight of water = 62.4 pcf (assumed)

Calculated total overburden stress at depth of 75.6 ft:

$$\sigma_{v,i,j=0} = \sum_{k=1}^{k=n} \gamma_k t_k = (126.90)(3) + (112.78)(5) + (126.90)(6) + (125.15)(5) +$$

$$(124.56)(11.25) + (127.77)(7) + (113.30)(8) + (124.48)(9.5) + (122.08)(3) +$$

$$(121.40)(14.75) = (127.35)(3.1) + 9{,}255.02 \text{ psf}$$

Assuming that the pore water was in equilibrium at the time construction of the embankment began:

$u_{i,j+1} = u_{ss,I} = \gamma_w(z_i - z_{gwt}) = 62.4(75.6 - 4.0) = 4{,}467.84$ psf

$\sigma'_{v,i,j=0} = \sigma_{v,i,j} - u_{i,j=0} = 9{,}255.02 - 4{,}467.84 = 4{,}787.18$ psf

Using Eq. D-5 along with the geotechnical parameters determined from laboratory testing, the equivalent strain used in Schmertmann's procedure is and was previously shown in Figure D-3.

$$\varepsilon_{58} = \frac{0.58(0.6516)}{1+0.6516}(100) = 22.883$$

The compression index, $C_{c\varepsilon}$, is calculated using the virgin compression portion of the stress-strain curve and is defined as Eq. D-6:

$$C_{c\varepsilon} = -\frac{d\varepsilon}{d\log\sigma'_v} = \frac{\varepsilon_2 - \varepsilon_1}{\log\frac{\sigma'_2}{\sigma'_1}} \qquad \text{(D-6)}$$

The preconsolidation stress was determined previously in this appendix using Casagrande's method.

$\sigma'_{v1} = 14.8$ ksf

Extending the virgin compression slope to the equivalent strain of 22.833, the effective vertical stress:

$\sigma'_{v2} = 280$ ksf

The strain corresponding to σ'_p:

$\varepsilon_1 = 0.133$

The strain corresponding to σ'_v (the intersection of the extension of the virgin compression curve and the horizontal line at $0.58e_0/(1+e_0)$.:

$\varepsilon_{58} = \varepsilon_2 = 22.883$

$C_{c\varepsilon}$ was calculated using D-6 from Appendix D:

$$C_{c\varepsilon} = -\frac{d\varepsilon}{d\log\sigma'_v} = \frac{\varepsilon_2 - \varepsilon_1}{\log\frac{\sigma'_2}{\sigma'_1}} = \frac{(22.833 - 0.133)0.01}{\log\left(\frac{280}{14.8}\right)} = 0.178$$

The recompression ratio, $C_{r\varepsilon}$, is calculated using the rebound portion of the stress-strain curve and is defined in the as Eq. D-7:

$$C_{r\varepsilon} = -\frac{d\varepsilon}{d\log\sigma'_v} = \frac{\varepsilon_2 - \varepsilon_1}{\log\frac{\sigma'_2}{\sigma'_1}} \qquad \text{(D-7)}$$

Stress-strain results from one-dimensional loading produced the following effective vertical stresses, σ'_v, and their corresponding strains, ε:

$\sigma'_{v1} = 61{,}902.72$ psf

$\varepsilon_1 = 13.205$ %

$\sigma'_{v2} = 7{,}190.64$ psf

$\varepsilon_2 = 12.199$ %

$C_{r\varepsilon}$ was calculated using Eq. D-7 from Appendix D:

$$C_{r\varepsilon} = -\frac{d\varepsilon}{d\log\sigma'_v} = \frac{\varepsilon_2 - \varepsilon_1}{\log\frac{\sigma'_2}{\sigma'_1}} = \frac{(13.205 - 12.199)0.01}{\log\left(\frac{61{,}902.72}{7{,}190.64}\right)} = 0.0108$$

REFERENCES

Adboun, T., and Bennett, V. (2008, March). A new wireless MEMS-based system for real-time deformation monitoring. *Geotechnical News*, 36-40.

Andersland, A.-K. a. (1992). *Geotechnical engineering and soil testing.* New York: Saunder College Publishing.

ASTM. (1985). Dry preparation of soil samples for particle-size analysis and determination of soil contents. In *D421 - 85.* West Conshohockon, PA.

ASTM. (2008). Standard test method for field vane shear test in cohesive soils. In *D2573 - 08.* West Conshohocken, PA.

ASTM. (2005). Standard test method for liquid limit, plastic limit, and plasticity index of soils. In *D4318 - 05.* West Conshohocken, PA.

ASTM. (2006). Standard test method for one-dimensional consolidation properties of saturated cohesive soils using controlled-strain loading. In *D4186 - 06.* West Conshohocken, PA.

ASTM. (1963). Standard test method for particle size analysis of soils. In *D422 - 63.* West Conshohocken, PA

Becker, D. (1987). Work as a criterion for determining in situ and yield stresses in class. *Canadian Geotechnical Journal, 24*, 549-564.

Biot, M. (1941, February). General theory of three-dimensional consolidation. *Journal of Applied Physics, 12* (2), 155-164.

Bowles, J. E. (1988). *Foundation analysis and design.* New York: McGraw-Hill.

Farnsworth, C. B., Bartlett, Steven (2008, March). Rapid construction and settlement behavior of embankment systems on soft foundation soils. *Journal of Geotechnical and Geoenvironmental*, 289-301.

Casagrande, A. (1936b). The determination of the pre-consolidation load and its practical significance. *Proceedings of the First International Conference on Soil Mechanics and Foundation Engineering, III.* 60-64. Cambridge.

Chang, K.-H., Kovacs, W. D., and Wu, M.-J. (1994). Comparison of predicted and measured settlement of a test embankment over soft soil. In A. T. Yeung, and G. Y. Felio, *Vertical and horizontal deformations of foundations and embankments* (Vol. 2, . 1164-1175). College Station: American Society of Civil Engineers.

Das, B. M. (2008). *Advanced soil mechanics.* New York: Taylor and Francis.
Dasenbrock, D. D. *Autommated landslide instrumentation programs on US Route 2 in Crookeston, MN.* Maplewood, Minnesota.

Davis, E. H., and Poulus, H. G. (1972). Rate of settlement under two- and three-dimensional conditions. *Geotechnique, 22* (1), 95-114.

Davis, E. H., and Raymond, G. P. (1965). A non-linear theory of consolidation. *Geotechnique, 15* (2), 161-173.

Duncan, J. M. (1993, September 8). Limitations of consolidation analysis of consolidation settlement. *Journal of Geotechnical Engineering, 119* (9), 1333-1359.

Dunnicliff, J. (1993). *Geotechnical instrumentation for monitoring field performance.* New York,: John Wiley & Sons Inc.

Gibson, R. E., Schiffman, R. L., and Cargill, K. W. (1981). The theory of one-dimensional consolidation of saturated clays. *Canadian Geotechnical Journal, 18*, 280-293.

Jamiolkowski, M. (1985). New developemeмnts in field and laboratory testing of soils. *Proc. of the llth Intl. Conference of Soil Mechanincs and Foundation Engineering, 1*, 57-153. San Francisco.

Kulhawy, F. H., and Mayne, P. W. (1990). Manual of estimating soil properties for foundation design. In *El-6800* (p. 306). Palo Alto: Electric Research Power Inst.

Learoueil, S., Tavenas, F., Mieussens, C., and Peifnaud, M. (1978). Construction pore pressuresc in clay foundations under embankments part II: gerneralized behaviour. *Canadian Geotechnical Journal, 15*, 66-82.

Leathers, F. D., and Ladd, C. C. (1978). Behavior of an embankment on New York varved clay. *Canadian Geotechnical Journal, 15*, 250-268.

Leroueil, S., Tavenas, F., Trak, B., La Rochelle, P., and Roy, M. (1978). Construction pore pressures in clay foundations under embankments part I: the Saint Alban test fills. *Canadian Geotechnical Journal, 15*, 54-65.

Ozer, A. T. (2005). *Estimation of consolidation and drainage properties for Lake Bonneville clays thesis.* Salt Lake City, UT: Univeristy of Utah, Department of Civil and Environmental Engineering.

Pilot, G., Trak, B., and La Rochelle, P. (1986). Effective stress analysis of the stability of embankments on soft soils. *Canadian Geotechnical Journal*, 255-256.

Ripley, C. F. (1995). Preloading a thick compressible subsoils: a case history. *Canadian Geotechnical Journal*, 465-480.

Seed, H. B., and Booker, J. R. (1976). Stabilization of potentially liquefiable sand deposits using gravel drain systems. *Report No. EERC 76-10.*

Sivaram, B., and Swamee, P. K. (1977). A computational method for consolidation-coefficient. *Soils and Foundations, 17* (2), 48-52.

Skempton, A. W., and Bjerrum, L. (1957). A contribution to the settlement analysis of foundations on clays. *Geotechnique, 12*,168-178.

Tavenas, F., Blanchet, R., Garneau, R., and Leroueil, S. (1978). The stability of stage-constructed embankments on soft clay. *Canadian Geotechnical Journal*, 283-305.